5-2008

RENEWABLE RESOURCE LACTIDE DERIVED MATERIALS: SCALED-UP SYNTHESIS, CHARACTERIZATION AND APPLICATIONS

Akhilesh Singh
Clemson University, asingh@g.clemson.edu

RENEWABLE RESOURCE LACTIDE DERIVED MATERIALS: SCALED-UP SYNTHESIS, CHARACTERIZATION AND APPLICATIONS

A Dissertation
Presented to
the Graduate School of
Clemson University

In Partial Fulfillment
of the Requirements for the Degree
Doctor of Philosophy
Polymer and Fiber Science

---

by
Akhilesh Kumar Satyanarayan Singh
May 2008

Accepted by:
Dr. Michael J. Drews, Committee Chair
Dr. Dennis W. Smith, Jr., Committee Co-Chair
Dr. Gary C. Lickfield
Dr. Philip J. Brown

ABSTRACT

Renewable resource monomer, lactide, derived copolymers and terpolymers were synthesized on a few hundred gram scale with specialty/commodity co-monomers such as perfluoropolyether and bisphenol A derivatives. The modifications resulted in improved properties such as surface energy, crystallization, and glass transition temperature of the polylactide.

Ring-opening polymerizations of L-lactide were performed using different block length perfluoropolyethers as macro-initiators and tin octoate as the catalyst. The resultant polylactide-perfluoropolyether-polylactide block copolymers were characterized by various analytical and microscopic techniques such as differential scanning calorimetry, thermogravimetric analysis, nuclear magnetic resonance spectroscopy, dynamic mechanical analysis, wide-angle x-ray diffraction spectroscopy, polarized optical microscopy, etc.

The incorporation of low surface energy perfluoropolyether into the polylactide backbone modified its surface energy and the copolymers possessed a very low surface energy (16-20 mN/m) compared to that of polylactide (35-40 mN/m) even when at a very low concentration of perfluoropolyether.

The copolymerization affected the thermal properties of the polylactide and the copolymers exhibited lowered glass-transition, crystallization, and melting temperatures compared to the homopolymer, polylactide. The copolymers exhibited unique crystallization behavior and higher crystallinity and faster crystallization rates of the copolymers were found in comparison to polylactide. The enhanced crystallization properties of copolymers were speculated to be due to the nucleating action of perfluoropolyether. The high density and low surface energy perfluoropolyether enables it to behave as a foreign material and as an

ideal sight for nucleation. The crystallization half-time, spherulitic growth rate, Avarami's parameters, etc., were studied.

The hydrolytic stability of polylactide-perfluoropolyether-polylactide block copolymers was studied in acidic, alkaline and neutral conditions. Degradation parameters such as weight loss, decrease in molecular weight, and change in thermal properties, hydrolytic solution properties, and surface morphology were monitored. Films hydrolyzed in alkaline conditions showed significant weight loss whereas in acidic and neutral conditions, the weight loss was comparatively low. Initial resistance to the weight loss of the films in alkaline conditions can be seen for the copolymers due to their hydrophobic nature. Molecular weight loss was observed for both homopolymer and the copolymers in all of the hydrolytic conditions. The melting temperatures of hydrolyzed films decreased with increasing hydrolysis time as the ester cleaved chain ends acted as impurities in the crystalline phase.

Melt spinning of polylactide and block copolymers were performed to obtain monofilaments.

The terpolymerization of lactide and bisphenol A derivatives resulted in a moderate molecular weight (Mn ~ 12 kg/mol) and a high glass transition (ca. 100 °C) terpolymer. The terpolymer also showed better thermal stability than PLA and the surface properties were unchanged compared to the PLA. Successful electro-spinning of the terpolymer was performed from chloroform and tetrahydrofuran solutions.

DEDICATION

This work is dedicated to my wife Dr. Akanksha Singh, my parents Mr. and Mrs. S. N. Singh, and to the rest of my family members for their love and support.

ACKNOWLEDGMENTS

I extend my sincere appreciation to my advisors Prof. Michael J. Drews from the School of Materials Science and Engineering and Prof. Dennis W. Smith, Jr. from the Chemistry department. I am forever grateful for their joint-venture mentoring and their constant support during my research tenure. Their experience, knowledge and logical explanations have given me great guidance in framing and concluding my work. I am also thankful to them for the freedom they allowed me and their confidence in me as I completed my endeavor.

I would like to thank my committee members, Dr. Gary C. Lickfield and Dr. Philip J. Brown for their suggestions, constructive criticisms and guidance. I enjoyed Dr. Lickfield's teaching and his unconditional guidance whenever needed and Dr. Brown's stimulating and thought provoking questions like "*What next?*" which helped direct my future steps.

This dissertation would not have been completed without the unconditional support and guidance from Ms. Kimberly Ivey. I am deeply grateful for her help with the laboratory analytical instrumentation, experimental suggestions, and critical review of my dissertation. In addition, I am thankful to Dr. Amit K. Naskar for his continuing guidance and support throughout this work and more.

I warmly thank Dr. Richard Aspland, Dr. Bhuvenesh Goswami, Dr. Igor Luzinov, Dr. Stephen Foulger, and Dr. Michael Ellison for their wonderful teaching and guidance during my course work at Clemson University.

In particular, I would like to thank Dr. Igor Luzinov for allowing the use of the atomic force microscopy facility, Dr. JoAn Hudson, Dayton Cash, Amar Kumbhar, and Donald Mulwee for their help with electron microscopy, Dr. Graham M. Harrison for the

use of the rheological instrument, and Dr. Don VanDerveer for his help with the x-ray diffraction technique. In addition, I would like to thank Prof. Smith's research group, Dr. Karthik Ramaratnam, Dr. Ruslan Burtovyy, Dahlia Haynes, Saif Pathan, Joel Barden, Madan Banda, Sourabh Pansare, Stephen Budy, Scott Iacono, Jason Conrad, Nancy Belanger, James Lowe, Robbie Nicholson, Deidra Cade, and whoever helped me in my research.

And finally, I would like to thank the School of Materials Science and Engineering and the National Textile Center for their financial support and the Dow Chemical Company, Tetramer Technologies, L.L.C., Solvay Solexis and Poly-Med, Inc. for their generous donations of chemicals.

TABLE OF CONTENTS

Page

LIST OF TABLES

List of Tables (Continued)

Table Page

LIST OF FIGURES

List of Figures (Continued)

Figure Page

List of Figures (Continued)

Figure Page

List of Figures (Continued)

Figure Page

List of Figures (Continued)

Figure Page

List of Figures (Continued)

Figure Page

List of Figures (Continued)

Figure Page

List of Figures (Continued)

Figure Page

List of Figures (Continued)

Figure Page

List of Figures (Continued)

List of Figures (Continued)

Figure Page

List of Figures (Continued)

Figure Page

LIST OF SCHEMES

Schemes Page

CHAPTER 1

INTRODUCTION

1.1 Renewable Resource Biodegradable Polymers

The world is changing but not towards a sustainable, healthy and safe future. Global society and the natural world are in prominent danger due to climate change. Polymeric solid wastes adversely affect climate change by the generation of greenhouse gases during various steps such as extraction and processing of raw materials, manufacture of products, waste management, etc.[1] Generation of long-lived solid waste and pollution associated with the petrochemical-based polymers (PBPs) are key issues. Also, the continual rise in price, political instability in oil rich regions, and the scarcity of crude oil (raw material for PBPs) are expected to adversely affect the economics of producing PBPs.[2,3] Thus it is very important that the above problems be addressed. Prudent use of resources and efficient waste management such as reduction, re-use, recycling, incineration, landfill, etc. for a sustainable future is difficult to achieve in any single way.

On the other hand, polymers have undoubtedly improved our lifestyle because of their wide range of properties available at low cost and hence versatility in applications. It is unacceptable to avoid the use of polymeric materials and hence the need arises for the low cost, renewable resource polymeric materials which can provide the properties of a commodity polymer while minimizing any detrimental effects on the environment. Biodegradable synthetic polymers (BSPs), such as polylactide/poly(lactic acids) can play a significant role in the commodity area if they possess desired qualities. Although, to replace

the gamut of PBPs with handful of biodegradable polymers, there is need for the modification of BSPs for specific applications.

1.2 Project Objectives

The goal of this dissertation is to improve specific properties of polylactides by incorporating specialty or commodity monomers and to make them comparable to those of common PBPs such as polystyrene, polyethylene, polytetrafluoroethylene, etc. This goal was accomplished by achieving the following objectives:

1. Increase hydrophobicity.
2. Increase the crystallization rate and overall crystallinity.
3. Increase the glass transition temperature of polylactide by incorporation of commodity monomers.
4. Demonstrate the fabrication of the modified polymeric materials into application products such as fibers for filtration, clothing, etc.
5. Investigate the effect of surface energy and crystallinity change on the hydrolytic stability of modified polylactides.

1.3 Outline

The dissertation is organized into chapters to present the experimental findings clearly and in relevance. Chapter 2 contains the literature review on synthesis, mechanisms, production aspects and also explores the properties, modifications, degradation and applications areas of polylatides. Chapter 3 describes the experimental techniques used in this research. Chapter 4 describes the ring-opening polymerization of lactides using

perfluoropolyether as macro-initiator and discusses the characterization and surface energy analysis of the resulting perfluoropolyether-polylactide block copolymers. Chapter 5 discusses results of the study of the crystallization behavior of the resulting perfluoropolyether-polylactide block copolymers. Chapter 6 describes the results of the hydrolytic stability study of the homopolymer and the resulting perfluoropolyether-polylactide block copolymers. Chapter 7 describes the melt spinning of the homopolymer and the resulting perfluoropolyether-polylactide block copolymers. Chapter 8 discusses the synthesis, characterization, and electrospinning of fibers from terpolymers of lactide and bisphenol-A derivatives (fluorinated and non-fluorinated derivatives). The Appendices A-N includes additional experimental techniques and results from Chapter 4-Chapter 8.

1.4 References

1. Solid Waste Management and Greenhouse Gases: A Life-Cycle Assessment of Emissions and Sinks, 3rd Edition.*www.epa.gov*.(16 Jun 2007).
2. Azapagic, A., Emsley, A. & Hamerton, I. in *Polymers, the Environment and Sustainable Development* (ed. Hamerton, I.) 1-15 (John Wiley & Sons, Inc., West Sussex, 2003).
3. Erhand, G. *Designing with Plastics* (Hanser Gardner Publications, Cincinnati, 2006).

CHAPTER 2

LITERATURE REVIEW

2.1 Introduction

Polylactide/poly(lactic acid)

Polylactides or poly(lactic acid)s (PLAs) are biodegradable aliphatic polyesters known for their biomedical and pharmaceutical applications and ecological benefits.[1] PLAs can be produced from renewable resources such as starch and possess some comparable properties to petroleum-based polymers (PBPs) such as polyethylene, polypropylene and polystyrene yet is generally inferior as a semi-crystalline engineering thermoplastic.[1] The properties of PLAs can be controlled by the type of lactic acid (L or D enantiomers) used, extent of branching, and length of the polymer chain.[2] In general, PLAs can be synthesized by the condensation of lactic acid, or by the ring-opening polymerization of lactide, a cyclic dimer of lactic acid.[1,3] Properties such as thermal, hydrolytic stability and rate of biodegradation can be modified by altering molecular characteristics such crystallinity and can be achieved in variety of ways including copolymerization, blending, addition of additives, etc. In addition to medical and pharmaceutical applications, PLA is showing great potential for commodity applications because of the recent decrease in the cost of its production and the increase in cost and instability of fossil feedstock.

Lactic acid and lactide

The optically active lactic acid (2-hydroxy propionic acid) has two enantiomeric L- and D- (*S*- and *R*-) forms. The isolation of lactic acid was reported back in 1780[4], however, the linear dimer (lactoyl lactic acid) from lactic acid was first reported in 1845 by Pelouze.[1,5] Carothers et al.[6] reported the two-step synthesis of high molecular PLA from the cyclic dimer (lactide) of lactic acid. The cyclic dimerisation of lactic acids proceeds by condensation resulting in three different lactides. The chemical structure of lactic acid in two different optically active forms and its conversion in L-, D-, and *meso*-lactides are illustrated in Scheme 2.1.[1,3] The melting temperature of the lactic acids are ca. 17 °C. The melting temperature of L- and D-lactides (ca. 97 °C) are higher than the meso-lactide (ca. 53 °C).

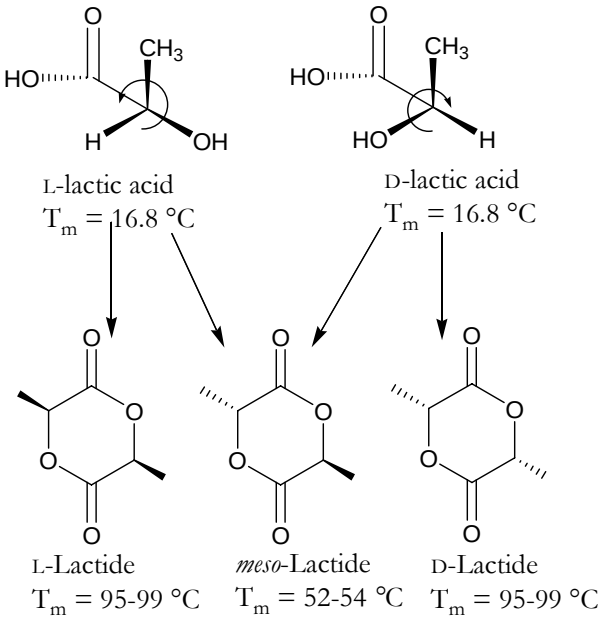

Scheme 2.1. Cyclic dimerization by condensation of L-, and D-lactic acids into L-, D-, and *meso*-lactides.

Biopolymers

In addition to PLA, other aliphatic polyesters which have good mechanical properties, hydrolyzability, and biocompatibility are derived from glycolide (GA), β-butyrolactone (β-BL), ε-caprolactone (ε-CL), and 1,5-dioxepan-2-one (DXO).[7] Scheme 2.2 illustrates the common lactones and their resultant polymer upon ring-opening polymerization. These polymers have shown tremendous potential, both as homopolymers and their copolymers. Copolymerization has been used to improve the mechanical, hydrophilic, and biodegradation properties of these polymers by utilizing various architectures such as linear random and block copolymers along with complex architectures such as stars, brushes, cyclic, cross-linked, hyperbranched aliphatic polyesters.[7-12]

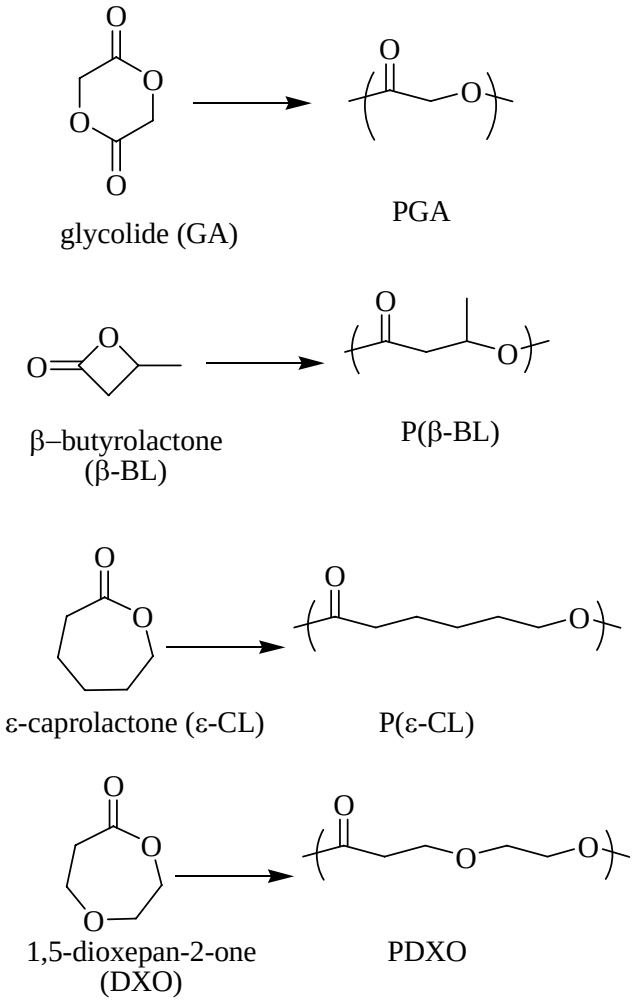

Scheme 2.2. Molecular structure of other lactones and aliphatic polyesters.

2.2 Synthesis, Mechanisms, and Commercial Production

Synthesis

PLA polymer can be prepared by the direct condensation of lactic acid or by the ring-opening polymerization (ROP) of lactide, the cyclic dimer of lactic acid. Scheme 2.3 shows a schematic of lactic acid production from starch and illustrates the synthesis of PLA by direct condensation and ring-opening routes.

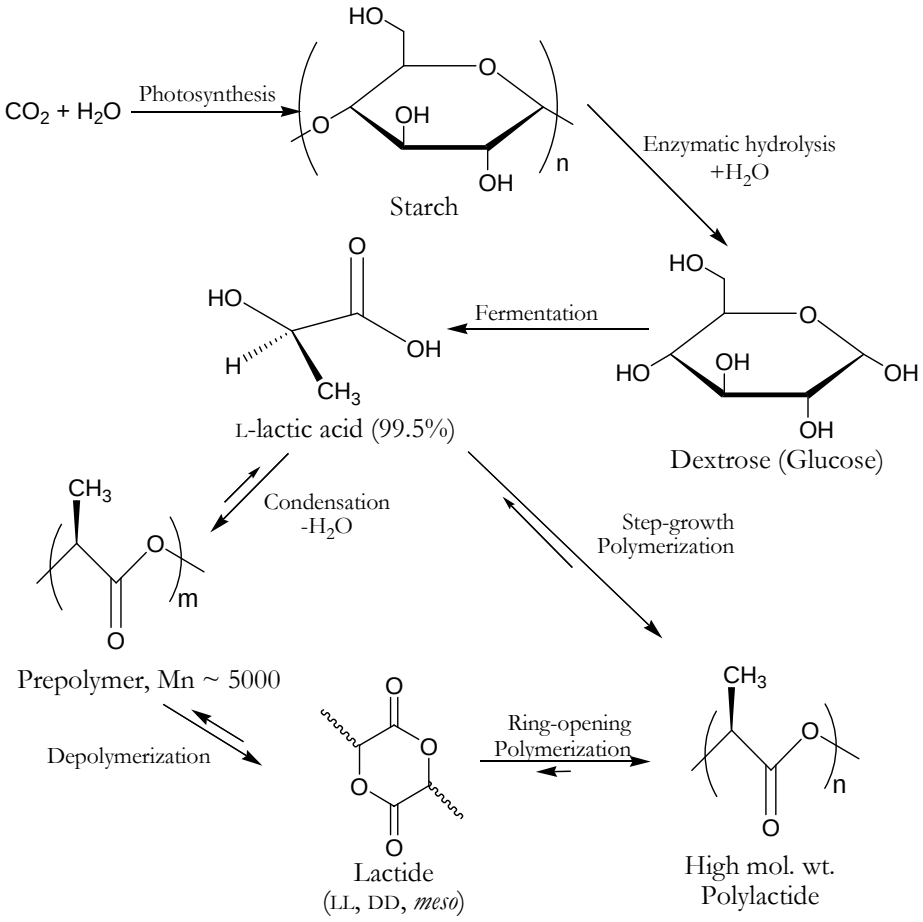

Scheme 2.3. Synthesis of lactic acid and poly(lactic acid).[13,14]

However, the condensation polymerization necessitates the removal of water even at traces level. Mitsui Toatsu Chemicals, Inc. invented a process for the efficient removal of water by azeotropic distillation and therefore, resulted in the production of high molecular weight (100-300 kD) PLA.[15,16] However, the feasibility of this process is greatly affected by the amount of catalyst, size of reactor, and the economical recovery of solvents.[16]

On the contrary, more versatile and efficient production of PLAs is achieved by ring-opening polymerization (ROP) of lactides in the presence of an initiator/catalyst. An efficient and versatile catalyst for the ROP of lactide is tin(II) 2-ethylhexanoate which is also known as stannous octoate ($Sn(Oct)_2$).[7] It offers benefits such as a very high catalytic activity, low levels of racemization, good solubility in the melt of lactide, and is an approved food additive.[16]

Stannous octoate does not initiate the polymerization of lactides and needs to be converted to tin(II)-alkoxides. The initiation requires presence of the hydroxyl or other nucleophilic species.[17,18] For lactides, impurities such as water, lactic acid, and linear dimers and trimers act as initiators.[19,20] Scheme 2.4 illustrates the ROP of lactide to PLA using alcohol and stannous octoate as catalyst system.

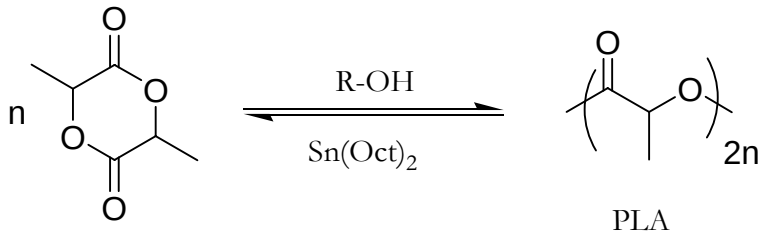

L-lactide PLA

Scheme 2.4. Polymerization of lactide to PLA using R-OH/$Sn(Oct)_2$ initiator/catalyst system.

Mechanisms

The reaction mechanisms for ROP of lactides are dictated by the catalyst/initiator systems and cationic, anionic, coordination mechanisms are a few of the proposed mechanisms based on the kinetics of reaction, side reactions and the end group analysis.[2,21] Complexes of tin, zinc, aluminum, lanthanides and strong bases such as metal alkoxides have been used as catalyst systems for ROP of lactides.[2] However, tin(II) 2-ethylhexanoate is the most commonly used catalyst/initiator for ROP of lactides. As mentioned earlier, initiation requires an active hydrogen compound.[22] The polymerization proceeds by the coordination of lactide in the active species and the propagation progresses by insertion of lactide units into the tin-oxygen bond.[23] There are two major proposed mechanisms for the co-ordination insertion polymerization of lactides, *viz*., the activated monomer mechanism[24,25] and coordination insertion[26-28] by formation of tin(II) alkoxides.

In the activated monomer mechanism, $Sn(Oct)_2$ forms a donor-acceptor complex with the monomer and activates the monomers towards the nucleophilic attack by the alcohol leading to the insertion of monomer into Sn-O (metal-oxygen) bond.[7,29] $Sn(Oct)_2$ is liberated at every propagation stage and Sn(II) atoms are not covalently bonded to polymer chains.[27] Scheme 2.5 demonstrates the activated monomer mechanism for ROP of lactide and other lactones.

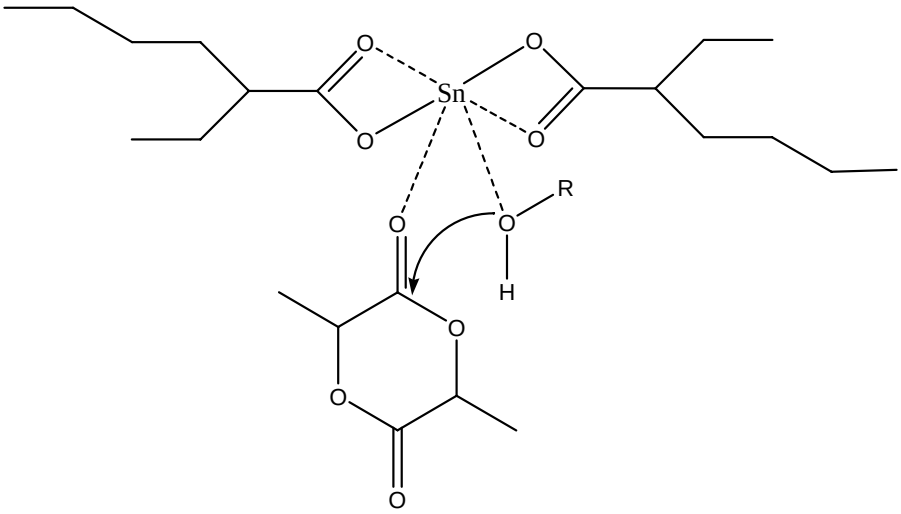

Scheme 2.5. Activated monomer mechanism for ROP of lactides using $Sn(Oct)_2$.

Penczek and co-workers proposed the coordination insertion mechanism based on observations involving the dissociation of at least one 2-ethylhexanoate group from $Sn(Oct)_2$ as 2-ethylhexanoic acid. The polymerization is thought to be initiated by compounds containing hydroxyl groups (added intentionally or present as impurities), resulting in the tin(II) alkoxide, a true initiator prior to polymerization.[27,30] Based on polymerization of GA and DXO, Albertsson and co-workers[31] suggested the nucleophilic attack of alkoxide (tin(II) alkoxide) on the carbonyl carbon of monomer followed by acyl-oxygen [C(O)--O]bond cleavage of the monomer which results in formation of R-O-C(O)-- and --O-Sn(Oct) end groups. The propagation proceeds by the addition of monomers to the Sn-O bond. Scheme 2.6 illustrates the Sn(II) alkoxide complex initiated ROP of lactides.

This mechanism was also supported by the Kricheldorf and co-workers[25,32] who reported dynamic complex systems based on $Sn(Oct)_2$/Initiator and that the system responds to any change in reaction conditions by a change in the concentration and structure

of active initiator species. Their conclusion was based on the observation of liberated octanoic acid during the reaction of alcohols and $Sn(Oct)_2$ and the presence of carboxylic acids decreases the reaction rate as it affects the equilibrium of complex formation. Also, information about the relationship between the molecular weight and monomer/initiator ratio was provided.

$$Sn(Oct)_2 + R\text{-}OH \rightleftharpoons Oct\text{-}Sn\text{-}OR + Oct\text{-}H$$

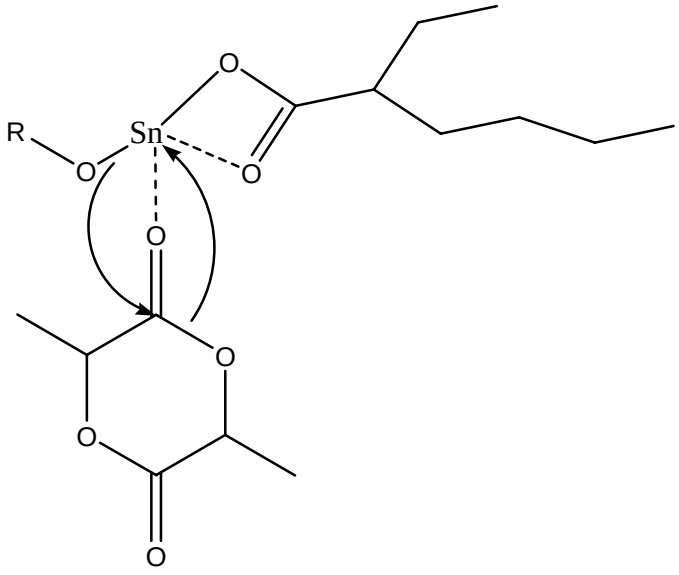

Scheme 2.6. Tin(II) alkoxide complex initiated ROP of lactides using $Sn(Oct)_2$.

Cationic polymerization mechanisms for the bulk polymerization of lactides in presence of $Sn(Oct)_2$ were proposed by Nijenhuis et al.(1992)[20] and Schwach et al.(1997)[33]. Pennings and co-workers (Nijenhuis et al.)[20] proposed a nucleophilic attack of hydroxyl compounds (R-OH) on the lactone/Sn^+(Oct) complex as shown in Scheme 2.7. The proposed mechanism is similar to transesterification mechanisms. The complex II generates a new species similar to complex I after reaction with lactones. It is proposed that the

catalyst is not chemically bound to growing polymer chain ends and that the catalyst can polymerize larger numbers of polymer chains than the number of catalyst molecules. This effectiveness of catalyst could decrease the number average molecular weight and also broaden the molecular weight distribution.

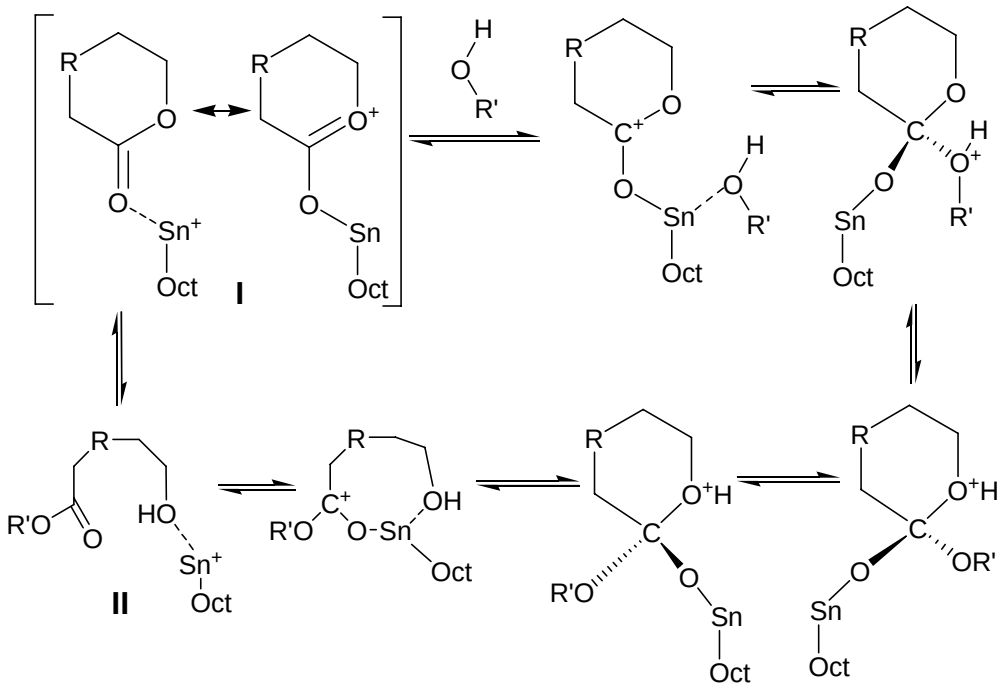

Scheme 2.7. Cationic polymerization mechanism for the $Sn(Oct)_2$/lactone system as proposed by Nijenhuis et al.

Vert and co-workers (Schwach et al.)[33] proposed a mechanism in which there is the formation of carbocations from lactones resulting after the reaction of the protonated catalyst, $Sn^+(Oct)$, on the carbonyl carbon of lactone. The cationic mechanism involving the co-initiation by lactic acid or octonoic acid is illustrated in Scheme 2.8.

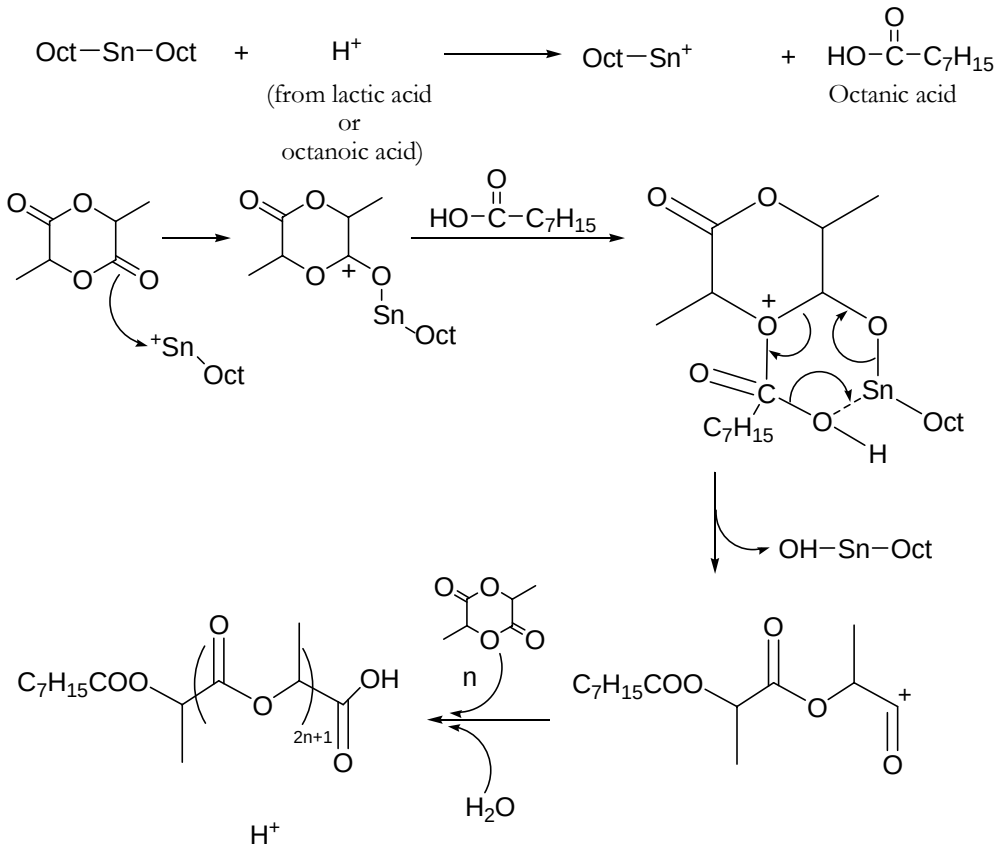

Scheme 2.8. Cationic polymerization mechanism for the $Sn(Oct)_2$/lactide system as proposed by Schwach et al.

Numerous mechanisms such as cationic, anionic, enzymatic, co-ordination insertion, etc., exist for the ring opening polymerization using organocatalysts as reviewed by Kamber et al.[34] Many other metal complexes such as aluminum complexes[35,36], iron complexes[37,38], zinc complexes[39,40] have been explored as catalysts for lactide polymerization. Coordination-insertion polymerization is the most widely accepted mechanism as it provides an explanation for the highly stereoregular polymers obtained with $Sn(Oct)_2$.[41] Hillmyer and co-workers reported a highly active metalloenzyme inspired dizinc catalyst for the controlled

polymerization of lactide.[39] Coates and co-workers[40] reported polymerization of *rac*-lactide using a zinc alkoxide complex that acts as a single-site, living initiator. Polymerization resulted in an amorphous heterotactic PLA with T_g of 49 °C and the probability of a racemic enchainment in the polymer of 0.94. Spassky et al. reported high stereoselectivity of PLA (88% enrichment at 19 % conversion) when *rac*-lactide was polymerized using a chiral Schiff's base/aluminium alkoxide as initiator.[42]

Commercial Production

Commercial scale production of PLA has been successfully achieved by both routes *viz.,* ROP of lactides and direct condensation of lactic acids.[43,44] Direct condensation utilizes azeotropic distillation to remove water from the reaction system and hence drives the reaction to attain a reasonable mol. wt. of PLA.[43,45] The properties of PLA produced from lactic acid were reported to be different compared to the PLA produced by ROP of lactides.[15] PLA polymer demands the control of the L/D composition and rheology depending on the end use properties and processing of the polymer.

Cargill Dow LLC has developed a process for the continuous production of PLA from lactic acid through lactide as an intermediate product. The schematic production of commercially viable biodegradable commodity polymer, PLA, is shown in Figure 2.1. Details about poly(lactic acid) production and technology can be found in work published by Drumright, Gruber, and Henton.[46] Dextrose obtained from the renewable resource, corn, was fermented to lactic acid. The lactic acid, then, condenses to pre-polymers (oligomers) in a continuous process. With the help of tin catalysts, the low molecular weight pre-polymers

are converted into lactide with higher rates and selectivity. The lactide is purified by vacuum distillation and lactic acids and its linear esters are recovered and fed back to the lactic acid tank. The pure lactides are separated into enantionmers. Melt polymerization of lactides can be performed using tin catalyst without any need for solvent. Unconverted monomers are recycled back to the lactic acid stage. NatureWorks LLC (currently joint venture of Cargill, USA and Teijin Limited, Japan) runs a plant with a 300 million lb/yr capacity in Blair, Nebraska, USA.[2]

Production of lactic acid is an important step for converting corn into PLA and is also the cost-determining step. Lactic acid can be obtained either by a chemical synthesis or a fermentation process. Musashino Chemical Laboratories (Japan) produces racemic lactic acid from lactonitrile. During fermentation, sugars (sucrose/dextrose) can be broken down into lactic acid by using microorganisms on a commercially viable scale. Different microorganisms are used depending on the production, optical purity, and cost of lactic acid. These microorganisms require nutrients such as salts and vitamins to function. As the lactic acid is produced the pH of the fermentation reaction drops and therefore affects the production. Hence, lime ($Ca(OH)_2$) and chalk ($CaCO_3$) are used to control the pH between 5.0 and 6.8. The fermentation product is a lactate salt which upon acidification or salt splitting results in lactic acid. The crude lactic acid is then subjected to purification by removal of microorganisms, separation of by-products, nutrients and residual sugars and finally concentrated to 60-70% with >98% optical purity.[2]

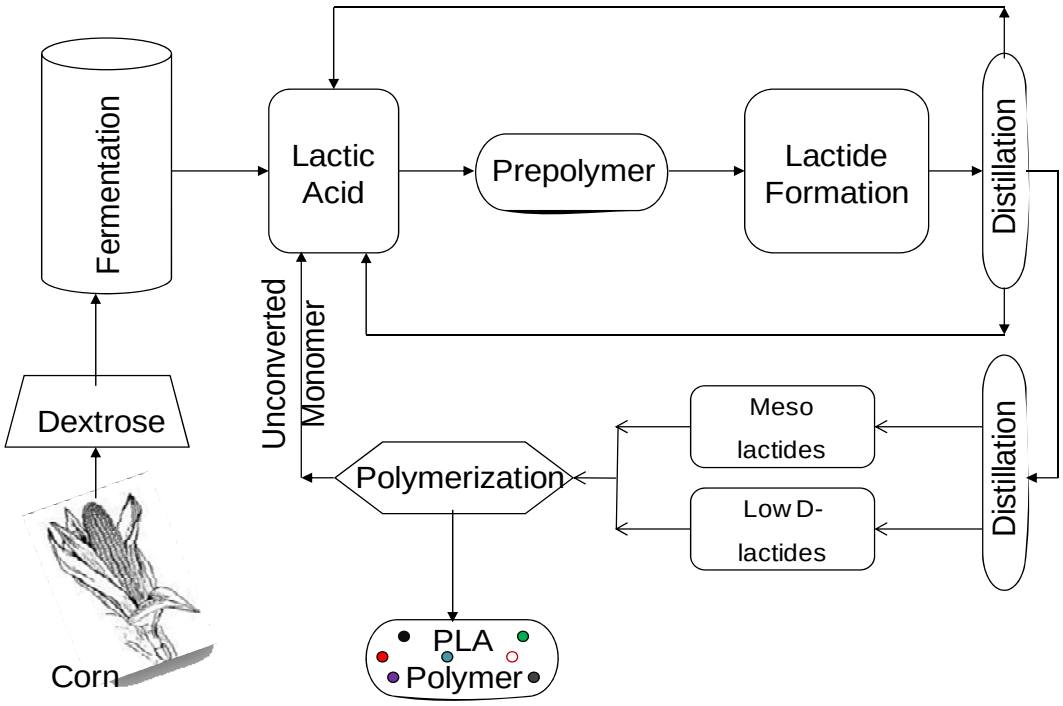

Figure 2.1. Block diagram for the production of lactide and high mol. wt. polylactide.[2,46]

2.3 Properties

Thermal Properties

PLA obtained from L- and D-lactides is semi-crystalline(0-37%) and a relatively hard material with melting temperatures ranging from 170-190 °C and glass transition temperatures ranging from 50-65 °C.[1,47,48] The melting temperatures can be as high as 220 °C and as low as 130 °C depending on the distribution of L- and D-lactides in the backbone.[49] Witzke reported that the melting temperatures decrease by 3 °C for every 1% intial *meso*-lactide concentration and almost no crystallinity, by ΔH_m, with 18% *meso*-lactide.[50] However, racemic crystallites have a melting temperature 50 °C higher than the PLLA or PDLA crystals. PLA has relatively low thermal stability and above 190 °C, the mol. wt. decreases and thermal degradation (weight loss) can be observed in the range of 235-255 °C.[48,51] Because of the semi-crystalline nature of PLA, physical properties such as changes in the crystalline/amorphous ratio are strongly affected by the thermal history.[52] The heat of fusion for 100% crystalline PLA from L-lactides ranges from 93-203 J/g as reported by different groups as listed in Table 2.1.

Crystallization

Crystallization of PLA has been thoroughly investigated by Fischer et al.[53] (melt and solution crystallization), Kalb and Pennings[47] (spherulitic growth from melt), Vasanthakumari and Pennings[54] (crystallization kinetics and crystal growth), Cohn et al[55]. (amorphous/crystalline morphology), Kishore et al.[56] (isothermal melt mechanism),

Kolstad[57] (crystallization kinetics), etc. Upon heating amorphous samples, crystallization rates increase with an increase in temperature (100 -160 °C) and reach a maximum before showing a decreasing trend.[59]

Table 2.1. Thermal properties of PLA.

Property	Value	Units	Reference
Degree of crystallinity, X_C	0-37	%	Gilding and Reed.[58]
Melting temperature, T_m	170-190	°C	Tsuji[1]
Equilibrium melting temperature, $T_m°$	205-215	°C	Tsuji and Ikada[47,59]
Heat of fusion for 100% crystalline PLLA	93-203	J/g	Fisher et al.[53], Miyata and Masuko[60], Jamshidi[48]
Glass transition temperature, T_g	50-65	°C	Tsuji[1]
Decomposition temperature, T_d	235-255	°C	Engelberg and Kohn[51]

The crystallization is strongly affected by the optical purity of PLA. The crystallization time for PLLA increased 40% with the incorporation of 1% *meso*-lactide.[57] Iannace and Nicolais reported a maximum crystallization rate at 105 °C and the overall rate of bulk crystallization follows the Avrami equation, which provides information on overall crystallization kinetics, with exponent close to 3.[61] According to the rate that the chains are deposited on the crystal surface, Hoffman divided the melt crystallization kinetics in three regimes.[62-64] As the temperature is lowered through regimes I, II, and III, the crystallization rate becomes larger than the nucleation rate. In PLA, the transition of crystallization kinetics from regime II to regime I was observed above 163 °C by Vasanthakumari and Pennings

whereas the transition of crystallization kinetics from regime III to regime II was observed around 115 °C by Iannace and Nicolais.[54,61] Di Lorenzo reported the transition of the crystallization kinetics from regime III to regime II at 120 °C by the Hoffman and Lauritzen theory.[65] Spherulitic growth rate was found to be function of crystallization temperature and molecular weight.[54] Growth rate (G) was observed to increase with a decrease in molecular weight. According to Vasanthakumari and Pennings, a viscosity-average molecular weight change from 150,000 g/mol to 690,000 g/mol reduces the growth rate from 5 μm/min to 2.5 μm/min.[54] Di Lorenzo and He et al. reported the growth rate of 6.7 and 9.1 μm/min, respectively for PLA isothermally crystallized at 130 °C.[65,66]

Optical, Spectroscopic, and Crystallographic Properties

The optical rotation, [α], for poly(lactic acid) has been reported to be in the range of. ±150 ° to ± 157 °.[67-70] Kobayashi et al.[71] reported the birefringence of fibers to be in the range of 1.9 x 10^{-2} to 3.1 x 10^{-2} depending on the draw ratios. Lalla and Chugh[72] observed the maximum absorption of ultraviolet radiation by PLA in chloroform at a wavelength of 240 nm and attributed the absorption to the ester functionality of PLA. Infrared spectroscopy absorption peaks and the corresponding assignments are briefly listed in Table 2.2 and more detailed information about Raman and infrared spectroscopy data for PLA can be found in the literature.[73] Younes and Cohn[74] assigned 755 cm^{-1} and 869 cm^{-1} peaks to the crystalline and amorphous phase of PLA and suggested the assessment of crystallinity can be related to the ratio of these peaks.

^{1}H and ^{13}C nuclear magnetic resonance (NMR) spectroscopy data for PLA are compiled in Table 2.2 and detailed information can be found in the referenced literature. PLLA has been reported to crystallize in different crystallographic forms such as α-form, β-form, γ-from, etc.[1] De Santis and Kovacs[75] proposed an α-form of PLA in pseudo-orthorhombic unit cell, of dimensions: a=1.07 nm, b=0.595 nm, and c= 2.78 nm; with two 10_3 helices. Hoogsteen et al.[76] reported an orthorhombic unit cell for the β-form of PLA with six 3_1 helices per unit cell and the cell dimensions: a=1.03 nm, b=1.82 nm, and c=0.90 nm. PLA in γ-form was reported by Cartier et al.[77] to be an orthorhombic unit cell (a=0.995 nm, b=0.625 nm, and c=0.88 nm) with two 3_1 helices per unit cell.

Table 2.2. IR, ^{1}H NMR, ^{13}C NMR Peak assignments for PLA.

Assignments	Comment	Peak Positions
	IR[73]	
Assignments	*Vibration*	*Peak positions [v(cm^{-1})]*
C-H (CH_3)	Asymmetric stretch	2997
C-H (CH_3)	Symmetric Stretch	2947
>C=O	Stretch	1760
C-H (CH_3)	Bend	1452
>C=O	Bend	1270
-C-O-C-	Stretch	1100-1090
Crystalline phase[74]	-	755
Amorphous Phase[74]	-	869
	^{1}H NMR[78,79]	
Assignments	*Peak Multiplicity*	*Chemical shift (ppm)/Peal multiplicity*
Hydroxyl proton	OH	7.30/singlet
Methine proton	CH	5.20/multiplet
Methyl proton	CH_3	1.55/doublet
	^{13}C NMR[73,78,79]	
Assignments	*Structure*	*Chemical shift (ppm)*
Methyl carbon	CH_3	16.7-16.9
Methine carbon	C-O	69.0-69.4
Carbonyl carbon	C=O	169.3-170.0

Physical Properties

The important physical properties of PLA are summarized in Table 2.3. The density of PLA was reported to be in the range of 1.25 to 1.29 g/cm^3 and the refractive index between 1.35-1.45.[49,80] Solubility parameter (δ) of PLA was reported in the range of 19.0-20.5 J$^{0.5}$cm$^{-1.5}$ and PLA is reported to be soluble in chloroform, methylene chloride, dichloroacetic acid, acetonitrile, and dioxane.[81] Crystalline PLA is not soluble in tetrahydrofuran, ethyl acetate, or acetone. PLA is insoluble in water, alcohols and alkanes and hence precipitates in alcohols and alkanes. The reported surface energy of PLA ranges from 35.9-43.9 mN/m depending on the processing and detailed information can be found in the literature by Biresaw and Carriere and references therein.[82] The permeability of PLA is an important factor for its packaging applications and depends on the crystalline/amorphous phase distribution as reported by Shogren, however, other common polymers such as polyethylene terephthalate and polypropylene have very low permeabilities (<1.3 g/m^2/day).[83]

Table 2.3. Physical properties of PLA.

Property	**Value**	**Units**	**Reference**
Density, ϱ	1.25-1.29	g/cm^3	Tsuji[1]
Refractive index (fiber)	1.35-1.45	--	Farrington et al.[49]
Solubility parameter, δ	19-20.5[b]	(J/cm^3)$^{1/2}$	Tsuji and Muramatsu[84]
Surface energy	35.9-43.9	mN/m	Biresaw and Carriere[82]
Permeability at 25 °C (Amorphous PLA)	172	g/m^2/day	Shogren[83]
Permeability at 25 °C (Crystalline PLA)	82	g/m^2/day	Shogren[83]

Rheological Properties and Processing

Knowledge of rheological properties of polymers are of importance from the processing aspect. The rheological properties of PLA including constants from the Mark-Houwink-Sakurada equation, entanglement molecular weight and characteristic ratio are listed in Table 2.4. The entanglement molecular weight (intermolecular entanglement of polymer chains) for linear PLA is ca. 9000 g/mol whereas for branched (4-arm star) PLA it was found to be about four times that of linear PLA at 35,000 g/mol.

Table 2.4. Rheological properties of PLA.

Property	Value	Units	Reference
Mark-Houwink-Sakurada equation, $[[\eta] = KM_v^a$			Perego et al.[70]
PLLA[a]	a= 0.73	--	
	K=5.45 x 10^{-4}	$cm^3\ mol^{1/2}\ g^{-3/2}$	
PDLA[a]	a= 0.77	--	
	K=2.21 x 10^{-4}	$cm^3\ mol^{1/2}\ g^{-3/2}$	
Entanglement mol. wt., M_e	9,000(linear)[b]	g/mol	Dorgan et al.[85]
	10, 500(linear) [d]	g/mol	Grijpma and Pennings[86]
	8,900(linear)[e]	g/mol	Grijpma and Pennings
	35,000 (branched)[c]	g/mol	Dorgan et al.[85]
Characteristic ratio, C_∞	2.0 (Isotactic PLA)	--	Tonelli and Flory[68]
	9.5 (Racemic PLA)	--	Joziasse et al.[87]
	11.8 (Isotactic PLA)	--	Joziasse et al.[87]

[a] at 25 °C in chloroform at a concentration of 0.20 g/dL; [b] (98:2::L:D) linear PLA;

[c] (98:2::L:D) 4-arm star PLA; [d] Crystallized PLA; [e] Amorphous PLA.

The characteristic ratio ($C_\infty = r^2/nl^2$ where n is the number of links, l is the length of each link, and r is end-to-end distance of a random coil) is a fundamental property related to chain stiffness and those reported for PLA have ranged from as low as 2 to as high as 12. Low values of C_∞ implies high flexibility of PLA chains and thus failure should happen in ductile fashion whereas PLA shows brittle failure and hence C_∞ should be high as reported by Joziasse et al.[85,87]

Fiber Spinning

Various techniques such as melt spinning[88], wet spinning[89], dry-jet-wet spinning[90], electrospinning[91], etc., have been employed to convert the PLA polymeric material into fibers. Agrawal and Bhalla[92] have reviewed the melt and solution spinning of PLA. Solution spinning results in high-strength fibers (tenacity 2.1 GPa, Young's modulus 16 GPa) but is restricted by limited production speeds.[93] Drug delivery devices utilize the as-spun hollow fibers produced using dry-jet-wet spinning methods. Biomedical applications requires high surface morphology and porosity and this requirement can be fulfilled by electrospinning techniques. Melt spinning, however, does not require solvent, and can also be performed at very high speed and can therefore be used to produce very low cost fibers for commodity applications.[94] Typical values for the tensile strength, tensile modulus and elongation at break for melt-spun PLA fibers are listed in Table 2.5.

Table 2.5. Tensile properties of melt-spun PLA fibers.

Property	Value	Units	Reference
Tensile strength	Up to 870[a]	MPa	Fambri et al.[88]
Tensile modulus	Up to 9200[a]	MPa	Fambri et al.[88]
Elongation at break	~ 25[b]	%	Eling et al.[95]

[a] 330, 000 g/mol PLA; [b] 350, 000 g/mol PLA.

PLA fibers have been produced in many forms and have potential applications in various areas as mentioned in Table 2.6. Ingeo™ is the new fiber from NatureWorks PLA and is expected to combine the physical properties of natural fibers, such as cotton, silk, wool, etc., with those of synthetic fibers from PBPs. PLA fibers have been reported to have superior hand and drape, better wicking, comfort, moisture management, ultraviolet resistance, and low odor retention.[96]

Table 2.6. Various forms and applications of PLA fibers.[97]

Various forms of PLA fibers/nonwovens	Various application of PLA fibers
Monofilament, multifilament, trilobal, staple fiber, bicomponent fiber, spun bonded nonwoven, needle punched nonwoven, knitted structure, woven structure, composite materials.	Apparel, furnishings, agricultural, hygiene, binder fibers sports wear, medical textiles, composites, catching and protection nets, industrial fabrics, filtration fabrics, packing material, geotextiles, transport, etc.

2.4 Modifications

Copolymers

One of the most important and most utilized methods of modification of PLA is copolymerization which results in a product that has combined effects of two or more polymers. Copolymers of PLA with various architectures such as block,[98-100] random,[68,98,101] alternating,[102,103] graft,[104-108] hyperbranched,[109-111] etc., have been reported. Polymerizations of L-lactide with other lactides and other polymer precursors result in copolymers with modified properties of PLA. The random copolymerization of L-lactide with small amounts of D-lactide reduces cystallinity as well as the substantially reducting the spherulitic growth rates.[101] The crystallization and microstructure of copolymers of L-lactides with *meso*-lactides have been reported by Huang et al.[112] Copolymers of PLA with numerous polymers such as polyglycolide (PGA),[113,114] poly(ε-caprolactone) (PCL),[115,116] polyisoprene,[117,118] polystyrene (PS),[119] polyethylene (PE),[120] polypropylene (PP),[121] poly(ethylene glycol) (PEG), poly(ethylene oxide) (PEO),[29,122,123] poly(methyl methacrylate) (PMMA),[124] etc., have been reported and produced with varying desired properties. The copolymers of glycolide with lactides are meticulously reviewed by Vert[125] and have applications in the medical and pharmaceutical fields. For highly crystallizable and hydrolytically stable PLA, Smith and co-workers[126] synthesized oligoethylene-end-capped PLA using hydroxy-terminated oligoethylene as macroinitiators for the ROP of L-lactide as shown in Scheme 2.9. Haynes et al.[127] used hydroxy-terminated perfluoropolyether as the macroinitiator for the ROP of L-lactide resulting in a very low surface energy PLA based copolymer with a water contact

angle above 100°. At the other extreme, PLA was made more hydrophilic, flexible and biodegradable by copolymerization with poly(ethylene oxide)/poly(ethylene glycol).[128] In addition to linear copolymers, PLA has been modified as graft copolymers, branched copolymers, and cross-linked polymers.[129-131]

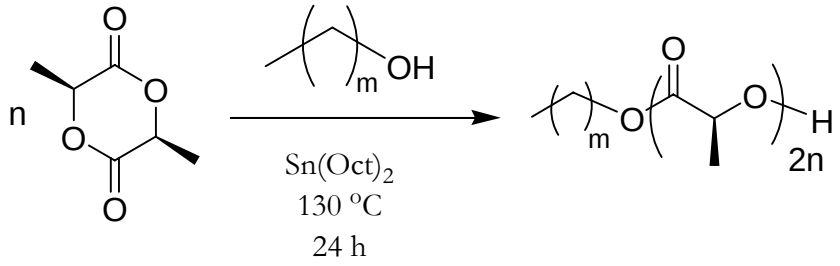

Scheme 2.9. Synthesis of oligoethylene-end-capped PLA.

Terpolymerization of equimolar ratios of L-lactide, diglycidyl ether of bisphenol A (DGEBA), and the 4,4'-hexafluoroisopropylidenediphenol (6F-Bis-A), catalyzed by 18-crown-6-ether and potassium chloride, resulted in an amorphous terpolymer with a glass transition of ca. 80 °C as reported by Abayasinghe and Smith.[132]

Smith and co-workers reported polylactide(PLA)-*block*-poly(hydroxyalkanoate (PHA) block copolymers (Mn ~ 25-50 kDa) by ring-opening polymerization of L-lactide using PHA as macro-initiator in presence of stannous octoate.[133] They also reported poly(ester amide) random copolymers by ring opening polymerization of L-lactide and novel depsipeptide monomer, 6,6'-dimethyl-2,5-morpholinedione, in presence of stannous octoate.[134]

PLA Blends

Blending provides an alternative modification route to copolymerization and is often less expensive. PLA has been blended with numerous polymeric materials to improve its physical properties, hydrolytic stability, degradation, hydrophilic properties, etc. Blends of PLA with PE,[135] PS,[82,136] PCL,[137] PMMA,[138] poly(sebacic anhydride),[139] polysaccharide,[140] poly(vinylpyrrolidone),[141] polyurethane,[142] poly(dimethyl siloxane),[143] chitosan,[144,145] poly(vinyl alcohol),[146] etc., have been reported. Wan et al.[144] prepared biodegradable blend membranes by blending PLA with chitosan using solvent-casting and solvent-extraction processing techniques and found a significant influence of processing conditions on the morphology. Interfacial properties of blends are important factors for a successful blend material and Biresaw and Carriere[82] measured the interfacial tension of PLA/PS blends at 170-200 °C by an embedded fiber retraction method and reported a value of 5.4 ± 1.3 mN/m. Wu and Liao compared the blend properties of hyaluronic acid with PLA and acrylic acid grafted PLA (PLA-*co*-AA) and reported higher melting temperatures and improved tensile strengths for the PLA-*co*-AA blends in comparison to PLA blends.[108]

Additives

PLA has been modified by the addition of inorganic/organic fillers/plasticizers to improve its mechanical properties and processability. PLA nanocomposites have been prepared by incorporating modified silicate, silica and mica. The interaction between clay particles and PLA improves the mechanical properties, thermal stability, crystallization behavior, etc. Stereocomplex (PLLA/PDLA) crystallites (<5%) have been used as nucleating

agents to enhance the crystallization rate of PLLA and were found to have better nucleating properties than the common nucleating agents such as talc.[147] Fujimoto et al.[148] reported the first biodegradable nanocellular polymeric foams from PLA/layered silicate nanocomposites using supercritical carbon dioxide as a foaming agent. Nam et al.[149] reported the improvement in the crystallization behavior of PLA after intercalation with organically modified montmorillonite. Li and Chang[150] investigated the pH compensation ability of bioactive inorganic fillers such as wollastonite and hydroxyapatite during acidic degradation of poly(lactic acid-*co*-glycolic acid) (PLGA) and found that the incorporation of wollastonite in the PLGA composite delays the degradation by compensating for the decrease in pH whereas hydroxyapatite accelerated the degradation. PLA and carbon fiber composites have been studied by Wan et al.[151] and it is reported that the nitric acid treated carbon fiber PLA composites had improved interfacial adhesion and hence better mechanical properties in comparison to carbon fiber (untreated) and PLA composites. The superior adhesion was attributed to the higher oxygen-containing functional groups on the surface of nitric acid treated carbon fibers as confirmed by XPS studies.

Polymers can be plasticized with small, relatively nonvolatile molecules, known as plasticizers, that dissolve in the polymer, therefore increasing the flexibility, processability, elongation or toughness and reducing melt viscosity, glass transition temperature, elastic modulus, melting temperature and/or extent of crystallinity in semicrystalline polymers, etc.[64,152] The semicrystalline, brittle, and stiff PLA polymer can be made flexibile by the addition of an efficient plasticizer which then separates the PLA chains from each other making reptation easier.[3,64] The remaining cyclic monomer can plasticize the PLA and the resultant polymer matrix showed microporous morphology extending from the surface to

the inner region.[153] Also, PLA plasticized with monomers gradually stiffens due to the migration of monomer/plasticizers to the surface upon heating or long storage time.

The compositional dependence of the glass transition temperature of the plasticized PLA polymer can be empirically expressed using the Fox equation[154] (Eq. 2.1), originally proposed for blends and copolymers, by considering the plasticizers as low T_g components. In Eq. 2.1 T_g is the glass transition temperature of plasticized material and w_i and T_{gi} are weight fractions and glass transition temperatures of two components.

$$\frac{1}{T_g} = \frac{w_1}{T_{g1}} + \frac{w_2}{T_{g2}} \qquad 2.1.$$

The depression in the melting temperature of plasticized PLA can be expressed by Flory equation[155] (Eq. 2.2) were $T_{m,d}$ and $T_{m,0}$ are the melting temperature of plasticized PLA and pure PLA, respectively; R is gas constant; ΔH_{pru} and V_{pru} are the heat of fusion and the molar volume per polymer repeating unit; V_1 is the molar volume of diluents/plasticizer; and χ is the polymer-plasticizer interaction parameter.

$$\frac{1}{T_{m,d}} - \frac{1}{T_{m,0}} = \frac{R}{\Delta H_{pru}} \cdot \frac{V_{pru}}{V_d}(\varphi_1 - \chi \cdot \varphi_1^2) \qquad 2.2.$$

Monomeric acetyl tri-*n*-butyl citrate (ATBC) and PEGs were used to plasticize PLA by Baiardo et al.[156] It was found that ATBC is miscible in PLA up to 50 wt% whereas the miscibility of PEG was in the range of 15-30 wt% depending on the molecular weight of the PEG. The glass transition and the melting temperatures of plasticized PLA decreased with increasing plasticizer concentration. Above the solubility limit, the decrease in the glass transition temperature drops with increasing PEG content and plasticizer efficiency of PEG increases with decreasing molecular weight. A significant increase in the elongation at break

of plasticized PLA was achieved along with a detrimental effect on the tensile and other mechanical properties.

Ren et al.[157] reported similar changes in the properties of PLA after plasticization with triacetin and oligomeric poly(1,3-butylene glycol adipate). Other plasticizers such as glycerol, citrate ester, PEG monolaurate, oligomeric lactic acid, triacetine, dioctyl maleate, etc., have been used to plasticize PLA.[158-161]

2.5 Degradation

All polymers degrade but it is the degradation rate which classifies polymers as biodegradable (degrades during or immediately after their application) and non-biodegradable (degrades after substantially longer time than the duration of their application) polymers.[162] Polymers can degrade by any combination of various degradation mechanisms including photo degradation by radiation, thermal degradation by heat, mechanical degradation by application of stress, degradation by chemical agents, etc. Aliphatic biodegradable polymers are susceptible to hydrolysis and biodegradation. Degradation is defined as a chemical phenomenon in which the polymer chains are converted to oligomers and oligomers to monomers by bond cleavage. Erosion is defined as a physical phenomenon which results in the depletion of material by dissolution and diffusion and is classified mainly into bulk and surface erosion.[163] For bulk erosion, material is lost from the entire volume and degradation rate decreases as the amount of material decreases, whereas, for surface erosion, the loss of material is from the surface of the specimen and thus the rate is proportional to the surface area. Core-accelerated bulk erosion is possible for the thicker polymer samples where low molecular weight degradation products are trapped inside the core of the sample and therefore accelerate degradation. A schematic for bulk, surface and core-accelerated bulk erosion are compared in Figure 2.2. Polymer degradation is affected by numerous material and hydrolysis media factors such as bond stability (amides>esters>ortho esters>anhydrides), hydrophobicity, water diffusivity, steric effects, microstructure (crystallinity/porosity), pH and temperature of hydrolysis media, effect of degraded products, polymer chain length, etc.[162,164] The effects of pH, temperature and catalyst on the hydrolysis of PLA are summarized in Table 2.7.

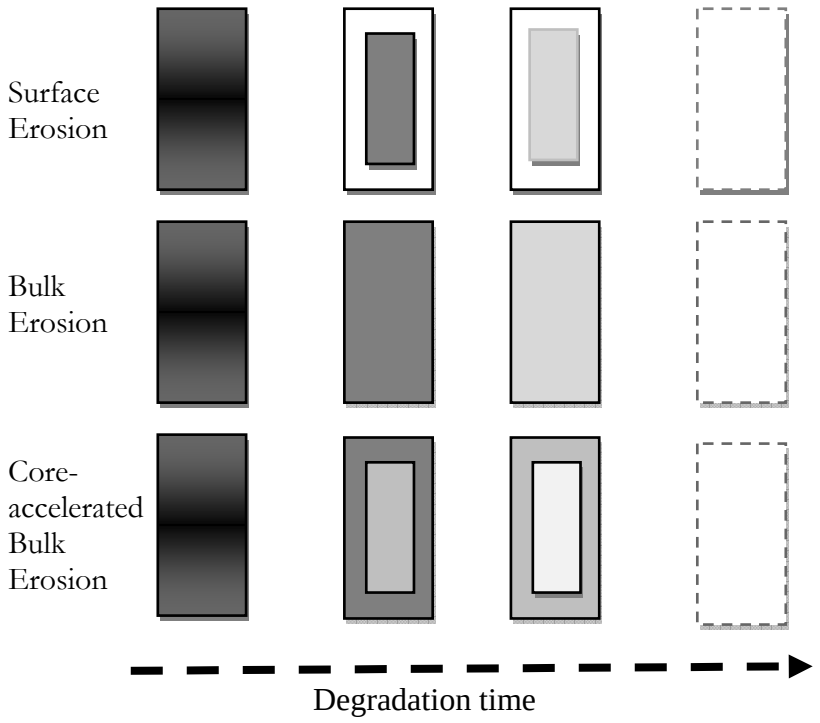

Figure 2.2. Hydrolysis mechanism for PLA.[1]

High mol. wt. PLA is water insoluble and hydrolysis of the ester linkage results in oligomeric products of lactic acid and a critical molecular weight (weight average mol. wt. of ca. 1.2 kg/mole)[165] must be reached before oligomers become water soluble. Hydrolysis of PLA can be achieved by any of the catalytic/non-catalytic, enzymatic/non-enzymatic, and autocatalytic mechanisms. PLA hydrolysis can be externally catalyzed by enzymes, acids and bases. Enzymatic hydrolysis of low molecular weight PLA (molecular weight ca. 2 kg/mole) has been achieved by esterase-type enzymes such as *Rhizopus delemer* lipase.[166] However, high mol. wt. PLA could only be hydrolyzed by enzymes such as Proteinase K and carboxylic esterase.[167,168]

Table 2.7. Effect of pH, temperature, and enzyme on the hydrolysis of PLA.[169]

pH	Temp, °C	Enzyme	Hydrolysis mechanism	
			Chain cleavage	Material erosion
2.0	37	--	Random in amorphous region	Bulk
7.4	37	--	Random in amorphous region	Bulk
12.0	37	--	Random in amorphous region	Surface
7.4	37	Proteinase K	Predominant cleavage at chains with free ends and tie chains in amorphous region	Surface
7.4	97	--	Random in amorphous region	Bulk

Hydrolysis (chain scission) is random for the base-catalyzed PLA and proceeds by surface erosion, whereas, in the case of acid-catalyzed PLA, major chain scission occurs at the end of polymer chain, also known as exo-chain scission, and bulk erosion is predominant.[170,171] Hydrolysis of PLA is autocatalyzed by the carboxyl acid chain ends and the rate of hydrolysis is affected by its concentration. Pitt and Gu reported faster hydrolysis of PGLA in comparison to PCL and PLA and attributed it to the intrinsic reactivity of glycolate linkage.[172] Hydrolysis of PLA has been extensively studied by Tsuji and co-workers and various aspects such as the effect of microstructure, different hydrolysis media and conditions have been investigated thoroughly.[169,171,173-180]

2.6 Applications

PLA and its copolymers have been heavily utilized in the biomedical field for specialty applications such as sutures, drug delivery, tissue guide, etc., in the forms of rods, plates, meshes, microspheres, etc.[1] Recent technological advances in the production of lactic acid have made PLA shift from a high price to high volume commodity polymer that could be seen as a substitute to PBPs. Excellent barrier properties for flavor constituents and heat sealability of the biaxially-oriented PLA films makes it ideal for food packaging applications.[181] Some of the important applications of PLA and its copolymers are listed in Table 2.8.

Table 2.8. Applications of PLA and their copolymer.[182]

Application	Fields	Examples
Industrial applications	Agriculture, forestry	Mulch films, temporary replanting pots, delivery system for fertilizers and pesticides
	Fisheries	Fishing lines and nets, fishhooks
	Civil engineering and construction industry	Forms, vegetation nets and sheets, water-retention sheets
	Outdoor sports	Golf tees, disposable plates, cups, bags, and cutlery
Composting	Food package	Package, containers, wrappings, bottles, bags, films, retail bags, six-pack rings
	Toiletry	Diapers, feminine hygiene products
	Daily necessities	Refuge bags, cups

In addition to the applications mentioned in Table 2.8, NatureWorks™ PLA polymer has been evaluated for a range of applications in the packaging, films, and fiber areas and these are listed segment-wise in detail in Table 2.9. In the future, a reduction in price, sustainability due to renewable raw materials, and also the positive environmental aspects of PLA could probably make it a potential commodity polymer.

Table 2.9. Commercial applications of compostable, NatureWorks™ PLA.[14]

Segments	Commercially available applications
Rigid thermoforms	Clear short shelf-life trays and lids, opaque dairy containers, consumer displays and electronics packaging,disposable articles, cold drink cups
Biaxially-oriented films	Shrink wrap for consumer goods packaging, twist wrap candy and flower wrap, windows for envelops, bags and cartons
Bottles	Short shelf-life milk and oil packaging
Apparel	Sport, active and underwear, fashion
Non-wovens	Agricultural and geotextiles, hygiene products, wipes, shoe liners
Household, industrial, and institutional fabrics	Bedding, drapery, table cloths, curtains, mattress ticking, wall and cubicle fabrics, upholstery
Carpet	Surface yarn and fibers
Fiberfill	Pillows, comforters, mattresses, duvets
Foams	Structural protective foams

2.7 References

1. Tsuji, H. in *Biopolymers for Medicinal and Pharmaceutical Applications* (eds. Steinbüchel, A. & Marchessault, R. H.) 183-231 (Wiley-VCH, Weinheim, 2005).
2. Gruber, P., Henton, D. E. & Starr, J. in *Biorefineries - Industrial Processes and Products: Status Quo and Future Directions* (eds. Kamm, B., Gruber, P. R. & Kamm, M.) 381-407 (Wiley-VCH, Weinheim, 2006).
3. Zhang, J.-F. & Sun, X. in *Biodegradable Polymers for Industrial Applications* (ed. Smith, R.) 251-288 (CRC Press, Washington, DC, 2005).
4. Holten, C. H., Müller, A. & Rehbinder, D. *Lactic Acid: Properties and Chemistry of Lactic Acid and Derivatives* (Verlag Chemie, Weinheim, 1971).
5. Pelouze, J. Ueber die Milchsäure. *Annalen der Chemie und Pharmacie* **53**, 112-124 (1845).
6. Carothers, W. H., Dorough, G. L. & Natta, F. J. v. Studies of Polymerization and Ring Formation. X. The Reversible Polymerization of Six-Membered Cyclic Esters. *Journal of the American Chemical Society* **54**, 761-772 (1932).
7. Albertsson, A.-C. & Varma, I. K. Recent Developments in Ring Opening Polymerization of Lactones for Biomedical Applications. *Biomacromolecules* **4**, 1466-1486 (2003).
8. Choi, Y. K., Bae, Y. H. & Kim, S. W. Star-Shaped Poly(ether-ester) Block Copolymers: Synthesis, Characterization, and Their Physical Properties. *Macromolecules* **31**, 8766-8774 (1998).
9. Finne, A. & Albertsson, A.-C. Controlled Synthesis of Star-Shaped L-Lactide Polymers Using New Spirocyclic Tin Initiators. *Biomacromolecules* **3**, 684-690 (2002).

10. Kricheldorf, H. R. & Eggerstedt, S. Macrocycles, 5. Ring Expansion of Macrocyclic Tin Alkoxides with Cyclic Anhydrides. *Macromolecular Chemistry and Physics* **200**, 587-593 (1999).

11. Palmgren, R., Karlsson, S. & Albertsson, A.-C. Synthesis of Degradable Crosslinked Polymers Based on 1,5-dioxepan-2-one and Crosslinker of *bis*-ε-caprolactone Type. *Journal of Polymer Science Part A: Polymer Chemistry* **35**, 1635-1649 (1997).

12. Shi, W. & Rånby, B. Photopolymerization of Dendritic Methacrylated Polyesters. I. Synthesis and Properties. *Journal of Applied Polymer Science* **59**, 1937-1944 (1996).

13. Mecking, S. Nature or Petrochemistry? - Biologically Degradable Materials. *Angewandte Chemie International Edition* **43**, 1078-1085 (2004).

14. Vink, E. T. H., Rabago, K. R., Glassner, D. A. & Gruber, P. R. Applications of Life Cycle Assessment to NatureWorks(TM) Polylactide (PLA) Production. *Polymer Degradation and Stability* **80**, 403-419 (2003).

15. Ajioka, M., Enomoto, K., Suzuki, K. & Yamaguchi, A. The Basic Properties of Poly(lactic acid) Produced by the Direct Condensation Polymerization of Lactic Acid. *Journal of Polymers and the Environment* **3**, 225-234 (1995).

16. Zhong, Z., Dijkstra, P. J. & Feijen, J. Controlled Synthesis of Biodegradable Lactide Polymers and Copolymers Using Novel *In Situ* Generated or Single-Site Stereoselective Polymerization Initiators. *Journal of Biomaterials Science- Polymer Edition* **15**, 929-946 (2004).

17. Penczek, S., Duda, A., Szymanski, R. & Biela, T. What We Have Learned in General from Cyclic Esters Polymerization. *Macromolecular Symposia* **153**, 1-15 (2000).

18. Schindler, A., Hibionada, Y. M. & Pitt, C. G. Aliphatic Polyesters. III. Molecular Weight and Molecular Weight Distribution in Alcohol-Initiated Polymerizations of ε-Caprolactone. *Journal of Polymer Science: Polymer Chemistry Edition* **20**, 319-326 (1982).

19. Zhang, X., MacDonald, D. A., Goosen, M. F. A. & McAuley, K. B. Mechanism of Lactide Polymerization in the Presence of Stannous Octoate: The Effect of Hydroxy and Carboxylic Acid Substances. *Journal of Polymer Science Part A: Polymer Chemistry* **32**, 2965-2970 (1994).

20. Nijenhuis, A. J., Grijpma, D. W. & Pennings, A. J. Lewis Acid Catalyzed Polymerization of L-lactide. Kinetics and Mechanism of the Bulk Polymerization. *Macromolecules* **25**, 6419-6424 (1992).

21. Stridsberg, K. M., Ryner, M. & Albertsson, A.-C. Controlled Ring-Opening Polymerization: Polymers with Designed Macromolecular Architecture. *Degradable Aliphatic Polyesters* **157**, 41-65 (2002).

22. Kafrawy, A. & Shalaby, S. W. A New Synthesis of 1,5-Dioxepan-2-one. *Journal of Polymer Science Part A: Polymer Chemistry* **25**, 2629-2630 (1987).

23. Mecerreyes, D., Jérôme, R. & Dubois, P. Novel Macromolecular Architectures Based on Aliphatic Polyesters: Relevance of the "Coordination-Insertion" Ring-Opening Polymerization. *Advances in Polymer Science* **147**, 1-59 (1999).

24. In't Veld, P. J. A., Velner, E. M., van de Witte, P., Hamhuis, J., Dijkstra, P. J. & Feijen, J. Melt Block Copolymerization of ε-Caprolactone and L-lactide. *Journal of Polymer Science Part A: Polymer Chemistry* **35**, 219-226 (1997).

25. Kricheldorf, H. R., Kreiser-Saunders, I. & Boettcher, C. Polylactones: 31. Sn(II)Octoate-Initiated Polymerization of L-Lactide: A Mechanistic Study. *Polymer* **36**, 1253-1259 (1995).

26. Duda, A., Penczek, S., Kowalski, A. & Libiszowski, J. Polymerizations of ε-Caprolactone and L,L-Dilactide Initiated with Stannous Octoate and Stannous Butoxide- A Comparison. *Macromolecular Symposia* **153**, 41-53 (2000).

27. Kowalski, A., Duda, A. & Penczek, S. Mechanism of Cyclic Ester Polymerization Initiated with Tin(II) Octoate. 2. Macromolecules Fitted with Tin(II) Alkoxide Species Observed Directly in MALDI-TOF Spectra. *Macromolecules* **33**, 689-695 (2000).

28. Kowalski, A., Duda, A. & Penczek, S. Kinetics and Mechanism of Cyclic Esters Polymerization Initiated with Tin(II) Octoate. 3. Polymerization of L,L-dilactide. *Macromolecules* **33**, 7359-7370 (2000).

29. Du, Y. J., Lemstra, P. J., Nijenhuis, A. J., van Aert, H. A. M. & Bastiaansen, C. ABA Type Copolymers of Lactide with Poly(ethylene glycol). Kinetic, Mechanistic, and Model Studies. *Macromolecules* **28**, 2124-2132 (1995).

30. Storey, R. F. & Taylor, A. E. Effect of Stannous Octoate on the Composition, Molecular Weight, and Molecular Weight Distribution of Ethylene Glycol-Initiated Poly(ε-Caprolactone). *Journal of Macromolecular Science- Part A* **35**, 723 - 750 (1998).

31. von Schenck, H., Ryner, M., Albertsson, A.-C. & Svensson, M. Ring-Opening Polymerization of Lactones and Lactides with Sn(IV) and Al(III) Initiators. *Macromolecules* **35**, 1556-1562 (2002).

32. Kricheldorf, H. R., Kreiser-Saunders, I. & Stricker, A. Polylactones 48. $Sn(Oct)_2$-Initiated Polymerizations of Lactide: A Mechanistic Study. *Macromolecules* **33**, 702-709 (2000).

33. Schwach, G., Coudane, J., Engel, R. & Vert, M. More About the Polymerization of Lactides in the Presence of Stannous Octoate. *Journal of Polymer Science Part A: Polymer Chemistry* **35**, 3431-3440 (1997).

34. Kamber, N. E., Jeong, W., Waymouth, R. M., Pratt, R. C., Lohmeijer, B. G. G. & Hedrick, J. L. Organocatalytic Ring-Opening Polymerization. *Chemical Reviews* (2007).

35. Montaudo, G., Montaudo, M. S., Puglisi, C., Samperi, F., Spassky, N., LeBorgne, A. & Wisniewski, M. Evidence for Ester-Exchange Reactions and Cyclic Oligomer Formation in the Ring-Opening Polymerization of Lactide with Aluminum Complex Initiators. *Macromolecules* **29**, 6461-6465 (1996).

36. Dubois, P., Jacobs, C., Jérôme, R. & Teyssié, P. Macromolecular Engineering of Polylactones and Polylactides. 4. Mechanism and Kinetics of Lactide Homopolymerization by Aluminum Isopropoxide. *Macromolecules* **24**, 2266-2270 (1991).

37. O'Keefe, B. J., Monnier, S. M., Hillmyer, M. A. & Tolman, W. B. Rapid and Controlled Polymerization of Lactide by Structurally Characterized Ferric Alkoxides. *Journal of the American Chemical Society* **123**, 339-340 (2001).

38. Stolt, M. & Sodergard, A. Use of Monocarboxylic Iron Derivatives in the Ring-Opening Polymerization of L-lactide. *Macromolecules* **32**, 6412-6417 (1999).

39. Williams, C. K., Brooks, N. R., Hillmyer, M. A. & Tolman, W. B. Metalloenzyme Inspired Dizinc Catalyst for the Polymerization of Lactide. *Chemical Communications*, 2132-2133 (2002).

40. Cheng, M., Attygalle, A. B., Lobkovsky, E. B. & Coates, G. W. Single-Site Catalysts for Ring-Opening Polymerization: Synthesis of Heterotactic Poly(lactic acid) from *rac*-lactide. *Journal of the American Chemical Society* **121**, 11583-11584 (1999).

41. Ryner, M., Stridsberg, K., Albertsson, A.-C., von Schenck, H. & Svensson, M. Mechanism of Ring-Opening Polymerization of 1,5-Dioxepan-2-one and L-Lactide with Stannous 2-Ethylhexanoate. A Theoretical Study. *Macromolecules* **34**, 3877-3881 (2001).

42. Spassky, N., Wisniewski, M., Pluta, C. & Le Borgne, A. Highly Stereoelective Polymerization of *rac*-(D,L)-lactide with a Chiral Schiff's Base/Aluminium Alkoxide Initiator. *Macromolecular Chemistry and Physics* **197**, 2627-2637 (1996).

43. Kashima, T., Kameoka, T., Higuchi, C., Ajioka, M. & Yamaguchi, A. Aliphatic Polyester and Preparation Process thereof. 5428126.United States.(1995).

44. Gruber, P. R., Hall, E. S., Kolstad, J. J., Iwen, M. L., Benson, R. D. & Borchardt, R. L. Continuous Process for Manufacture of Lactide Polymers with Purification by Distillation. 5357035.United States.(1994).

45. Enomoto, K., Ajioka, M. & Yamaguchi, A. Polyhydroxycarboxylic Acid and Preparation Process thereof. 5310865.United States.(1994).

46. Drumright, R. E., Gruber, P. R. & Henton, D. E. Polylactic Acid Technology. *Advanced Materials* **12**, 1841-1846 (2000).

47. Kalb, B. & Pennings, A. J. General Crystallization Behaviour of Poly(L-lactic acid). *Polymer* **21**, 607-612 (1980).

48. Jamshidi, K., Hyon, S.-H. & Ikada, Y. Thermal Characterization of Polylactides. *Polymer* **29**, 2229-2234 (1988).

49. Farrington, D. W., Lunt, J., Davies, S. & Blackburn, R. S. in *Biodegradable and Sustainable Fibres* (ed. Blackburn, R. S.) 191-220 (CRC Press LLC, Boca Raton, 2005).

50. Witzke, D. R. Introduction to Properties, Engineering, and Prospects of Polylactide Polymers. *PhD Dissertation. Michigan State University.* 56-80 (1997).

51. Engelberg, I. & Kohn, J. Physico-Mechanical Properties of Degradable Polymers Used in Medical Applications: A Comparative Study. *Biomaterials* **12**, 292-304 (1991).

52. Celli, A. & Scandola, M. Thermal Properties and Physical Ageing of Poly(L-lactic acid). *Polymer* **33**, 2699-2703 (1992).

53. Fischer, E. W., Sterzel, H. J. & Wegner, G. Investigation of the Structure of Solution Grown Crystals of Lactide Copolymers by Means of Chemical Reactions. *Colloid & Polymer Science* **251**, 980-990 (1973).

54. Vasanthakumari, R. & Pennings, A. J. Crystallization Kinetics of Poly(L-lactic acid). *Polymer* **24**, 175-178 (1983).

55. Cohn, D., Younes, H. & Marom, G. Amorphous and Crystalline Morphologies in Glycolic Acid and Lactic Acid Polymers. *Polymer* **28**, 2018-2022 (1987).

56. Kishore, K., Vasanthakumari, R. & Pennings, A. J. Isothermal Melting Behavior of Poly(L-lactic acid). *Journal of Polymer Science: Polymer Physics Edition* **22**, 537-542 (1984).

57. Kolstad, J. J. Crystallization Kinetics of Poly(L-lactide-*co-meso*-lactide). *Journal of Applied Polymer Science* **62**, 1079-1091 (1996).

58. Gilding, D. K. & Reed, A. M. Biodegradable Polymers for Use In Surgery-Polyglycolic/Poly(lactic acid) Homo- and Copolymers: 1. *Polymer* **20**, 1459-1464 (1979).

59. Tsuji, H. & Ikada, Y. Properties and Morphologies of Poly(L-lactide): 1. Annealing Condition Effects on Properties and Morphologies of Poly(L-lactide). *Polymer* **36**, 2709-2716 (1995).

60. Miyata, T. & Masuko, T. Crystallization Behaviour of Poly(L-lactide). *Polymer* **39**, 5515-5521 (1998).

61. Iannace, S. & Nicolais, L. Isothermal Crystallization and Chain Mobility of Poly(L-lactide). *Journal of Applied Polymer Science* **64**, 911-919 (1997).

62. Hoffman, J. D. Role of Reptation in the Rate of Crystallization of Polyethylene Fractions from the Melt. *Polymer* **23**, 656-670 (1982).

63. Hoffman, J. D. Regime III Crystallization in Melt-Crystallized Polymers: The Variable Cluster Model of Chain Folding. *Polymer* **24**, 3-26 (1983).

64. Sperling, L. H. *Introduction to Physical Polymer Science* (Wiley-Interscience, New York, 2001).

65. Di Lorenzo, M. L. Determination of Spherulite Growth Rates of Poly(L-lactic acid) Using Combined Isothermal and Non-Isothermal Procedures. *Polymer* **42**, 9441-9446 (2001).

66. He, Y., Fan, Z., Wei, J. & Li, S. in *Polymer Engineering and Science* 1583(7) (2006).

67. Ikada, Y., Jamshidi, K., Tsuji, H. & Hyon, S. H. Stereocomplex Formation Between Enantiomeric Poly(lactides). *Macromolecules* **20**, 904-906 (1987).

68. Tonelli, A. E. & Flory, P. J. The Configurational Statistics of Random Poly(lactic acid) Chains. I. Experimental Results. *Macromolecules* **2**, 225-227 (1969).

69. Tsuji, H. & Ikada, Y. Stereocomplex Formation Between Enantiomeric Poly(lactic acid)s. 6. Binary Blends from Copolymers. *Macromolecules* **25**, 5719-5723 (1992).

70. Perego, G., Cella, G. D. & Bastioli, C. Effect of Molecular Weight and Crystallinity on Poly(lactic acid) Mechanical Properties. *Journal of Applied Polymer Science* **59**, 37-43 (1996).

71. Kobayashi, J., Asahi, T., Ichiki, M., Oikawa, A., Suzuki, H., Watanabe, T., Fukada, E. & Shikinami, Y. Structural and Optical Properties of Poly(lactic acid)s. *Journal of Applied Physics* **77**, 2957-2973 (1995).

72. Lalla, J. K. & Chugh, N. N. Biodegradable Polymer: Poly(lactic acid): Part I: Synthesis, Evaluation and Structure Elucidation. *Indian Drugs* **27**, 516-522 (1990).

73. Kister, G., Cassanas, G. & Vert, M. Effects of Morphology, Conformation and Configuration on the IR and Raman Spectra of Various Poly(lactic acid)s. *Polymer* **39**, 267-273 (1998).

74. Younes, H. & Cohn, D. Phase Separation in Poly(ethylene glycol)/Poly(lactic acid) Blends. *European Polymer Journal* **24**, 765-773 (1988).

75. De Santis, P. & Kovacs, A. J. Molecular Conformation of Poly(*S*-lactic acid). *Biopolymers* **6**, 299-306 (1968).

76. Hoogsteen, W., Postema, A. R., Pennings, A. J., ten Brinke, G. & Zugenmaier, P. Crystal Structure, Conformation and Morphology of Solution-Spun Poly(L-lactide) Fibers. *Macromolecules* **23**, 634-642 (1990).

77. Cartier, L., Okihara, T., Ikada, Y., Tsuji, H., Puiggali, J. & Lotz, B. Epitaxial Crystallization and Crystalline Polymorphism of Polylactides. *Polymer* **41**, 8909-8919 (2000).

78. Rak, J., Ford, J., Rostron, C. & Walters, V. The Preparation and Characterization of Poly(D,L-lactic acid) for Use as a Biodegradable Drug Carrier. *Pharmaceutica Acta Helvetiae* **60**, 162-169 (1985).

79. Lu, L. & Mikos, A. G. in *Polymer Data Handbook* (ed. Mark, J. E.) 627-633 (Oxford University Press, New York, 1999).

80. Tsuji, H. Poly(lactide) Stereocomplexes: Formation, Structure, Properties, Degradation, and Applications. *Macromolecular Bioscience* **5**, 569-597 (2005).

81. Kharas, G. B., Sanchez-Riera, F. & Severson, D. K. in *Plastics from Microbes* (ed. Mobley, D. P.) 93-258 (Hanser Gardner, Munich, 1994).

82. Biresaw, G. & Carriere, C. J. Interfacial Tension of Poly(lactic acid)/Polystyrene Blends. *Journal of Polymer Science Part B: Polymer Physics* **40**, 2248-2258 (2002).

83. Shogren, R. Water Vapor Permeability of Biodegradable Polymers. *Journal of Polymers and the Environment* **5**, 91-95 (1997).

84. Tsuji, H. & Muramatsu, H. Blends of Aliphatic Polyesters. IV. Morphology, Swelling Behavior, and Surface and Bulk Properties of Blends from Hydrophobic Poly(L-lactide) and Hydrophilic Poly(vinyl alcohol). *Journal of Applied Polymer Science* **81**, 2151-2160 (2001).

85. Dorgan, J. R., Williams, J. S. & Lewis, D. N. Melt Rheology of Poly(lactic acid): Entanglement and Chain Architecture Effects. *Journal of Rheology* **43**, 1141-1155 (1999).

86. Grijpma, D. W. & Pennings, A. J. Copolymers of L-lactide, 2. Mechanical Properties. *Macromolecular Chemistry and Physics* **195**, 1649-1663 (1994).

87. Joziasse, C. A. P., Veenstra, H., Grijpma, D. W. & Pennings, A. J. On the Chain Stiffness of Poly(lactide)s. *Macromolecular Chemistry and Physics* **197**, 2219-2229 (1996).

88. Fambri, L., Pegoretti, A., Fenner, R., Incardona, S. D. & Migliaresi, C. Biodegradable Fibres of Poly(L-lactic acid) Produced by Melt Spinning. *Polymer* **38**, 79-85 (1997).

89. Tsuji, H., Ikada, Y., Hyon, S.-H., Kimura, Y. & Kitao, T. Stereocomplex Formation Between Enantiomeric Poly(lactic acid). VIII. Complex Fibers Spun from Mixed Solution of Poly(D-lactic acid) and Poly(L-lactic acid). *Journal of Applied Polymer Science* **51**, 337-344 (1994).

90. van de Witte, P. et al. Formation of Porous Membranes for Drug Delivery Systems. *Journal of Controlled Release* **24**, 61-78 (1993).

91. Kim, K. et al. Control of Degradation Rate and Hydrophilicity in Electrospun Non-Woven Poly(D,L-lactide) Nanofiber Scaffolds for Biomedical Applications. *Biomaterials* **24**, 4977-4985 (2003).

92. Agrawal, A. K. & Bhalla, R. Advances in the Production of Poly(lactic acid) Fibers. A Review. *Polymer Reviews* **43**, 479 - 503 (2003).

93. Leenslag, J. W. & Pennings, A. J. High-Strength Poly(L-lactide) Fibers by a Dry-Spinning/Hot-Drawing Process. *Polymer* **28**, 1695-1702 (1987).

94. Solarski, S., Ferreira, M. & Devaux, E. Characterization of the Thermal Properties of PLA Fibers by Modulated Differential Scanning Calorimetry. *Polymer* **46**, 11187-11192 (2005).

95. Eling, B., Gogolewski, S. & Pennings, A. J. Biodegradable Materials of Poly(L-lactic acid): 1. Melt-Spun and Solution-Spun Fibers. *Polymer* **23**, 1587-1593 (1982).

96. Gruber, P. R. Cargill Dow LLC. *Journal of Industrial Ecology* **7**, 209-213 (2004).

97. Lunt, J. & Shafer, A. L. Polylactic Acid Polymers from Com. Applications in the Textiles Industry. *Journal of Industrial Textiles* **29**, 191-205 (2000).

98. Duda, A., Biela, T., Libiszowski, J., Penczek, S., Dubois, P., Mecerreyes, D. & Jérôme, R. Block and Random Copolymers of ε-Caprolactone. *Polymer Degradation and Stability* **59**, 215-222 (1998).

99. Kataoka, K., Harada, A. & Nagasaki, Y. Block Copolymer Micelles for Drug Delivery: Design, Characterization and Biological Significance. *Advanced Drug Delivery Reviews* **47**, 113-131 (2001).

100. Huang, C.-I., Tsai, S.-H. & Chen, C.-M. Isothermal Crystallization Behavior of Poly(L-lactide) in Poly(L-lactide)-*block*-Poly(ethylene glycol) Biblock Copolymers. *Journal of Polymer Science Part B: Polymer Physics* **44**, 2438-2448 (2006).

101. Baratian, S., Hall, E. S., Lin, J. S., Xu, R. & Runt, J. Crystalization and Solid-State Structure of Random Polylactide Copolymers: Poly(L-lactide-*co*-D-lactide)s. *Macromolecules* **34**, 4857-4864 (2001).

102. Nishikubo, T., Kameyama, A. & Kawakami, S. A Novel Synthesis of Poly(ester-*alt*-sulfide)s by the Ring-Opening Alternating Copolymerization of Oxiranes with γ-Thiobutyrolactone Using Quaternary Onium Salts or Crown Ether Complexes as Catalysts. *Macromolecules* **31**, 4746-4752 (1998).

103. Bechtold, K., Hillmyer, M. A. & Tolman, W. B. Perfectly Alternating Copolymer of Lactic Acid and Ethylene Oxide as a Plasticizing Agent for Polylactide. *Macromolecules* **34**, 8641-8648 (2001).

104. Cai, Q., Wan, Y. Q., Bei, J. Z. & Wang, S. G. Synthesis and Characterization of Biodegradable Polylactide-grafted Dextran and its Application as Compatilizer. *Biomaterials* **24**, 3555-3562 (2003).

105. Wu, Y., Zheng, Y. L., Yang, W. L., Wang, C. C., Hu, J. H. & Fu, S. K. Synthesis and Characterization of a Novel Amphiphilic Chitosan-Polylactide Graft Copolymer. *Carbohydrate Polymers* **59**, 165-171 (2005).

106. Barakat, I., Dubois, P., Jérôme, R., Teyssié, P. & Goethals, E. Macromolecular Engineering of Polylactones and Polylactides. XV. Poly(D,L)-lactide Macromonomers as Precursors of Biocompatible Graft Copolymers and Bioerodible Gels. *Journal of Polymer Science Part A: Polymer Chemistry* **32**, 2099-2110 (1994).

107. Janorkar, A. V., Metters, A. T. & Hirt, D. E. Modification of Poly(lactic acid) Films: Enhanced Wettability from Surface-Confined Photografting and Increased Degradation Rate due to an Artifact of the Photografting Process. *Macromolecules* **37**, 9151-9159 (2004).

108. Wu, C. S. & Liao, H. T. A New Biodegradable Blends Prepared from Polylactide and Hyaluronic Acid. *Polymer* **46**, 10017-10026 (2005).

109. Gottschalk, C. & Frey, H. Hyperbranched Polylactide Copolymers. *Macromolecules* **39**, 1719-1723 (2006).

110. Pitet, L. M., Hait, S. B., Lanyk, T. J. & Knauss, D. M. Linear and Branched Architectures from the Polymerization of Lactide with Glycidol. *Macromolecules* **40**, 2327-2334 (2007).

111. Adeli, M. & Haag, R. Multiarm Star Nanocarriers Containing A Poly(ethylene imine) Core and Polylactide Arms. *Journal of Polymer Science Part A: Polymer Chemistry* **44**, 5740-5749 (2006).

112. Huang, J., Lisowski, M. S., Runt, J., Hall, E. S., Kean, R. T., Buehler, N. & Lin, J. S. Crystallization and Microstructure of Poly(L-lactide-*co*-*meso*-lactide) Copolymers. *Macromolecules* **31**, 2593-2599 (1998).

113. Hollinger, J. O. Preliminary Report on the Osteogenic Potential of a Biodegradable Copolymer of Polyactide (PLA) and Polyglycolide (PGA). *Journal of Biomedical Materials Research* **17**, 71-82 (1983).

114. Min, C. C., Cui, W. J., Bei, J. Z. & Wang, S. G. Biodegradable Shape-Memory Polymer- Polylactide-*co*-Poly(glycolide-*co*-caprolactone) Multiblock Copolymer. *Polymers for Advanced Technologies* **16**, 608-615 (2005).

115. Li, G., Cai, Q., Bei, J. & Wang, S. Relationship Between Morphology Structure and Composition of Polycaprolactone/Poly(ethylene oxide)/Polylactide Copolymeric Microspheres. *Polymers for Advanced Technologies* **13**, 636-643 (2002).

116. Helminen, A. O., Korhonen, H. & Seppala, J. V. Cross-linked Poly(ε-caprolactone/D,L-lactide) Copolymers with Elastic Properties. *Macromolecular Chemistry and Physics* **203**, 2630-2639 (2002).

117. Frick, E. M. & Hillmyer, M. A. Synthesis and Characterization of Polylactide-*block*-Polyisoprene-*block*-Polylactide Triblock Copolymers: New Thermoplastic Elastomers

Containing Biodegradable Segments. *Macromolecular Rapid Communications* **21**, 1317-1322 (2000).

118. Schmidt, S. C. & Hillmyer, M. A. Synthesis and Characterization of Model Polyisoprene-Polylactide Diblock Copolymers. *Macromolecules* **32**, 4794-4801 (1999).

119. Zalusky, A. S., Olayo-Valles, R., Wolf, J. H. & Hillmyer, M. A. Ordered Nanoporous Polymers from Polystyrene-Polylactide Block Copolymers. *Journal of the American Chemical Society* **124**, 12761-12773 (2002).

120. Wang, Y. & Hillmyer, M. A. Polyethylene-Poly(L-lactide) Diblock Copolymers: Synthesis and Compatibilization of Poly(L-lactide)/Polyethylene Blends. *Journal of Polymer Science Part A: Polymer Chemistry* **39**, 2755-2766 (2001).

121. Schmidt, S. C. & Hillmyer, M. A. Morphological Behavior of Model Poly(ethylene-*alt*-propylene)-*block*-Polylactide Diblock Copolymers. *Journal of Polymer Science Part B: Polymer Physics* **40**, 2364-2376 (2002).

122. Li, F., Li, S. & Vert, M. Synthesis and Rheological Properties of Polylactide/Poly(ethylene glycol) Multiblock Copolymers. *Macromolecular Bioscience* **5**, 1125-1131 (2005).

123. Kubies, D., Rypacek, F., Kovarova, J. & Lednicky, F. Microdomain Structure in Polylactide-*block*-Poly(ethylene oxide) Copolymer Films. *Biomaterials* **21**, 529-536 (2000).

124. Gautier, S., Grudzielski, N., Goffinet, G., De Hassonville, S. H., DeLattre, L. & Jerome, R. Preparation of Poly(D,L-lactide) Nanoparticles Assisted by Amphiphilic Poly(methyl methacrylate-*co*-methacrylic acid) Copolymers. *Journal of Biomaterials Science- Polymer Edition* **12**, 429-450 (2001).

125. Vert, M. in *Biopolymers for Medicinal and Pharmaceutical Applications* (eds. Steinbüchel, A. & Marchessault, R. H.) 159-182 (Wiley-VCH, Weinheim, 2005).

126. Abayasinghe, N. K., Glaser, S., Perera, P. U. & Smith, D. W., Jr. Oligoethylene-End-Capped Polylactides. *Journal of Polymer Science Part A: Polymer Chemistry* **43**, 5257-5266 (2005).

127. Haynes, D., Naskar, A. K., Singh, A., Yang, C.-C., Burg, K. J., Drews, M., Harrison, G. & Smith, D. W., Jr. Poly(L-lactic acid) with Segmented Perfluoropolyether Enchainment. *Macromolecules* **40**, 9354-9360 (2007).

128. Lemmouchi, Y., Perry, M. C., Amass, A. J., Chakraborty, K. & Schué, F. Novel Synthesis of Biodegradable Poly(lactide-*co*-ethylene glycol) Block Copolymers. *Journal of Polymer Science Part A: Polymer Chemistry* **45**, 2235-2245 (2007).

129. Breitenbach, A. & Kissel, T. Biodegradable Comb Polyesters: Part 1 - Synthesis, Characterization and Structural Analysis of Poly(lactide) and Poly(lactide-*co*-glycolide) Grafted onto Water-Soluble Poly(vinyl alcohol) as Backbone. *Polymer* **39**, 3261-3271 (1998).

130. Kitamura, T. & Matsumoto, A. Synthesis of Poly(lactic acid) with Branched and Network Structures Containing Thermally Degradable Junctions. *Macromolecules* **40**, 509-517 (2007).

131. Helminen, A. O., Korhonen, H. & Seppala, J. V. Crosslinked Poly(ester anhydride)s Based on Poly(ε-caprolactone) and Polylactide Oligomers. *Journal of Polymer Science Part A: Polymer Chemistry* **41**, 3788-3797 (2003).

132. Abayasinghe, N. K. & Smith, D. W., Jr. Terpolymers from Lactide and Bisphenol A Derivatives: Introducing Renewable Resource Monomers into Commodity Thermoplastics. *Macromolecules* **36**, 9681-9683 (2003).

133. Haynes, D., Abayasinghe, N. K., Harrison, G. M., Burg, K. J. & Smith, D. W., Jr. In Situ Copolyesters Containing Poly(L-lactide) and Poly(hydroxyalkanoate) Units. *Biomacromolecules* **8**, 1131-1137 (2007).

134. Abayasinghe, N. K., Perera, K. P. U., Thomas, C., Daly, A., Suresh, S., Burg, K., Harrison, G. M. & Smith, D. W., Jr. Amido-modified Polylactide for Potential Tissue Engineering Applications. *Journal of Biomaterials Science-Polymer Edition* **15**, 595-606 (2004).

135. Anderson, K. S., Lim, S. H. & Hillmyer, M. A. Toughening of Polylactide by Melt Blending with Linear Low-Density Polyethylene. *Journal of Applied Polymer Science* **89**, 3757-3768 (2003).

136. Sarazin, P. & Favis, B. D. Morphology Control in Co-Continuous Poly(L-lactide)/Polystyrene Blends: A Route Towards Highly Structured and Interconnected Porosity in Poly(L-lactide) Materials. *Biomacromolecules* **4**, 1669-1679 (2003).

137. Cabedo, L., Feijoo, J. L., Villanueva, M. P., Lagaron, J. M. & Gimenez, E. Optimization of Biodegradable Nanocomposites Based on a PLA/PCL Blends for Food Packaging Applications. *Macromolecular Symposia* **233**, 191-197 (2006).

138. Eguiburu, J. L., Iruin, J. J., Fernandez-Berridi, M. J. & Roman, J. S. Blends of Amorphous and Crystalline Polylactides with Poly(methyl methacrylate) and Poly(methyl acrylate): A Miscibility Study. *Polymer* **39**, 6891-6897 (1998).

139. Davies, M. C., Shakesheff, K. M., Shard, A. G., Domb, A., Roberts, C. J., Tendler, S. J. B. & Williams, P. M. Surface Analysis of Biodegradable Polymer Blends of Poly(sebacic anhydride) and Poly(DL-lactic acid). *Macromolecules* **29**, 2205-2212 (1996).

140. Dubois, P. & Narayan, R. Biodegradable Compositions by Reactive Processing of Aliphatic Polyester/Polysaccharide Blends. *Macromolecular Symposia* **198**, 233-243 (2003).

141. Zhang, G., Zhang, J., Zhou, X. & Shen, D. Miscibility and Phase Structure of Binary Blends of Polylactide and Poly(vinylpyrrolidone). *Journal of Applied Polymer Science* **88**, 973-979 (2003).

142. Yuan, Y. M. & Ruckenstein, E. Polyurethane Toughened Polylactide. *Polymer Bulletin* **40**, 485-490 (1998).

143. Lee, J. K., Kim, M. R., Lee, H. J., Chung, I., Lim, K. T., Jeon, S. & Lee, W. K. Surface Structure and Stereocomplex Formation of Enantiomeric Polylactide Blends Using Poly(dimethyl siloxane) as a Probe Polymer. *Macromolecular Symposia* **239**, 91-96 (2006).

144. Wan, Y., Wu, H., Yu, A. & Wen, D. Biodegradable Polylactide/Chitosan Blend Membranes. *Biomacromolecules* **7**, 1362-1372 (2006).

145. Peesan, M., Supaphol, P. & Rujiravanit, R. Preparation and Characterization of Hexanoyl Chitosan/Polylactide Blend Films. *Carbohydrate Polymers* **60**, 343-350 (2005).

146. Tsuji, H. & Muramatsu, H. Blends of Aliphatic Polyesters. IV. Morphology, Swelling Behavior, and Surface and Bulk Properties of Blends from Hydrophobic Poly(L-lactide) and Hydrophilic Poly(vinyl alcohol). *Journal of Applied Polymer Science* **81**, 2151-2160 (2001).

147. Anderson, K. S. & Hillmyer, M. A. Melt Preparation and Nucleation Efficiency of Polylactide Stereocomplex Crystallites. *Polymer* **47**, 2030-2035 (2006).

148. Fujimoto, Y., Ray, S. S., Okamoto, M., Ogami, A., Yamada, K. & Ueda, K. Well-Controlled Biodegradable Nanocomposite Foams: From Microcellular to Nanocellular. *Macromolecular Rapid Communications* **24**, 457-461 (2003).

149. Nam, J. Y., Ray, S. S. & Okamoto, M. Crystallization Behavior and Morphology of Biodegradable Polylactide/Layered Silicate Nanocomposite. *Macromolecules* **36**, 7126-7131 (2003).

150. Li, H. Y. & Chang, J. pH-compensation Effect of Bioactive Inorganic Fillers on the Degradation of PLGA. *Composites Science and Technology* **65**, 2226-2232 (2005).

151. Wan, Y. Z., Wang, Y. L., Li, Q. Y. & Dong, X. H. Influence of Surface Treatment of Carbon Fibers on Interfacial Adhesion Strength and Mechanical Properties of PLA-based Composites. *Journal of Applied Polymer Science* **80**, 367-376 (2001).

152. Katz, H. S. in *Handbook of Plastic Materials and Technology* (ed. Rubin, I. I.) 675-681 (John Wiley & Sons, Inc., New York, 1990).

153. Nakamura, T., Hitomi, S., Watanabe, S., Shimizu, Y., Jamshidi, K., Hyon, S.-H. & Ikada, Y. Bioabsorption of Polylactides with Different Molecular Properties. *Journal of Biomedical Materials Research* **23**, 1115-1130 (1989).

154. Fox, T. G. Influence of Diluent and of Copolymer Composition on the Glass Temperature of a Polymer System. *Bulletin of the American Physical Society* **1**, 123 (1956).

155. Mandelkern, L., Garrett, R. R. & Flory, P. J. Heats of Fusion of Aliphatic Polyesters. *Journal of the American Chemical Society* **74**, 3949-3951 (1952).

156. Baiardo, M., Frisoni, G., Scandola, M., Rimelen, M., Lips, D., Ruffieux, K. & Wintermantel, E. Thermal and Mechanical Properties of Plasticized Poly(L-lactic acid). *Journal of Applied Polymer Science* **90**, 1731-1738 (2003).

157. Ren, Z., Dong, L. & Yang, Y. Dynamic Mechanical and Thermal Properties of Plasticized Poly(lactic acid). *Journal of Applied Polymer Science* **101**, 1583-1590 (2006).

158. Martin, O. & Averous, L. Poly(lactic acid): Plasticization and Properties of Biodegradable Multiphase Systems. *Polymer* **42**, 6209-6219 (2001).

159. Labrecque, L. V., Kumar, R. A., Davé, V., Gross, R. A. & McCarthy, S. P. Citrate Esters as Plasticizers for Poly(lactic acid). *Journal of Applied Polymer Science* **66**, 1507-1513 (1997).

160. Ljungberg, N. & Wesslén, B. The Effects of Plasticizers on the Dynamic Mechanical and Thermal Properties of Poly(lactic acid). *Journal of Applied Polymer Science* **86**, 1227-1234 (2002).

161. Zhang, J.-F. & Sun, X. Mechanical and Thermal Properties of Poly(lactic acid)/Starch Blends with Dioctyl Maleate. *Journal of Applied Polymer Science* **94**, 1697-1704 (2004).

162. Göpferich, A. Mechanisms of Polymer Degradation and Erosion. *Biomaterials* **17**, 103-114 (1996).

163. Tamada, J. A. & Langer, R. Erosion Kinetics of Hydrolytically Degradable Polymer. *Proceedings of the National Academy of Sciences* **90**, 552-556 (1993).

164. Göpferich, A. & Langer, R. Modeling of Polymer Erosion. *Macromolecules* **26**, 4105-4112 (1993).

165. Park, T. G. Degradation of Poly(D,L-lactic acid) Microspheres: Effect of Molecular Weight. *Journal of Controlled Release* **30**, 161-173 (1994).

166. Fukuzaki, H., Yoshida, M., Asano, M. & Kumakura, M. Synthesis of Copoly(D,L-lactic acid) with Relatively Low Molecular Weight and *In Vitro* Degradation. *European Polymer Journal* **25**, 1019-1026 (1989).

167. Williams, D. F. Enzymatic Hydrolysis of Polylactic Acid. *Engineering in Medecine* **10**, 5-7 (1981).

168. Makino, K., Arakawa, M. & Kondo, T. Preparation and Invitro Degradation Properties of Polylactide Microcapsules. *Chemical & Pharmaceutical Bulletin* **33**, 1195-1201 (1985).

169. Tsuji, H. & Nakahara, K. Poly(L-lactide). IX. Hydrolysis in Acid Media. *Journal of Applied Polymer Science* **86**, 186-194 (2002).

170. Shih, C. Chain-End Scission in Acid Catalyzed Hydrolysis of Poly (D,L-lactide) in Solution. *Journal of Controlled Release* **34**, 9-15 (1995).

171. Tsuji, H. & Ikada, Y. Properties and Morphology of poly(L-lactide). II. Hydrolysis in Alkaline Solution. *Journal of Polymer Science Part A: Polymer Chemistry* **36**, 59-66 (1998).

172. Pitt, C. G. & Gu, Z.-w. Modification of the Rates of Chain Cleavage of Poly(ε-caprolactone) and Related Polyesters in the Solid State. *Journal of Controlled Release* **4**, 283-292 (1987).

173. Tsuji, H., Ogiwara, M., Saha, S. K. & Sakaki, T. Enzymatic, Alkaline, and Autocatalytic Degradation of Poly(L-lactic acid): Effects of Biaxial Orientation. *Biomacromolecules* **7**, 380-387 (2006).

174. Tsuji, H., Mizuno, A. & Ikada, Y. Properties and Morphology of Poly(L-lactide). III. Effects of Initial Crystallinity on Long-Term *In Vitro* Hydrolysis of High Molecular Weight Poly(L-lactide) Film in Phosphate-Buffered Solution. *Journal of Applied Polymer Science* **77**, 1452-1464 (2000).

175. Tsuji, H., Ikarashi, K. & Fukuda, N. Poly(L-lactide): XII. Formation, Growth, and Morphology of Crystalline Residues as Extended-Chain Crystallites Through Hydrolysis of Poly(L-lactide) Films in Phosphate-Buffered Solution. *Polymer Degradation and Stability* **84**, 515-523 (2004).

176. Tsuji, H. & Ikarashi, K. *In vitro* Hydrolysis of Poly(L-lactide) Crystalline Residues as Extended-Chain Crystallites - III. Effects of pH and Enzyme. *Polymer Degradation and Stability* **85**, 647-656 (2004).

177. Tsuji, H. & Ikarashi, K. *In vitro* Hydrolysis of Poly(L-lactide) Crystalline Residues as Extended-Chain Crystallites. Part I: Long-Term Hydrolysis in Phosphate-Buffered Solution at 37 °C. *Biomaterials* **25**, 5449–5455 (2004).

178. Tsuji, H. & Ikarashi, K. *In Vitro* Hydrolysis of Poly(L-lactide) Crystalline Residues as Extended-Chain Crystallites: II. Effects of Hydrolysis Temperature. *Biomacromolecules* **5**, 1021-1028 (2004).

179. Tsuji, H. & Carpio, C. A. D. *In Vitro* Hydrolysis of Blends from Enantiomeric Poly(lactide)s. 3. Homocrystallized and Amorphous Blend Films. *Biomacromolecules* **4**, 7-11 (2003).

180. Tsuji, H. *In vitro* Hydrolysis of Blends from Enantiomeric Poly(lactide)s. Part 4:Well Homo-crystallized Blend and Nonblended Films. *Biomaterials* **24**, 537-547 (2003).

181. Smith, P. B., Leugers, A., Kang, S., Yang, X. & Hsu, S. L. Raman Characterization of Orientation in Poly(lactic acid) Films. *Macromolecular Symposia* **175**, 81-94 (2001).

182. Ikada, Y. & Tsuji, H. Biodegradable Polyesters for Medical and Ecological Applications. *Macromolecular Rapid Communications* **21**, 117–132 (2000).

CHAPTER 3

EXPERIMENTAL

3.1 Materials

L-Lactide (LA) was generously donated by Poly-Med Inc. (Pendleton, SC) and was recrystallized from ethyl acetate and vacuum dried to remove solvent and moisture. Polylactide (PLA) was generously donated by Cargill Dow Polymers, LLC (United States).

Poly(tetrafluoroethylene oxide-co-difluoromethylene oxide) α,ω-diol (Fomblin® Z DOL) (PFPE) with number average molecular weight of 1500, 2000, 4200 g mol^{-1} was generously donated by Solvay-Solexis (Italy). PFPE used were colorless clear liquids with density 1.8 g cm^{-3}, x/y≈1 and functionality of ~ 1.8-1.9 with following chemical structure:

$HO\text{-}CH_2\text{-}CF_2\text{-}(CF_2\text{-}CF_2\text{-}O)_x\text{-}(CF2\text{-}O)_y\text{-}CF_2\text{-}CH_2\text{-}OH$

Diglycidyl ether of bisphenol A (DGEBA), 4,4'-(hexafluoroisopropylidene)diphenol (6F-Bis-A) and 1-phenoxy-2-propanol (Dowanol™) were used generously donated by Dow Chemical Company (United States). Stannous Octoate ($Sn(Oct)_2$, 18-Crown-6-Ether (18C6E) and potassium chloride (KCl) were purchased from Sigma Aldrich (United States) and were used as received. All other chemicals and reagents were purchased from Fisher (United States) or Sigma Aldrich and used as received unless otherwise stated.

3.2 Instrumentation

Polymerization Reactor

Polymerization was carried out using a high pressure/moderate temperature stirred, series 4540, reactor (Parr Instrument Company, Moline, IL) with the 600 ml capacity moveable reaction vessel shown in Figure 3.1. This movable floor stand reactor offers working pressures of up to 5000 psi at 350 °C. The reactor is accompanied by a controller (Model 4843) which regulates the temperature and the stirrer drive, and also displays the pressure in the reaction vessel. The progress of the reaction can be qualitatively evaluated by monitoring the change in torque generated on the stirrer drive.

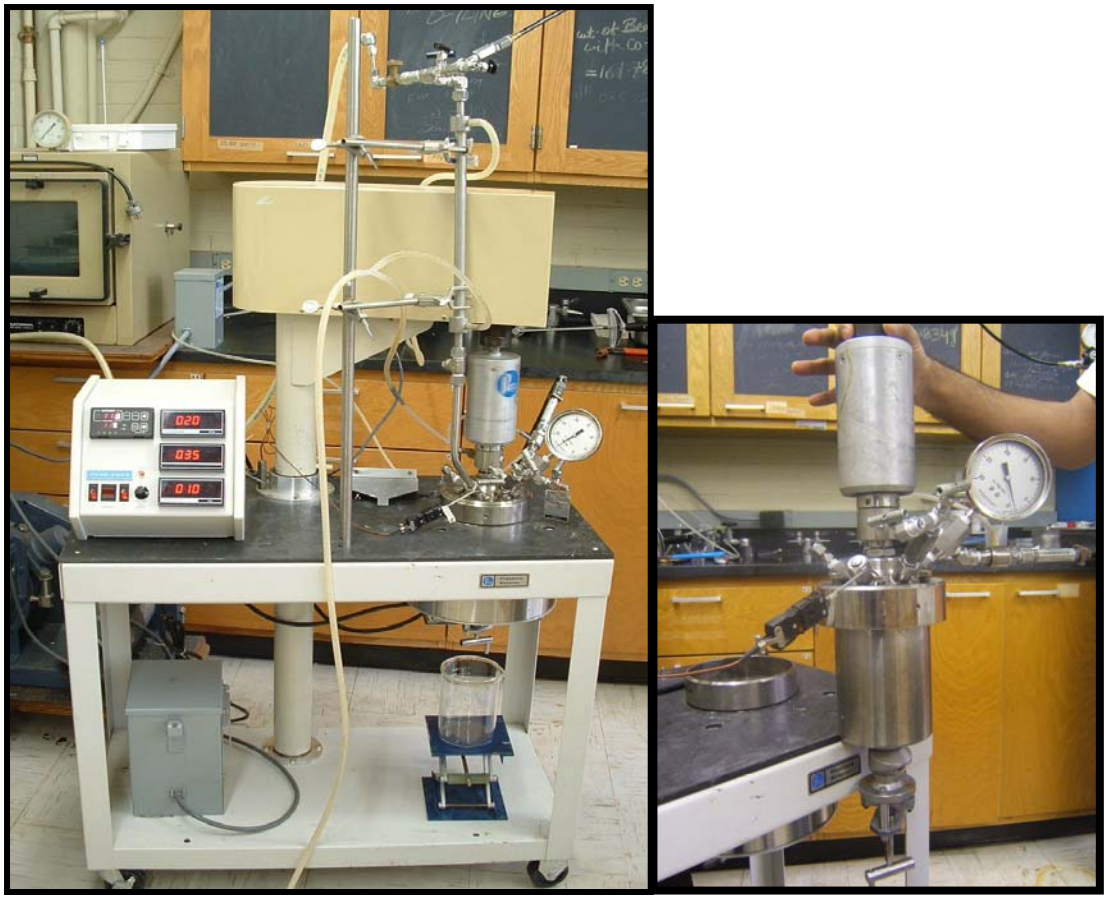

Figure 3.1. Photographs of the high pressure/moderate temperature reactor used for polymerization. Movable floor stand reactor (left) and reaction vessel with stirrer drive (right).

Gel Permeation Chromatography (GPC)

The number and weight average molecular weights of polymers were characterized using a Waters "Breeze" GPC system (Waters, Milford, MA) interfaced with a Polymer Lab (Amherst, MA) PL-ELS 2100 detector. Two Waters columns were used in series (Styragel HR4E & HR5E). The mobile phase was chloroform (Burdick & Jackson, HPLC grade) at 1

ml/min. Polystyrene standards (Polysciences, Inc., Warrington, PA) of number average molecular weights 1,000,000; 600,000; 400,000; 200,000; 105,200; 50,000; 20,000; 4,000; 436 Dalton (Polydispersity Index ≤1.1) were used to calibrate the system.

Differential Scanning Calorimetry

Differential Scanning Calorimentry (DSC) analysis was conducted using a TA Instruments (New Castle, Delaware) Q1000 DSC. Data was analyzed using TA Instruments Universal Analysis 2000 version 4.1D software. The samples (6-8 mg standard aluminum pans) were initially heated to 225 °C to erase the thermal history and then cooled to -50 °C, and finally heated from -50 °C to 225 °C. A heating rate of 10 °C/min was used for all segments mentioned above. The glass transition temperatures were obtained as the inflection point of the step transition. Temperature values of the endothermic and exothermic peak maxima's were considered as melting and crystallization temperatures, and the integral of the peak area was used to calculate heats of fusion and crystallization respectively.

Thermal Gravimetric Analysis

Thermal Gravimetric Analysis (TGA) was conducted using a TA Instruments (New Castle, Delaware) 2950 TGA. Data was analyzed using TA Instruments Universal Analysis 2000 version 4.1D software. Samples were heated at the rate of 10 °C/min from room temperature to 400 °C under a nitrogen purge.

Dynamic Mechanical Analysis

Dynamic Mechanical Analysis (DMA) was performed using a DMS 210 Tension Module (Seiko Instruments Inc., Japan) with specimen dimension of 40 mm x 10 mm and an effective gauge length of 20 mm. Samples were evaluated over a temperature range of -130 °C to 125 °C at a heating rate of 2 °C min^{-1} at a frequency of 1 Hz and a deformation amplitude of 10 μm. Data were analyzed using EXSTAR6000 software.

Rheology

The rheological properties of the polymers were measured using a TA Instruments (New Castle, Delaware) Advanced Rheometric Expansion System (ARES) shown schematically in Figure 3.2. Experiments were carried out using a cone-and-plate fixture with diameter of 25 mm and angular gap of 0.1 radian. Steady shear rate sweep tests, from 0.1 s^{-1} to 100 s^{-1}, were carried out on samples at 180 °C. Shear viscosities for PLA and FluoroPLAs were measured as a function of the shear rate. Data were analyzed using TA Instruments Orchestrator™ software.

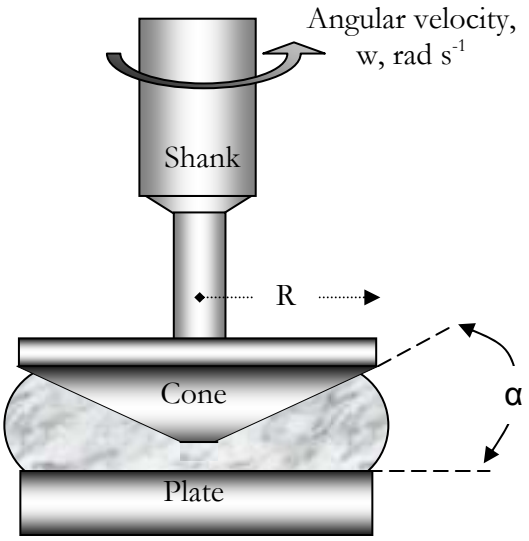

Figure 3.2. Schematic of cone-and-plate AR rheometer.

The pellets were prepared from fibrous polymeric materials using a Carver Laboratory Press mold. A load of 15,000 pounds was applied on the material and left under vacuum for 2 min. Circular pellets, approximately 12 mm in diameter and 3-4 mm in thickness, were obtained and dried at 90 °C for 1 hr before subjected to rheological study. The pellets were placed between cone and plate and heated to 180 °C under inert atmosphere before the steady shear rate tests were initiated.

Nuclear Magnetic Resonance (NMR) Spectroscopy

^{19}F NMR spectra were obtained using a JEOL (Tokyo, Japan) Eclipse+ 300 MHz NMR spectrometer. Highly concentrated solutions (~10 (w/v) %) of polymer in deuterated chloroform were placed in 5 mm NMR tubes and 128 scans were collected. Trichlorofluoromethane ($CFCl_3$) was used as internal reference (0 ppm).

X-ray Diffraction (XRD)

Diffraction patterns of polymers were collected at room temperature using SCINTAG XDS 2000 (Scintag, Inc., Cupertino, CA) diffractometer equipped with Cu Kα radiation at a wavelength of 1.54 Å. The instrument was operated at 40 kV and 40 mA with a collimator diameter of 0.5 mm. Solution-cast polymer films were scanned at 2°/min (2θ value) from 6° to 60°. Percent crystallinity was calculated by dividing total counts under crystalline peaks by total area under the curve. Data were analyzed using DMSNT™ version 1.37 software.

Fourier Transform Infrared (FTIR) Spectroscopy

FTIR spectroscopy was performed using a Thermo-Nicolet Magna - IR™ 550 spectrometer (Thermo Nicolet, Waltham, MA) equipped with a Thermo Spectra-Tech Foundation Series Endurance diamond attenuated total reflectance (ATR) accessory. Sample spectra were collected by performing 32 scans at a resolution of 4 cm^{-1} from 4000 cm^{-1} to 525 cm^{-1} and were ratioed against background spectra collected in the same fashion. Data was analyzed using OMNIC E.S.P. v 7.2 software.

Dip Coating of Polymer on Silicon Wafer

Silicon wafers were oxidized by immersion in the pirana solution (3 part 95-98% H_2SO_4 + 1 part 30% H_2O_2) at 80 °C for 45 minutes. The thickness of the resultant SiO_2 layer was measured by ellipsometry and found ca. 1.4 nm. Solutions of 2 % (w/v)

homopolymer and copolymer in chloroform were prepared and filtered through a Whatman 0.2 μm polytetrafluoroethylene membrane syringe filter. Dip coating of oxidized silicon wafers were carried out using a dip coater (Mayer Feintechnik D-3400, Göttingen, Germany). Dip coated samples were air dried and then the film thickness was measured using ellipsometry.

Atomic Force Microscopy (AFM)

A Dimension 3100 (Veeco Inc., Woodbury, NY) atomic force microscope (AFM) equipped with Nanoscope IIIa controller was used to image the surface of the dip-coated polymer film on silicon wafers. All AFM characterization experiments were performed using a silicon AFM tip (MicroMash Inc., nominal force constant 40 N/m, tip radius <10 nm) in the non-contact (tapping) mode.

Scanning Electron Microscopy (SEM)

Scanning electron microscopy (SEM) images of electrospun fibers and hydrolysed samples were obtained on Hitachi S3400N (Hitachi High-Technologies, Japan) microscope at an accelerating voltage of 20 kV. A Hummer®6.2 (Anatech Ltd., Hayward, CA) sputter coater was used to pre-coat the samples with a 4-5 nm layer of platinum.

Contact Angle Measurements

Static contact angle measurements were performed using the sessile drop method on a Drop Shape Analysis (KRÜSS Instruments, Hamburg, Germany) system. Test liquid drops

with an average volume between 5 to 10 μL were placed on the dip coated polymer films and the equilibrium contact angles were measured after an equilibration time of 30 seconds. A schematic of the contact angle measurement is shown Figure 3.3.

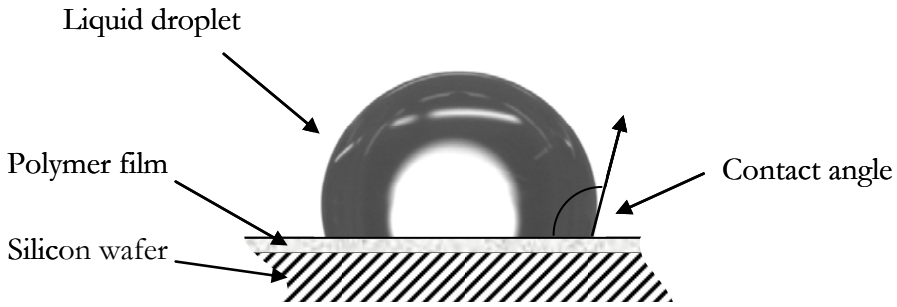

Figure 3.3. Schematic of static contact angle.

Polarized Optical Microscopy

Morphological studies were executed on James Swift Polarising Microscope (James Swift, London, England) equipped with Mettler Toledo (Columbus, OH) FP90 central processor and Mettler Toledo FP80HT hot stage. Digital images were captured using Sony 3CCD camera and analyzed using *Image-Pro PLUS* (version 4.0) software (Media Cybernetics, MD, USA). A Fisher Micromaster (Fisher Scientific) microscope stage micrometer was used for measurement calibration.

Solutions of polymer in chloroform (2 (w/v) %) were placed as single drops on to glass slides and dried under vacuum. Samples were then covered with a coverslip and placed onto the mount. Samples were heated to 200 °C at a rate of 20 °C/min and held for 5 min. Samples were then cooled to selected crystallization temperature (Tc) at a rate of 20 °C/min

and held isothermally to observe the growth of spherulites. Growths in spherulite's radii were measured at fixed time intervals. Samples were cooled to room temperature at 20 °C from crystallization temperature. The above was repeated for each selected crystallization temperature with new samples each time. The selected crystallization temperatures were 140, 130, 120, 110, 100, 90 °C.

Electrospinning

Polymer solutions of concentrations between 25-35 (w/v) % in chloroform and tetrahydrofuran were electrospun using the electrospinning equipment illustrated in Figure 3.4. Solutions were placed in a 10 ml syringe and then extruded through a 16 ½ gauge needle at a rate of 6 ml/hr. A 15 kV voltage was applied to the needle and the polymer jet was collected on a grounded surface at distance of 10 cm. The electrospun sample was then vacuum dried at 60 °C for 1 hour.

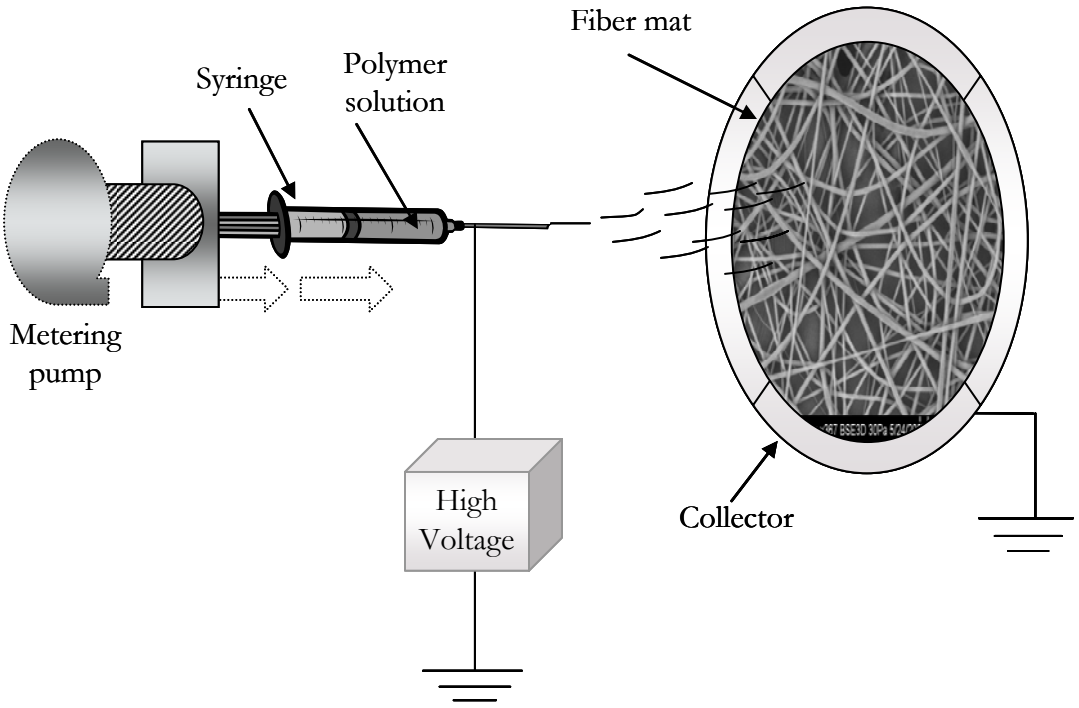

Figure 3.4. Schematic of electrospinning process for fiber spinning.

3.3 Polymerization Procedure

Scaled-up synthesis of PLA and FluoroPLA

A solution of 10 mL of toluene, 0.42 g of $Sn(Oct)_2$, and 5 g of PFPE was prepared and shaken well. Then L-Lactide (100 g) and above mixture were added to the Parr reaction vessel, sealed and blanketed with the inert (argon) atmosphere. The reaction mixtures were stirred at 20 rpm and the temperature was gradually raised (~2 °C/min) to 130 °C and held for 24 hrs. After polymerization, the reactor was allowed to cool and a solid light yellow mass was removed by opening the reactor. The reaction product was dissolved in and diluted with chloroform followed by precipitation in swirling methanol at room temperature. The precipitated material was then dried under vacuum at 70 °C for one hour. Various batches of the copolymer of PLA and PFPE were prepared with ~ 5 (wt) % PFPE (LA:PFPE::20:1, wt/wt) of different molecular weights (Mn= 1.5kD, 2.0kD, 4.2kD). A control PLA homopolymer batch was synthesized without any PFPE in above mentioned reaction mixture.

Scaled-up synthesis of Terpolymer

The terpolymerization of lactide (LA), diglycidyl ether of bisphenol A (DGEBA) and 4,4'-(hexafluoroisopropylidene)diphenol (6F-Bis-A) was carried out in molar ratio of 1:1:1. Catalyst (KCl and 18C6E) was stirred overnight in 10 ml Dowanol™ and added to the reaction system. Reaction mixtures were prepared using the following recipe:

Reactants	Mole	
LA	1.0	
DGEBA	1.0	
6F-Bis-A	1.0	
KCl	2.7	$x10^{-3}$
18C6E	2.9	$x10^{-3}$
Dowanol	0.7	

The prepared reaction mixture (~300 g) was then added to the reaction vessel, purged and sealed under 15 psi of inert (argon) atmosphere. The temperature was gradually (~2 °C/min) heated to 115 °C and held for 24 hrs and the mixture was stirred slowly (20 rpm) throughout. The terpolymerization product was removed from the bottom drain valve of the reactor and cooled. Extraction of product was carried out by dissolving in tetrahydrofuran and precipitating in methanol and n-hexane sequentially. The precipitated terpolymer was then vacuum dried at 90 °C for 1 hour.

CHAPTER 4

SCALED-UP SYNTHESIS, CHARACTERIZATION AND SURFACE PROPERTIES OF POLYLACTIDE AND POLYLACTIDE-PERFLUOROPOLYETHER BLOCK COPOLYMERS

4.1 Introduction

Polylactide (PLA), a biodegradable and biocompatible aliphatic polyester, is well known in the medical and pharmaceutical fields and is now rapidly evolving as a commodity polymer. PLA is commercially synthesized from lactide, a renewable resource monomer and is seen as a potential alternative to petroleum based commodity polymers as the latter faces problems associated with waste disposal and increased cost of production.[1-7] PLA is semicrystalline (glass transition temperature range 50-60 °C, melting temperature range 170-180 °C) and melt-processable with products having some comparable properties to the petroleum-based plastics such as polystyrene and polypropylene, however, PLA is more brittle.[4,6,8] The future prospects of PLA depend mainly on availability of raw material, energy consumed for producing these materials, cost of further processing and acceptance of the processed material as a commodity.[9] In order to make PLA versatile and deliver tailor made crystallinity, surface morphology, hydrolytic degradation, molecular distribution and other useful properties for commodity applications, there is a need for its modification by either copolymerization, blending and/or plasticization with other polymers having the desired properties.[10-13]

The ring-opening polymerization (ROP) of lactide can be carried out by using complexes of aluminum, iron, tin, yttrium, zinc and various other metals.[14-18] Tin(II) 2-ethylhexanoate (Figure 4.1) is one of the most commonly used catalysts/initiators for bulk

polymerization of lactides because of its high efficiency, low risk of racemization and extremely low toxicity.[2,19,20]

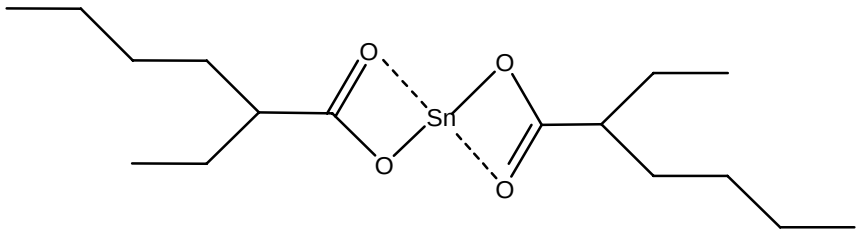

Figure 4.1. Tin(II) 2-Ethylhexanoate [$Sn(Oct)_2$].

Two of the major ROP mechanisms proposed are the activated monomer mechanism and the coordination-insertion mechanism and both mechanisms are thought to be alcohol-initiated.[21] In the activated monomer mechanism a donor-acceptor complex is formed between $Sn(Oct)_2$ and the monomer, activating the monomer towards an attack by the alcohol as shown in Scheme 2.5 (Chapter 2).[2,21]

A two-step coordination-insertion mechanism is proposed by the complexation of lactone to metal alkoxides containing favorable energy, vacant p- or d-orbitals, followed by insertion of the monomer into the metal-oxygen bond as shown in Scheme 2.6 (Chapter 2).[22]

Since ROP is not initiated by $Sn(Oct)_2$ and octoate has to be converted to an alkoxide, the polymerization is very sensitive to the relative content of hydroxyl impurities in monomer and catalyst thus explaining the difficulties reported in controlled molecular weight synthesis. [2,22,23] Even when there is no added alcohol or acid in the system, impurities present in the monomer and/or catalyst initiate the system.[24] Impurities such as water, lactic acid, lactoyl lactic acid are present in the monomer and catalyst (hygroscopic nature).[25,26] This

problem is also seen as an opportunity and work has been done to improve the properties of PLA.[27]

Fluorinated polymers have excellent properties such as chemical inertness, low coefficient of friction, and low surface energy.[28] Semifluorinated hybrid materials can be prepared by blending, copolymerization, chemical reaction of fluorinated materials with polymers such as poly(acrylates), poly(methacrylate), polystyrene, poly(ε-caprolactone), and others.[29-31] Copolymerization of monomers requires relatively higher amounts of fluorinated materials for a considerable change in surface properties of the resultant copolymer and lead to an expensive material.[28] Surface modification of pre-molded articles with fluorinated materials is also an expensive technique.[32] Blending of small amounts of fluorinated materials with nonfluorinated polymeric materials can enhance the surface properties by segregation of fluorinated materials on surface, however, thermodynamic separation of two phases can lead to poor mechanical properties.[28,33,34]

In our study, we modified the surface and bulk properties of PLA using telechelic poly(fluoroalkylene oxide)s with reactive hydroxyl groups as a macrointiator leading to polylactide-poly(fluoroalkylene oxide)s-polylactide block copolymer (FluoroPLA). The ability of the fluorinated segments to migrate towards/on the surface thereby enriching the surface with fluorine even at very low concentration has been very well demonstrated in previous studies [28,35-37] In this chapter we describe the scaled-up synthesis of FluoroPLA for different monomer/initiator concentrations and their thermal, dynamic mechanical and surface characterization.

4.2 Experimental Section

Materials

Poly(tetrafluoroethylene oxide-*co*-difluoromethylene oxide) α,ω-diol (Fomblin® Z DOL) (Perfluoropolyether, PFPE) with number average molecular weight of 1500, 2000, 4200 g mol^{-1} was generously donated by Solvay-Solexis (Italy). PFPE used were colorless clear liquids with a density of 1.8 g cm^{-3}, x/y≈1 and a functionality of ~ 1.8-1.9 with following chemical structure:

$$HO\text{-}CH_2\text{-}CF_2\text{-}(CF_2\text{-}CF_2\text{-}O)_x\text{-}(CF_2\text{-}O)_y\text{-}CF_2\text{-}CH_2\text{-}OH \equiv (HO\text{-}PFPE\text{-}OH).$$

L-Lactide (LA) was generously donated by Poly-Med Inc. (Pendleton, SC) and was recrystallized from ethyl acetate and vacuum dried to remove solvent and moisture. Stannous ethylhexanoate ($Sn(Oct)_2$) was purchased from Sigma Aldrich (United States) and was used as received. All other chemicals and reagents were purchased from Fisher or Sigma Aldrich and were used as received unless otherwise stated.

Synthesis of Homopolymer and Block Copolymer

A solution of 10 ml of toluene, 0.42g of $Sn(Oct)_2$, and 5 g of PFPE was prepared and shaken well. Then L-Lactide (100g) and the above mixture were added to the reaction vessel, sealed and blanketed with the inert (argon) atmosphere. The temperature was gradually (~2 °C/min) raised to 130 °C, and held for 24 hrs. The reaction mixture was slowly stirred at 20 rpm throughout the polymerization process. After polymerization, the reactor was allowed to cool and a solid light yellow mass was removed by opening the

reactor. The reaction product was then dissolved in and diluted with chloroform (1000 cm^3) followed by drop-wise precipitation in swirling methanol (~500 cm^3) at room temperature. The precipitated material was then dried under vacuum at 70 °C for one hour. Various batches of the copolymer of PLA and PFPE were prepared with ~5 wt% PFPE of different molecular weights (Mn= 1.5, 2.0, 4.2 kg mol^{-1}). In the following discussion the abbreviation FluoroPLA**x(y)** for copolymers contains two numbers where the '**x**' represents the percentage of PFPE in the feed and the '**y**' (in parenthesis) represents the number average molecular weight (by NMR) of PFPE will be used. A control PLA homopolymer batch was synthesized without any PFPE in the above mentioned reaction mixture.

Characterization

The number and weight average molecular weights of all of the polymers were characterized using a Waters "Breeze" GPC system (Waters, Milford, MA) interfaced with a Polymer Lab (Amherst, MA) PL-ELS 2100 detector. Two Waters columns were used in series (Styragel HR4E & HR5E). The mobile phase was chloroform (Burdick & Jackson, HPLC grade) at 1 cm^3/min. Polystyrene standards (Polysciences, Inc., Warrington, PA) of number average molecular weights 1,000,000; 600,000; 400,000; 200,000; 105,200; 50,000; 20,000; 4,000; 436 Dalton (Polydispersity Index ≤1.1) were used to calibrate the system.

^{19}F NMR spectra were obtained using a JEOL (Tokyo, Japan) Eclipse+ 300 MHz NMR spectrometer. Highly concentrated solutions (~10 (w/v) %) of polymer in deuterated chloroform were placed in 5 mm NMR tubes and 128 scans were collected. Trichlorofluoromethane ($CFCl_3$) was used as internal reference (0 ppm).

Differential Scanning Calorimentry (DSC) analysis was conducted using a TA Instruments (New Castle, Delaware) Q1000 DSC. Data was analyzed using TA Instruments Universal Analysis 2000 version 4.1D software. The samples (6-8 mg in standard aluminum pans) were initially heated to 225 °C to erase the thermal history and then cooled to -50 °C, and finally heated from -50 °C to 225 °C. A heating rate of 10 °C was used for all segments mentioned above. The glass transition temperatures were obtained as the inflection point of the step transition. Temperature values of the endothermic and exothermic peak maxima's were considered as melting and crystallization temperatures, and the integral of the peak areas was used to calculate heats of fusion and crystallization respectively.

Thermal Gravimetric Analysis (TGA) was conducted using a TA Instruments (New Castle, Delaware) 2950 TGA. Data was analyzed using TA Instruments Universal Analysis 2000 version 4.1D software. Samples were heated at the rate of 10 °C/min from room temperature to 400 °C under a nitrogen purge.

Diffraction patterns of polymers were collected at room temperature using SCINTAG XDS 2000 (Scintag, Inc., Cupertino, CA) diffractometer equipped with Cu Kα radiation at a wavelength of 1.54 Å. The instrument was operated at 40 kV and 40 mA with a collimator diameter of 0.5 mm. Solution-cast polymer films were scanned at 2 °/min (2θ value) from 6 ° to 60 °. The percent crystallinity was calculated by dividing the total counts under crystalline peaks by total area under the curve. Data were analyzed using DMSNT™ version 1.37 software.

Dynamic Mechanical Analysis (DMA) was performed using a DMS 210 Tension Module (Seiko Instruments Inc., Japan) with specimen dimensions of 40 mm x 10 mm and an effective gauge length of 20 mm. Samples were evaluated over a temperature range of -

130 °C to 125 °C at a heating rate of 2 °C min^{-1} at a frequency of 1 Hz and a deformation amplitude of 10 μm. Data were analyzed using EXSTAR6000 software.

Silicon wafers were oxidized by immersion in the pirana solution (3 part 95-98% H_2SO_4 + 1 part 30% H_2O_2) at 80 °C for 45 minutes. The thickness of the resultant SiO_2 layer was measured by ellipsometry and found to be ~ 1.4 nm. The solutions of 2 % (w/v) homopolymer and copolymer in chloroform were prepared and filtered through a Whatman 0.2 μm polytetrafluoroethylene membrane syringe filter. Dip coating of oxidized silicon wafers were carried out using a dip coater (Mayer Feintechnik D-3400, Göttingen, Germany). Dip coated samples were air dried and then the film thickness was measured using ellipsometry.

A Dimension 3100 (Veeco Inc., Woodbury, NY) atomic force microscope (AFM) equipped with Nanoscope IIIa controller was used to image the surface of the dip-coated polymer film on silicon wafers. All AFM characterization experiments were performed using a silicon AFM tip (MicroMash Inc., nominal force constant 40 N/m, tip radius <10 nm) in the non-contact (tapping) mode.

Static contact angle measurements were performed using the sessile drop method on a Drop Shape Analysis (KRÜSS Instruments, Hamburg, Germany) system. Liquid drops with an average volume between 5 to 10 μL were placed on the dip coated polymer films and the equilibrium contact angles were measured after an equilibration time of 30 seconds.

4.3 Results and Discussion

Synthesis, Mechanism and Molecular Properties

The synthesis of ABA triblock copolymer of PFPE and PLA was carried out by ROP of L-lactide using $Sn(Oct)_2$ as a catalyst/initiator. $Sn(Oct)_2$ is an effective catalyst for ROP of lactones and widely accepted as a food additive or contaminant in PLA in pharmaceutical applications.[2,38] Two series of polymerizations (with and without PFPE) were conducted. Homopolymerization was carried out without PFPE, and impurities such as water, lactic acid, lactoyl lactic acid acted as initiators.[24] Copolymerization were performed with ~5 wt% PFPE of different molecular weights and the molar concentration of PFPE varies depending on its molecular weights. All polymerizations were carried out at 130 °C for 24 hrs under 18-20 psi of argon gas. The overall reaction of the copolymerization is shown in Scheme 4.1 and the effect of different PFPE loading on thermal and surface properties copolymers is already reported.[39]

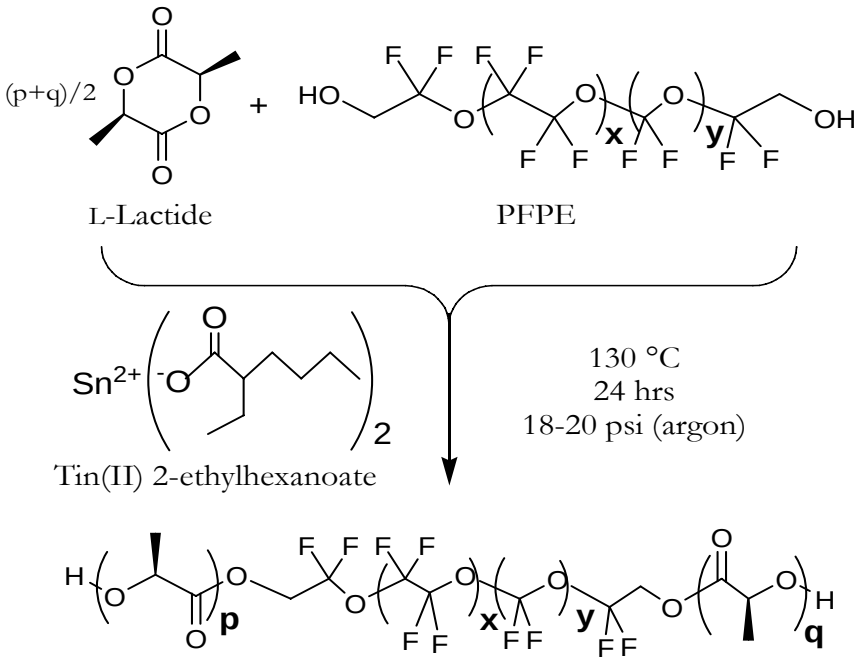

FluoroPLA
(PLA-PFPE-PLA Block Copolymer)

Scheme 4.1. Ring-opening polymerization of L-Lactide with $Sn(Oct)_2$ as catalyst/initiator and PFPE as macro-initiator.

Controlled ROP of six and seven membered cyclic esters can be carried out by using alkoxides formed by the reaction of carboxylate and hydroxyl group containing species.[16] Propagation takes place by nucleophilic attack of the alcoholate active species at the ester group leading to an acyl-oxygen bond scission.[40] Hydroxyl group containing species, in addition to their initiator behavior, can also act as transfer agents resulting in broadening of the molecular weight distribution of the resultant polymer.[41,42] Many parameters such as composition of feed, temperature of polymerization, solvent, extent of conversion, and relative rate of reactions (Scheme 4.2) determines the various steps involved in the reaction

mechanism. A few of the important steps involved in the ROP of lactide by the insertion mechanism are shown in Scheme 4.2 and more detailed mechanisms can be found in the literature.[16,42-44]

1. $Sn(Oct)_2$ + HO-PFPE-OH → Oct-Sn-O-PFPE-OH + OctH

2. $Sn(Oct)_2$ + Oct-Sn-O-PFPE-OH → Oct-Sn-O-PFPE-O-Sn-Oct + OctH

3. Oct-Sn-O-PFPE-O-Sn-Oct + (p+q)LA →

   Oct-Sn-$(LA)_p$-O-PFPE-O-$(LA)_q$-Sn-Oct

4. Oct-Sn-$(LA)_p$-O-PFPE-O-$(LA)_q$-Sn-Oct + OctH →

   H-$(LA)_p$-O-PFPE-O-$(LA)_q$-H + $Sn(Oct)_2$

Scheme 4.2. Important steps involved in reaction mechanism for the PLA-PFPE-PLA block copolymer.

There is the possibility of the formation of diblock to multiblock copolymers depending on other combinations of species shown in Scheme 4.2. A schematic representation of the A-B-A type triblock of PLA (A) and PFPE (B) is shown in Figure 4.2. A higher hydroxyl content of the initiator molecule can accelerate the polymerization rate and result in different moieties with PLA blocks.[45]

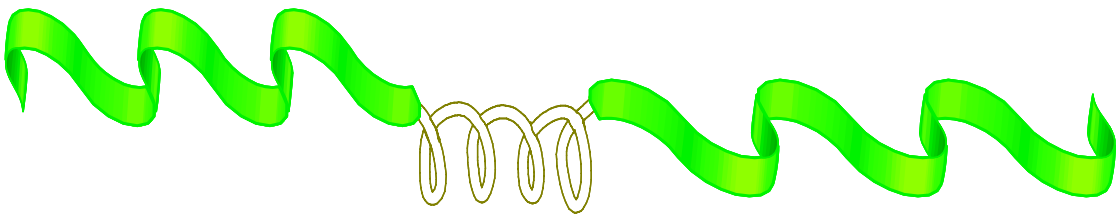

Figure 4.2. Schematic representation of A-B-A type block copolymer of PLA (A) and PFPE (B).

The effect of the initial molar concentration of $[PFPE]_0$ for a fixed $[Sn(Oct)2]_0$, on the molar masses and molar distribution of resultant polymer were studied. The dependence of molecular weight of resultant polymer on $[PFPE]_0$ is shown in Figure 4.3. As $[PFPE]_0$ increases, molecular weights decrease and PLA (homopolymer) elutes first in the GPC analysis, followed by FluoroPLA5(4.2k), FluoroPLA5(2.0k), FluoroPLA5(1.5k) with higher elution times. The elution peaks have similar shapes which are indicative of similar distribution of molar masses. For $[PFPE]_0$ from 0 to 4.6 x 10^{-3} mole, molecular weight (Mn) decreases from 144 x 10^3 g mol^{-1} (PLA) to 68 x 10^3 g mol^{-1} (FluoroPLA5(1.5k)) as shown in Table 4.1, suggesting more active initiating species are formed with the higher $[PFPE]_0$ resulting in lower molecular weight of polymerization products. The negligible effect of $[PFPE]_0$ on distribution of molar masses suggests that polymerization proceeds by similar mechanisms in case of all the polymers. If the ratio $[PFPE]_0/[LA]_0$ is higher than catalytic amounts, then the molecular weight decreases below the critical molecular weight and the molecular weight based properties are adversely affected.

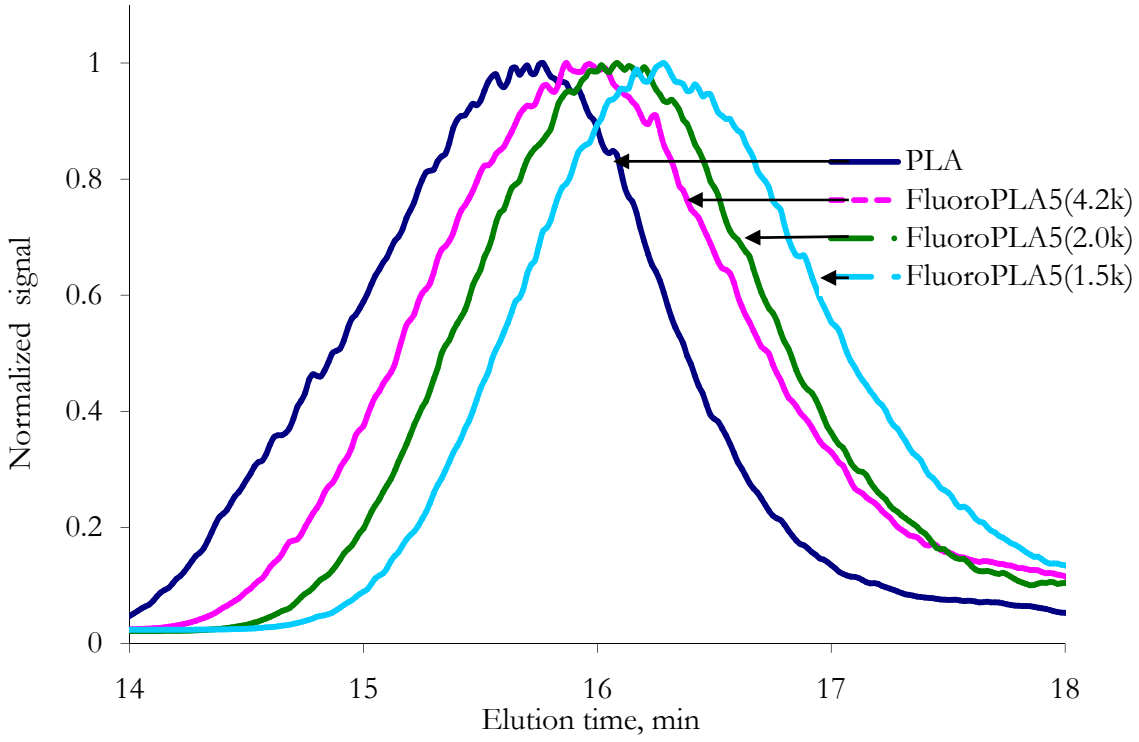

Figure 4.3. Gel permeation chromatographs for PLA and FluoroPLAs.

Molar ratios of reactants in feed and resulting molecular weights from chromatographic analysis are summarized in Table 4.1. For fixed molar amounts of LA (1 mole) and $Sn(Oct)_2$ (1.5 x 10^{-3} mole), as the PFPE content increases from 0 to 4.6 x 10^{-3} mole, Mn decreases from 144 x 10^3 g mol^{-1} (PLA) to 68 x 10^3 g mol^{-1} (FluoroPLA5(1.5k)) with polydispersity index (PDI) in the range of 1.6-1.8. The theoretical molecular weight (Mn_T) was obtained using equation 4.1 with assumptions that all hydroxyl groups participate as initiators and remain as part of the polymer chain and no other reactant or existing impurities act as initiators.[46]

$$Mn_T = \left[{}^{LA}\Big/_{\left\{\frac{PFPE}{2}\right\}} \right]_0 \times \{Mol.wt.of\ Lactide\ unit\} + Mol.wt.of\ PFPE \quad 4.1.$$

Table 4.1. Molar ratio of monomer, macro-initiator and catalyst with molar masses and distribution of PLA and FluoroPLA.

Polymer	Molar Ratio	Molecular Weight		
	LA: PFPE : $Sn(Oct)_2$	Mn_E [a,c]	PDI [b,c]	Mn_T [d]
PLA	1 : 0.0000 : 0.0015	144	1.67	--
FluoroPLA5(4.2k)	1 : 0.0017 : 0.0015	95	1.76	173
FluoroPLA5(2.0k)	1 : 0.0037 : 0.0015	83	1.67	80
FluoroPLA5(1.5k)	1 : 0.0046 : 0.0015	68	1.63	64

[a] Mn values are expressed in kD; [b] Polydispersity Index (PDI) = Mw/Mn; [c] By GPC;

[d] Theoretical mol wt (Mn_T), Mol wt of lactide – 144.1 g mol^{-1}.

The theoretical mol wt (Mn_T) for PLA is not shown in Table 4.1 because no initiator (PFPE) was added and only the impurities containing hydroxyl groups resulted in the polymerization of the LA. The concentration of hydroxyl group containing impurities was calculated from the molar mass of PLA and molecular weight of the resulting polymer under the assumption that each hydroxyl group initiates growth of a polymer chain and the impurities are monofunctional. The calculated impurity concentration was ~ 1 x 10^{-3} mole per mole of lactide (or reaction mixture) and it should be noted that the impurity concentration changes with the functionality of the impurities.

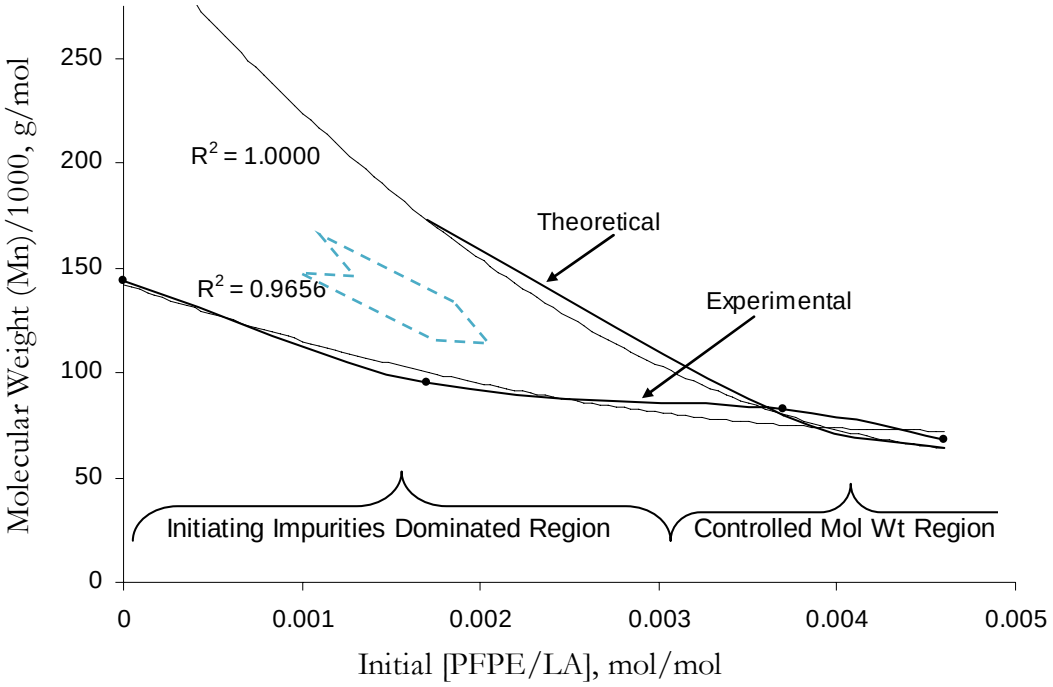

Figure 4.4. Comparison of experimentally obtained number average molecular weight with theoretically calculated values and their dependence on initial [PFPE/LA].

The theoretical and experimental number average molecular weights (Mn) are shown as a function of the initial ratio of [PFPE] to [LA] in Figure 4.4. Discrepancies in the theoretical and experimental Mn values are due to the presence of initiating impurities such as water, lactic acid, lactoyl lactic acid.[25,26] The difference in molecular weights decreases as the relative concentration of PFPE over impurities increases. For [PFPE] ≫ [Impurities], controlled molecular weight can be obtained but very high [PFPE] can have detrimental effects on the molecular weights. Hence, the concentration of PFPE should be carefully decided depending on the desired molecular weight and surface properties.

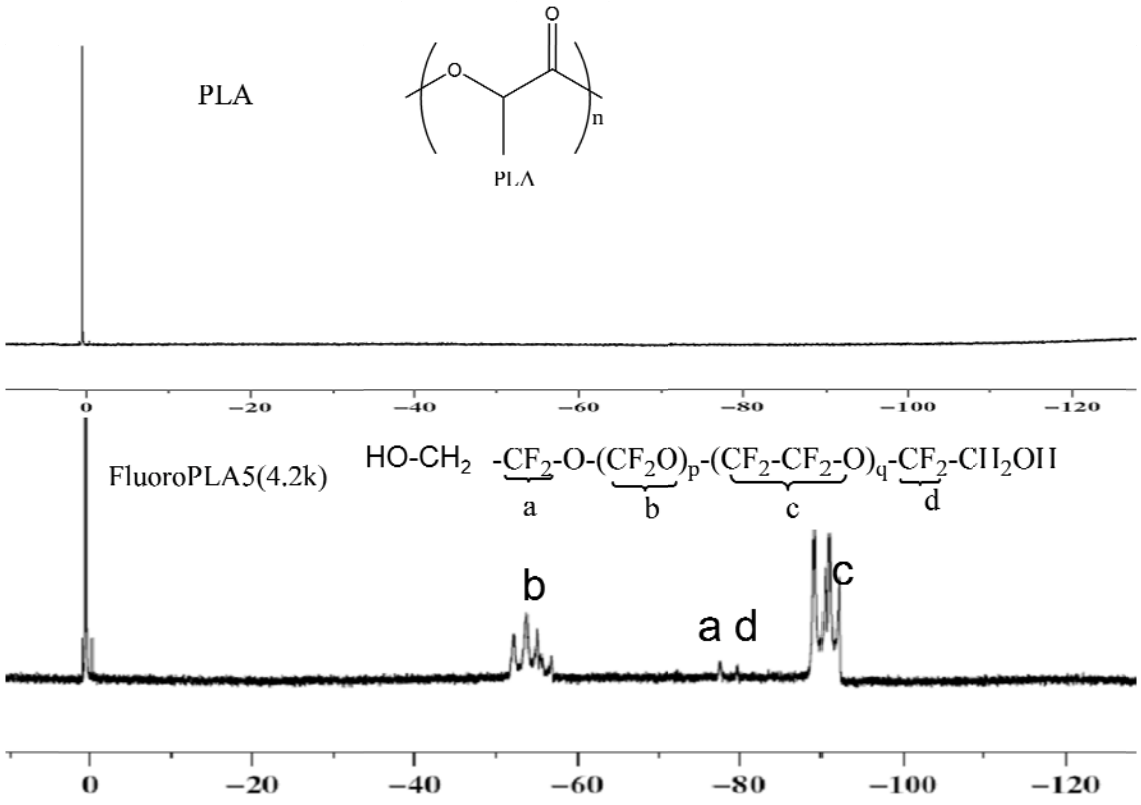

Figure 4.5. ^{19}F NMR spectra of PLA and FluoroPLA5(4.2k) in $CDCl_3$.

Confirmation of the presence of the PFPE block in copolymers was performed by obtaining ^{19}F NMR spectrum of the homopolymer and copolymer. Figure 4.5 shows the ^{19}F NMR spectrum for PLA and FluoroPLA5(4.2k). As expected the PLA does not show peaks in NMR spectrum suggesting the absence of fluorinated segments whereas the FluoroPLA5(4.2k) shows the appearance of peaks corresponding to the molecular structure of PFPE. Other FluoroPLAs show similar ^{19}F spectra and are shown in Appendix A. In PFPE, the perfluoromethylene oxide units shows three peaks (-51.5, -53.1, -54.8 ppm) while the perfluoroethylene oxide units show two peaks (-88.5, -90.1 ppm) and the two end groups

show peaks at -80.7, -82.7 ppm.[47] A shift in the end group peak positions are due to the linkage of the PFPE block to the PLA blocks. Chemical shifts of the end segments and the internal segments for PFPE are as summarized in Table 4.2.[47]

Table 4.2. ^{19}F chemical shift for end segments and internal segments of PFPE.

Segments	Chemical shift (ppm)
$-OCF_2OCF_2CH_2OH$	-80.7
$-OCF_2CF_2OCF_2CH_2OH$	-82.7
$-OCF_2OCF_2OCF_2O-$	-54.8
$-OCF_2CF_2OCF_2CF_2OCF_2CF_2O-$	-88.5

Thermal, Dynamic Mechanical and Crystallographic Properties

Representative differential scanning calorimetry (DSC) thermograms for PLA and FluoroPLAs are compared in Figure 4.6. The characteristic transitions such as the glass transition step, the exothermic crystallization peak and the endothermic melting peak can be observed in DSC traces. All the transitions are shifted to lower temperature from PLA to FluoroPLA5(4.2k) to FluoroPLA5(2.0k) to FluoroPLA5(1.5k). There is ca. 10 °C difference between all the transitions of PLA and FluoroPLA(1.5k).

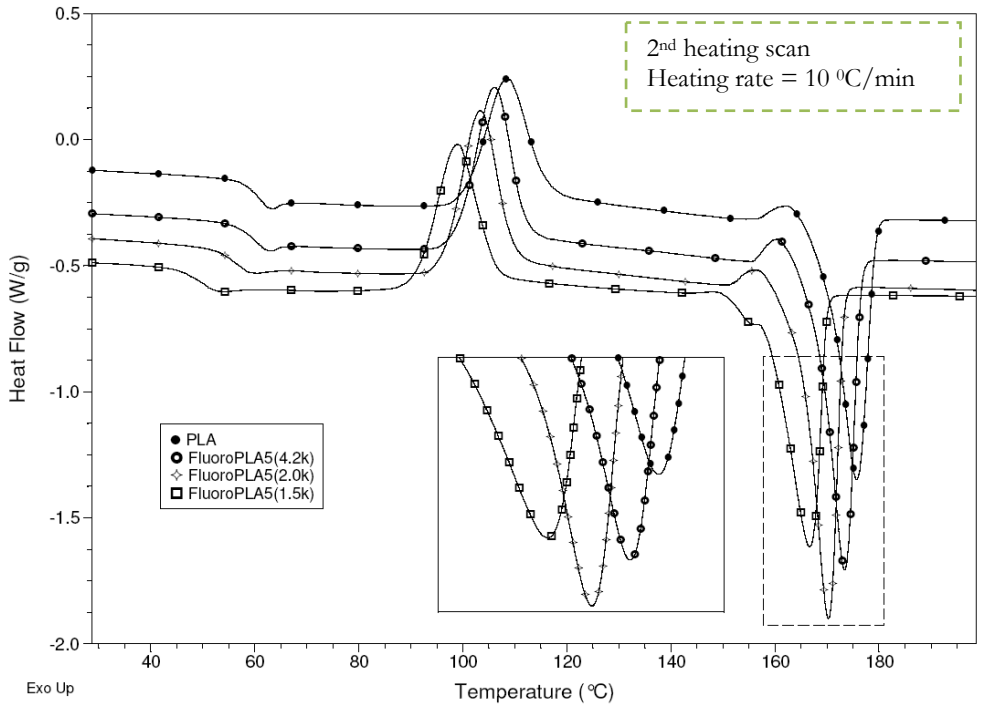

Figure 4.6. Thermal transitions of PLA and FluoroPLAs by differential scanning calorimetry.

Representative thermogravimetric analysis (TGA) thermograms for PLA, PFPE and FluoroPLAs are compared in Figure 4.7. The curve showing the lowest temperature weight loss is PFPE of molecular weight 4, 200 g mol^{-1} and is very similar to degradation of hydroxyl terminated PFPE in inert atmosphere results reported in earlier studies.[48] The thermal decomposition of PFPE results in low molecular weights gaseous products with the main component hexafluoropropylene (CF_2=CF-CF_3).[48] The onset of degradation is strongly dependent on the molecular weight of PFPE with the same chemical structure and molecular distribution.[48] The degradation begins at lower temperatures for lower molecular weight PFPE's.

Based on the TGA results PLA exhibited higher thermal stability than the FluoroPLAs. FluoroPLA5(1.5k) show the lowest stability among the FluoroPLAs. The decrease in thermal stability of FluoroPLAs can be attributed to the incorporation of the comparatively low thermal stability PFPE segments in PLA backbone. In addition, the differences observed in the degradation temperatures of FluoroPLAs could be due to the molecular weight effect on degradation of PFPE as previously discussed. A decrease of ca. 50 °C in the degradation temperatures (temperature at 10 % weight loss) of PLA and FluoroPLA5(1.5k) was observed.

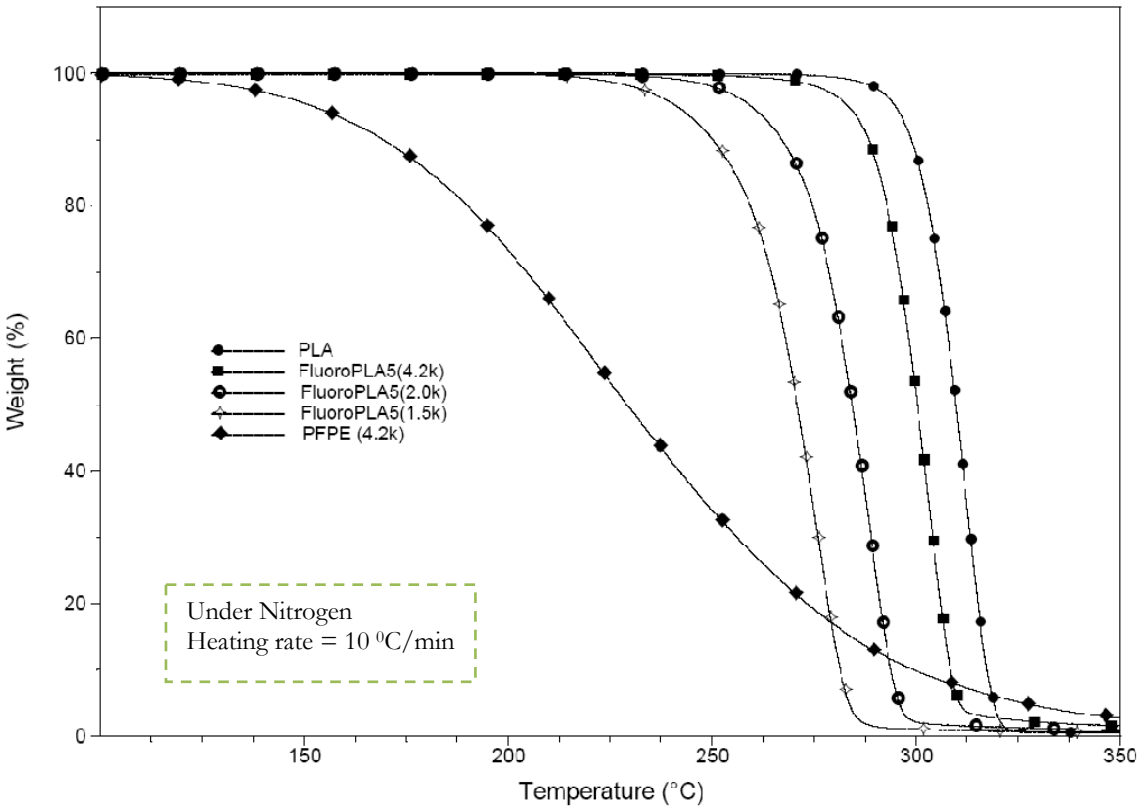

Figure 4.7. Thermal degradation behavior of PLA, FluoroPLAs and PFPE by thermogravimetric analysis.

Thermal properties of PLA and FluoroPLAs are shown in Table 4.3 and in Figure 4.8. The glass transition, melting, crystallization and the degradation temperatures for the FluoroPLAs depends on PFPE content in copolymer. With an increase in the PFPE content, the temperatures of all of the transitions are lowered.

Table 4.3. Thermal properties of PLA and FluoroPLAs. (T_g: glass transition temperature; T_m: Melting temperature; T_c: crystallization temperature; T_d: degradation temperature; ΔH_f: enthalpies of fusion; ΔH_C: enthalpy of crystallization); FluoroPLA**x(y)** where '**x**' represents the percentage of PFPE in the feed and the '**y**' (in parenthesis) represents the number average molecular weight of PFPE.

Polymer	Temperature (°C)				Heat (J/g)	
	T_g [a]	T_c [a]	T_m [a]	T_d [b]	ΔH_f [a]	ΔH_C [a]
PLA	61.4	108.5	175.7	298.9	43.0	28.8
FluoroPLA5(4.2k)	59.7	105.9	173.4	288.4	48.0	30.9
FluoroPLA5(2.0k)	55.7	103.3	170.3	267.2	48.4	31.5
FluoroPLA5(1.5k)	50.7	98.9	166.7	250.3	46.3	30.4

[a] DSC data for quenched samples heated at the rate of 10 °C/min, second heating cycle.

[b] TGA data for annealed films for 10% weight loss at heating rate of 10 °C/min.

As illustrated by the data in Table 4.3, a trend was observed that showed a decrease in all the transition temperatures with the increasing molar content of PFPE. The order of this decrease in transition temperatures for the PLA and FluoroPLAs was PLA >

FluoroPLA5(4.2k) > FluoroPLA5(2.0) > FluoroPLA5(1.5k). The glass transition temperature falls from ca. 61 °C for PLA to ca. 51 °C for FluoroPLA5(1.5k). PLA exhibits a crystallization temperature of ca. 109 °C whereas FluoroPLA5(1.5k) gave a crystallization temperature of ca. 99 °C only. Similarly, a decrease in melting temperature was observed. The transition temperatures for FluoroPLA5(4.2k) and FluoroPLA5(2.0k) falls between the values for PLA and FluoroPLA5(1.5k).

The relationship between the glass transition temperature and the molecular weight of polymer is well explained by Fox and Flory as shown in equation 4.2:[49,50]

$$T_g = T_{g\infty} - \frac{C}{M_n} \qquad 4.2.$$

where $T_{g\infty}$ is glass transition temperature at infinite molecular weight, C is a positive constant depending on the polymer. The dependence of T_g on the molecular weight is very strong below the critical molecular weight (M_C) of polymer (due to the large free volume associated with the chain ends) but above M_C, T_g is practically independent of molecular weight. The molecular weight of FluoroPLAs are much higher than the reported M_C (9.6×10^3 g mol^{-1}) for PLA.[51] Hence, the decrease in molecular weight from PLA to FluoroPLA5(1.5k) is not responsible for lowering of the T_g. This lower temperature shift in the T_g ($T_{g,PFPE} \sim -115$ °C, $T_{g,PLA} \sim 60$ °C)[52] can be explained by appreciable mixing between PFPE and PLA segments of phase-separated block copolymers as shown in equation 4.3.[53]

$$\frac{1}{T_g} = \frac{M_{PFPE}}{T_{g,PFPE}} + \frac{M_{PLA}}{T_{g,PLA}} \qquad 4.3.$$

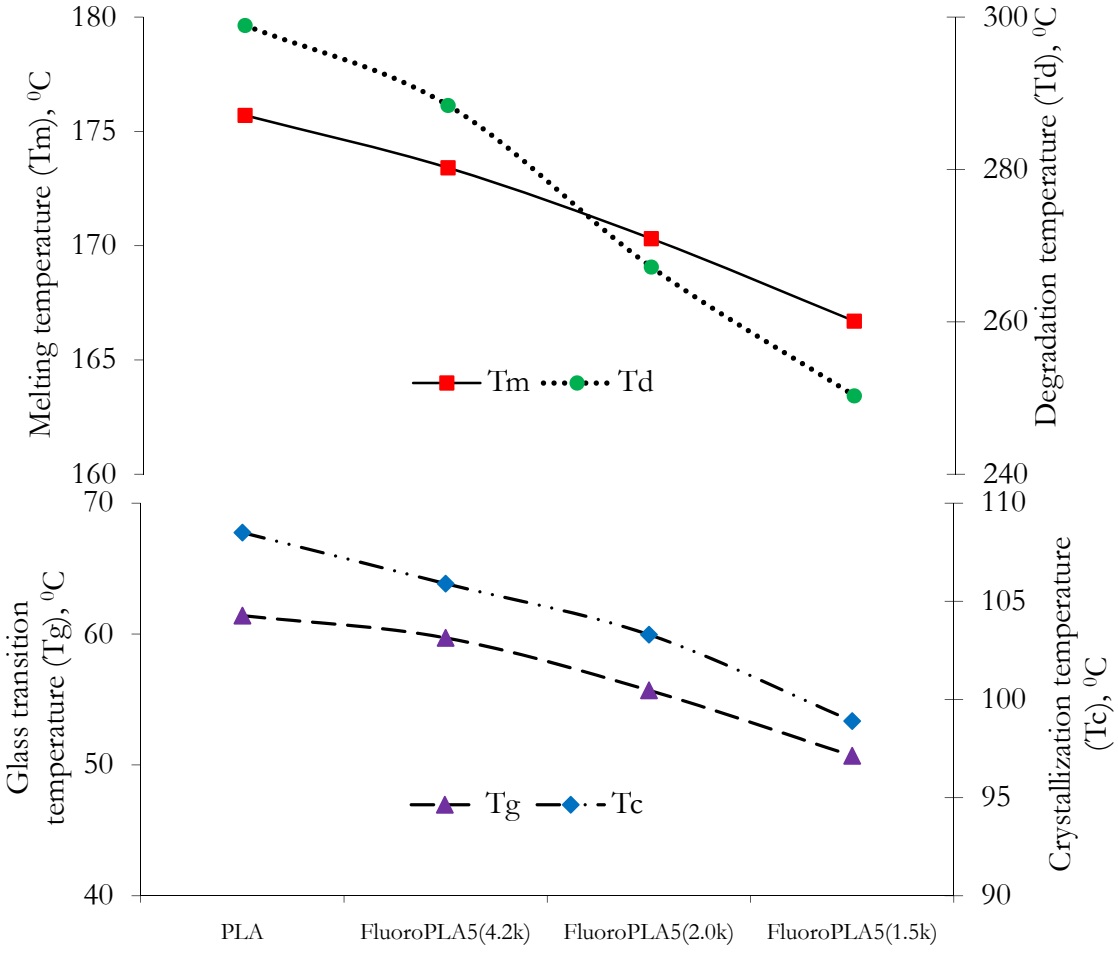

Figure 4.8. Thermal transitions of PLA and FluoroPLAs.

The depression in the melting point (T_m) can be explained by equation 4.4 where $T_{m,0}$ is the melting point of pure crystalline state (PLA homopolymer), ΔH_m is the heat of fusion

$$\frac{1}{T_m} - \frac{1}{T_{m,0}} = \frac{R}{\Delta H_m} M_{PFPE} \qquad 4.4.$$

per mole of crystalline (PLA) mers, R is molar gas constant and M_{PFPE} is mole fraction of noncrystallizable PFPE incorporated into crystalline PLA domains.[53,54]

The enthalpies of fusion and crystallization were higher for FluoroPLAs than for PLA due to the nucleating action of PFPE leading to a higher level and a higher rate of crystallization of FluoroPLAs.[55] This suggests that the activation energy of diffusion of PLA segments in crystallization site decreases as the PFPE molar content increases.[56] The reporting of percentage crystallinity of PLA and FluoroPLAs was avoided as it would be erroneous to use the same ΔH_m^0 (heat of fusion for 100% crystalline material) for the homopolymer and the copolymers. The depression in melting points of FluoroPLAs are responsible for the decrease in crystallization temperature as crystallization can occur only after the temperature has fallen below the theoretical melting temperature.[57] In comparison to PLA, the lower thermal stability of PFPE (Figure 4.7) shifts the FluoroPLAs degradation to lower temperatures. The degradation temperature of FluoroPLAs depends strongly on the content of PFPE.

The dynamic mechanical analysis (DMA) provides information about the mechanical properties of the polymer. Samples were subjected to oscillating stress along the axis (tension mode) and resulting deformation (strain) in the sample was measured. The complex modulus (E^*) is the ratio of the stress amplitude to the strain amplitude as shown in equation 4.5. In

$$|E^*| = \frac{\sigma_A}{\varepsilon_A} \qquad 4.5.$$

the linear-viscoelastic range, the stress response has the same frequency (ω) as the input deformation. The phase angle (δ) is the phase difference between the dynamic strain and the

dynamic stress due to the viscoelastic nature of materials. The complex modulus is composed of the storage modulus (E') (i.e. the real part) and the loss modulus (E'') (i.e. the

$$|E^*| = \sqrt{[E'(w)]^2 + [E''(w)]^2} \quad 4.6.$$

imaginary part) as shown in equation 4.6. The storage modulus (equation 4.7) represents the stiffness of a viscoelastic material and is proportional to the energy stored during a loading

$$E'(w) = |E^*| \cdot \cos\delta \quad 4.7.$$

$$E''(w) = |E^*| \cdot \sin\delta \quad 4.8.$$

cycle and the loss modulus (equation 4.8) is proportional to the energy dissipated (energy lost as heat) during a loading cycle. The elastic and viscous properties of polymer are related to the real and the imaginary parts of modulus respectively. The loss factor ($\tan\delta$) represents the mechanical damping or the internal friction in a viscoelastic system. As shown in equation 4.9, the loss factor is the ratio of energy loss to recoverable energy.[57]

$$\tan\delta = \frac{\sin\delta}{\cos\delta} = \frac{E''(w)}{E'(w)} \quad 4.9.$$

Figure 4.9 shows the plot of storage moduli of PLA and FluoroPLAs as a function of temperature. Analysis was performed on annealed (annealing temperature 90 °C) solution cast films from ~ 2% chloroform solution of PLA and FluoroPLAs. At low temperatures, the storage moduli of FluoroPLAs are higher than that of PLA. FluoroPLA5(1.5k) shows the highest storage modulus (>4.5 GPa above -125 °C) which is about 1 GPa higher than that of PLA. Below the glass transition temperature, the storage modulus of PLA remains constant whereas the modulus of FluoroPLA decreases gradually with temperature. This is possibly due to the presence of amorphous PFPE segments (which are above their glass transition temperature) in the FluoroPLAs. The softening of the amorphous domains in the

glass transition region (60-80 °C) results in a sharp decrease in storage moduli of the homopolymer and the block copolymers.

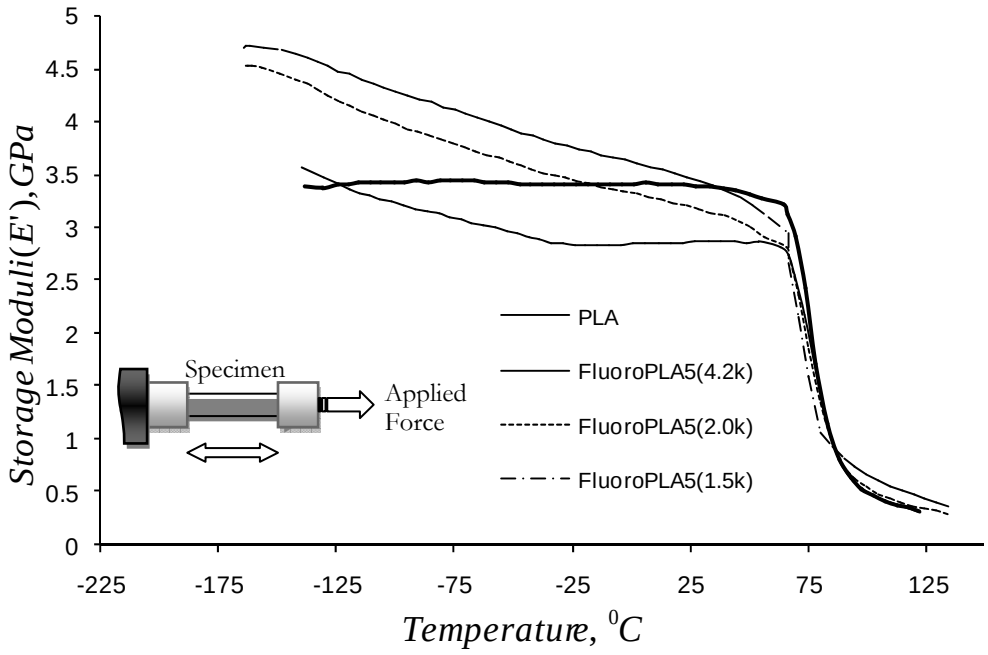

Figure 4.9. Storage Moduli (***E***′) of PLA and FluoroPLAs.

Loss moduli of PLA and FluoroPLAs are shown in Figure 4.10. In the glass transition region, a decrease in peak area (area under the peak) is noted for the FluoroPLAs as compared with the PLA. The FluoroPLA5(1.5k) shows the smallest peak area. It can be concluded that as PFPE content increases, the peak height and area decreases. Figure 4.11 shows the plot of the loss factor against temperature in the upper transition region (PLA, α relaxation) and Figure 4.12 shows the plot of the loss factor against temperature in the lower transition region (PFPE, α relaxation). The loss modulus and loss factor maxima were found in a narrow temperature range of 75-80 °C for both PLA and the FluoroPLAs. The

relaxation transitions found in the lower temperature region (-150 °C to -25 °C) are possibly the contributions from α relaxation of the PFPE (-120 °C to -90 °C)[52,58,59] and the broad β relaxation of PLA (~ -50 °C).[60]

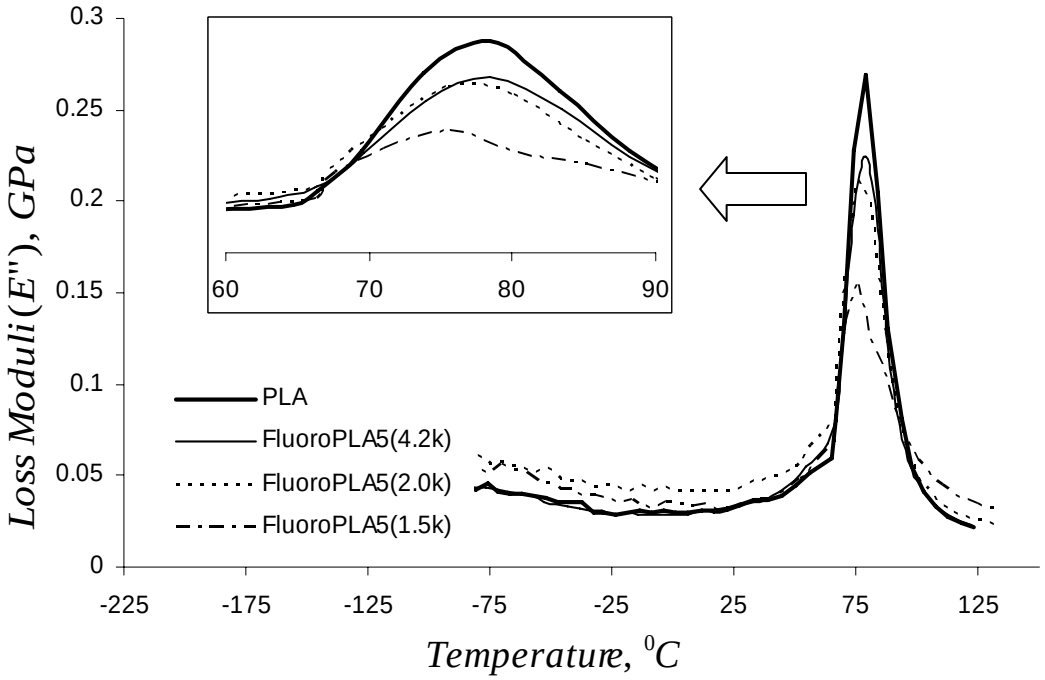

Figure 4.10. Loss Moduli (E'') of PLA and FluoroPLAs.

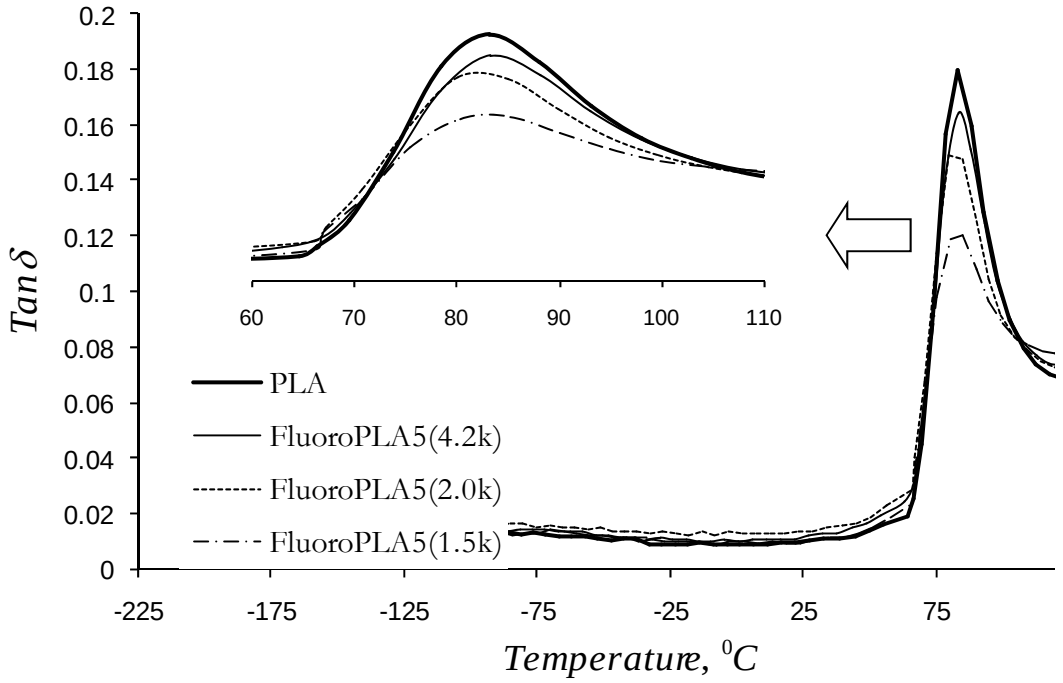

Figure 4.11. Loss factor of PLA and FluoroPLAs in higher transition regions.

The change in magnitude of the loss modulus or the loss factor (which occurs in the same sequence) is indicative of a difference in crystallinity.[57] From the loss modulus or the loss factor graph, it is very clear that the magnitudes of peaks of FluoroPLAs are smaller than the magnitude PLA peak and this observation suggests that the FluoroPLAs are more crystalline than the PLA. This phenomenon is supportive of the higher enthalpies of fusion and crystallization of the copolymer. Among the FluoroPLAs, FluoroPLA5(1.5k) shows smallest loss factor/loss modulus peak and hence the FluoroPLA5(1.5k) is the most crystalline polymer among the three FluoroPLAs.

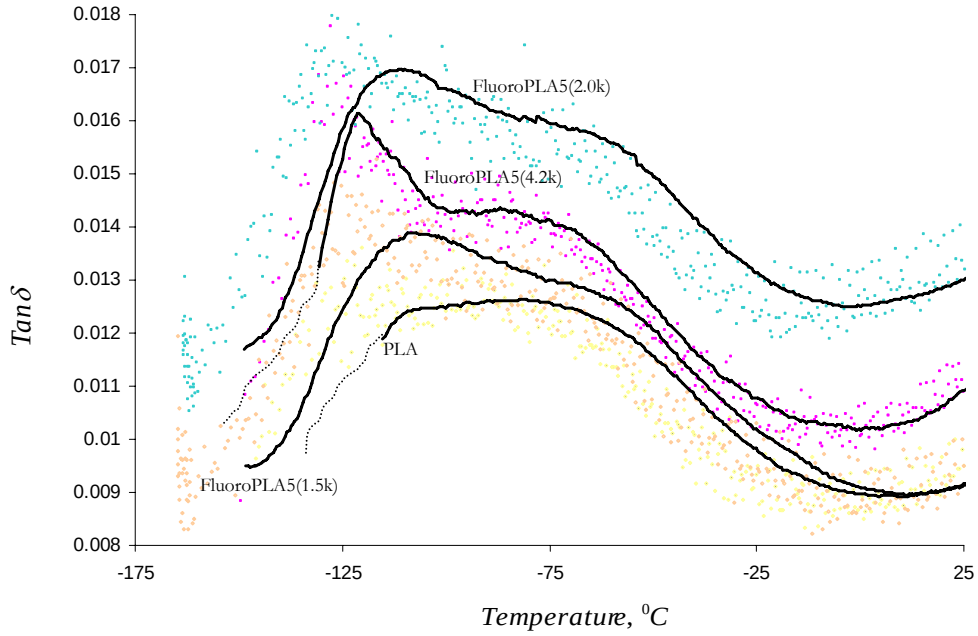

Figure 4.12. Loss factor (Tanδ) of PLA and FluoroPLAs in the lower temperature region. (Dots are data points) Solid lines are the moving average trendlines with different periods fitted to data. FluoroPLA5(4.2k) and PLA trendlines are extended in the lower region based on data points.

Wide-angle x-ray diffraction (WAXD) analysis of annealed PLA and FluoroPLAs are shown in Figure 4.13. The PLA and the FluoroPLAs exhibit diffraction peaks at 2θ values of 14.7, 16.5-16.7, 19.0 and 22.2 which are assigned to 010, 200/110, 203, and 015, respectively, and characteristic of the PLA α-crystal orthorhombic cell with a=1.060 nm, b=0.605 nm, and c=2.880 nm.[13,61,62] This suggests that PLA and FluoroPLAs have similar crystal structures and it appears that there is no significant deformation in the crystal structure of PLA due to the incorporation of PFPE blocks. The WAXD analysis supports the observation by DSC and DMA that the FluoroPLAs are more crystalline than the PLA. The

FluoroPLA5(1.5k) shows the highest crystallinity of 44% (approx.) among the other FluoroPLAs and much higher than PLA which has crystallinity of 34% (approx.) which is close to the upper limit crystallinity of PLA reported in literature(0-37%)[63].

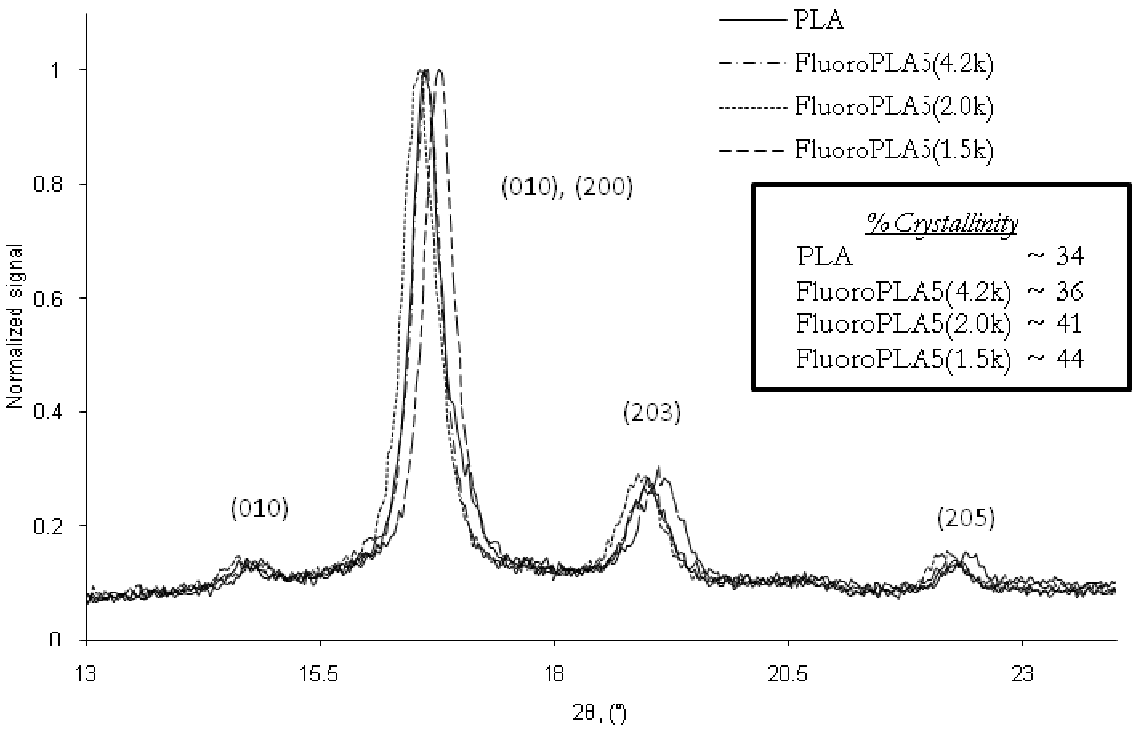

Figure 4.13. Wide angle X-ray diffraction plot of annealed PLA and FluoroPLAs films.

Surface Morphology and Properties

The atomic force microscope (AFM) analysis in the non-contact (tapping) mode was performed on the dip coated films. Figure 4.14 shows the surface morphology of PLA and FluoroPLAs. PLA shows a very flat morphology whereas the FluoroPLAs showed distinct morphology in comparison to PLA. The differences in the morphology of the FluoroPLAs copolymers themselves are not very obvious. The microphase separation or contrast

observed in the morphology of FluoroPLAs is possibly due to the well known fluoro-enrichment of the surface.

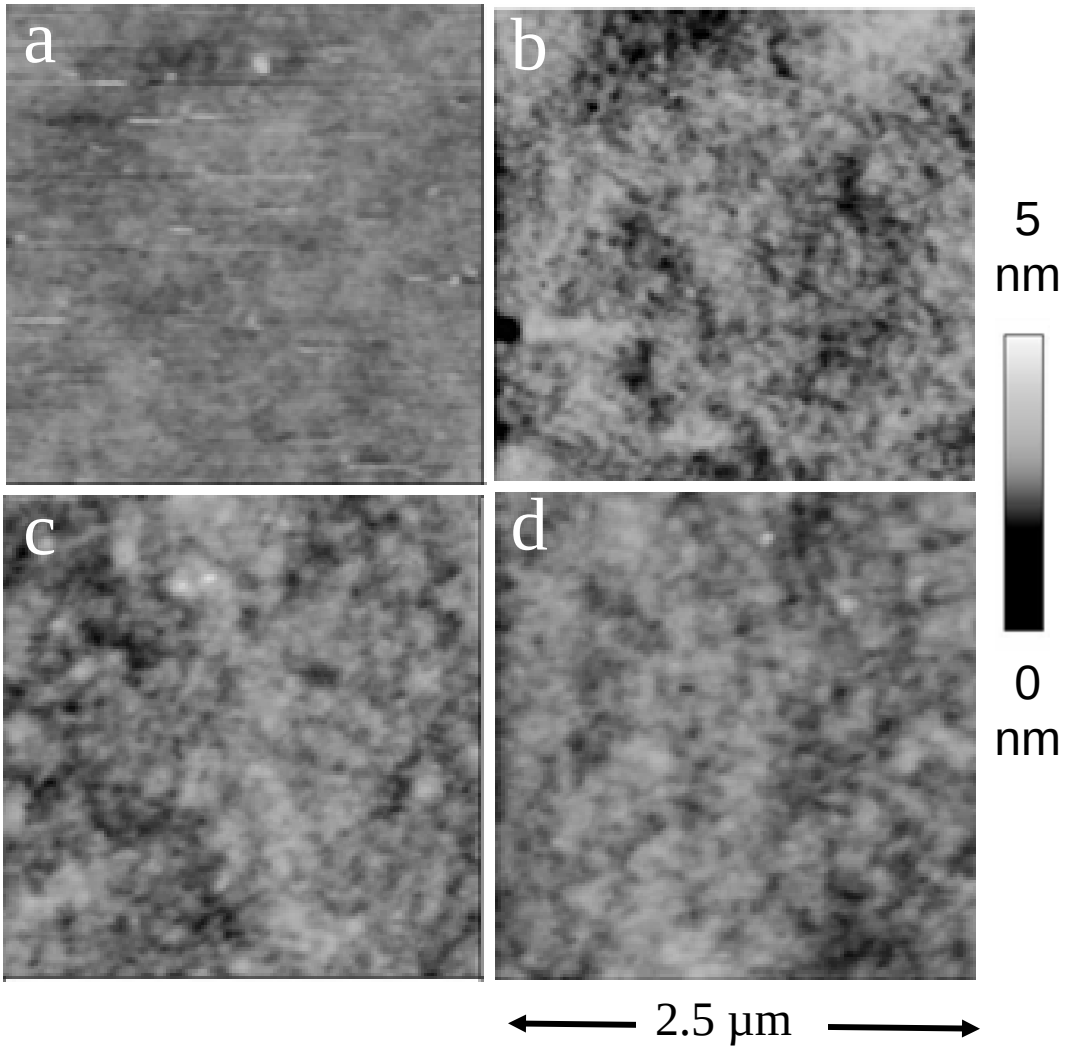

Figure 4.14. AFM topography images of dip-coated PLA (a), FluoroPLA5(4.2k) (b), FluoroPLA5(2.0k) (c) and FluoroPLA5(1.5k) (d). Pre-oxidized silicon wafers were dip-coated in 2% solutions of PLA and FluoroPLAs in chloroform.

Surface phenomenon such as adsorption, wetting and adhesion are governed by the surface energy of the materials. Polymers are low surface energy materials and direct determination of surface energy is difficult due to poor mobility of molecules in the solid state. The contact angle measurement on polymer surfaces with chosen liquids can be used to determine the surface energy of the polymer.[64] The Owens-Wendt-Rabel-Kaelble (WORK) method was used to investigate the surface energies of PLA and FluoroPLAs.

The evaluation of the surface energy can be performed using various methods as proposed by Neumann, Schultz, Fowkes, Good, Owens, Wu, Zisman, Young, Dupré and their coworkers.[65] The background of evaluation of the surface energy can be explained by combining the work of Fowkes, Good, Girifalco, Owens, Wendt, Rabel, Kaelble.[65-67]

The basic relationship between the interfacial tension between two phases (*s:solid, l:liquid*) given by the ANTONOW rule is the interfacial tension (γ_{sl}) of two phases as shown in equation 4.10. Good and Girifalco introduced an interaction parameter (φ) and proposed equation 4.11. The interaction parameter is a function of molecular size and can only be determined empirically and hence is not known before the measurement.[656464]

$$\gamma_{sl} = |\gamma_s - \gamma_l| \qquad 4.10.$$

$$\gamma_{sl} = \gamma_s + \gamma_l - 2 \cdot \varphi \sqrt{\gamma_s \cdot \gamma_l} \qquad 4.11.$$

Considering the contribution of dispersion forces at an interface, Fowkes suggested equation 4.12 for the calculation of surface energy. Combining Young's equation (equation 4.13) with equation 4.12 and rearranging, results in equation 4.14. With known γ_l, γ_l^d values, it is possible to approximately calculate the γ_s^d from a single measurement of the contact angle (θ) between the two phases.[66]

$$\gamma_{sl} = \gamma_s + \gamma_l - 2\sqrt{\gamma_s^d \cdot \gamma_l^d} \quad 4.12.$$

$$\gamma_s = \gamma_{sl} + \gamma_l \cdot (\cos\theta) \quad 4.13.$$

$$(1 + \cos\theta) = 2\sqrt{\gamma_s^d} \cdot \frac{\sqrt{\gamma_l^d}}{\gamma_l} \quad 4.14.$$

For cases where polar (non-dispersive) forces operate, equation 4.12 needs modification by incorporation of the polar component of surface energy. Based on Fowkes's theoretical consideration of attractive forces at interfaces, WORK suggested (equation 4.15) that the surface energy can be broken into its polar and dispersive components and that these components are independent and additive in nature.[65,66] The surface energies of solids and liquids can be presented in the form of equation 4.16 and equation 4.17 respectively.

$$\gamma = \gamma^d + \gamma^p \quad 4.15.$$

$$\gamma_s = \gamma_s^d + \gamma_s^p \quad 4.16.$$

$$\gamma_l = \gamma_l^d + \gamma_l^p \quad 4.17.$$

With the assumption that the interaction parameter $(\varphi) \approx 1$ in equation 4.11, WORK extended the equation 4.11 to the more general form as shown in equation 4.18.

$$\gamma_{sl} = \gamma_s + \gamma_l - 2\left(\sqrt{\gamma_s^d \cdot \gamma_l^d} + \sqrt{\gamma_s^p \cdot \gamma_l^p}\right) \quad 4.18.$$

Equation 4.18 combined with equation 4.13 results in equation 4.19 which upon rearrangement leads to equation 4.20.

$$\gamma_l \cdot (1 + \cos\theta) = 2\left(\sqrt{\gamma_s^d \cdot \gamma_l^d} + \sqrt{\gamma_s^p \cdot \gamma_l^p}\right) \quad 4.19.$$

$$\frac{(1+\cos\theta)}{2} \cdot \left(\frac{\gamma_l}{\sqrt{\gamma_l^d}}\right) = \sqrt{\gamma_s^d} + \sqrt{\gamma_s^p} \cdot \left(\frac{\sqrt{\gamma_l^p}}{\sqrt{\gamma_l^d}}\right) \quad 4.20.$$

By measuring the contact angle of a liquid with the known dispersive and polar components of surface energy on a polymer surface, the dispersive and polar components of surface energy of polymer can be evaluated from equation 4.20 which can be represented as a straight line equation (equation 4.21).

$$Y = c + mX \quad 4.21.$$

From the plot of Y versus X (from equation 4.22), the intercept and slope of the line can be interpreted and thus the square of the intercept and slope provides γ_s^d and γ_s^p for the polymer.

$$Y = \frac{\gamma_l \cdot (1+\cos\theta)}{2\sqrt{\gamma_l^d}} \qquad and \qquad X = \frac{\sqrt{\gamma_l^p}}{\sqrt{\gamma_l^d}} \quad 4.22.$$

$$c^2 = \gamma_s^d \qquad and \qquad m^2 = \gamma_s^p \quad 4.23.$$

Owens and Wendt used only two test liquids where as Kaelble and Rabel used several liquids. The Kaelble method provides the average value of the surface energies from several pairs of liquids. Rabel used a regression method using several liquids.[656464] These

methods are in good agreement and can be used for low surface energy materials such as polymers.

Work of adhesion is the measure of attraction forces at an interface and can be defined as the work required to separate two phases thereby creating a unit area of two phases at the expense of a unit area of their interface. The W_A can be expressed in terms of surface energy components as shown in equation 4.24 and equation 4.25 and can also be expressed as a function of contact angle as shown in equation 4.26.[68]

$$W_A = \gamma_s + \gamma_l - \gamma_{sl} \quad 4.24.$$

$$W_A = 2\left(\sqrt{\gamma_s^d \cdot \gamma_l^d} + \sqrt{\gamma_s^p \cdot \gamma_l^p}\right) \quad 4.25.$$

$$W_A = \gamma_l(1 + \cos\theta) \quad 4.26.$$

The surface energies of PLA and FluoroPLAs were evaluated by measuring the contact angles of five liquids on dip coated polymer films. Five liquids were selected to cover the whole range of polarity from highly polar to non polar (water, glycerol, formamide, methylene iodide, n-hexadecane). The dispersive and polar components of the surface energy for the five selected liquids are summarized in Table 4.4.

Table 4.4. Dispersive and Polar Components of Liquid Surface Energy at 20 °C.[67]

Liquid	Surface Energy of Liquids (mN/m)		
	Dispersive	Polar	Total
Water	21.8	51.0	72.8
Glycerol	37.0	26.4	63.4
Formamide	39.5	18.7	58.2
Methylene Iodide	48.5	2.3	50.8
n-Hexadecane	27.6	0.0	27.6

Static contact angle measurements were performed using the sessile drop method with an equilibration time of 30 seconds. Figure 4.15 shows the plot of contact angles of five probe liquids on PLA and FluoroPLAs and the contact values for PLA and FluoroPLAs are summarized in Table 4.5. A significant difference in the contact angles of PLA and FluoroPLAs can be seen for all test liquids. FluoroPLAs showed higher contact angles than the PLA for all the liquids. Though there is not a significant difference between the contact angles among the FluoroPLAs.

Water has a relatively high surface tension (72 mN/m) and interfacial forces have a significant contribution from intermolecular forces such as hydrogen bonding. In the case of n-hexadecane, which has surface tension of 27 mN/m, only dispersion forces contribute to the interfacial tension. The highly polar water forms larger contact angles on FluoroPLAs surfaces as the interaction forces are very weak. However, in the case of PLA, intermolecular forces such as hydrogen bonding make strong interactions, thus, resulting in lower contact

angles. The difference in the contact angles of PLA and FluoroPLAs for liquids with different polarity was observed in the range of 30-40 °.

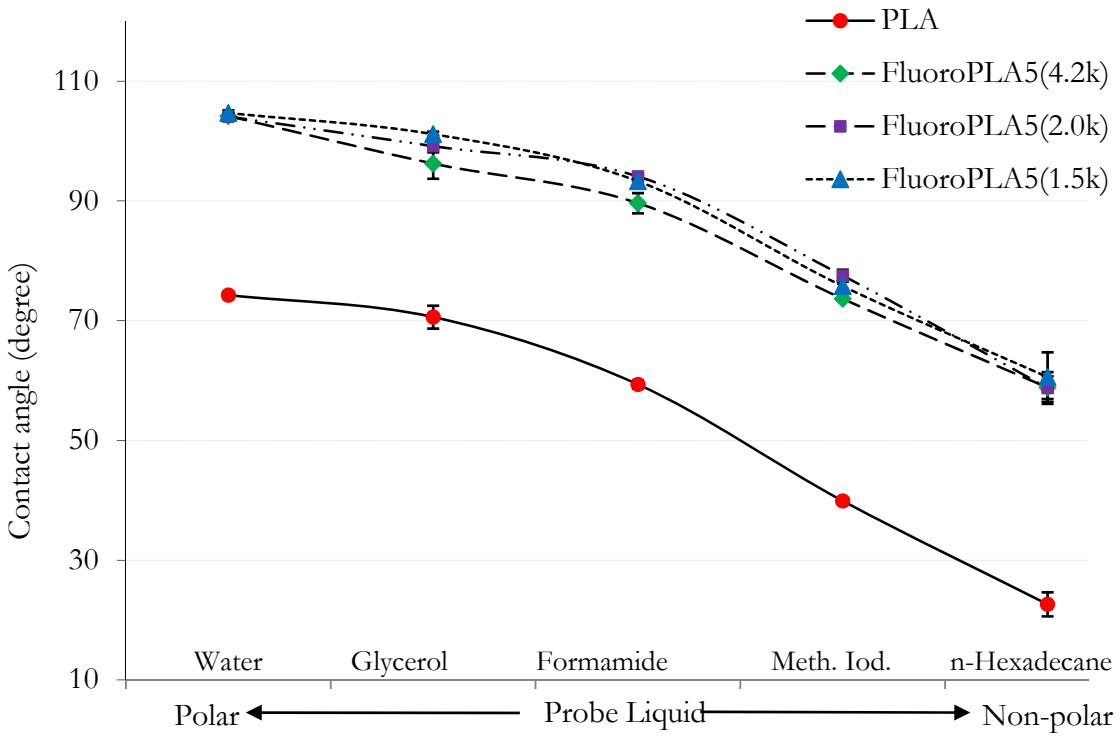

Figure 4.15. Contact angle of water, glycerol, formamide, methylene iodide and n-hexadecane on PLA and FluoroPLA dip coated on silicon wafers.

Table 4.5. Static contact angle values for PLA and FluoroPLAs.

Polymer	Contact angle in degrees (Mean[a] ± standard deviation)				
	Water	Glycerol	Formamide	Methylene Iodide	n-Hexadecane
PLA	74.3 ± 0.6	70.6 ± 1.9	59.4 ± 0.7	39.9 ± 0.3	22.6 ± 2.0
FluoroPLA5(4.2k)	104.2 ± 0.5	96.2 ± 2.5	89.6 ± 1.7	73.7 ± 0.3	58.8 ± 1.9
FluoroPLA5(2.0k)	104.1 ± 0.4	99.2 ± 1.0	94.1 ± 0.5	77.5 ± 1.0	58.8 ± 2.7
FluoroPLA5(1.5k)	104.7 ± 0.5	101.2 ± 0.4	93.3 ± 1.1	75.8 ± 0.8	60.6 ± 4.1

[a] Mean of at least 3 measurements.

Figure 4.16 illustrates the difference in the behavior of water on PLA and FluoroPLAs surfaces. Water forms a bead (θ>90 °) on FluoroPLA surfaces whereas a wetting phenomenon (θ>90 °) is observed on PLA films. The increase in contact angle of water on FluoroPLA is due to the segregation of PFPE segments on the film surface of films due to very low surface tension.[44]

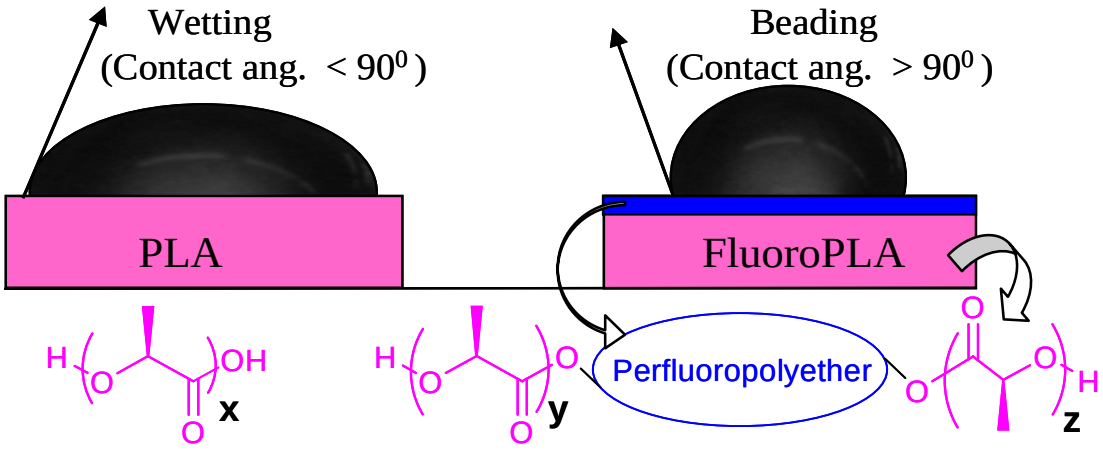

Figure 4.16. Schematic of surface properties of PLA and FluoroPLA. Low surface energy FluoroPLA shows a very high water contact angle.

The dispersive and polar components of the total surface energies of PLA and FluoroPLAs calculated by WORK equation are summarized in Table 4.6. The plots of $\frac{\gamma_l \cdot (1+\cos\theta)}{2\sqrt{\gamma_l^d}}$ vs $\frac{\sqrt{\gamma_l^p}}{\sqrt{\gamma_l^d}}$ for Rabel and Kaelble methods are shown in Appendix E and Appendix F, respectively. The two methods have good agreement and show that there is a significant difference in dispersive, polar and total surface energies of PLA and FluoroPLAs. For PLA, the dispersive component of surface energy by Kaelble and Rabel method was 29.7 mN/m and 26.9 mN/m respectively and the polar component of surface energy by Kaelble and Rabel method was 10.5 mN/m and 8.2 mN/m. For FluoroPLAs, the range of dispersive component of surface energy by Kaelble and Rabel method was 15.2-17.2 mN/m and 15.0-16.6 mN/m respectively and the range of polar component of surface energy by Kaelble and Rabel method was 1.7-2.2 mN/m and 1.1-1.2 mN/m. There is no considerable effect of incorporation of different block lengths of PFPE on the surface energies of FluoroPLAs

because the overall fluorine content of FluoroPLAs remains nearly the same irrespective of block lengths.

Figure 4.17 shows the plot of surface energies of PLA and FluoroPLAs by the Kaelble method. Significant drop in both the components of surface energies was observed from PLA to FluoroPLAs. The difference in surface energies of PLA and FluoroPLAs varied in the range of ca. 15-20 mN/m. The surface energies of FluoroPLAs are close to those obtained from fluorinated materials such as polytetrafluoroethylene (Teflon™).[69,70]

Table 4.6. Surface energy and its components for PLA and FluoroPLAs.

Polymer	Surface energy (mN/m)					
	Kaelble (Average)			Rabel (Regression)		
	Dispersive	Polar	Total	Dispersive	Polar	Total
PLA	29.7	10.5	40.2	26.9	8.2	35.1
FluoroPLA5(4.2k)	17.2	2.0	19.2	16.6	1.1	17.7
FluoroPLA5(2.0k)	15.2	1.7	16.8	15.0	1.2	16.2
FluoroPLA5(1.5k)	16.4	2.2	18.5	15.1	1.1	16.2

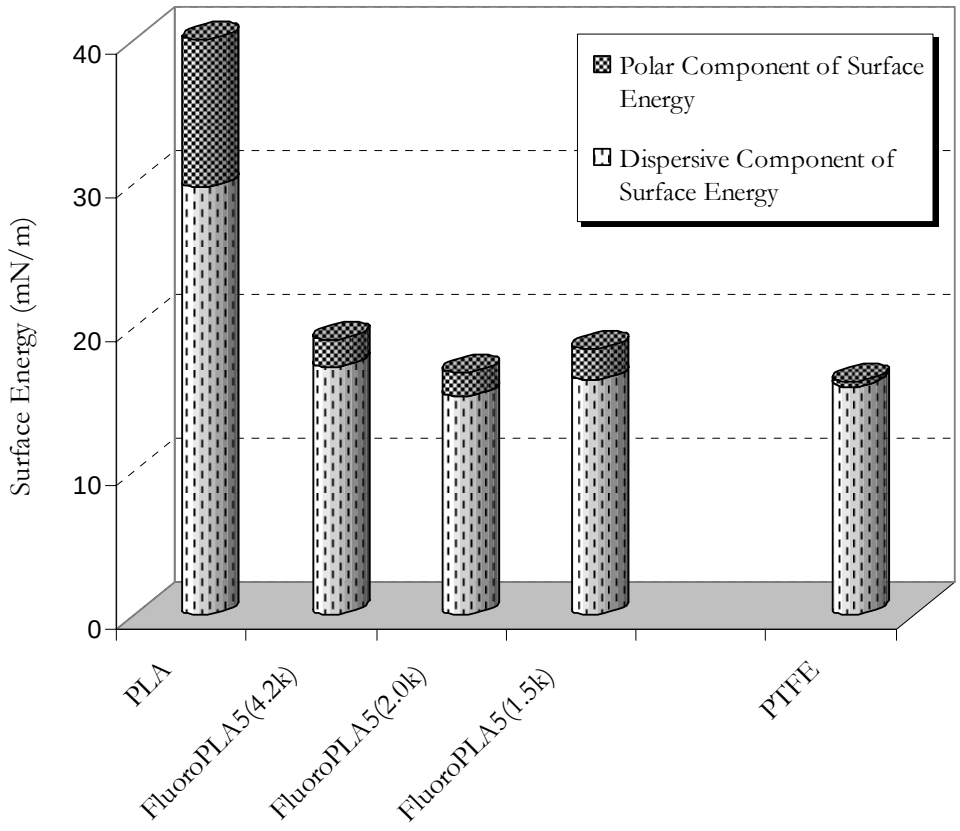

Figure 4.17. Surface free energy and its components for PLA, FluoroPLAs and PTFE by the Kaelble method.

The repellency of a liquid droplet from a polymer surface can be considered as the work of adhesion (W_A). The relation among the work of adhesion, the contact angle and the surface energy of probe liquids is as shown in equation 4.26. As the contact angle increases for a given test liquid, W_A decreases, and the surface becomes repellent in nature. Figure 4.18 shows W_A for PLA and FluoroPLAs using water, glycerol, formamide, methylene iodide, and n-hexadecane and calculated using equation 4.26 and the mean values of contact angle from Table 4.5. The work of adhesion for FluoroPLAs is lower than that of PLA in all five liquids.

For water, the difference between the works of adhesion of PLA and FluoroPLAs was ca. 40 mN/m. A similar difference was observed for glycerol. The difference decreases from formamide to methylene iodide to n-hexadecane. The lowest difference of ca. 15 mNm was observed in case of non-polar n-hexadecane as only the dispersive forces contribute. Hence FluoroPLAs have better hydrophobicity and lipopholicity than PLA.

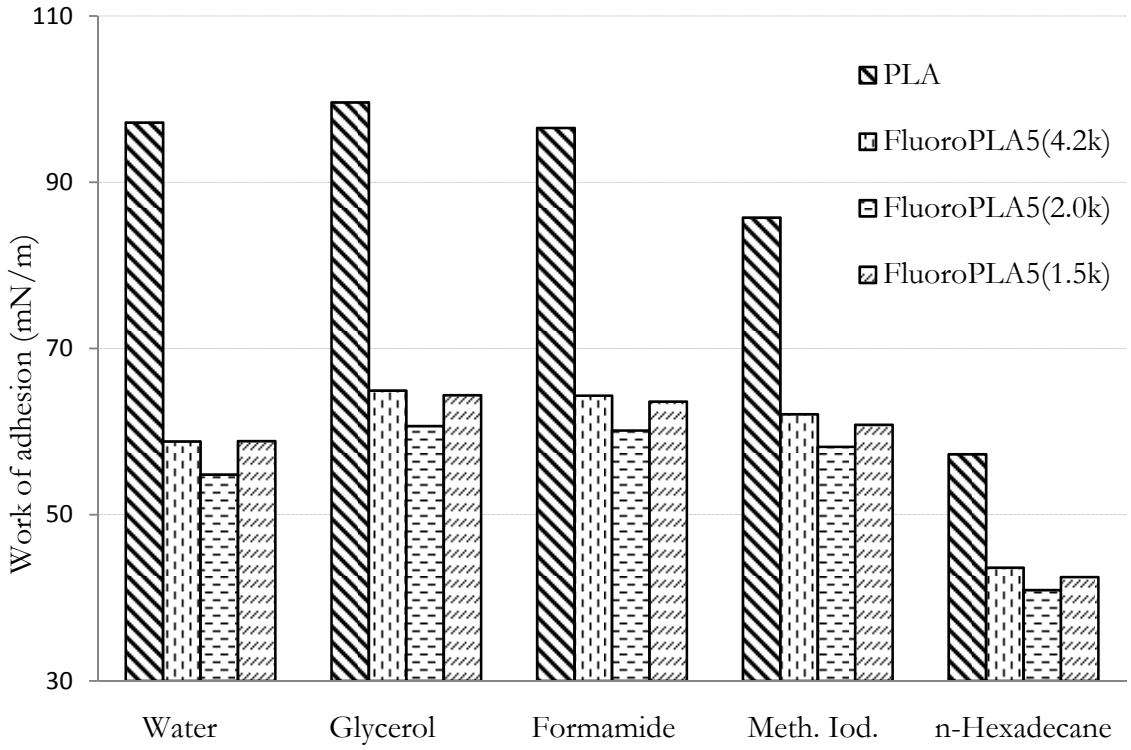

Figure 4.18. Work of adhesion for PLA & FluoroPLAs using water, glycerol, formamide, methylene iodide and n-hexadecane.

4.4 Conclusions

Scaled up synthesis of PLA and FluoroPLAs were successfully carried out by ring opening polymerization of lactide using telechelic hydroxyl terminated PFPE as macro-initiator and $Sn(Oct)_2$ as catalyst/initiator. High molecular weight (> 60,000 g mol^{-1}) copolymer (FluoroPLA) of PLA and PFPE were obtained with controlled distribution of molar masses. Molecular weights were dependent on the molar content of the PFPE in feed.

As expected, the copolymers showed lower glass transition, melting, and degradation temperatures than the homopolymer (PLA). These shifts in temperatures were due to incorporation of PFPE segments in molecular chains of PLA. The extent of lowering of the transition temperatures was strongly dependent on the molar content of PFPE in feed.

Surprisingly, FluoroPLAs showed higher heats of fusion and degrees of crystallization indicative of higher crystallinity and probably higher rates of crystallization than that of PLA. The increase in crystallization of FluoroPLAs are possibly due to the nucleating behavior of PFPE segments, which decreases the activation energy of diffusion of PLA segments at crystallization sites.

Incorporation of low energy segments in the PLA block modified its surface morphology and surface properties markedly. Surface energy dropped from 35-40 mN/m to 16-20 mN/m with very small amounts of PFPE. FluoroPLAs showed better hydrophobic and lipophobic properties than PLA.

4.5 References

1. Gross, R. A. & Kalra, B. Biodegradable Polymers for the Environment. *Science* **297**, 803 (2002).
2. Albertsson, A.-C. & Varma, I. K. Recent Developments in Ring Opening Polymerization of Lactones for Biomedical Applications. *Biomacromolecules* **4**, 1466-1486 (2003).
3. Sinclair, R. G. The Case for Poly(lactic acid) as a Commodity Packaging Plastic. *Journal of Macromolecular Science-Pure and Applied Chemistry* **A33**, 585-597 (1996).
4. Radano, C. P., Baker, G. L. & Smith, M. R. Stereoselective Polymerization of a Racemic Monomer with a Racemic Catalyst: Direct Preparation of the Polylactic Acid Stereocomplex from Racemic Lactide. *Journal of the American Chemical Society* **122**, 1552-1553 (2000).
5. Amass, W., Amass, A. & Tighe, B. A Review of Biodegradable Polymers: Uses, Current Developments in the Synthesis and Characterization of Biodegradable Polyesters, Blends of Biodegradable Polymers and Recent Advances in Biodegradation Studies. *Polymer International* **47**, 89-144 (1998).
6. Stefan Mecking. Nature or Petrochemistry? - Biologically Degradable Materials. *Angewandte Chemie International Edition* **43**, 1078-1085 (2004).
7. Mehta, R., Kumar, V., Bhunia, H. & Upadhyay, S. N. Synthesis of Poly(lactic acid): A Review. *Polymer Reviews* **45**, 325 - 349 (2005).
8. Huang, J., Lisowski, M. S., Runt, J., Hall, E. S., Kean, R. T., Buehler, N. & Lin, J. S. Crystallization and Microstructure of Poly(L-lactide-*co*-*meso*-lactide) Copolymers. *Macromolecules* **31**, 2593-2599 (1998).

9. Erhand, G. *Designing with Plastics* (Hanser Gardner Publications, Cincinnati, 2006).

10. Grijpma, D. W., Van Hofslot, R. D. A., Supèr, H., Nijenhuis, A. J. & Pennings, A. J. Rubber Toughening of Polylactide by Blending and Block Copolymerization. *Polymer Engineering and Science* **34**, 1674-1684 (1994).

11. Anderson, K. S., Lim, S. H. & Hillmyer, M. A. Toughening of Polylactide by Melt Blending with Linear Low-Density Polyethylene. *Journal of Applied Polymer Science* **89**, 3757-3768 (2003).

12. Piorkowska, E., Kulinski, Z., Galeski, A. & Masirek, R. Plasticization of Semicrystalline Poly(L-lactide) with Poly(propylene glycol). *Polymer* **47**, 7178-7188 (2006).

13. Abayasinghe, N. K., Glaser, S., Perera, P. K. U. & Smith, D. W., Jr. Oligoethylene-End-Capped Polylactides. *Journal of Polymer Science Part A: Polymer Chemistry* **43**, 5257-5266 (2005).

14. Dubois, P., Jacobs, C., Jérôme, R. & Teyssié, P. Macromolecular Engineering of Polylactones and Polylactides. 4. Mechanism and Kinetics of Lactide Homopolymerization by Aluminum Isopropoxide. *Macromolecules* **24**, 2266-2270 (1991).

15. Kricheldorf, H. R. & Boettcher, C. Polylactones .27. Anionic Polymerization of L-Lactide - Variation of Endgroups and Synthesis of Block Copolymers with Poly(ethylene oxide). *Makromolekulare Chemie-Macromolecular Symposia* **73**, 47-64 (1993).

16. Kowalski, A., Duda, A. & Penczek, S. Mechanism of Cyclic Ester Polymerization Initiated with Tin(II) Octoate. 2. Macromolecules Fitted with Tin(II) Alkoxide

Species Observed Directly in MALDI-TOF Spectra. *Macromolecules* **33**, 689-695 (2000).

17. Chamberlain, B. M., Jazdzewski, B. A., Pink, M., Hillmyer, M. A. & Tolman, W. B. Controlled Polymerization of DL-Lactide and ε-Caprolactone by Structurally Well-Defined Alkoxo-Bridged Di- and Triyttrium(III) Complexes. *Macromolecules* **33**, 3970-3977 (2000).

18. Cheng, M., Attygalle, A. B., Lobkovsky, E. B. & Coates, G. W. Single-Site Catalysts for Ring-Opening Polymerization: Synthesis of Heterotactic Poly(lactic acid) from *rac*-Lactide. *Journal of the American Chemical Society* **121**, 11583-11584 (1999).

19. Kricheldorf, H. R., Kreiser-Saunders, I. & Stricker, A. Polylactones 48. $Sn(Oct)_2$-Initiated Polymerizations of Lactide: A Mechanistic Study. *Macromolecules* **33**, 702-709 (2000).

20. Kricheldorf, H. R., Kreiser-Saunders, I. & Boettcher, C. Polylactones: 31. Sn(II)Octoate-Initiated Polymerization of L-Lactide: A Mechanistic Study. *Polymer* **36**, 1253-1259 (1995).

21. Ryner, M., Stridsberg, K., Albertsson, A.-C., von Schenck, H. & Svensson, M. Mechanism of Ring-Opening Polymerization of 1,5-Dioxepan-2-one and L-Lactide with Stannous 2-Ethylhexanoate. A Theoretical Study. *Macromolecules* **34**, 3877-3881 (2001).

22. Dubois, P., Ropson, N., Jérôme, R. & Teyssié, P. Macromolecular Engineering of Polylactones and Polylactides. 19. Kinetics of Ring-Opening Polymerization of ε-

Caprolactone Initiated with Functional Aluminum Alkoxides. *Macromolecules* **29**, 1965-1975 (1996).

23. Penczek, S., Duda, A., Szymanski, R. & Biela, T. What We have Learned in General from Cyclic Esters Polymerization. *Macromolecular Symposia* **153**, 1-15 (2000).

24. Zhang, X., MacDonald, D. A., Goosen, M. F. A. & McAuley, K. B. Mechanism of Lactide Polymerization in the Presence of Stannous Octoate: The Effect of Hydroxy and Carboxylic Acid Substances. *Journal of Polymer Science Part A: Polymer Chemistry* **32**, 2965-2970 (1994).

25. Nijenhuis, A. J., Grijpma, D. W. & Pennings, A. J. Lewis Acid Catalyzed Polymerization of L-Lactide. Kinetics and Mechanism of the Bulk Polymerization. *Macromolecules* **25**, 6419-6424 (1992).

26. Diez, F. V., Sastre, H. & Coca, J. Effect of the Operating Conditions on the Preparation of Stannous Octanoate from Stannous Oxide. *Industrial & Engineering Chemistry Research* **27**, 845-847 (1988).

27. Kricheldorf, H. R., Rost, S., Wutz, C. & Domb, A. Stereocomplexes of A-B-A Triblock Copolymers Based on Poly(L-Lactide) and Poly(D-Lactide) A Blocks. *Macromolecules* **38**, 7018-7025 (2005).

28. Pilati, F., Toselli, M., Messori, M., Priola, A., Bongiovanni, R., Malucelli, G. & Tonelli, C. Poly(ε-caprolactone)-Poly(fluoroalkylene oxide)-Poly(ε-caprolactone) Block Copolymers. 1. Synthesis and Molecular Characterization. *Macromolecules* **32**, 6969-6976 (1999).

29. Hillmyer, M. A. & Lodge, T. P. Synthesis and Self-Assembly of Fluorinated Block Copolymers. *Journal of Polymer Science Part A: Polymer Chemistry* **40**, 1-8 (2002).

30. Radhakrishnan, K., Switek, K. A. & Hillmyer, M. A. Synthesis of Semifluorinated Block Copolymers by Atom Transfer Radical Polymerization. *Journal of Polymer Science Part A: Polymer Chemistry* **42**, 853-861 (2004).

31. Synytska, A., Appelhans, D., Wang, Z. G., Simon, F., Lehmann, F., Stamm, M. & Grundke, K. Perfluoroalkyl End-Functionalized Oligoesters: Correlation between Wettability and End-Group Segregation. *Macromolecules* **40**, 297-305 (2007).

32. Hopkins, J. & Badyal, J. P. S. Nonequilibrium Glow Discharge Fluorination of Polymer Surfaces. *The Journal of Physical Chemistry* **99**, 4261-4264 (1995).

33. Thomas, R. R., Lloyd, K. G., Stika, K. M., Stephans, L. E., Magallanes, G. S., Dimonie, V. L., Sudol, E. D. & El-Aasser, M. S. Low Free Energy Surfaces Using Blends of Fluorinated Acrylic Copolymer and Hydrocarbon Acrylic Copolymer Latexes. *Macromolecules* **33**, 8828-8841 (2000).

34. Koh, K. et al. Precision Synthesis of a Fluorinated Polyhedral Oligomeric Silsesquioxane-Terminated Polymer and Surface Characterization of Its Blend Film with Poly(methyl methacrylate). *Macromolecules* **38**, 1264-1270 (2005).

35. Bottino, F. A., Di Pasquale, G., Pollicino, A., Pilati, F., Toselli, M. & Tonelli, C. XPS Study on Surface Segregation in Poly(ethylene-iso/terephthalate)-Perfluoropolyether Block Copolymers. *Macromolecules* **31**, 7814-7819 (1998).

36. Pilati, F., Toselli, M., Re, A., Bottino, F. A., Pollicino, A. & Recca, A. Surface Investigation by ESCA of Poly(ethylene terephthalate)-Perfluoropolyether Block Copolymers. *Macromolecules* **23**, 348-350 (1990).

37. Toselli, M., Messori, M., Bongiovanni, R., Malucelli, G., Priola, A., Pilati, F. & Tonelli, C. Poly(ε-caprolactone)-Poly(fluoroalkylene oxide)-Poly(ε-caprolactone) Block Copolymers. 2. Thermal and Surface Properties. *Polymer* **42**, 1771-1779 (2001).

38. Stevels, W. M., Ankoné, M. J. K., Dijkstra, P. J. & Feijen, J. Stereocomplex Formation in ABA Triblock Copolymers of Poly(lactide) (A) and Poly(ethylene glycol) (B). *Macromolecular Chemistry and Physics* **196**, 3687-3694 (1995).

39. Haynes, D., Naskar, A. K., Singh, A., Yang, C.-C., Burg, K. J., Drews, M., Harrison, G. & Smith, D. W., Jr. Poly(L-lactic acid) with Segmented Perfluoropolyether Enchainment. *Macromolecules* **40**, 9354-9360 (2007).

40. Duda, A., Biela, T., Libiszowski, J., Penczek, S., Dubois, P., Mecerreyes, D. & Jérôme, R. Block and Random Copolymers of ε-caprolactone. *Polymer Degradation and Stability: Biodegradable Polymers and Macromolecules* **59**, 215-222 (1998).

41. Slomkowski, S., Sosnowski, S. & Gadzinowski, M. Polyesters from Lactides and ε-Caprolactone. Dispersion Polymerization versus Polymerization in Solution. *Polymer Degradation and Stability: Biodegradable Polymers and Macromolecules* **59**, 153-160 (1998).

42. Kowalski, A., Duda, A. & Penczek, S. Kinetics and Mechanism of Cyclic Esters Polymerization Initiated with Tin(II) Octoate. 3. Polymerization of L,L-Dilactide. *Macromolecules* **33**, 7359-7370 (2000).

43. Libiszowski, J., Kowalski, A., Duda, A. & Penczek, S. Kinetics and Mechanism of Cyclic Esters Polymerization Initiated with Covalent Metal Carboxylates, 5. *Macromolecular Chemistry and Physics* **203**, 1694-1701 (2002).

44. Bongiovanni, R., Malucelli, G., Messori, M., Pilati, F., Priola, A., Tonelli, C. & Toselli, M. Poly(ε-caprolactone-*co*-lactide)/Perfluoropolyether Block Copolymers: Synthesis, Thermal, and Surface Characterization. *Journal of Polymer Science Part A: Polymer Chemistry* **43**, 3588-3599 (2005).

45. Korhonen, H., Helminen, A. & Seppala, J. V. Synthesis of Polylactides in the Presence of Co-Initiators with Different Numbers of Hydroxyl Groups. *Polymer* **42**, 7541-7549 (2001).

46. Tsuji, H., Miyase, T., Tezuka, Y. & Saha, S. K. Physical Properties, Crystallization, and Spherulite Growth of Linear and 3-Arm Poly(L-lactide)s. *Biomacromolecules* **6**, 244-254 (2005).

47. Karis, T. E., Marchon, B., Hopper, D. A. & Siemens, R. L. Perfluoropolyether Characterization by Nuclear Magnetic Resonance Spectroscopy and Gel Permeation Chromatography. *Journal of Fluorine Chemistry* **118**, 81-94 (2002).

48. Hoshino, M., Kimachi, Y. & Terada, A. Thermogravimetric Behavior of Perfluoropolyether. *Journal of Applied Polymer Science* **62**, 207-215 (1996).

49. Fox, J., Thomas G. & Flory, P. J. Second-Order Transition Temperatures and Related Properties of Polystyrene. I. Influence of Molecular Weight. *Journal of Applied Physics* **21**, 581-591 (1950).

50. Ajroldi, G., Marchionni, G. & Pezzin, G. The Viscosity-Molecular Weight Relationships for Diolic Perfluoropolyethers. *Polymer* **40**, 4163-4164 (1999).

51. Zhang, J.-F. & Sun, X. in *Biodegradable Polymers for Industrial Applications* (ed. Smith, R.) 251-288 (CRC Press, Washington, DC, 2005).

52. Turri, S., Sanguineti, A. & Levi, M. Molecular Characterization and Chain Flexibility of Linear Polyacetals Containing Poly(Perfluoro(oxymethylene-*ran*-oxyethylene)) Macromers. *Macromolecular Chemistry and Physics* **198**, 3215-3228 (1997).

53. Sperling, L. H. *Introduction to Physical Polymer Science* (Wiley-Interscience, New York, 2001).

54. Keller, A., Hikosaka, M., Rastogi, S., Toda, A., Barham, P. J. & Goldbeck-Wood, G. An Approach to the Formation and Growth of New Phases with Application to Polymer Crystallization: Effect of Finite Size, Metastability, and Ostwald's Rule of Stages. *Journal of Materials Science* **29**, 2579-2604 (1994).

55. Tonelli, C., Pilati, F., Toselli, M., Turturro, A. & Gattiglia, E. Fluoromodified polyesters having improved processability. 352825.U.S. Patent # 5686522.(1997).

56. Huang, C.-I., Tsai, S.-H. & Chen, C.-M. Isothermal Crystallization Behavior of Poly(L-lactide) in Poly(L-lactide)-*block*-Poly(ethylene glycol) Biblock Copolymers. *Journal of Polymer Science Part B: Polymer Physics* **44**, 2438-2448 (2006).

57. Ehrenstein, G. W., Riedel, G. & Trawiel, P. *Thermal Analysis of Plastics - Principles and Practice* (Hanser Gardner Publications, Cincinnati, US, 2004).

58. Meroni, G., Pogliani, C., Zompatori, A., Trombetta, T. & Tonelli, C. in *Proceeding of the 8th Polymers for Advanced Technologies International Symposium* (Budapest, Hungary, 2005).

59. Stefano Turri, A. S., Marinella Levi,. Molecular characterization and chain flexibility of linear polyacetals containing poly-perfluoro(oxymethylene-*ran*-oxyethylene) macromers. *Macromolecular Chemistry and Physics* **198**, 3215-3228 (1997).

60. Starkweather, H. W., Avakian, P., Fontanella, J. J. & Wintersgill, M. C. Internal Motions in Polylactide and Related Polymers. *Macromolecules* **26**, 5084-5087 (1993).

61. Kobori, Y., Iwata, T., Doi, Y. & Abe, H. Synthesis, Solid-State Structure, and Surface Properties of End-Capped Poly(L-lactide). *Biomacromolecules* **5**, 530-536 (2004).

62. Brizzolara, D., Cantow, H.-J., Diederichs, K., Keller, E. & Domb, A. J. Mechanism of the Stereocomplex Formation between Enantiomeric Poly(lactide)s. *Macromolecules* **29**, 191-197 (1996).

63. Gilding, D. K. & Reed, A. M. Biodegradable Polymers for Use In Surgery-Polyglycolic/Poly(lactic acid) Homo- and Copolymers: 1. *Polymer* **20**, 1459-1464 (1979).

64. Ho, C. C. & Khew, M. C. Surface Free Energy Analysis of Natural and Modified Natural Rubber Latex Films by Contact Angle Method. *Langmuir* **16**, 1407-1414 (2000).

65. KRÜSS Application Notes. *www.kruss.info*. (August 2007).

66. Owens, D. K. & Wendt, R. C. Estimation of the Surface Free Energy of Polymers. *Journal of Applied Polymer Science* **13**, 1741-1747 (1969).

67. Kaelble, D. H. *Physical Chemistry of Adhesion* (Wiley-Interscience, New York, 1971).

68. Owens, D. K. Some Thermodynamic Aspects of Polymer Adhesion. *Journal of Applied Polymer Science* **14**, 1725-1730 (1970).

69. Kaelble, D. H. & Cirlin, E. H. Dispersion and Polar Contributions to Surface Tension of Poly(methylene oxide) and Na-treated Polytetrafluoroethylene. *Journal of Polymer Science Part B: Polymer Physics* **9**, 363-368 (1971).

70. Legeay, G., Coudreuse, A., Legeais, J.-M., Werner, L., Bulou, A., Buzare, J.-Y., Emery, J. & Silly, G. AF Fluoropolymer for Optical Use: Spectroscopic and Surface Energy Studies; Comparison with Other Fluoropolymers. *European Polymer Journal* **34**, 1457-1465 (1998).

CHAPTER 5

CRYSTALLIZATION BEHAVIOR OF POLYLACTIDE AND POLYLACTIDE-PERFLUOROPOLYETHER BLOCK COPOLYMERS

5.1 Introduction

The study of the crystallization phenomenon of polymers is of utmost importance as the crystallization behavior of materials affects their end use properties and applications. The bulk and the solution crystallization of polylactide has been studied extensively and various aspects such as spherulitic growth, molecular weight effects, crystallization regimes, influence of history, stereoselective crystallization, etc., have been reported.[1-4] However, the crystallization of complex polymer architectures such as block copolymers are still not completely understood.

Block copolymers can be designed with different morphologies with components in either the amorphous state or the crystalline state under ambient conditions and hence, the control of properties of the block copolymers depends on the composition of these chemically linked components.[5]

In the case of more than one crystallizable block in the polymer chain (e.g. Polycaprolactone-*block*-Polylactide, Polylactide-*block*-Poly(ethylene oxide)-*block*-Polylactide, etc.), the crystallization can occur in a simultaneous or sequential fashion, depending on the thermal properties of the block. Each block can therefore have a dramatic effect on the nucleation and crystallization kinetics of the other blocks. Hence, the morphology and properties of block copolymers depend on factors such as the molecular weight of the blocks, the chemical nature of the constituent units, the molecular architecture and the number of crystallizable blocks, etc.[6]

On the other hand, where only one block crystallizes, the crystallization is expected to compete with the microphase separation at low temperatures.[5] The chain folding during crystallization in a homopolymer is kinetically controlled whereas a block copolymer (with crystallizable and non-crystallizable blocks) crystallizes through equilibrium chain folding and the equilibrium number of chain folds are controlled by the size of non-crystallizable block.[7] A block copolymer with very high block incompatibilies can lead to an ordered melt microphase (nanometer length scale domains such as spheres, cylinders, lamellae, etc.) and these microdomains can affect the crystallization and morphology of the resultant block copolymer.[8,9]

Isothermal calorimetric and microscopic experiments aid in the study of the nucleation and growth mechanisms during crystallization. On the other hand, non-isothermal crystallization experiments are also very important as the polymer processing occurs mostly under non-isothermal conditions.

The surface, bulk and crystallization properties of PLA were modified by using telechelic poly(fluoroalkylene oxide)s with reactive hydroxyl groups as a macrointiator for ring-opening polymerization of lactides which resulted in polylactide-poly(fluoroalkylene oxide)s-polylactide block copolymers (FluoroPLA). The ability of the fluorinated segments to migrate towards the surface, thereby enriching the surface with fluorine even at very low concentrations is very well demonstrated in previous studies. [10-13]

This chapter discusses the isothermal and non-isothermal crystallization of PLA and FluoroPLA. FluoroPLA shows a higher crystallization rate and higher overall crystallinity when compared to PLA.

5.2 Materials and Methods

Polylactide-perfluoropolyether-polylactide (FluoroPLA) block copolymers were synthesized using hydroxyl terminated perfluoropolyether (PFPE) as a macro-initiator for the ring opening polymerization of lactide. Various batches of the copolymer of PLA and PFPE were prepared with ~5 wt% PFPE of different molecular weights (Mn= 1.5, 2.0, 4.2 kg mol^{-1}). The abbreviation FluoroPLA**x**(**y**) for copolymers contains two numbers with 'x' representing the weight percentage of PFPE in the feed and 'y' (in parenthesis) representing the number average molecular weight (by NMR) of PFPE. A control PLA homopolymer batch was synthesized without any PFPE in the above mentioned reaction mixture.

The number average molecular weight (Mn), polydispersivity index (PDI), cold crystallization temperature (Tc) and melting temperature (Tm) for PLA and the FluoroPLAs are summarized in Table 5.1. The Mn of the PLA homopolymer, was 144 kg mol^{-1}; while the Mn of the FluoroPLA5(1.5k) was 68 kg mol^{-1}, which was the lowest among the molecular weights of all the polymers. The PDIs of PLA and the FluorPLAs were very similar. The molar characteristics of block copolymer can be designed by adding calculated amounts of PFPE. The Tc of PLA was ca. 109 °C and the Tm 176 °C. All of the FluorPLAs had lower Tc's and Tm's than PLA, with FluoroPLA5(1.5k) having the lowest values.

Table 5.1. The Mn's, PDI's, Tc's, and Tm's of PLA and the FluoroPLAs.

Polymer	Mn[a] kg mol^{-1}	PDI[a]	Tc[b] °C	Tm[b] °C
PLA	144	1.7	107.9 ± 0.3	176.0 ± 0.2
FluoroPLA5(4.2k)	95	1.8	103.5 ± 1.4	173.4 ± 0.1
FluoroPLA5(2.0k)	83	1.7	103.3 ± 0.1	171.6 ± 0.7
FluoroPLA5(1.5k)	68	1.6	99.0 ± 0.1	167.4 ± 0.7

[a]Results from GPC; [b]Results from DSC, heating rate 10 °C/min, 2nd heating cycle.

Morphological studies were conducted using a James Swift Polarising Microscope (James Swift, England) equipped with a Mettler Toledo (Columbus, OH) FP90 central processor and a Mettler Toledo FP80HT hot stage. Digital images were captured using a Sony 3CCD camera and analyzed using *Image-Pro PLUS* (version 4.0) software. A Fisher Scientific stage micrometer was used for measurement calibration.

Solutions of polymer in chloroform (2 (w/v) %) were placed as single drops on the glass slides and dried under vacuum. Samples were then covered with a coverslip and placed in the hot stage. Samples were heated to 200 °C at a rate of 20 °C/min and held for 5 min, thereafter; samples were cooled to selected crystallization temperatures (Tc) at the rate of 20 °C/min and held isothermally to observe the growth of spherulites. Growth in selected, isolated, spherulites' radial direction was measured at fixed time intervals. Samples were then cooled to room temperature at 20 °C/min from the crystallization temperature. This process

was repeated for each selected crystallization temperature with a new sample each time. The selected crystallization temperatures were 140, 130, 120, 110, 100, 90 °C.

Differential Scanning Calorimetry (DSC) analysis was conducted using a TA Instruments (New Castle, Delaware) Q1000 DSC. Data was analyzed using TA Instruments Universal Analysis 2000 version 4.1D software. The isothermal melt crystallization of PLA and FluoroPLAs was performed by heating the samples (8-10 mg in standard aluminum pans) at 20 °C/min to 200 °C/min and the polymer melt was held isothermally for 5 min before it was rapidly cooled at 30 °C/min to the crystallization temperature and then held isothermally for 30 min. The cooling rate of 30 °C/min was employed as the higher cooling rates resulted in a sudden drop in the heat flow in the initial cooling stage and the slower cooling rates resulted in the crystallization of the melt before the isothermal crystallization temperature was reached. The non-isothermal crystallization kinetics was investigated by heating the cooled samples (200 °C to 0 °C at 20 °C/min) at different rates of 2.5, 5, 10, 20, 40 °C/min. The heat capacity signals obtained during the cold crystallization were plotted against the temperature for different heating rates. Heat of fusion for the samples annealed at 120 °C for different annealing time were measured with DSC at heating rate of 10 °C/min.

5.3 Results and Discussion

The effect of annealing time at 120 °C on the heats of fusion of PLA and FluoroPLAs are shown in Figure 5.1. Overall, the PLA heats of fusion were lower at every annealing time when compared to the FluoroPLAs. The heats of fusion for the FluoroPLA5(1.5k) were the highest at all annealing times and also in the case of the unannealed sample. All the polymer samples showed an increase in the heat of fusion (increase in crystallinity) with an increase in annealing time. For the FluoroPLA5(1.5k), the curve flattens out after only 12 hours of annealing time which is suggestive of a higher crystallization rate. For the FluoroPLA5(2.0k), the curve flattens out after 24 hours whereas FluoroPLA5(4.2k) still shows a slight increase in the heat of fusion with annealing time similar to the PLA. For the FluoroPLA5(1.5k), the heat of fusion reached the maximum value fastest and overall, FluoroPLAs showed higher and faster attainment of the maximum heat of fusion compared to the PLA which is indicative of slower rate of crystallization and the lower crystallinity of the PLA compared to those of the FluoroPLAs.

Contrary to the expected trend of a decrease in crystallinity upon copolymerization in the copolymers, an increase in the crystallization rate and the overall crystallinity relative to PLA was observed by incorporation of the perfluoropolyether linkage in the polymer chain. Consequently the study of the crystallization behavior of FluoroPLAs was of interest.

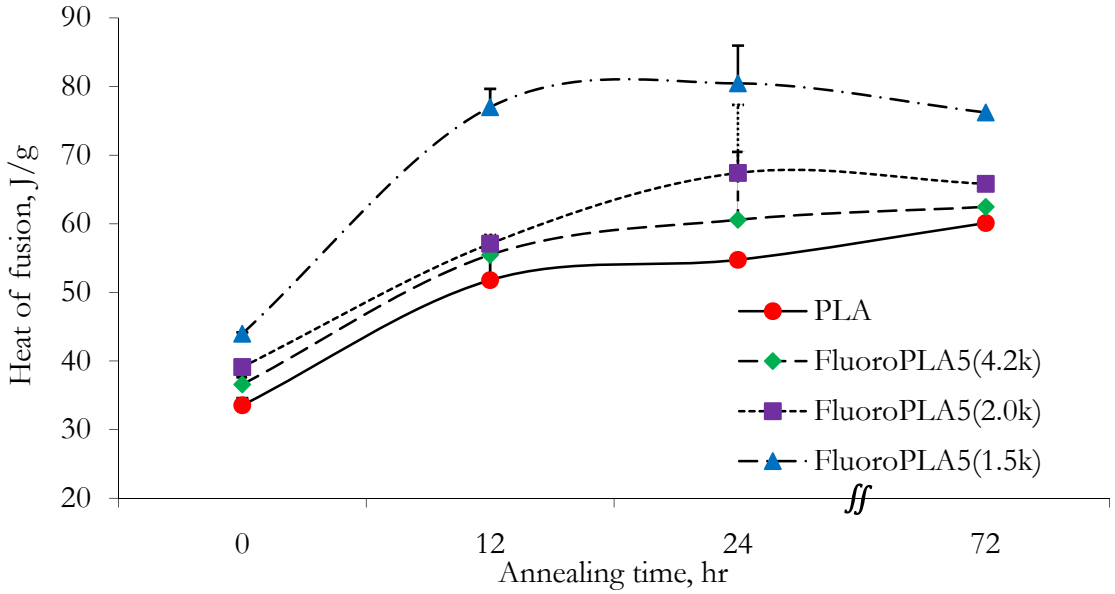

Figure 5.1. Influence of annealing time on the heat of fusion of PLA and FluoroPLAs annealed at 120 °C.

PLA and PFPE are two chemically distinct polymeric materials and both would be expected to retain their behavior upon copolymerization with each other. As shown in Table 5.2, there is a large difference between the densities and solubility parameters of PLA and PFPE. The solubility parameter of PFPE is about half that of the PLA and the density is almost 1.4 times higher than that of PLA. It is proposed that PFPE could behave as nuclei for PLA chains.[14]

Table 5.2. Solubility parameters and densities of PLA and PFPE.

Polymer	Solubility parameter (δ), $J^{1/2}cm^{3/2}$	Density, g cm^{-3}
PLA	19-22[15]	1.3[16]
PFPE	10-11[17]	1.8[18]

Figure 5.2 shows the schematic of the proposed nucleating action of PFPE and its comparison with the polarized optical micrograph of FluoroPLA5(1.5k). The red color represents the PFPE as the nuclei and the green color represents the PLA rich portion. Nucleating action of PFPE enhances the overall crystallinity of FluoroPLA5(1.5k) in comparison to PLA. Melt crystallization of FluoroPLA5(1.5k) results in branded spherulites easily and is discussed in detail under optical microscopic measurement section of this chapter.

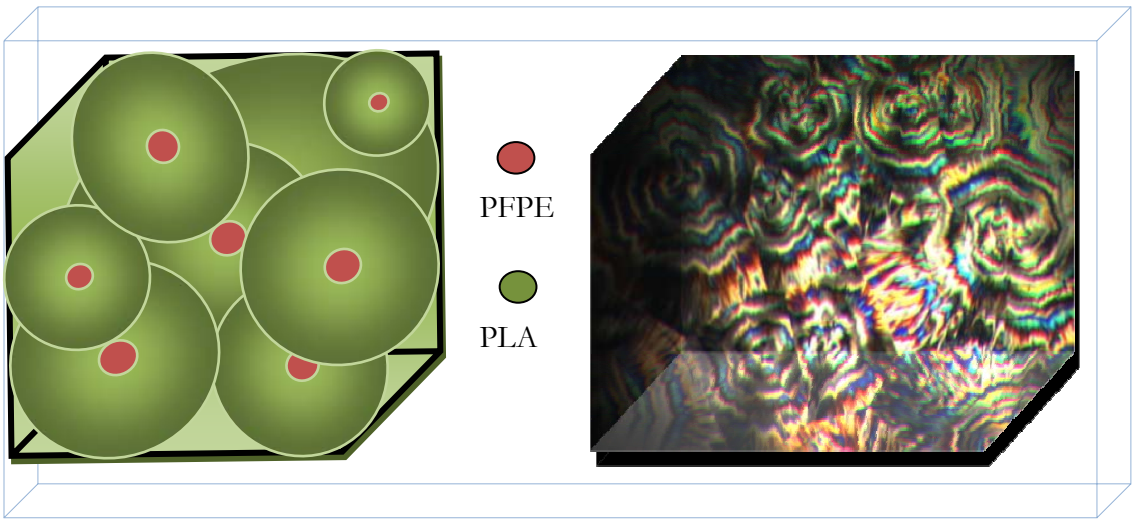

Figure 5.2. Schematic representation showing the nucleating action of PFPE.

Isothermal Crystallization: Differential Scanning Calorimetry

In Figure 5.3(a), Figure 5.4(a), Figure 5.5(a) and Figure 5.6(a) the heats evolved (normalized to sample weight)(W/g) during isothermal crystallization as a function of time in the DSC for the PLA, FluoroPLA5(4.2k), FluoroPLA5(2.0k) and FluoroPLA5(1.5k) are shown. The corresponding relative crystallinity (*Xt*) data for PLA, FluoroPLA5(4.2k), FluoroPLA5(2.0k) and the FluoroPLA5(1.5k) are shown in Figure 5.3(b), Figure 5.4(b), Figure 5.5(b) and Figure 5.6(b), respectively. The relative crystallinity of the samples was calculated using equation 5.1:[19,20]

$$X_t = \frac{\int_0^t [dH/dt] \cdot dt}{\int_0^\infty [dH/dt] \cdot dt} \qquad 5.1.$$

where X_t is the fraction of crystallized material. The numerator in equation 5.1 is the amount of heat evolved during crystallization until time t and the denominator is the amount of the heat evolved upon complete crystallization. As the crystallization temperature is approached, the heat flow peak becomes sharp and the relative crystallization curve reaches the complete relative crystallinity (X_∞) faster. The heat flow curve corresponding to 130 °C for the PLA is sharper than for the FluoroPLAs and the opposite behavior is seen for the heat flow curve corresponding to 90 °C where the FluoroPLA5(1.5k) shows the sharper peak compared to the other FluoroPLAs and the PLA. This is suggestive of shift in the crystallization temperature to lower value as we move from PLA to FluoroPLA5(4.2k) to FluoroPLA5(2.0k) to FluoroPLA5(1.5k). A similar trend is seen in the relative crystallinity curve.

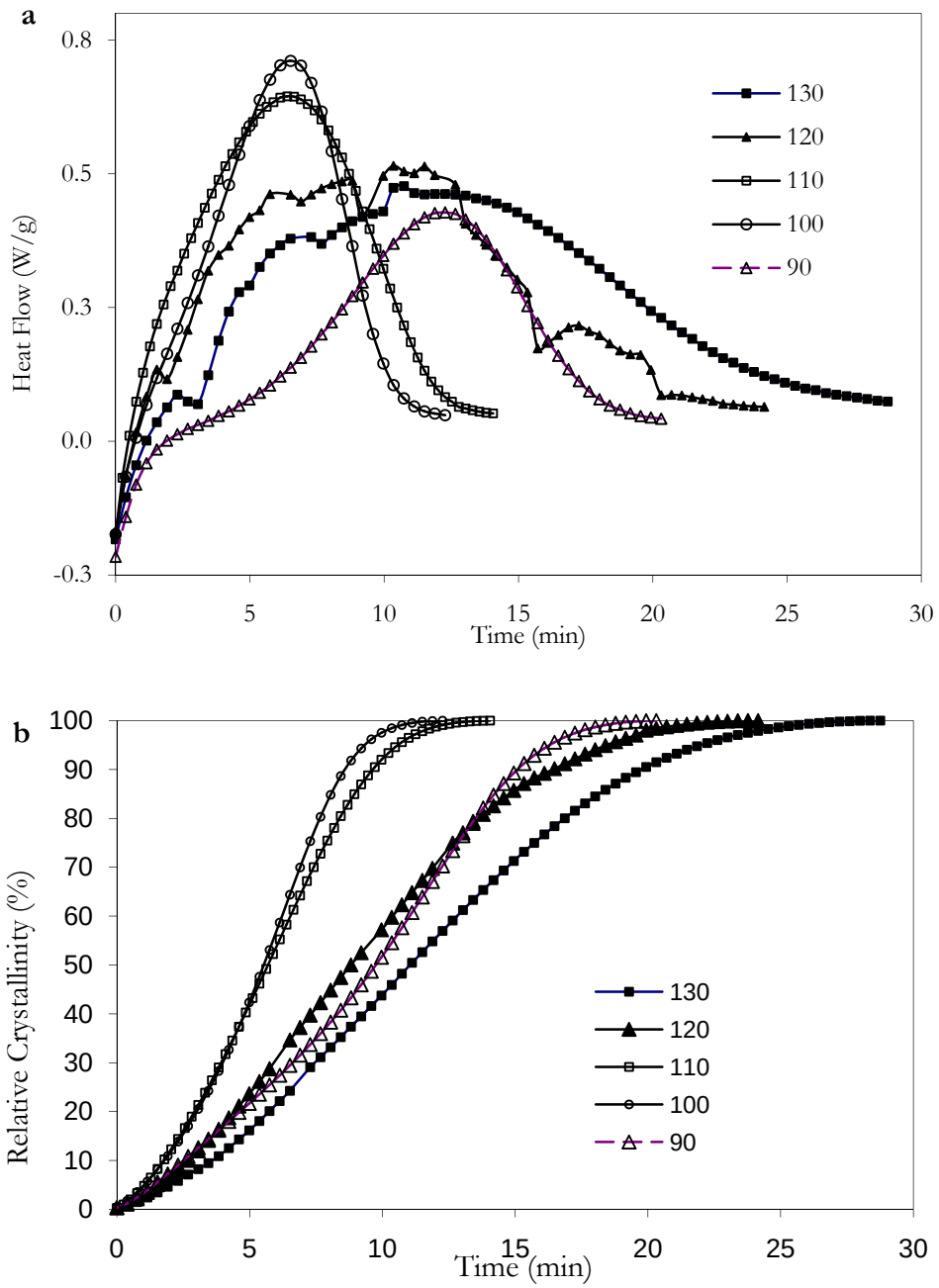

Figure 5.3. Normalized heat flow (a) and relative crystallinity (b) curves for isothermal crystallization of PLA at different temperatures.

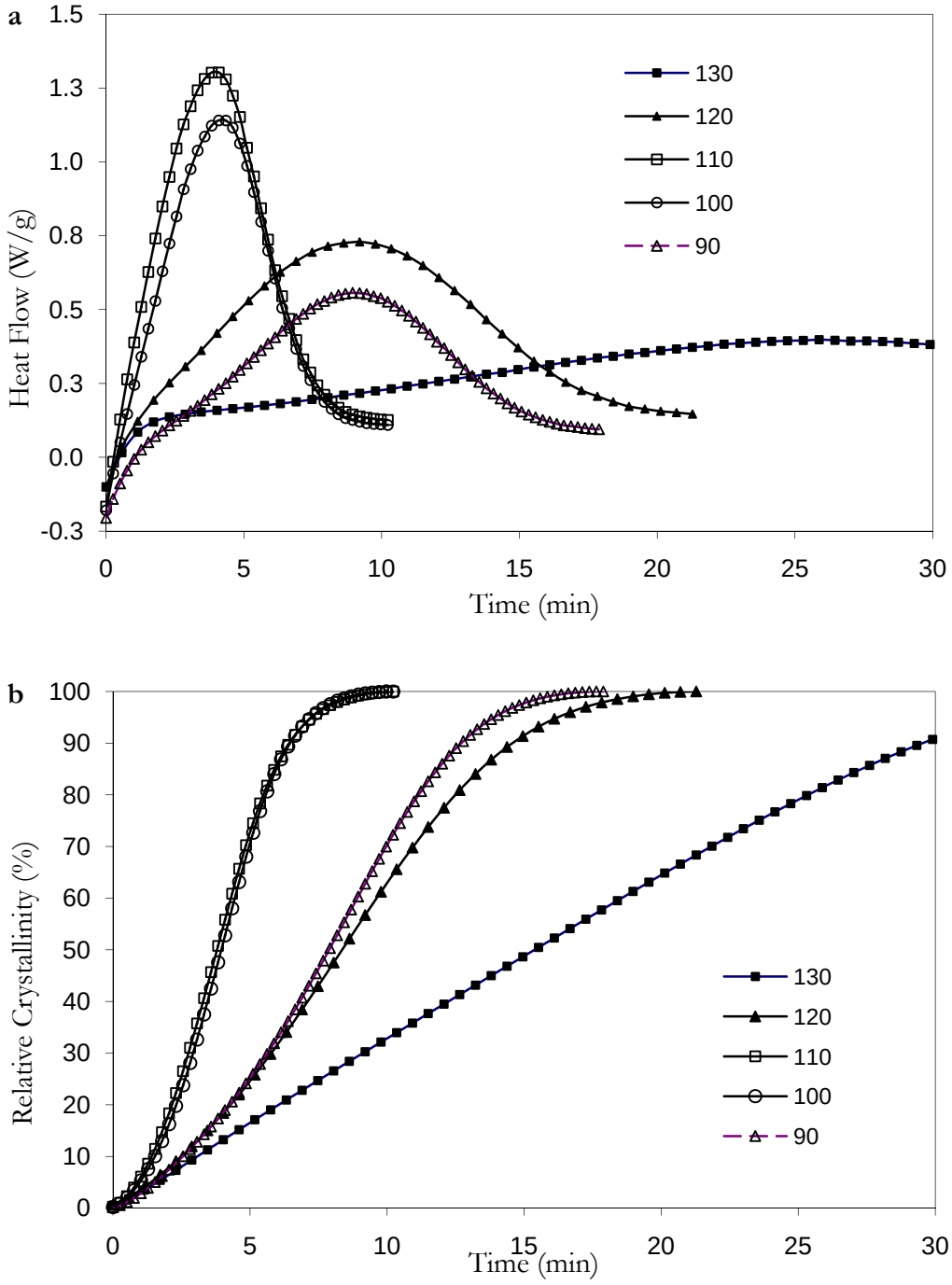

Figure 5.4. Normalized heat flow (a) and relative crystallinity (b) curves for isothermal crystallization of FluoroPLA5(4.2k) at different temperatures.

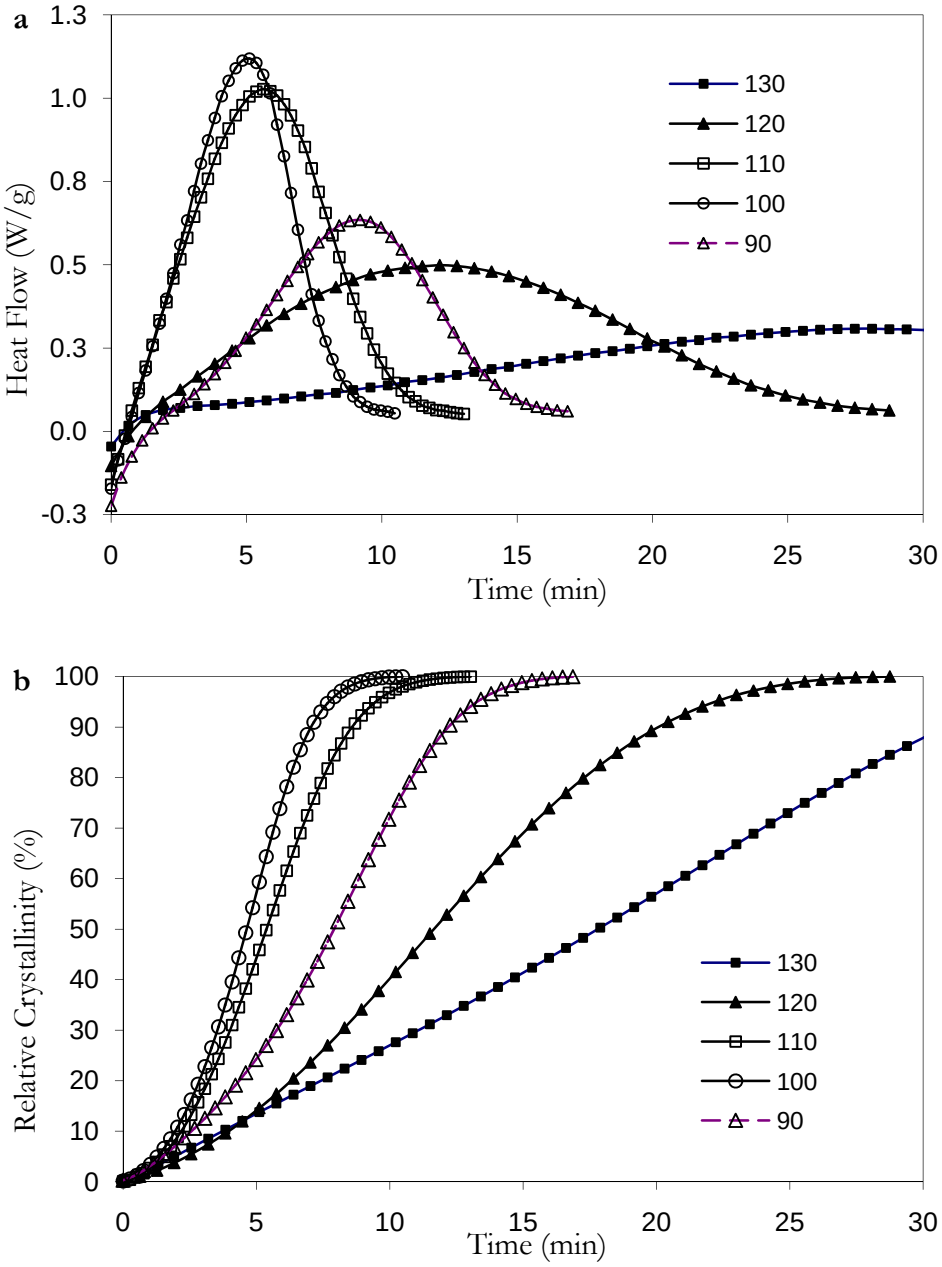

Figure 5.5. Normalized heat flow (a) and relative crystallinity (b) curves for isothermal crystallization of FluoroPLA5(2.0k) at different temperatures.

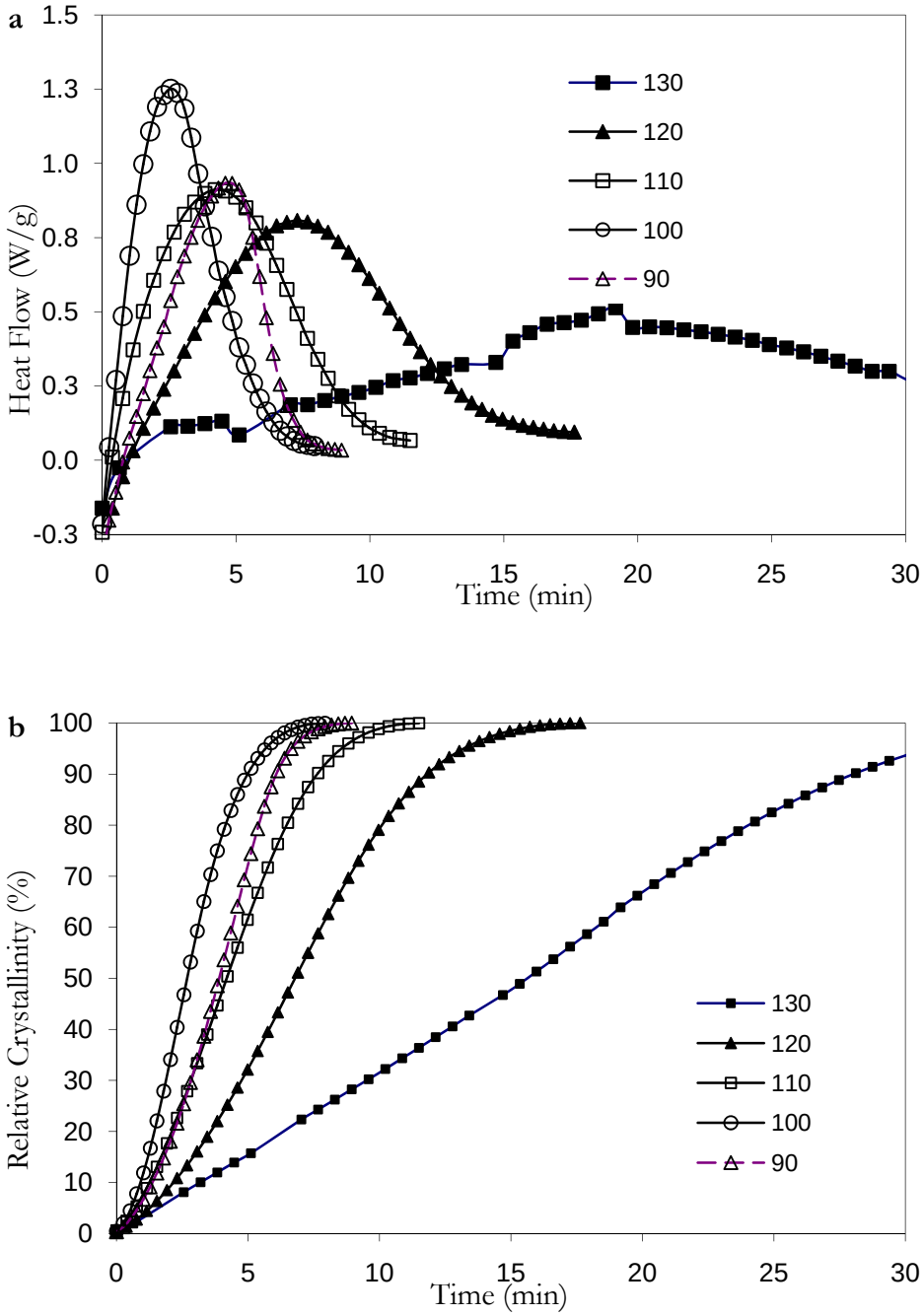

Figure 5.6. Normalized heat flow (a) and relative crystallinity (b) curves for isothermal crystallization of FluoroPLA5(1.5k) at different temperatures.

The kinetics of the isothermal crystallization of polymers was studied using the Avrami equation as shown in equation 5.2, where X_t is the fraction of crystallized material and Z and n are constants.[21]

$$X_t = 1 - exp\,(-Zt^n) \qquad 5.2.$$

The constant, n, called the Avrami exponent, depends on the mode of domain growth whereas Z is a temperature-dependent constant which contains the nucleation and geometry information. These constants can be extracted from double logarithmic plots of the experimental data.

The Avrami equation is based on various assumptions such as the free growth approximation, no change in the volume during crystallization, etc.[22] A typical derivation of the Avrami equation for the case of an athermal (fixed number of nuclei at start) nucleation and constant linear growth of crystals is shown in the following paragraph.[22-25]

With the assumption that only spherical crystals are formed, the volume of the i^{th} crystal ($V_{c,i}^t$) at time t is given by equation 5.3 where G is the constant linear growth rate with time.

$$V_{c,i}^t = \frac{4}{3}\pi G^3 t^3 \qquad 5.3.$$

Assuming no impingement of the crystals, the total crystalline volume is given by equation 5.4 where N is the fixed number of nuclei in the sample.

$$V_{c,total}^t = \sum V_{c,i}^t = \frac{4}{3}\pi N G^3 t^3 \qquad 5.4.$$

The volume fraction crystallinity (X_f) of sample of volume V can be written as in equation 5.5 where N_0 is the number of nuclei per unit volume.

$$X_t = \frac{V_{c,total}^t}{V} = \frac{\frac{4}{3}\pi N_0 G^3 t^3}{V} \quad 5.5.$$

The probability *Ix* that a point is crossed by x fronts of growing spherulites is given by Poisson's equation (equation 5.6) where A represents the average number of fronts

$$I_x = \frac{e^{-A}A^x}{x!} \quad 5.6.$$

of all such points in the sample. The probability that the point has not been crossed by any

$$I_0 = \frac{e^{-A}A^0}{0!} = e^{-A} \quad 5.7.$$

such fronts is given by equation 5.7 i.e. the point is in an amorphous region of sample as given in equation 5.8.

$$I_0 = 1 - X_t \quad 5.8.$$

From equation 5.7 and equation 5.8, the probability of finding a point in an amorphous portion of the sample is given by equation 5.9.

$$I_0 = 1 - X_t = e^{-A} \quad 5.9.$$

For bulk crystallization of polymers, X_t may be considered related to the volume of crystallized material, $V_{c,total}^t$ and leads to equation 5.10.

$$1 - X_t = e^{-\left(\frac{4}{3}\pi N_0 G^3 t^3\right)} \quad 5.10.$$

The general form of Avrami equation is written as in equation 5.11 and the logarithmic form is given in equation 5.12.

$$1 - X_t = e^{-(Zt^n)} \quad 5.11.$$

$$\ln(1 - X_t) = -Zt^n \quad 5.12.$$

The double logarithmic form of equation 5.11 can be written in the form of equation 5.13 and we can extract the constants, Z and n, by observing the change in *Xt* of sample with time.

$$log[-\ln(1 - X_t)] = log\ Z + n\ log\ t \qquad 5.13.$$

The Avrami equation can take different forms depending on the type of nucleation and growth geometry. The dimensionality of the growth for the primary nucleation with pre-existing nuclei and with a constant rate is illustrated in Table 5.3.[25] The one, two, and three-dimensional growth is typically represented by rod-like, disc-like, and spherical domains, respectively. Practically, a mixed case is often observed with simultaneous existence of heterogeneous and homogeneous nucleation.[25]

Table 5.3. Avrami exponent with pre-existing and constant rate primary nucleation with linear growth domains.[25]

Domain growth	Primary nucleation	
	Pre-existing (heterogeneous)	Constant rate (homogeneous)
One-dimensional	1	2
One-dimensional	2	3
One-dimensional	3	4

Figure 5.7 shows the Avrami plot for PLA where log(-ln(1-X_t)) is plotted against log(t) for various isothermal crystallization temperatures. The 110 and 100 °C curves overlap and 90 °C curve overlaps with 120 °C curve and it could be concluded that the

crystallization temperature of PLA is between 100 and 110 °C. Figure 5.8, Figure 5.9 and Figure 5.10 show the Avrami plot for FluoroPLA5(4.2k), FluoroPLA5(2.0k) and FluoroPLA5(1.5k) respectively. For the FluoroPLA5(1.5k), the 90 °C curve shifts left and overlaps with 110 °C curve and this suggests that crystallization temperature of FluoroPLA5(1.5k) is very close to 100 °C. The crystallization behavior of FluoroPLA5(4.2k) and FluoroPLA5(2.0k) falls between that of PLA and FluoroPLA5(1.5k).

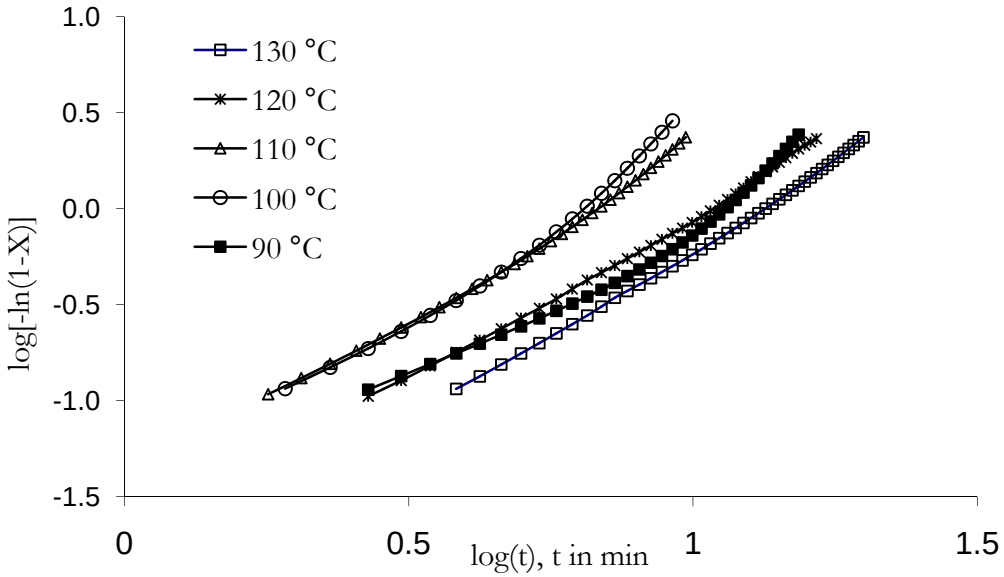

Figure 5.7. Avrami plot for PLA at different crystallization temperatures.

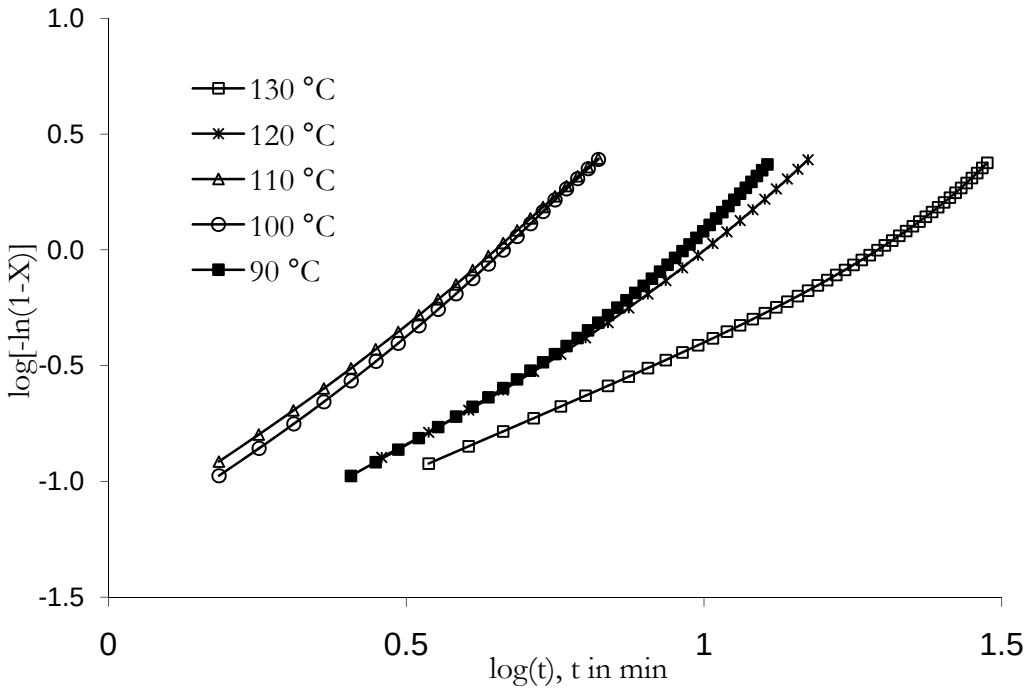

Figure 5.8. Avrami plot for FluoroPLA5(4.2k) at different crystallization temperatures.

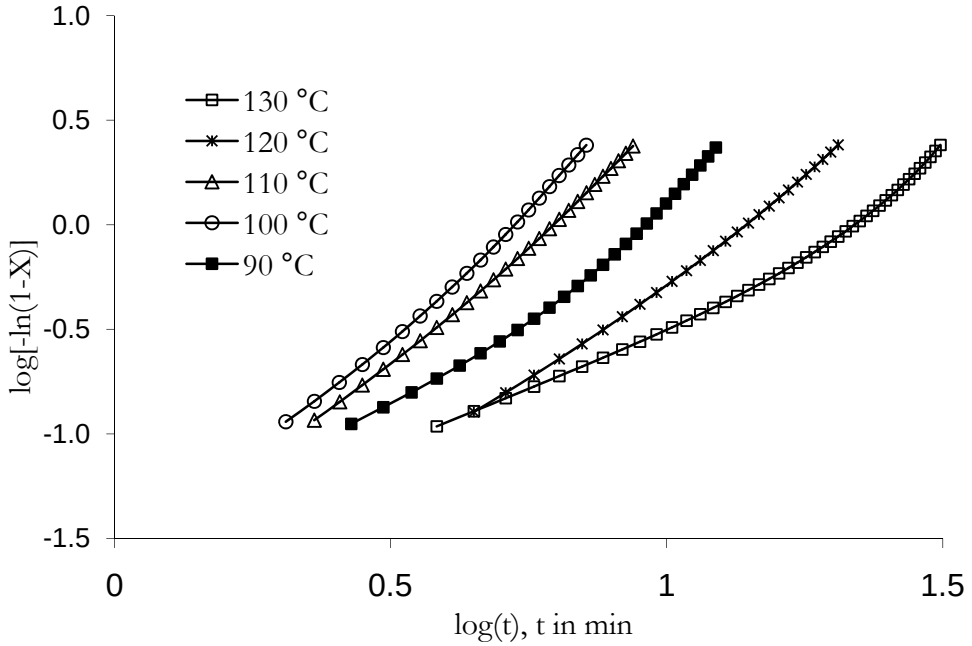

Figure 5.9. Avrami plot for FluoroPLA5(2.0k) at different crystallization temperatures.

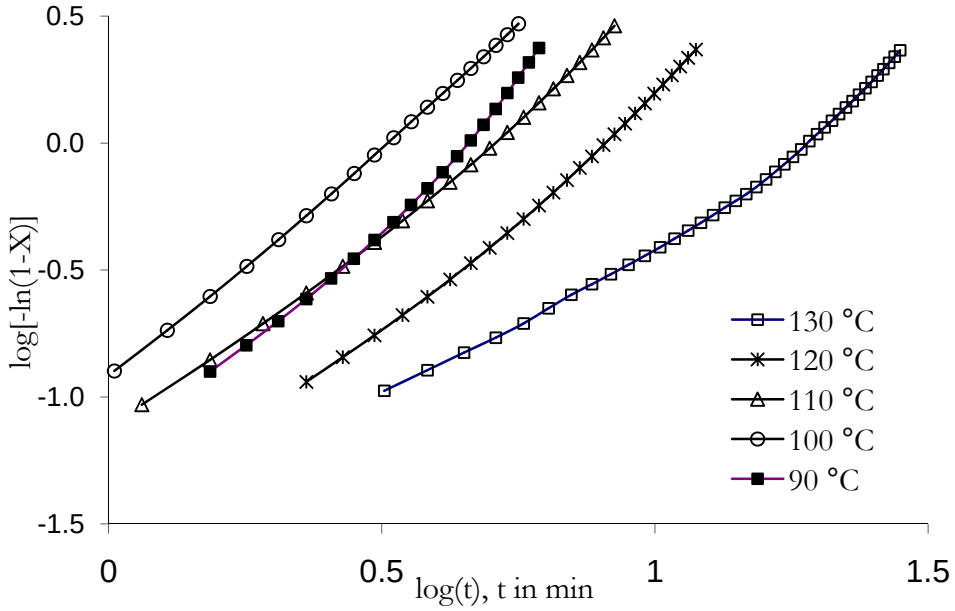

Figure 5.10. Avrami plot for FluoroPLA5(1.5k) at different crystallization temperatures.

The Avrami parameters n and k were estimated by fitting equation 5.13 to the plots of log(-ln(1-X_t)) versus log(t) from Figure 5.7-Figure 5.10. The calculated Avrami parameters and the $t_{1/2}$ for PLA and FluoroPLAs for temperatures in the range of 90-130 °C are summarized in Table 5.4.

Table 5.4. Kinetic parameters obtained by fitting the Avrami equation to the isothermal crystallization data obtained by DSC.

Polymer	Avrami parameters				$t_{1/2}$ (min)	
	Temp., °C	n	Z x 10^3, Min^{-n}	R^2	$\left(\frac{\ln 2}{Z}\right)^{1/n}$	From DSC
PLA	130	1.8	9.1	1.000	10.7	11.4
	120	1.7	17.0	0.997	8.5	9.1
	110	1.8	31.2	0.991	5.4	5.9
	100	2.1	23.1	0.981	5.2	6.0
	90	1.7	15.3	0.968	8.9	10.2
FluoroPLA5(4.2k)	130	1.4	17.9	0.986	14.3	15.2
	120	1.8	15.5	0.993	8.0	8.3
	110	2.1	44.6	0.998	3.7	3.6
	100	2.2	36.2	0.996	3.8	3.9
	90	2.0	13.4	0.988	7.5	7.8
FluoroPLA5(2.0k)	130	1.5	11.6	0.977	16.3	17.7
	120	2.0	6.1	0.996	11.3	11.6
	110	2.3	15.3	0.997	5.3	5.3
	100	2.5	16.9	0.995	4.5	4.8
	90	2.0	11.6	0.981	7.5	8.0
FluoroPLA5(1.5k)	130	1.4	15.3	0.981	14.2	15.6
	120	1.9	20.6	0.994	6.6	6.6
	110	1.7	62.0	0.994	4.0	4.2
	100	1.9	112.7	0.999	2.6	2.9
	90	2.1	42.3	0.988	3.7	3.6

The overall crystallization mechanism can be subdivided into three processes which are nucleation, crystal growth and crystal perfection.[23] The calculated values of n and k are plotted against the isothermal crystallization temperatures in Figure 5.11 (a) and Figure 5.11 (b) respectively. The PLA and the FluoroPLAs have calculated Avrami exponent values between 1.5 to 2.5. With the assumption of pre-existing nuclei (heterogeneous nucleation), two dimensional domain growth is suggested for n=2. However, optical microscopic observations of the crystallization suggest that the overall nucleation has a contribution from both heterogeneous nucleation (pre-existing nuclei) and homogeneous nucleation (sporadic growth of the nuclei). The n values for the FluoroPLAs were higher than the n value for PLA at the lower crystallization temperatures. This could possibly be due to the nucleating action of PFPE segments resulting in higher nucleation rate. At 90 °C, FluoroPLA5(1.5k) showed the highest n value (n=2.1) due to lower crystallization temperature (T_c= 98.9) and higher mobility of the polymer chains. The constant, Z, provides information about the growth rate of spheres, discs or one-dimensional domains. In the case of pre-existing nuclei, $Z^{1/n}$ is proportional to the growth rate of domains. The FluoroPLA5(1.5k) shows a significantly higher constant (Z) value below 100 °C, suggesting that the polymer chains still have a higher mobility compared to the PLA and other FluoroPLAs polymer chains and contributes significantly to the growth of spherulites.

Overall, the Avrami equation offers a good representation of the data in thermal analysis rather than a precise analysis of the crystallization mechanism. The Avrami equation fits well for the initial crystallization (i.e. primary crystallization with no impingement of spherulites) but does not fit that well for the secondary crystallization (growth of spherulites in amorphous interstices).[23,24]

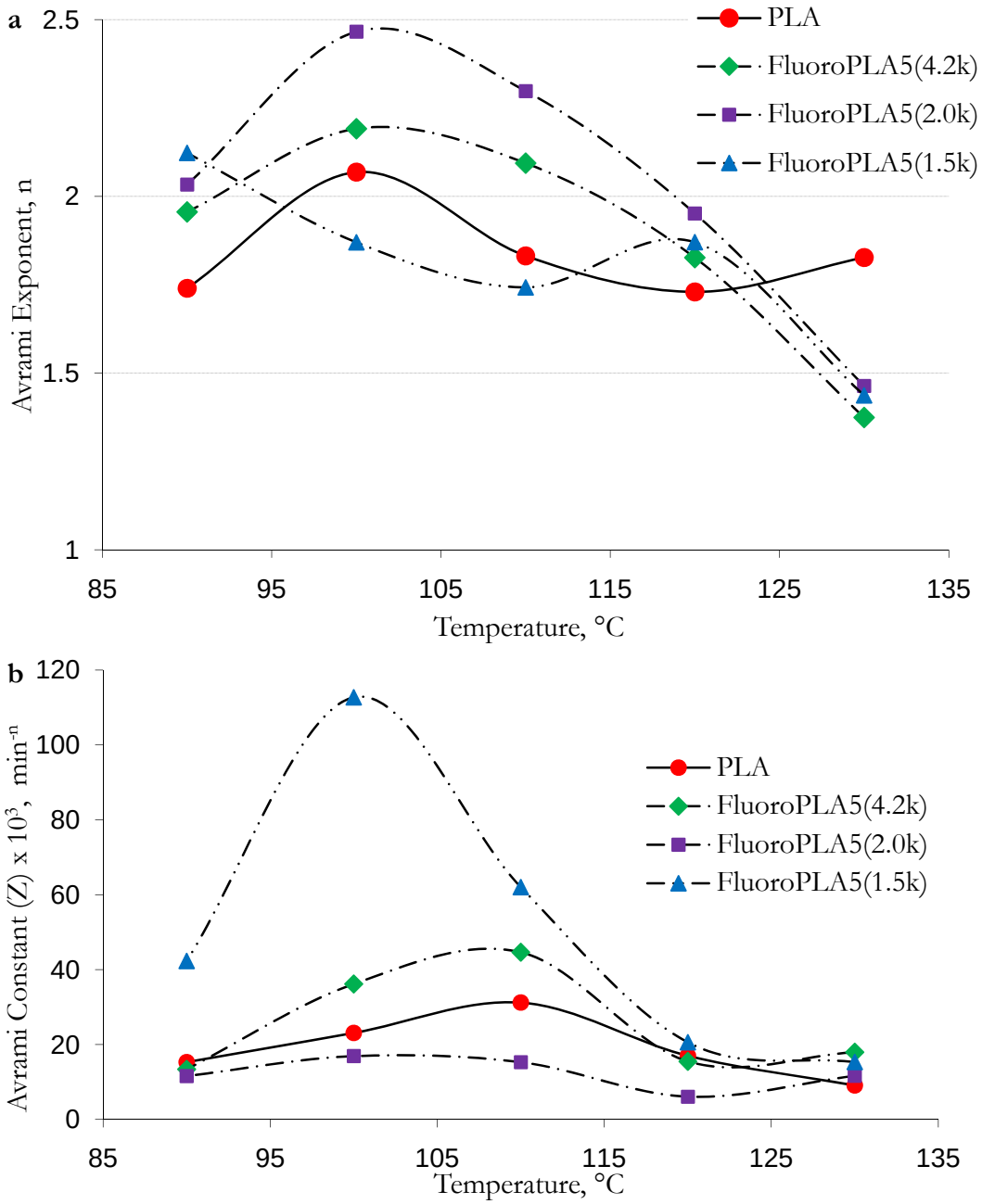

Figure 5.11. Avrami exponent (a) and constant (b) for PLA and FluoroPLAs.

The crystallization half time, $t_{1/2}$, can be defined as the time required to attain 50% relative crystallinity i.e. the completion of half crystallization of the sample. The $t_{1/2}$ is related to the constant Z by equation 5.14. Table 5.4 shows the $t_{1/2}$ values obtained from the DSC curves and equation 5.14.

$$t_{1/2} = \left(\frac{\ln(2)}{Z}\right)^{1/n} \qquad 5.14.$$

Figure 5.12 is the plot of the half-time of crystallization for PLA and FluoroPLAs versus various crystallization temperatures. At 130 °C, the $t_{1/2}$ for PLA (11.4 min) is lower than the $t_{1/2}$ of any FluoroPLAs (>15.2 min). Below 110 °C, the $t_{1/2}$ for PLA is higher than

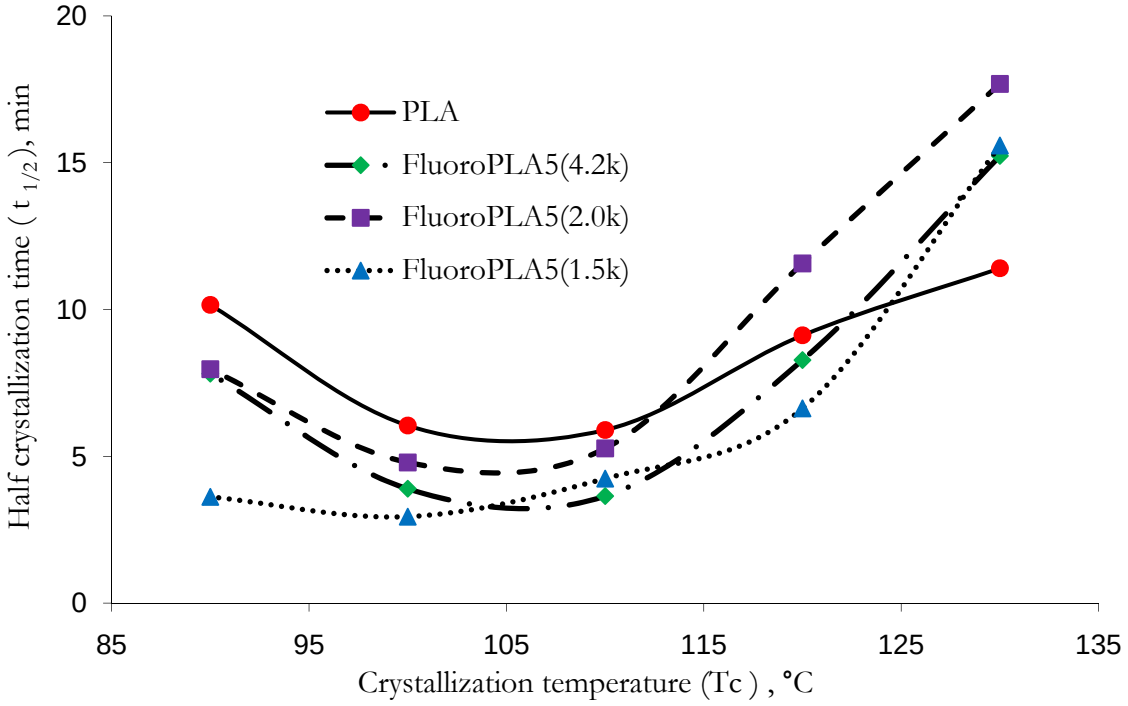

Figure 5.12. The half-time of crystallization ($t_{1/2}$) for PLA and FluoroPLAs at the various crystallization temperatures.

those for the FluoroPLAs, suggesting a slower rate of crystallization for PLA. Above 110 °C, PLA shows a lower $t_{1/2}$ values compared to those for the FluoroPLAs. However, there is a significant drop in the $t_{1/2}$ of the FluoroPLAs from 130 °C to 110 °C and at or below 110 °C, the $t_{1/2}$ for FluoroPLAs was lower than that of the PLA. The FluoroPLA5(1.5k) shows the lowest $t_{1/2}$, suggesting a higher crystallization rate among FluoroPLAs. At 90 °C when chain mobility decreases and crystallization becomes sluggish for PLA, FluoroPLA5(4.2k), and FluoroPLA5(2.0), the FluoroPLA5(1.5k) showed the lowest $t_{1/2}$ value (3.6 min) suggesting considerably more polymer chain mobility resulting in a higher crystallization rate.

Isothermal Crystallization: Optical Microscopic Measurements of Spherulitc Growth Rates

The spherulitic growth rates (G), which are the microscopic change in the diameter of the spherulites as a function of time during the isothermal crystallization, of polymers were measured during melt crystallization. The growth rates were monitored at isothermal temperatures ranging from 140 °C to 90 °C after cooling from the melt at 200 °C. The measurements were difficult for temperatures below 110 °C due to very high nucleation density. However, the linearity in the growth rate of individual spherulite was maintained for all the polymer systems (PLA and FluoroPLAs) through the range of isothermal crystallization temperatures. Spherulitic growth rates of PLA and FluoroPLAs are shown in Figure 5.13. As the isothermal temperature was lowered from 140 °C to 90 °C, a maximum was observed in the growth rates due to the increase in the driving force (degree of cooling) as the temperature decreases. However, the molecular motion becomes sluggish with continuing decrease in temperature and the growth rate decreases. The maximum growth

rate was observed at 15-20 °C above the measured crystallization temperatures obtained from the DSC experiments. The FluoroPLA5(1.5k) had the highest growth rate (ca. 11 μm/min at 110 °C) over the whole temperature range, most likely due to the molecular weight effect and its highly crystallizable nature. At 110 °C, the G values for PLA, FluoroPLA5(4.2k), FluoroPLA5(2.0k), and the FluoroPLA5(1.5k) were ca. 6.61, 6.64, 7.60, 11.09 μm/min, respectively. The growth rate of PLA at 130 °C was ca. 8 μm/min which is consistent with values published in previous studies (6.7, 9.1 μm/min).[26,27]

The growth rate of polymer spherulites has been described by the classical Turnbull-Fisher expression shown in equation 5.15, where G_0 represents a pre-exponential factor; $\Delta E_{d,T}$, the activation energy

$$G = G_0 \cdot e^{-\left(\frac{\Delta E_{d,T}}{kT_c}\right)} \cdot e^{-\left(\frac{\Delta E_{d,N}}{kT_c}\right)} \qquad 5.15.$$

of transport of a crystallizing segment across the melt-crystal interface; $\Delta E_{d,N}$, the activation energy to form a nucleus of critical size; Tc, crystallization temperature; and k, Boltzmann's constant. A Gaussian-like function is proposed for the growth rate of spherulites as a function of crystallization temperature.[28] In practice, as illustrated in Figure 5.13, the growth rate curve does not exhibit the simple Gaussian-like shape.

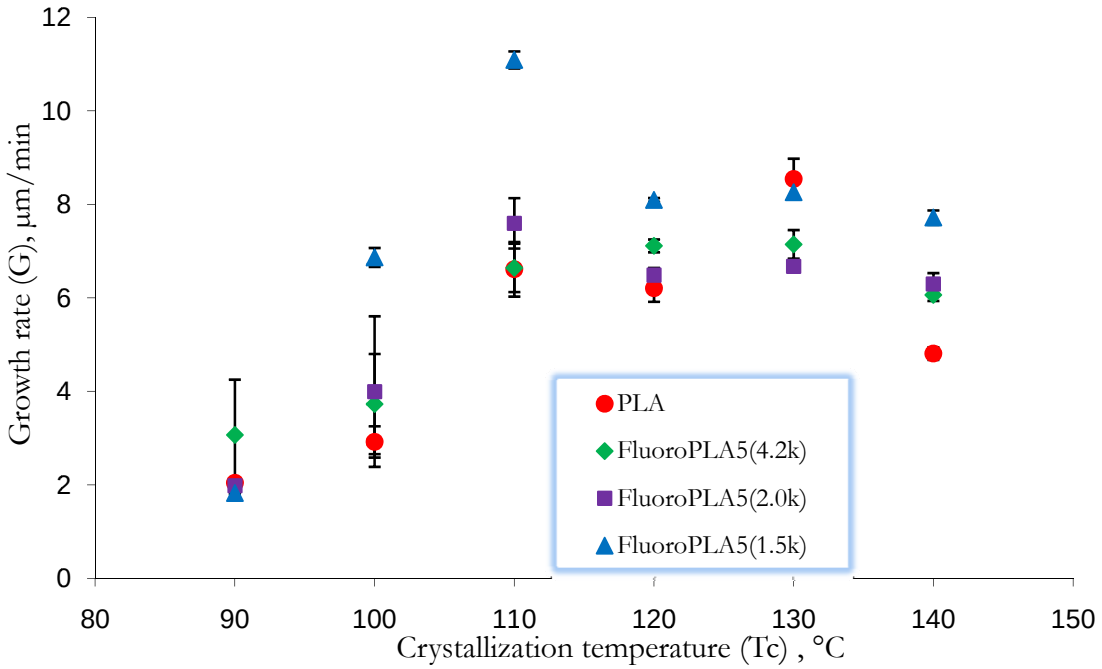

Figure 5.13. Spherulitic growth rate (G) for PLA and FluoroPLAs as a function of crystallization temperatures.

The crystallization temperature influences the radial growth rate and morphology of spherulites and thus controls the chain folding and packing. The rate of crystallization is nucleation-controlled when the temperature is above the crystallization temperature and it becomes diffusion controlled in the lower crystallization temperature range (below Tc).[28]

The nucleation density (N') can be roughly estimated using the assumption that the spherulites are identical in size.[29,30] The density can be expressed as:[31]

$$N' = (3/4\pi)(2/D_m^a)^3 \qquad 5.16.$$

where D_m^a the average maximum attainable diameter of the spherulites before any impingement. The observed D_m^a and the calculated N' for the PLA and the FluoroPLAs at 120 °C are shown in Figure 5.14 and the degree of cooling (Tm-Tc), observed D_m^a and calculated N' data for PLA and FluoroPLAs are summarized in Table 5.5. The nucleation density drops sharply when comparing PLA to the FluoroPLAs and the average maximum diameter increases linearly from PLA to FluoroPLA5(1.5k).

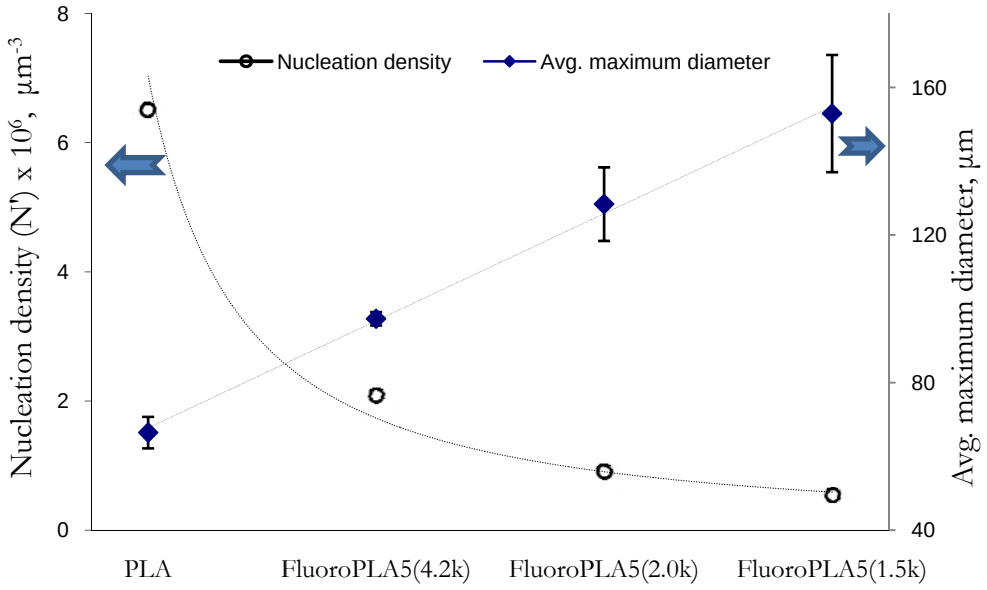

Figure 5.14. Nucleation density and maximum diameter of PLA and FluoroPLAs at 120 °C.

Table 5.5. The effect of degree of cooling on the primary average nucleation density at 120 °C.

Polymer	Degree of cooling, (Tm-Tc)[a], °C	Avg. Maximum diameter[b], µm	Nucleation density[c] (N'), μm^{-3}
PLA	55.7	66.5 ± 4.3	6.51×10^{-6}
FluoroPLA5(4.2k)	53.7	97.3 ± 1.8	2.07×10^{-6}
FluoroPLA5(2.0k)	50.3	128.4 ± 9.9	0.90×10^{-6}
FluoroPLA5(1.5k)	46.7	152.9 ± 15.9	0.53×10^{-6}

[a] Tc = 120 °C, [b] Mean ± standard dev, [c] primary average nucleation density.

At 120 °C, the degree of cooling for PLA is ca. 56 °C and ca. 47 °C for FluoroPLA5(1.5k). The difference in the degree of cooling between PLA and FluoroPLAs, increases from FluoroPLA5(4.2k) to FluoroPLA5(2.0k) to FluoroPLA5(1.5k) and the maximum difference between PLA and FluoroPLA5(1.5k) of 9 °C was observed. The measurement of D_m^a and N' is difficult below 120 °C as the nucleation density is very high and the maximum diameter (before impingement) of spherulites considerably smaller.

The spherulitic morphologies of the PLA and FluoroPLAs obtained after isothermal crystallization at 120 °C for 20 min are shown in Figure 5.15. At 120 °C, the D_m^a increases from PLA to FluoroPLA5(4.2k) to FluoroPLA5(2.0k) to FluoroPLA5(1.5k). It is clearly observed that the FluoroPLA5(1.5k) has the lower number of spherulites per unit area and larger spherulite than the PLA, FluoroPLA5(4.2k), and FluoroPLA5(2.0k).

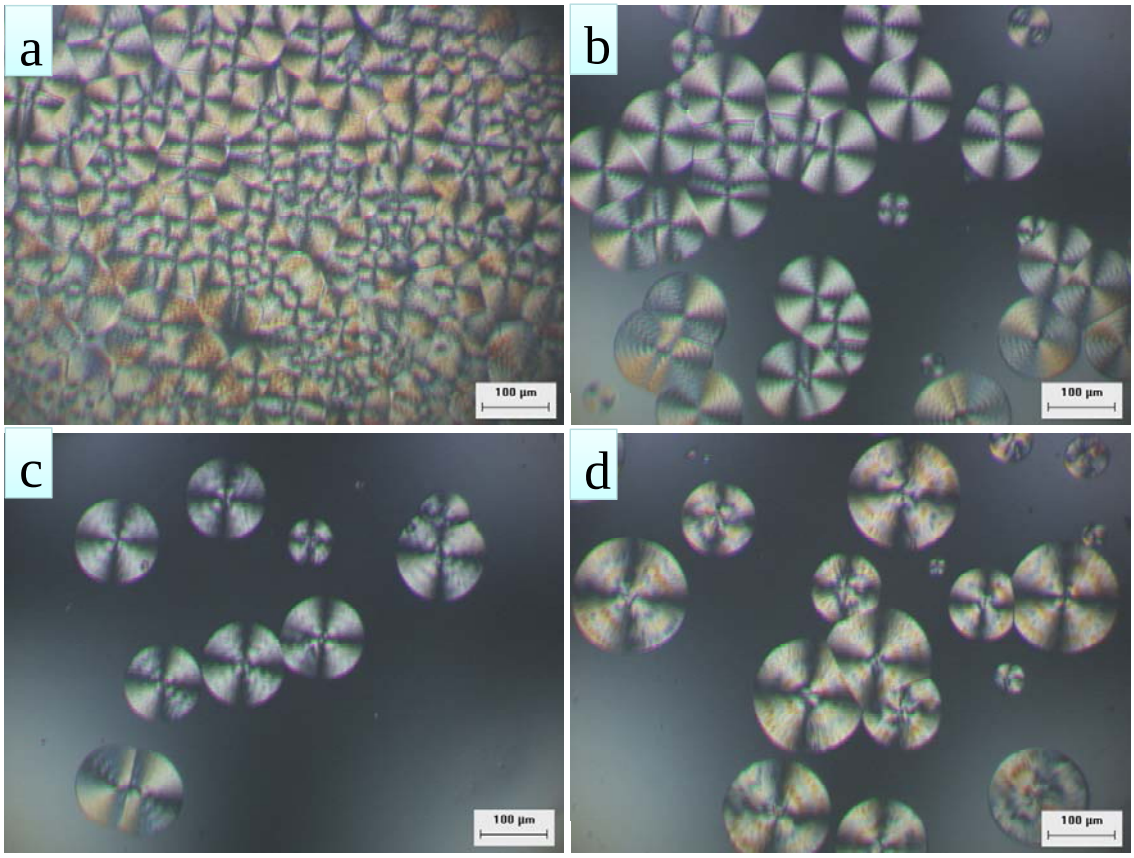

Figure 5.15. Polarized optical micrographs of PLA (a), FluoroPLA5(4.2k) (b), FluoroPLA5(2.0k) (c) and FluoroPLA5(1.5k) (d) isothermally crystallized from melt at 120 °C for 20 minutes.

The PLA crystals occur in three different forms: α-form with 10_3 helical conformation, β-form with 3_1 helical conformation and γ-form.[32-34] The α-form is the most common conformation and generally obtained during melt or solution crystallization.[35] Two types of spherulites are observed in polymers, Maltese cross (no band) and ringed (banded) spherulites. The appearance of different patterns is not dependent on the chemical nature or molecular characteristics of the polymer, but rather governed by its thermal properties. It is

commonly believed that lamellar twisting leads to a periodic extinction pattern (radial banding) in spherulites.[36] PLA does not show the distinct appearance of ringed (banded) spherulites at any temperature between 90 °C to 140 °C. However, the appearance of ringed spherulites was observed in the FluoroPLAs spherulites at 120 °C and above. FluoroPLA5(4.2k) show concentric ringed spherulites whereas the FluoroPLA5(2.0k) and FluoroPLA5(1.5k) show distorted bands.

Above 120 °C the appearance of ringed (or banded) spherulites were often observed in FluoroPLAs which was different from the appearance of the maltese cross in the case of PLA. Figure 5.16 shows an optical micrograph of FluoroPLA5(1.5k) under polarized and non-polarized light after isothermal crystallization at 130 °C for 120 min. The periodical bands result from lamellar twisting and the negative birefringent bands show edge-on lamellae and the positive birefringent bands show flat-on lamellae.[35] The interference colors observed in the spherulites can be attributed to the retardation expressed as[37] $r = t * \Delta n$; where r is the retardation or interference color (nm); t, the sample thickness (nm); and Δn, the birefringence. The relationship between the interference color and retardation is described in the Michael-Lévy interference color chart.[37,38] It is proposed that incorporation of fluorinated segments (PFPE) in the PLA backbone induces flexibility in the polymer chain and this could possibly facilitate the lamellae twisting.

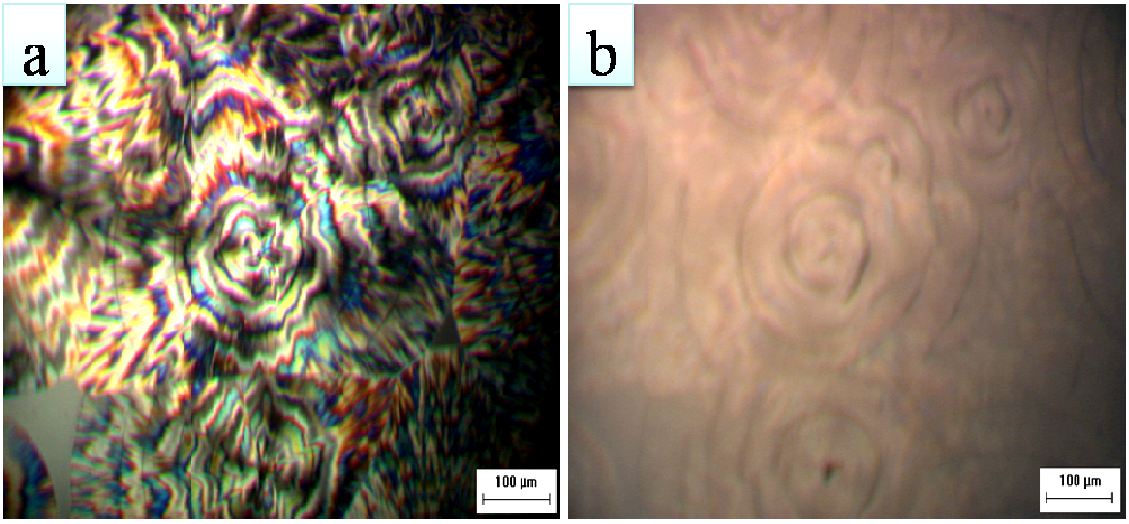

Figure 5.16. FluoroPLA5(1.5k) under polarized (a) and non-polarized (b) light after isothermal crystallization at 130 °C for 120 minutes.

Non-Isothermal Crystallization: Differential Scanning Calorimetry - Heat Capacities

A non-isothermal crystallization study during cooling is difficult in the case of PLA and FluoroPLAs as crystallization is not observed until a very slow rate of cooling (<10 °C/min) is employed. The crystallization can also be studied during the heating process i.e. cold crystallization. All the samples were first heated to 200 °C, and then were cooled at the rate of 20 °C/min to 25 °C and then subjected to different heating rates. Figure 5.17 shows the plot of heat capacities for PLA and FluoroPLAs (only crystallization transition shown) as a function of temperature for the different heating rates. All of the heat flow signals show an increase in the crystallization peak area with an increase in heating rate. In the following discussion the heat capacity data are used for comparing the polymers at the different heating rates.

Under non-isothermal conditions, the observed crystallization exotherm will be a function of crystallization temperature, heating rate and instrumental parameters. As shown in Figure 5.17, as the heating rate increased, the crystallization curves were observed to shift to higher temperatures for PLA and FluoroPLAs. The change in heating rate from 2.5 °C/min to 20 °C/min shifts the curve by 28 °C for PLA and ca. 21 ± 2.6 °C for FluoroPLAs. The FluoroPLA5(1.5k) show the smallest shift of 18 °C.

For the heating rate of 2.5 °C/min, the FluoroPLA5(1.5k) crystallization peak appears at 83 °C, whereas the PLA crystallization peak appears at 95 °C and the FluoroPLA5(4.2k) and the FluoroPLA5(2.0k) show crystallization peaks between 83 – 95 °C (at 93, 91 °C respectively). Hence, FluoroPLAs crystallize at lower temperatures and this observation is well supported by the isothermal crystallization study.

For the heating rate of 40 °C, almost no crystallization peak is observed in case of PLA but the FluoroPLAs show a developing peak. FluoroPLA5(1.5k) shows the well developed crystallization peak even at the crystallization rate of 40 °C/min. Hence, we can conclude that FluoroPLAs have higher crystallization rates than the PLA and this behavior can be explained by hypothesizing the nucleating action of PFPE segments.

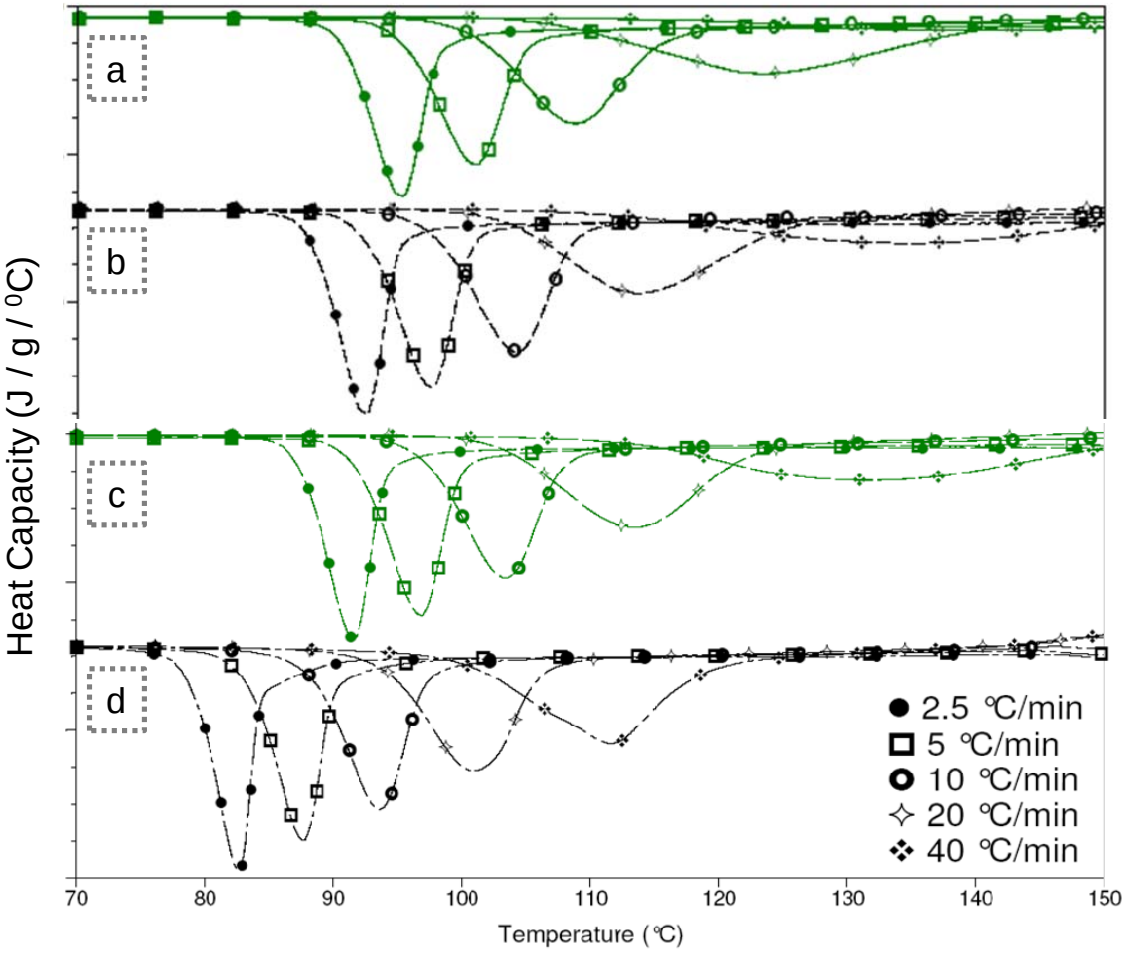

Figure 5.17. Heat capacity curves for non-isothermal cold crystallization of PLA (a), FluoroPLA5(4.2k) (b), FluoroPLA5(2.0k) (c) and FluoroPLA5(1.5k) (d) obtained during various heating rates.

DSC is a very sensitive tool for the measurement of small heat changes and hence, is a useful technique for the determination of the activation energies associated with kinetic process such as crystallization.[39] During the crystallization, upon heating a relatively amorphous semi-crystalline polymer sample or cooling a semi-crystalline polymer melt, the change in the heat content and the thermal properties of the sample is indicated by an exothermic deflection (peak). The position of the peak varies with the heating rate if other experimental parameters were kept constant.[40] The Kissinger method can be utilized to calculate the activation energies associated with non-isothermal cold crystallization of polymer.[41-43] The Kissinger equation[40,44] can be written as

$$\frac{d \ln\left(\frac{\beta}{T_p^2}\right)}{d\left(\frac{1}{T_p}\right)} = -\frac{E_a}{R} \qquad 5.17.$$

where R is the gas constant, T_P is the temperature corresponding to the maximum of crystallization curve (with the assumption that the reaction rate is maximum at T_P), E_a is the activation energy and β (=dT/dt) is the heating rate. The equation can be solved and rearranged in the form:

$$-\ln\left(\frac{\beta}{T_p^2}\right) = Const + \left(\frac{E_a}{R}\right)\frac{1}{T_p} \qquad 5.18.$$

The value of E_a is determined from the plot of $-\ln(\beta/T_P^2)$ vs $1/T_P$ for different heating rates which results in a straight line with slope E_a/R.

The plots of $-\ln(\beta/T_P^2)$ against $1/T_P$ for PLA and the FluoroPLAs are shown in Figure 5.18. The activation energies of PLA and the FluoroPLAs are summarized in Table

5.6. The activation energy from the non-isothermal cold crystallization for PLA was 69.1 kJ/mol and for FluoroPLA5(4.2k), FluoroPLA5(2.0k) and the FluoroPLA5(1.5k) was 71.1, 74.8 and 125.0 kJ/mol respectively. The higher activation energies of FluoroPLAs suggest the higher crystallizability (energy is released during crystallization) and amongst the FluoroPLAs, FluoroPLA5(1.5k) shows highest activation energy and this could possibly be due to the nucleating action of PFPE segments.

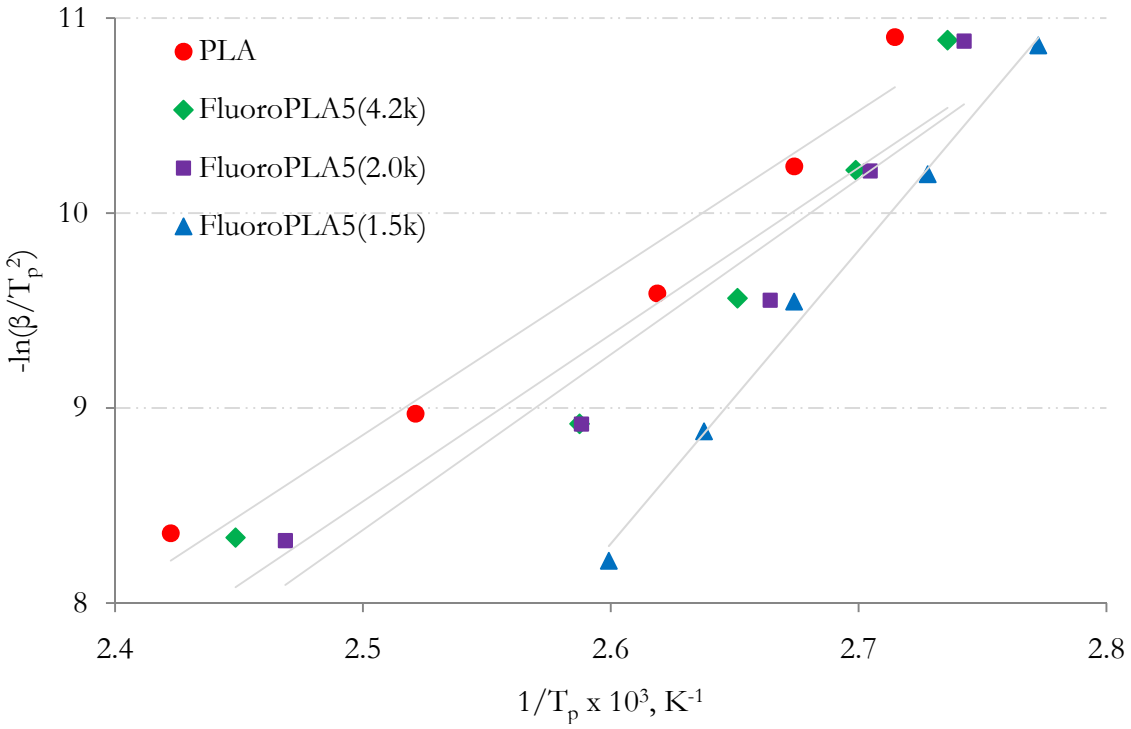

Figure 5.18. Plot of $-\ln(\beta/T_p^2)$ against $1/T_p$ for PLA and the FluoroPLAs.

Table 5.6. Activation energies of PLA and FluoroPLAs calculated from Kissinger's equation.

Polymer	Heating rate (°C/min)	T_P (°C)	E_a (kJ/mol)	R^2
PLA	2.5	95.2	69.1	0.959
	5.0	100.8		
	10.0	108.7		
	20.0	123.5		
	40.0	139.7		
FluoroPLA5(4.2K)	2.5	92.4	71.1	0.909
	5.0	97.4		
	10.0	104.1		
	20.0	113.3		
	40.0	135.3		
FluoroPLA5(2.0K)	2.5	91.5	74.8	0.925
	5.0	96.6		
	10.0	102.2		
	20.0	113.2		
	40.0	131.9		
FluoroPLA5(1.5K)	2.5	87.5	125.0	0.994
	5.0	93.4		
	10.0	100.8		
	20.0	106.0		
	40.0	111.6		

Solution Crystallization

Figure 5.19 shows polarized optical micrographs of solution crystallized PLA and FluoroPLAs. The micrograph for PLA shows a few isolated crystalline areas in bulk and the PLA solution crystallized films contains many similar spots. The micrographs of the FluoroPLAs show a uniform growth of spherulites throughout the sample. Hence, FluoroPLAs appear to have better crystallization properties in solution too.

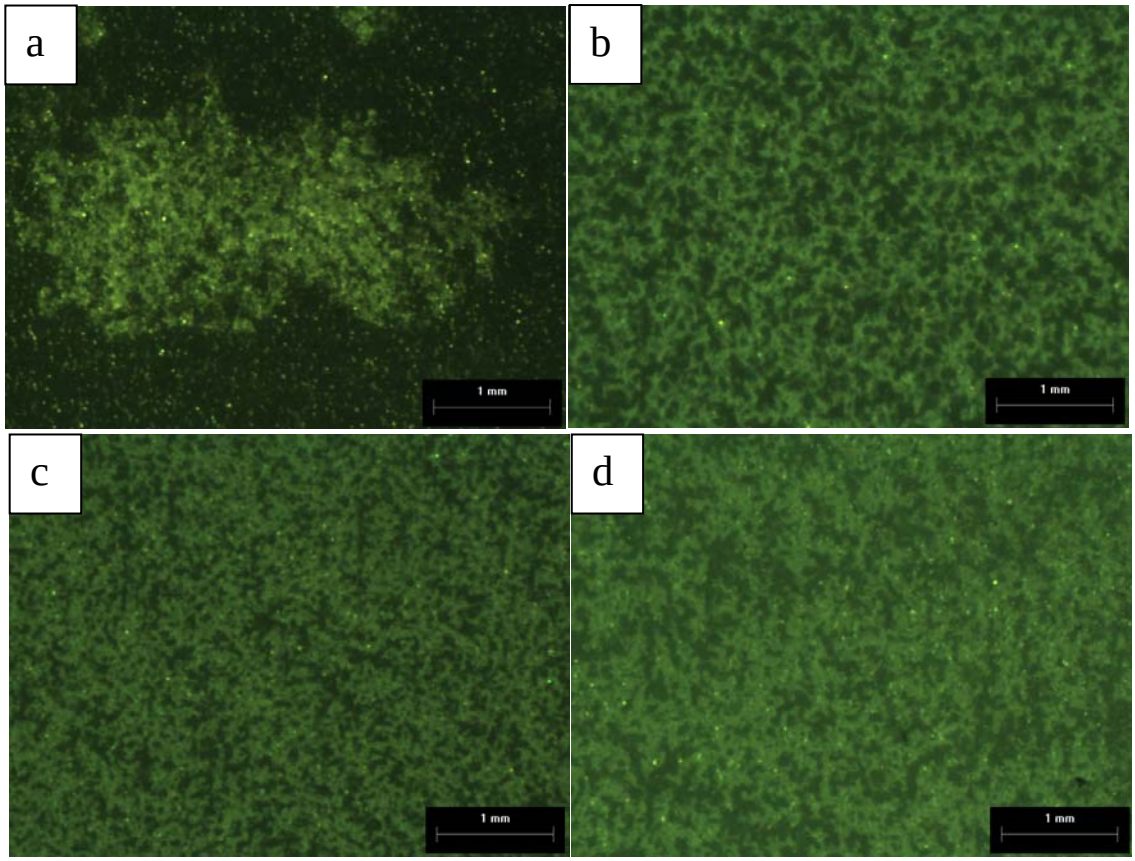

Figure 5.19. Polarized optical micrographs of PLA (a), FluoroPLA5(4.2k) (b), FluoroPLA5(2.0k) (c) and FluoroPLA5(1.5k) (d) crystallized from 3.75 %(w/v) solution in chloroform for 72 hour. Scale bar 1 mm.

5.4 Conclusion

The incorporation of high density, low surface energy PFPE in the PLA backbone by the ring-opening polymerization results in a low surface energy (Ch. 4), high crystallinity novel material (FluoroPLA). It is proposed that the FluoroPLAs show higher crystallization rates than the homopolymer PLA due to the nucleating action of the PFPE segments. The molar content of PFPE affects the crystallization temperature and the melting peak temperatures. The increase in molar PFPE content lowers the crystallization and melting temperature of the copolymer. Hence, the copolymer with the higher PFPE content can be processed at lower temperatures. The crystallization half time ($t_{1/2}$) for FluoroPLAs are very low even at lower temperature (90 °C). The higher crystallization rate and overall crystallinity of FluoroPLAs are retained even in solution crystallization. These results demonstrate that it is possible to design the molar and thermal characteristics of block copolymers by the controlled addition of macro-initiator, PFPE.

5.5 References

1. Vasanthakumari, R. & Pennings, A. J. Crystallization Kinetics of Poly(L-lactic acid). *Polymer* **24**, 175-178 (1983).
2. Kalb, B. & Pennings, A. J. General Crystallization Behaviour of Poly(L-lactic acid). *Polymer* **21**, 607-612 (1980).
3. Masirek, R., Piorkowska, E., Galeski, A. & Mucha, M. Influence of Thermal History on the Non-Isothermal Crystallization of Poly(L-lactide). *Journal of Applied Polymer Science* **105**, 282-290 (2007).
4. Sarasua, J.-R., Rodriguez, N. L., Arraiza, A. L. & Meaurio, E. Stereoselective Crystallization and Specific Interactions in Polylactides. *Macromolecules* **38**, 8362-8371 (2005).
5. Hamley, I. W. et al. Crystallization in Oriented Semicrystalline Diblock Copolymers. *Macromolecules* **29**, 8835-8843 (1996).
6. Müller, A. J., Arnal, M. L. & Balsamo, V. Crystallization in Block Copolymers with More than One Crystallizable Block. *Lecture Notes in Physics* **714**, 229-259 (2007).
7. Hamley, I. W. in *Developments in Block Copolymers Science and Technology* (ed. Hamley, I. W.) 1-30 (John Wiley & Sons Ltd., Hoboken, NJ, 2004).
8. Rangarajan, P. et al. Crystallization of a Weakly Segregated Polyolefin Diblock Copolymer. *Macromolecules* **28**, 4932-4938 (1995).
9. Loo, Y.-L., Register, R. A. & Ryan, A. J. Modes of Crystallization in Block Copolymer Microdomains: Breakout, Templated, and Confined. *Macromolecules* **35**, 2365-2374 (2002).

10. Bottino, F. A. et al. XPS Study on Surface Segregation in Poly(ethylene-iso/terephthalate)-Perfluoropolyether Block Copolymers. *Macromolecules* **31**, 7814-7819 (1998).

11. Pilati, F. et al. Surface Investigation by ESCA of Poly(ethylene terephthalate)-Perfluoropolyether Block Copolymers. *Macromolecules* **23**, 348-350 (1990).

12. Pilati, F. et al. Poly(ε-caprolactone)-Poly(fluoroalkylene oxide)-Poly(ε-caprolactone) Block Copolymers. 1. Synthesis and Molecular Characterization. *Macromolecules* **32**, 6969-6976 (1999).

13. Toselli, M. et al. Poly(ε-caprolactone)-Poly(fluoroalkylene oxide)-Poly(ε-caprolactone) Block Copolymers. 2. Thermal and Surface Properties. *Polymer* **42**, 1771-1779 (2001).

14. Claudio, T., Francesco, P., Maurizio, T., Antonio, T. & Ercole, G. Fluoromodified Polyesters Having Improved Processability. U.S. Patent 5686522.(1997).

15. Tsuji, H. & Muramatsu, H. Blends of Aliphatic Polyesters. IV. Morphology, Swelling Behavior, and Surface and Bulk Properties of Blends from Hydrophobic Poly(L-lactide) and Hydrophilic Poly(vinyl alcohol). *Journal of Applied Polymer Science* **81**, 2151-2160 (2001).

16. Fischer, E. W., Sterzel, H. J. & Wegner, G. Investigation of the Structure of Solution Grown Crystals of Lactide Copolymers by Means of Chemical Reactions. *Colloid & Polymer Science* **251**, 980-990 (1973).

17. Turri, S., Sanguineti, A. & Levi, M. Molecular Characterization and Chain Flexibility of Linear Polyacetals Containing Polyperfluoro(oxymethylene-*ran*-oxyethylene) Macromers. *Macromolecular Chemistry and Physics* **198**, 3215-3228 (1997).

18. Fomblin Z Derivatives - Product Data Sheet.*www.solvaysolexis.com.*(September 2007).

19. Kim, J. Y., Park, H. S. & Kim, S. H. Unique Nucleation of Multi-Walled Carbon Nanotube and Poly(ethylene 2,6-naphthalate) Nanocomposites During Non-Isothermal Crystallization. *Polymer* **47**, 1379-1389 (2006).

20. Sung, Y.-t. et al. Rheological Properties and Crystallization Kinetics of Polypropylene Block Copolymer with Repeated Extrusion. *Korea-Australia Rheology Journal* **17**, 21-25 (2005).

21. Avrami, M. Kinetics of Phase Change. II Transformation-Time Relations for Random Distribution of Nuclei. *The Journal of Chemical Physics* **8**, 212-224 (1940).

22. Turi, E. A. *Thermal Characterization of Polymeric Materials* (Academic Press, New York, 1981).

23. Wunderlich, B. *Thermal Analysis* (Academic Press, Boston, 1990).

24. Sperling, L. H. *Introduction to Physical Polymer Science* (Wiley-Interscience, New York, 2001).

25. Sorai, M. *Comprehensive Handbook of Calorimetry and Thermal Analysis* (J. Wiley, Hoboken, NJ, 2005).

26. Di Lorenzo, M. L. Determination of Spherulite Growth Rates of Poly(L-lactic acid) Using Combined Isothermal and Non-Isothermal Procedures. *Polymer* **42**, 9441-9446 (2001).

27. He, Y., Fan, Z., Wei, J. & Li, S. in *Polymer Engineering and Science* 1583(7) (2006).

28. Marentette, J. M. & Brown, G. R. Polymer Spherulites II. Crystallization Kinetics. *Journal of Chemical Education* **70**, 539-542 (1993).

29. Nam, J. Y. et al. Morphology and Crystallization Kinetics in a Mixture of Low-Molecular Weight Aliphatic Amide and Polylactide. *Polymer* **47**, 1340-1347 (2006).

30. Sinha Ray, S., Yamada, K., Okamoto, M., Ogami, A. & Ueda, K. New Polylactide/Layered Silicate Nanocomposites. 3. High-Performance Biodegradable Materials. *Chemistry of Materials* **15**, 1456-1465 (2003).

31. Maiti, P., Nam, P. H., Okamoto, M., Hasegawa, N. & Usuki, A. Influence of Crystallization on Intercalation, Morphology, and Mechanical Properties of Polypropylene/Clay Nanocomposites. *Macromolecules* **35**, 2042-2049 (2002).

32. De Santis, P. & Kovacs, A. J. Molecular Conformation of Poly(*S*-lactic acid). *Biopolymers* **6**, 299-306 (1968).

33. Hoogsteen, W., Postema, A. R., Pennings, A. J., ten Brinke, G. & Zugenmaier, P. Crystal Structure, Conformation and Morphology of Solution-Spun Poly(L-lactide) Fibers. *Macromolecules* **23**, 634-642 (1990).

34. Cartier, L. et al. Epitaxial Crystallization and Crystalline Polymorphism of Polylactides. *Polymer* **41**, 8909-8919 (2000).

35. Xu, J. et al. Observation of Banded Spherulites in Pure Poly(L-lactide) and its Miscible Blends with Amorphous Polymers. *Polymer* **46**, 9176-9185 (2005).

36. Raimo, M. A Thermo-Conductive Approach to Explain the Origin of Lamellar Twisting in Banded Spherulites. *Journal of Materials Science* **42**, 998-1003 (2007).

37. Marentette, J. M. & Brown, G. R. Polymer Spherulites I. Birefringence and Morphology. *Journal of Chemical Education* **70**, 435-439 (1993).

38. Yun, J. H., Kuboyama, K., Chiba, T. & Ougizawa, T. Crystallization Temperature Dependence of Interference Color and Morphology in Poly(trimethylene terephthalate) Spherulite. *Polymer* **47**, 4831-4838 (2006).

39. Donthu, S., Vora, M., Lahiri, S., Thompson, C. & Yi, S. Activation Energy Determination for Recrystallization in Electroplated-Copper Films Using Differential Scanning Calorimetry. *Journal of Electronic Materials* **32**, 531-534 (2003).

40. Kissinger, H. E. Reaction Kinetics in Differential Thermal Analysis. *Analytical Chemistry* **29**, 1702-1706 (1957).

41. Vyazovkin, S. Is the Kissinger Equation Applicable to the Processes that Occur on Cooling? *Macromolecular Rapid Communications* **23**, 771-775 (2002).

42. Soliman, A. A. Derivation of the Kissinger Equation for Non-Isothermal Glass Transition Peaks. *Journal of Thermal Analysis and Calorimetry* **89**, 389-392 (2007).

43. Lee, Y.-K. et al. Activation Energy and Curing Behavior of Resol- and Novolac-Type Phenolic Resins by Differential Scanning Calorimetry and Thermogravimetric Analysis. *Journal of Applied Polymer Science* **89**, 2589-2596 (2003).

44. Kissinger, H. E. Variation of Peak Temperature with Heating Rate in Differential Thermal Analysis. *Journal of Research of the National Bureau of Standards* **57**, 217-221 (1956).

CHAPTER 6

HYDROLYTIC STABILITY OF POLYLACTIDE AND POLYLACTIDE-PERFLUOROPOLYETHER BLOCK COPOLYMERS

6.1 Introduction

Plastics are inexpensive, light-weight, strong, easily processable and energy efficient materials and heavily utilized in modern society. However, irreversible build-up of these non-biodegradable polymeric materials in landfills impacts the environment severely and is thus driving the need for more biodegradable polymeric materials. Degradable polymeric materials possess inherent sensitivity to physical, chemical, mechanical or biological agents.[1]

One such biodegradable polymer is polylactide / poly(lactic acid) (PLA) from the aliphatic polyester group. The first synthesis of poly(lactic acid) was reported by Carothers et al. in 1932.[2] The medical applications of PLA and its copolymers for surgical implants and tissue repair began in the 1960s.[3] In addition to the biomedical and pharmaceutical applications, PLA and its copolymers are showing a significant rise in their use in commodity applications because they are made from a renewable monomer resource, they have comparable mechanical properties to petroleum-based polymers, they degrade in the natural environments with very low toxicity, and above all, recent developments in technology have lead to comparable prices to petroleum-based commercial polymers.[4,5] Various modification have been recently used to alter the intrinsic properties of PLA. The enhancement of properties has been due to the use of novel catalysts and modifications by blending, plasticization and copolymerization with other polymers and/or compounds are reported.[6-9]

The commodity application of PLA as film, fiber, molded components, etc., requires the prediction of durability after which a sudden decline in mechanical and tensile properties

occurs due to hydrolysis. The hydrolytic degradation of aliphatic polyesters such as PLA has been extensively investigated.[10-15] Degradation is a very complex process influenced by various factors such as crystallinity, swellability, hydrophobicity/hydrophilicity, polymer chain length, diffusivity, glass transition temperature (T_g), type of hydrolysable linkage, etc.[16-18] The comparative rates of diffusion and degradation governs the mode of erosion i.e. bulk or surface erosion. Surface erosion prevails when degradation is significantly faster than diffusion and only rapidly degrading polymers such as polyanhydrides and poly(ortho esters) have been reported to show surface erosion.[19] Pitt et al. (1987) reported a kinetic relationship between the number average molecular weight and time as $M_{n,t}/M_{n,0} = \exp(-kt)$ for aliphatic polyesters such as poly(ε-caprolactone) and PLA in phosphate buffer (pH 7.4) and concluded that the hydrolysis of these polyesters proceeds by the autocatalytic random chain scission catalyzed by carboxylic acid end groups.[20,21]

In this study, we modified the surface and bulk properties of PLA using telechelic poly(fluoroalkylene oxide)s with reactive hydroxyl groups as a macrointiator leading to polylactide-poly(fluoroalkylene oxide)s-polylactide block copolymer (FluoroPLA). FluoroPLAs (surface energy of ca. 16-19 mN/m) shows better hydrophobicity and lipophilicity than PLA (surface energy of ca. 35-40 mN/m). In this study, the hydrolytic degradation of PLA and FluoroPLA in alkaline, acidic and aqueous media and the effect of degradation on thermal, molecular and surface properties are described.

6.2 Materials and Methods

Materials

PLA and FluoroPLAs were synthesized for the study as described and discussed in Chapter 4. The molecular characterstics and thermal properties of the synthesized PLA and FluoroPLAs used in this study are summarized in Table 6.1. Solution cast films were prepared from ~2(wt/v)% polymer in $CHCl_3$ and the resultant films were annealed at 90 °C for 12 h. From the cast films, specimens were prepared by cuting to a size of 40 mm x 10 mm with thickness ca. 0.17mm. The sodium hydroxide (0.05N), hydrochloric acid (0.05N), acetic acid (1.0N) and water (HPLC grade, Burdick & Jackson) were purchased from VWR. Buffer solutions (pH 8 and pH 6) were purchased from Fisher Scientific.

Hydrolytic Degradation

The hydrolytic degradation of films was performed in 50 ml of the appropriate solution (Water, 0.5N NaOH, 0.05N HCl or 0.05N Acetic acid) at 60 °C for up to 15 weeks. Films (40 mm x 10 mm x ~0.17mm, 82.3 ± 5.2 mg) were placed in 80 ml plastic (HDPE) bottles with 50 ml of solution and the whole batch was held isothermally at 60 °C. Samples for each polymer and for all the treatments were removed after 1, 2, 3, 4, 6, 8, 11 and 15 weeks. The sample bottles were removed, cooled to room temperature, and thereafter, the hydrolyzed films were removed and washed with deionized water, neutralized in buffer solutions (pH 8 and pH 6 for acidic and alkaline treated films respectively) and washed again with distilled water thoroughly to prevent further degradation. The washed degraded films

were dried in a desiccator over silica for 36 h. The dried films were utilized to monitor any change in weight, molecular weight and thermal properties of the hydrolyzed films.

Table 6.1. Molecular characterstics and thermal properties of PLA and FluoroPLAs. (Mn: number average molecular weight; PDI: Molecular weight distribution; Tg: glass transition temperature; Tm: Melting temperature; Tc: crystallization temperature;

Polymer	PFPE/LA (mol/mol)	Mn[a] (kD)	PDI[a]	Tg[b,c] (°C)	Tc[b,c] (°C)	Tm[b,c] (°C)	ΔHm[b,d] (J/g)	Contact Angle[e] (°)	Surface Energy[f] (mN/m)
PLA	0.0000/1	144	1.66	61.9±0.4	107.8±0.1	176.1±0.0	39.3±1.4	74.3 ± 0.6	40.2
FluoroPLA5(4.2k)	0.0017/1	94	1.76	60.5±0.5	102.9±0.2	173.4±0.1	46.5±2.2	104.2 ± 0.5	19.1
FluoroPLA5(2.0k)	0.0038/1	82	1.68	59.7±0.4	103.3±0.1	171.9±0.1	50.8±1.0	104.1 ± 0.4	16.8
FluoroPLA5(1.5k)	0.0045/1	67	1.64	51.0±1.1	99.1±0.0	167.8±0.4	54.9±0.9	104.7 ± 0.5	18.5

[a] GPC; [b] DSC data for samples heated at the rate of 10 °C/min; [c] 2nd heating cycle; [d] 1st heating cycle (annealed); [e] Equilibrium static contact angle (degrees) of water on the dip coated polymer films on silicon wafer; [f] by Kaelble method.

Measurements

The percent weight loss values were calculated using the measured weight of each film before and after degradation ($W_{initial}$ and W_{final}, respectively) and equation 6.1.

$$W_{loss}(\%) = \left[\left(W_{initial} - W_{final}\right)/W_{initial}\right] \times 100 \qquad 6.1$$

The pH measurements were performed on the solutions after removal of the degraded films using a Beckman Electrode Series 511050 (Beckman Coulter, Fullerton, CA). The number and weight average molecular weights of polymers were characterized using a Waters "Breeze" GPC system (Waters, Milford, MA) interfaced with a Polymer Lab (Amherst, MA) PL-ELS 2100 detector. Two Waters columns were used in series (Styragel HR4E & HR5E). The mobile phase was chloroform (Burdick & Jackson, HPLC grade) at 1 ml/min. Polystyrene standards (Polysciences, Inc., Warrington, PA)of number average molecular weights 1,000,000; 600,000; 400,000; 200,000; 105,200; 50,000; 20,000; 4,000; 436 Dalton (Polydispersity Index ≤1.1) were used to calibrate the system.

Differential Scanning Calorimentry (DSC) analysis was conducted using a TA Instruments (New Castle, Delaware) Q1000 DSC. Data was analyzed using TA Instruments Universal Analysis 2000 version 4.1D software. The samples (6-8 mg in standard aluminum pans) were heated from 0 °C to 200 °C at a heating rate of 10 °C/min. The temperature values of the endothermic peak maxima's were considered as melting temperatures, and the integral of the peak area was used as the heat of fusion.

Diffraction patterns of polymers were collected at room temperature using SCINTAG XDS 2000 (Scintag, Inc., Cupertino, CA) diffractometer equipped with Cu Kα source at a wavelength of 1.54 Å. The instrument was operated at 40 kV and 40 mA with a

collimator diameter of 0.5 mm. Solution-cast polymer films were scanned at 2 °/min (2θ value) from 6 ° to 60 °. The percent crystallinity was calculated by dividing the total counts under crystalline peaks by the total area under the curve. Data were analyzed using DMSNT™ version 1.37 software.

Scanning electron microscopy (SEM) images of the hydrolyzed samples were obtained using a Hitachi S3400N (Hitachi High-Technologies, Japan) Microscope at an accelerating voltage of 20 kV. A Hummer®6.2 (Anatech Ltd., Hayward, CA) sputter coater was used to pre-coat the samples with a 4-5 nm layer of platinum.

6.3 Results and Discussion

Weight Change (Erosion)

The erosion of the polymer film leads to weight loss during hydrolysis. Figure 6.1 shows the weight loss of PLA films as a function of the hydrolysis time in different hydrolytic media. The weight loss of the PLA films in water and acidic solutions showed an induction period of 4 weeks with a slow weight loss observed for all films. However for the films in NaOH solutions, almost linear loss in weight versus time was observed with complete erosion of the film observed by the 4th week. The weight loss of PLA films in NaOH can be explained by the surface erosion of the film, and the weight loss in water, HCl and acetic acid due to a bulk erosion phenomenon.[19]

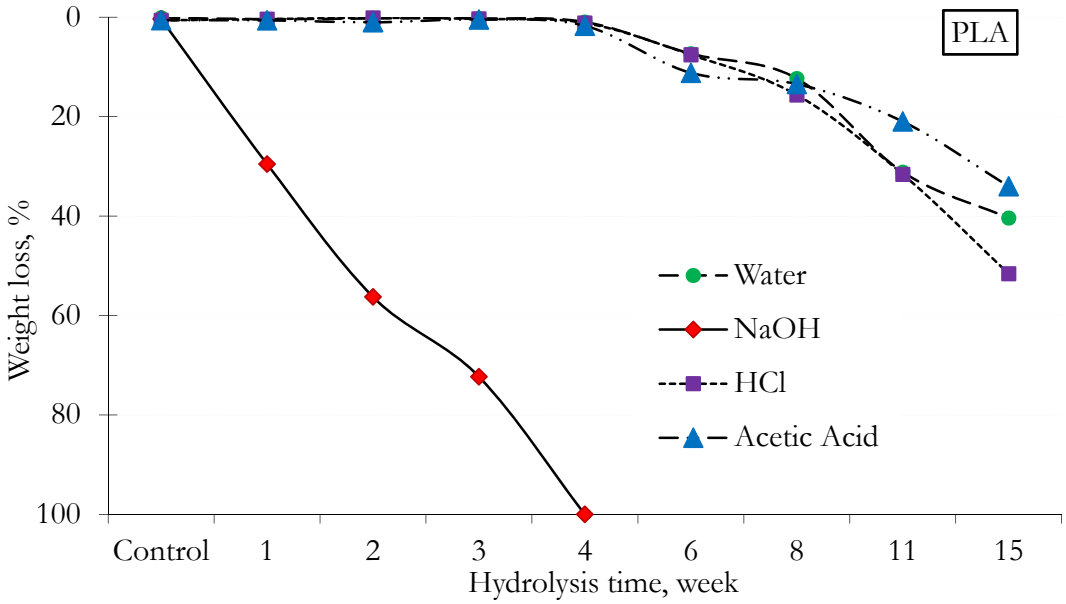

Figure 6.1. Percentage weight loss in PLA films in different hydrolytic solutions as a function of hydrolysis time.

Figure 6.2 shows the weight loss of the FluoroPLA5(4.2k) films as a function of the hydrolysis times in the different hydrolytic media. In alkaline medium, complete weight loss was observed by 2nd week. However, weight loss is of only ca. 76 % in HCl solution, ca. 46 % in water and ca. 40 % in acetic acid solution were observed after 15th week. The weight loss in acetic acid and water were similar except for the 3rd week data which could be possibly due to handling the fragile degraded films.

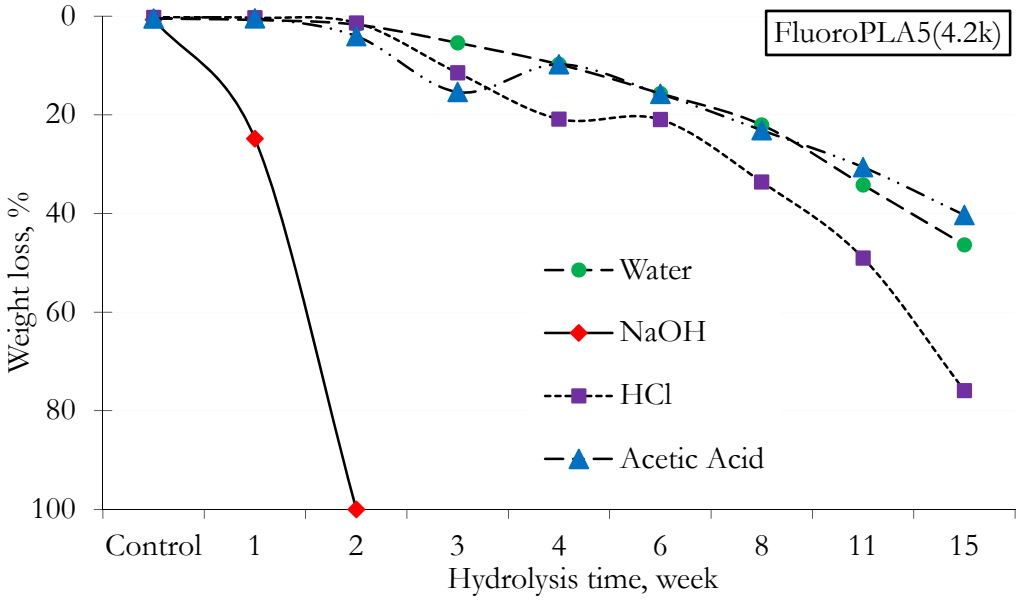

Figure 6.2. Percentage weight loss in FluoroPLA5(4.2k) films in different hydrolytic solutions as a function of hydrolysis time.

The weight loss of FluoroPLA5(2.0k) films in aqueous, acidic, and alkaline conditions as a function of hydrolysis time is shown in Figure 6.3. The complete degradation and disintegration of films were observed in alkaline solution by 4th week, whereas weight loss is of only ca. 58 % in HCl solution, ca. 33 % in acetic acid solution, and ca. 31 % were

observed for the FluoroPLA5(2.0k) films. The weight loss in water and acetic acid showed similar trend throughout the hydrolytic study whereas weight loss in HCl solution was accelerated for the 11th and 15th week.

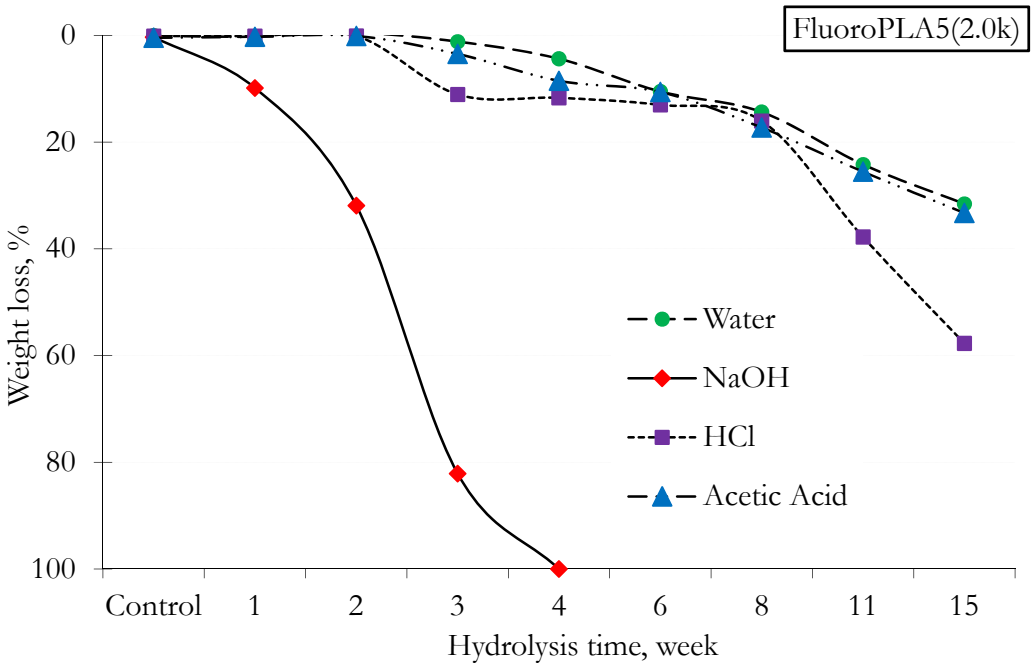

Figure 6.3. Percentage weight loss in FluoroPLA5(2.0k) films in different hydrolytic solutions as a function of hydrolysis time.

Figure 6.4 shows the weight loss of FluoroPLA5(1.5k) films as function of hydrolysis time in aqueous, acidic, and alkaline medium. The films are completely degraded and disintegrated in alkaline solution by the 4th week. In case of water and acetic acid, similar weight loss was observed in films except for the 15th week where weight loss in water was high (ca. 74 % compared to ca. 32% in acetic acid). At the end of 15th week, the weight loss in HCl solution was ca. 51 % .

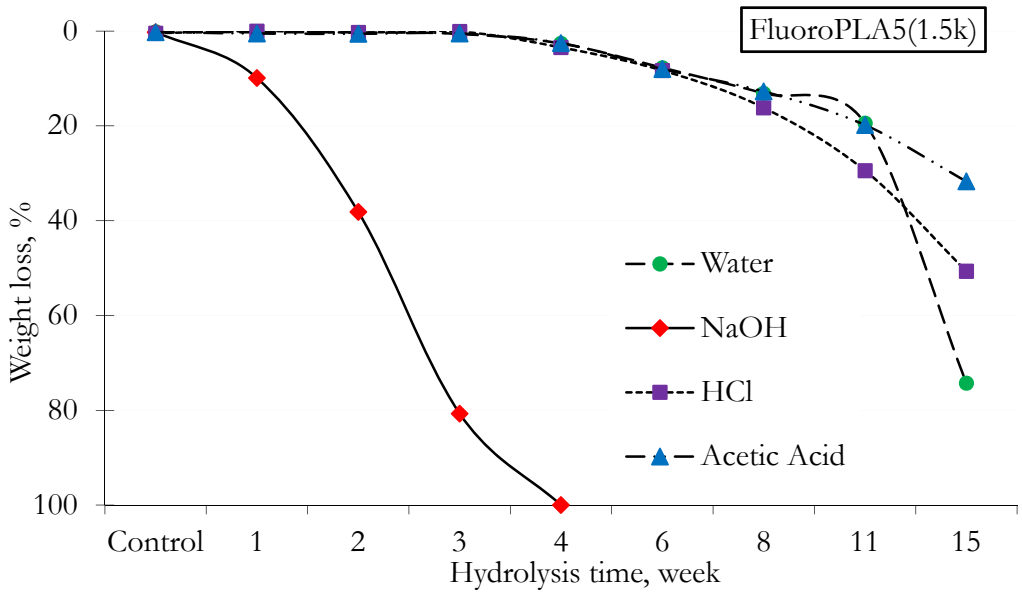

Figure 6.4. Percentage weight loss in FluoroPLA5(1.5k) films in different hydrolytic solutions as a function of hydrolysis time.

The FluoroPLA5(4.2k) showed faster weight loss compared to FluoroPLA5(2.0k) and FluoroPLA5(1.5k) in all the hydrolytic media. Complete weight loss of FluoroPLA5(4.2k) film in NaOH solution was observed by the 2nd week whereas the complete weight loss of FluoroPLA5(2.0k) and the FluoroPLA5(1.5k) in NaOH was only observed after the 4th week. In HCl solutions and by the end of 15th week, FluoroPLA5(4.2k) showed the highest weight loss (ca. 76%) whereas FluoroPLA5(2.0k), PLA, and FluoroPLA5(1.5k) films lost ca. 58%, 52%, and 51% of the original weights respectively. In general, the weight loss for the water and the acetic acid treated films were similar for PLA and FluoroPLAs.

Figure 6.5 shows the weight loss of PLA and the FluoroPLAs films hydrolyzed in alkaline conditions for 4 weeks. The weight loss of PLA films showed a linear (R^2=0.992)

profile with time whereas FluoroPLAs showed a resistance to weight loss initially. The weight losses for the FluoroPLA5(2.0k) and FluoroPLA5(1.5k) films were smaller than that of the PLA for the initial 2 weeks and for FluoroPLA5(4.2k) for 1 week and this could be due to the hydrophobic properties (higher contact angle) of FluoroPLAs. The complete weight loss of PLA and FluoroPLAs films could be explained by the surface erosion of the films by the alkaline hydrolysis of the ester groups. The oligomeric hydrolysis products ($RCOO^-$) with the hydrophilic properties would have a tendency to diffuse in the alkaline solution.

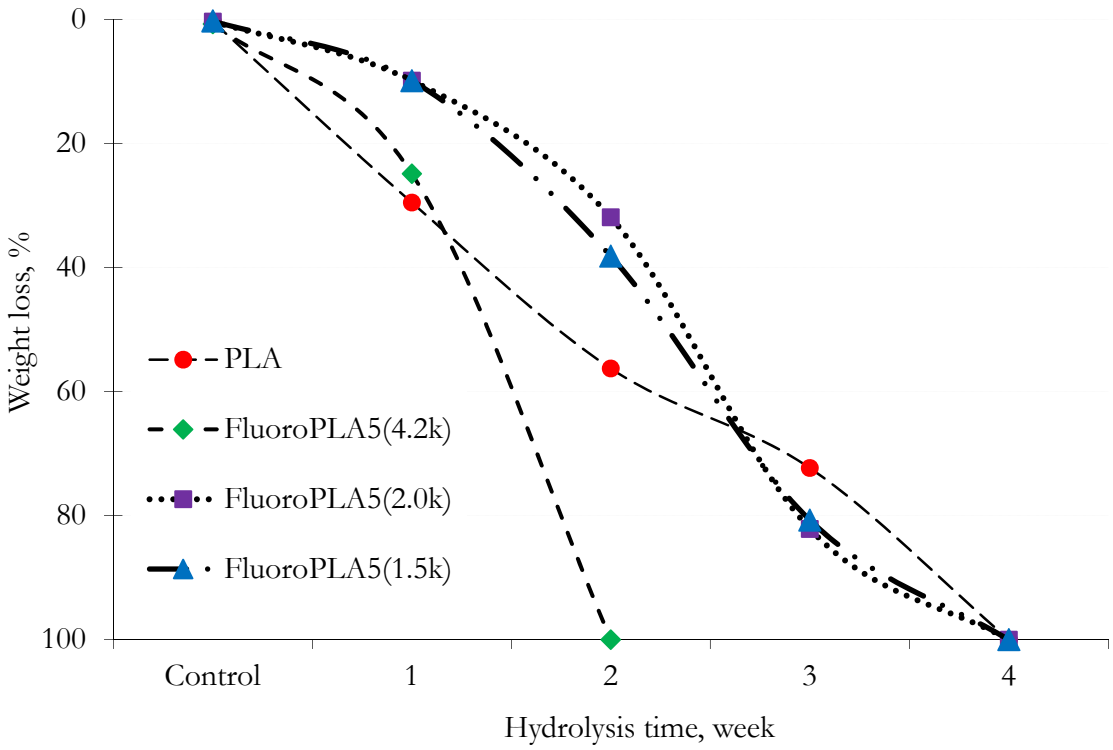

Figure 6.5. Percentage weight loss of PLA and FluoroPLAs films in alkaline solution (0.05 N NaOH) as a function of hydrolysis time.

Molecular Weight Decrease (Degradation)

Polymer degradation can be measured by changes in the molecular weight during degradation. The degradation of polyesters proceeds by the cleavage of ester linkages in the backbone and can be driven either by acidic or basic conditions.[22] Alkaline hydrolysis proceeds by the acyl-oxygen fission whereas for either neutral or acidic hydrolysis, alkyl-oxygen fission prevails.[23-26] The mechanism of the hydrolysis of esters has been explained in detail by Datta et al. and Roberts et al.[26,27]

The mechanisms for hydrolysis of ester linkages in neutral, acidic, and alkaline environments are very well explained in literature.[23,24,26] In general, the acid-catalyzed hydrolysis of esters is driven by the electrophilic attack at the carbonyl oxygen by hydrogen ions and the alkaline hydrolysis proceeds via nucleophilic attack of hydroxide ions on the lowest electron density carbon (carbonyl).[22] The hydrolytic degradation in alkaline condition proceeds by random chain scission, however, in acidic media, chain scission is faster for the ester bonds towards chain ends than the internal ester bonds.[28,29] In the textile industry, the weight reduction and softening of the surface of polyesters (poly(ethylene terephthalate) is often carried out by treatment with mild alkaline solution.[30] The alkaline hydrolysis of esters is strongly dependent on both pH and the temperature of the hydrolytic solution. A unit change in the pH causes a 10-fold change in the reaction rate and a shift in temperature from 0 to 20 °C causes a similar change in the reaction rate (ethyl acetate model).[22]

Figure 6.6 shows the percentage loss in the number average molecular weight (Mn) of PLA in different hydrolytic mediums. A simultaneous decrease in Mn was observed for PLA in the case of all hydrolytic solutions. Figure 6.7, Figure 6.8, and Figure 6.9 shows the

percentage loss in the number average molecular weight (Mn) of FluoroPLA5(4.2k), FluoroPLA5(2.0k), FluoroPLA5(1.5k), respectively in different hydrolytic mediums. Among the FluoroPLAs, FluoroPLA5(4.2k) shows faster degradation compared to PLA and the two other FluoroPLAs. The lower molecular weight polymer (FluoroPLA5(4.2k) degrades faster than higher molecular weight polymer (PLA). FluoroPLA5(4.2k) has a bigger block length (4,200 g mol^{-1}) of PFPE. In Chapter 5, it was observed that FluoroPLAs show higher enthalpy of fusion compared to PLA The higher enthalpies (or crystallinity) of FluoroPLAs are due the nucleating action of chemically different, highly dense PFPE segments. Hence, comparatively low enthalpies of fusion for FluoroPLA5(4.2k) versus other FluoroPLAs and the lower molecular weight of FluoroPLA5(4.2k) compared to PLA, makes it a faster degrading polymer among PLA and FluoroPLAs.

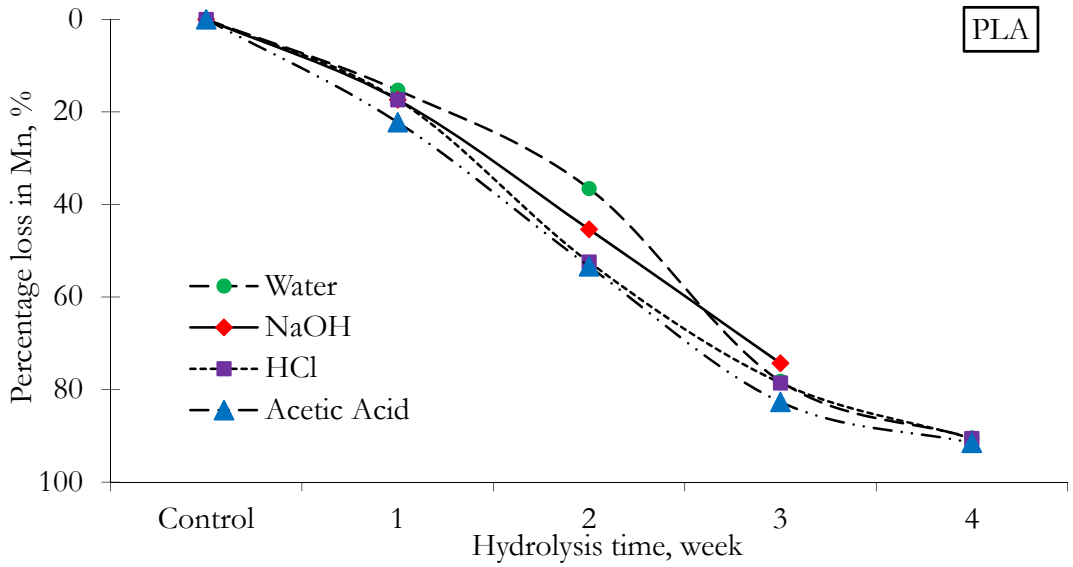

Figure 6.6. Percentage loss in number average mol. wt. of PLA films in different hydrolytic solutions as a function of hydrolysis time.

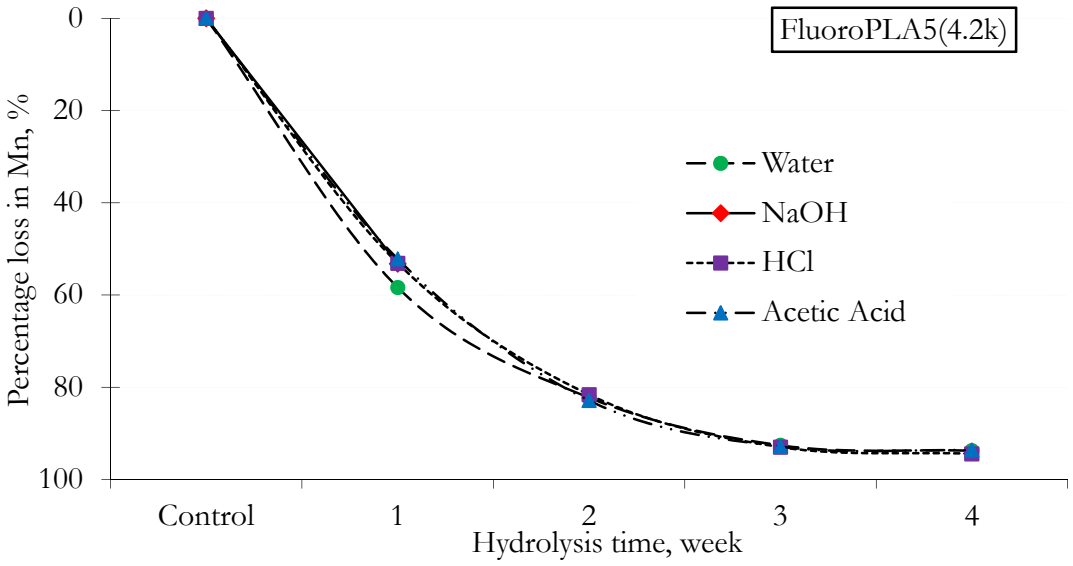

Figure 6.7. Percentage loss in number average mol. wt. of FluoroPLA5(4.2k) films in different hydrolytic solutions as a function of hydrolysis time.

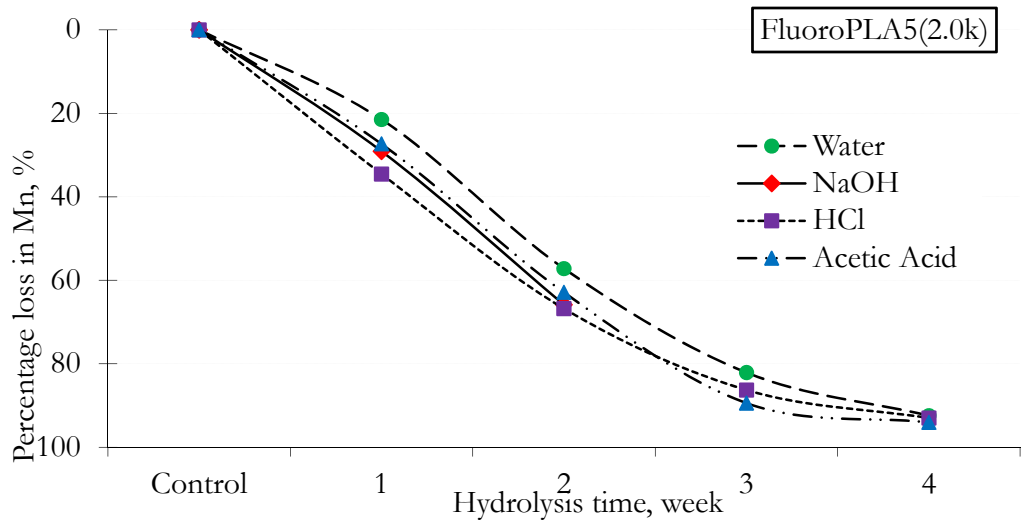

Figure 6.8. Percentage loss in number average mol. wt. of FluoroPLA5(2.0k) films in different hydrolytic solutions as a function of hydrolysis time.

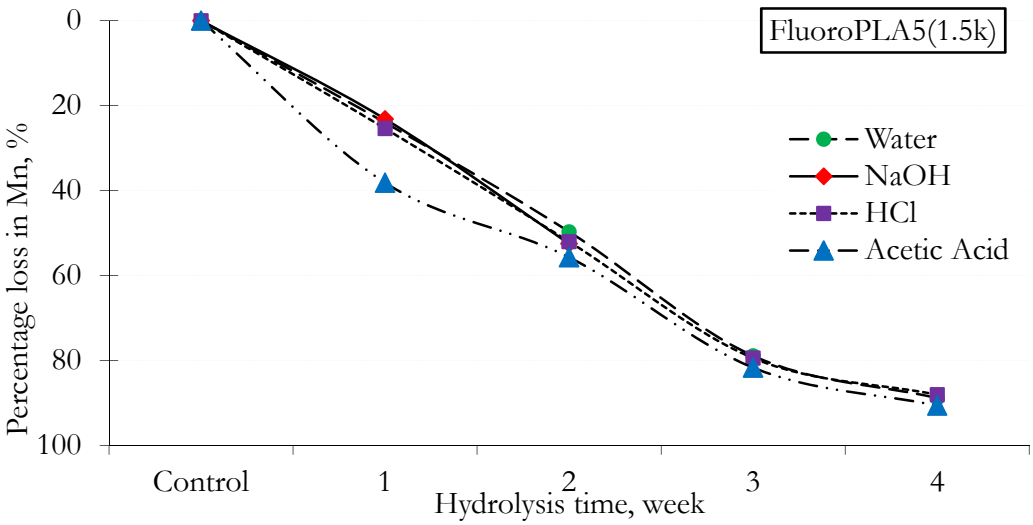

Figure 6.9. Percentage loss in number average mol. wt. of FluoroPLA5(1.5k) films in different hydrolytic solutions as a function of hydrolysis time.

pH Change During Hydrolysis

The chain scission during hydrolysis, degrades the polymer to oligomer and finally to monomers. The ester functional groups are cleaved into carboxylic acids and alcohols. Hence, the pH of the hydrolytic solution is affected. Figure 6.10 shows the variation of the pH of the hydrolytic solutions with the PLA films as a function of the hydrolysis time. No significant change in pH was observed for the NaOH, HCl and acetic acid solutions during hydrolysis. However, significant changes in pH of water were seen as the hydrolysis proceeded. After 15 weeks of hydrolysis of the PLA in water, the pH dropped from ca. 5.7 to 3.0. The hydrolytic degradation of polyesters is the result of hydrolysis of the ester groups which generate carboxylic groups. As hydrolysis progresses, there is an increase in the concentration of carboxylic groups. Huffman et al. reported that during hydrolysis of aliphatic polyesters in deionized water at 37 °C, log [COOH] increases linearly with time.[11]

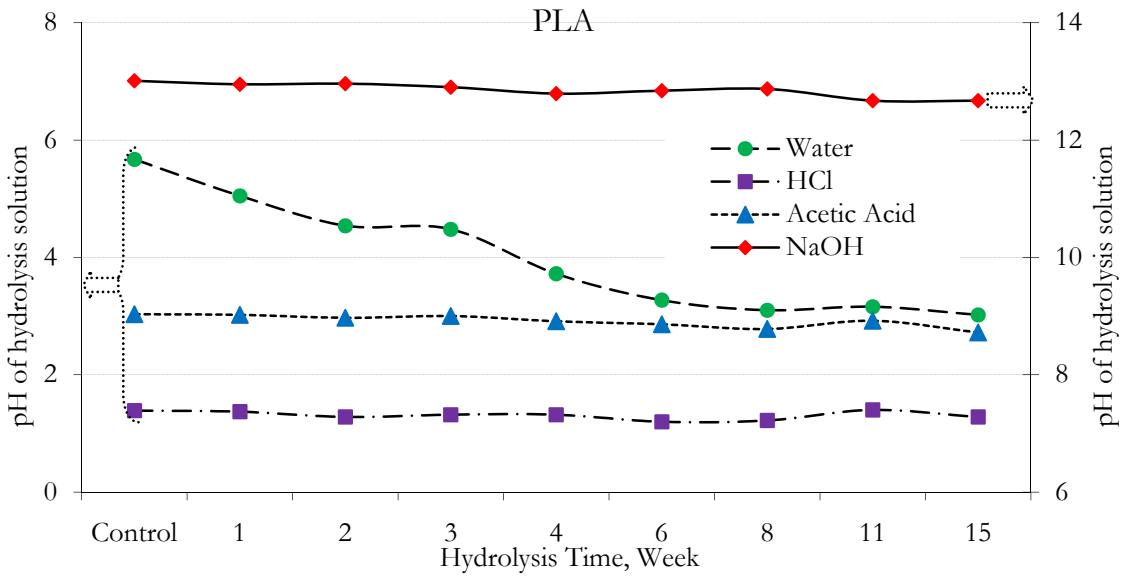

Figure 6.10. pH of different hydrolytic solutions during hydrolytic degradation of PLA films as a function of hydrolysis time.

Since the pH is an inverse logarithmic representation of hydrogen ion (hydronium ion) concentration, a unit change in pH requires ten fold changes in concentration of hydrogen ions and also the carboxylic acid ($K_{a,\ acetic\ acid}$= 1 x 10^{-5}) weakly dissociates. Hence, any change in pH below 2.9-3 and above 11 is not feasible by carboxylic acid groups generated by degradation.

Figure 6.11, Figure 6.12, and Figure 6.13 show the variation in pH of the different hydrolytic solutions used for hydrolysis of FluoroPLA5(4.2k), FluoroPLA5(2.0k), and FluoroPLA5(1.5k) respectively. In the case of PLA and the FluoroPLAs, the pH of NaOH, HCl and acetic acid solutions falls from 13.0 to ca. 12.6-12.7, 1.39 to ca. 1.24-1.28, and 3.0 to ca. 2.72-2.8 respectively.

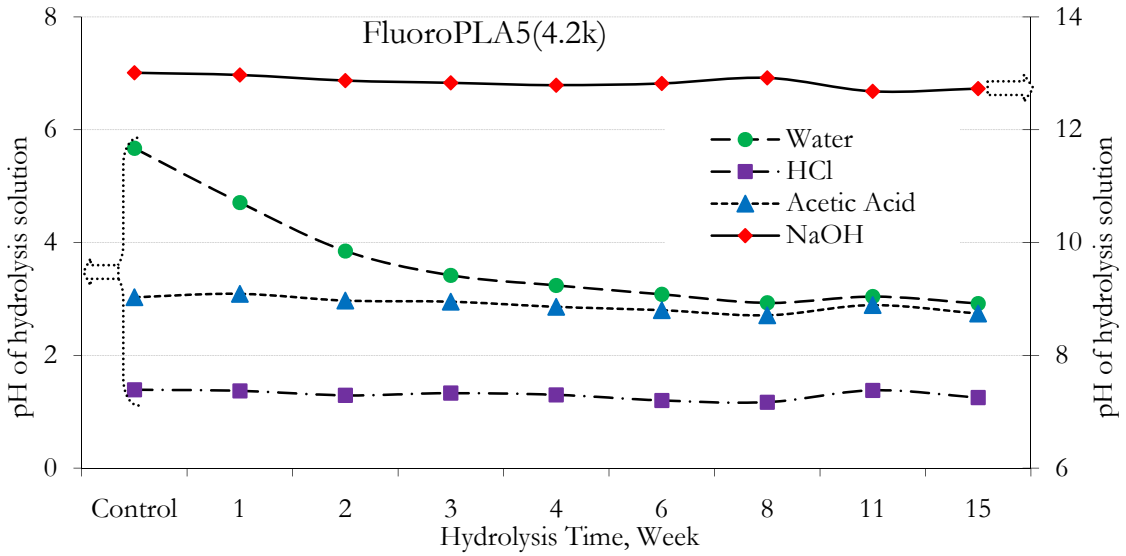

Figure 6.11. pH of different hydrolytic solutions during hydrolytic degradation of FluoroPLA5(4.2k) films as a function of hydrolysis time.

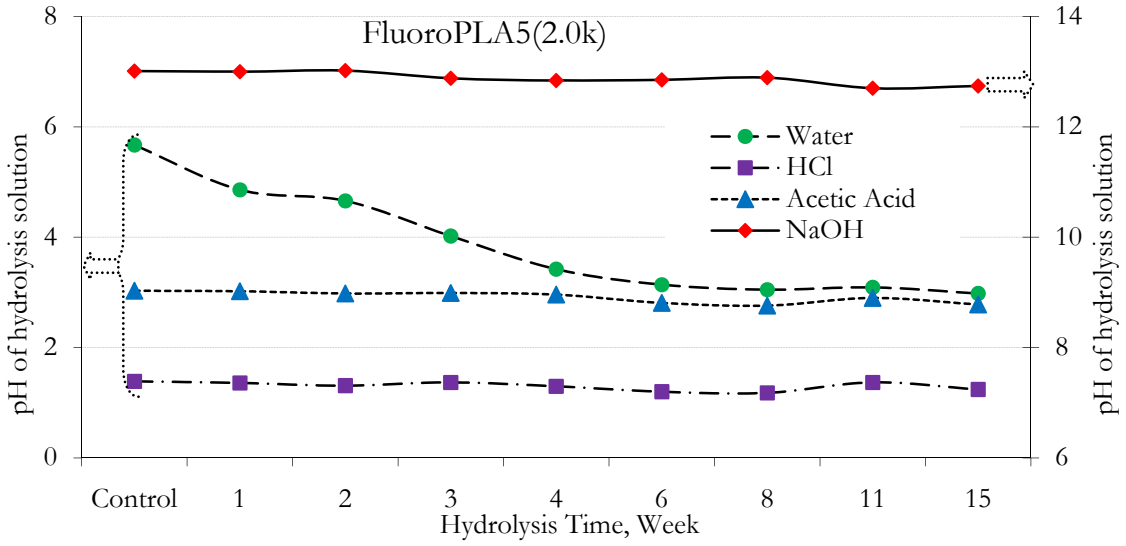

Figure 6.12. pH of different hydrolytic solutions during hydrolytic degradation of FluoroPLA5(2.0k) films as a function of hydrolysis time.

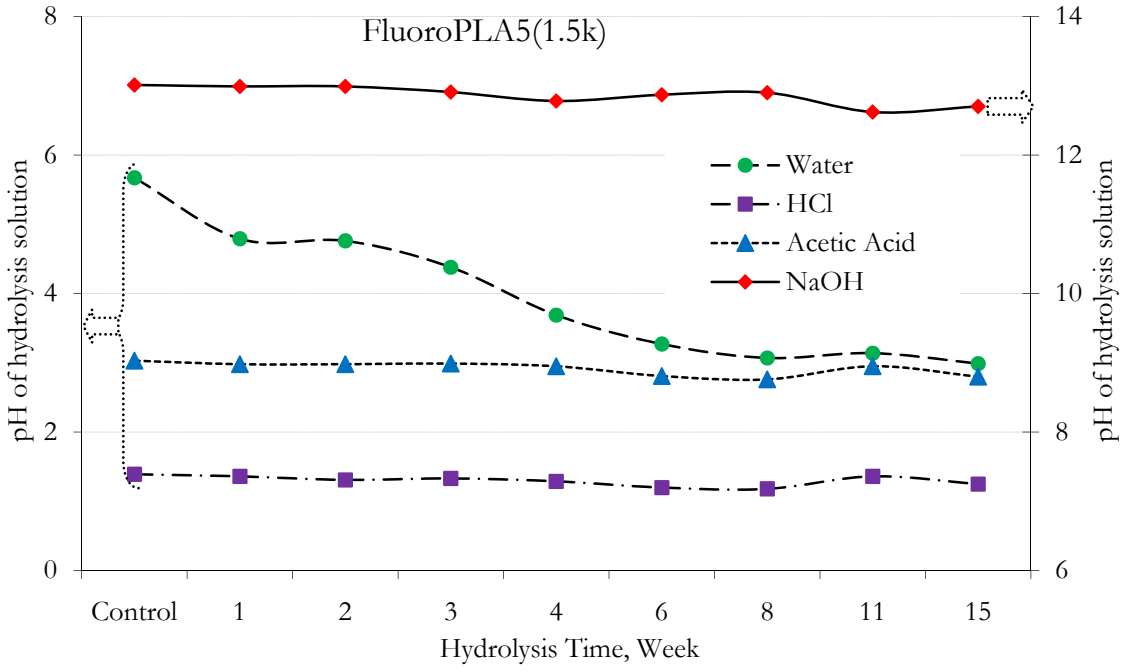

Figure 6.13. pH of different hydrolytic solutions during hydrolytic degradation of FluoroPLA5(1.5k) films as a function of hydrolysis time.

Figure 6.14 shows the pH of water during the hydrolysis of PLA and the FluoroPLAs as a function of hydrolysis time. The pH falls from 5.7 to ca. 2.9-3.0 in the case of all the polymers. The decrease of the pH is a result of the carboxyl groups generated due to the hydrolytic degradation of the ester linkages of the PLA chains. During the initial period (up to 4 weeks) FluoroPLA5(4.2k) shows a more rapid change in the pH of water compared to that of PLA, FluoroPLA5(2.0k) and the FluoroPLA5(1.5k). This observation supports the faster degradation of FluoroPLA5(4.2k) observed in the weight loss and molecular weight experiments.

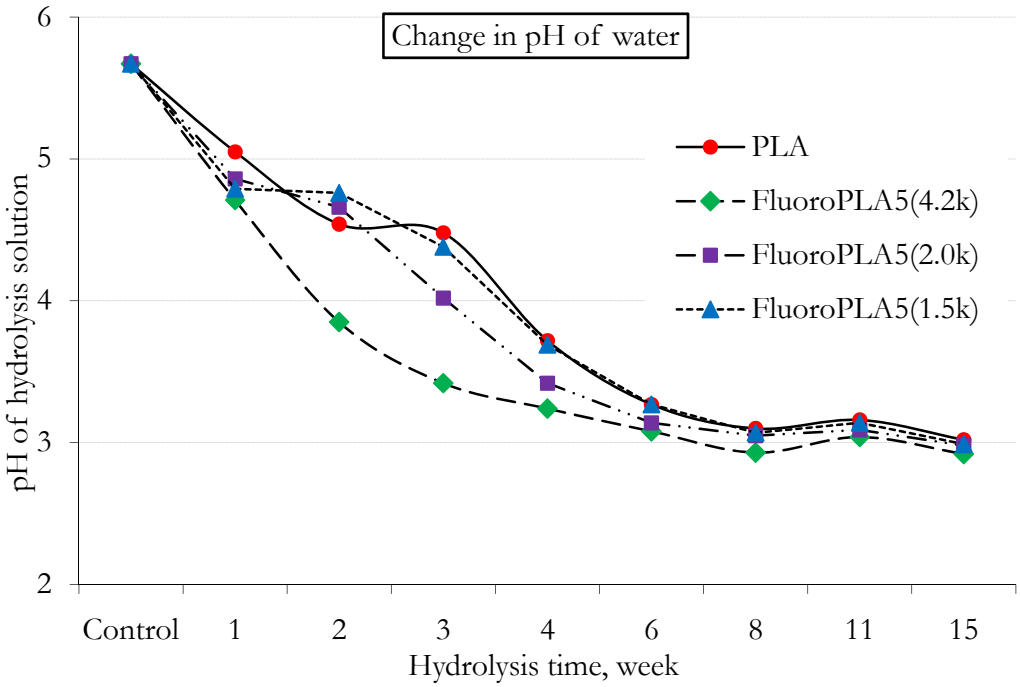

Figure 6.14. pH of water during hydrolytic degradation of PLA and FluoroPLAs films as a function of hydrolysis time.

Thermal Properties

When a semi-crystalline polymer such as polylactide films are immersed in an aqueous solution, water molecules easily penetrate the amorphous phase of the film, but have very low or no degree of penetration into the crystalline phase. Hence, the hydrolytic degradation begins in the amorphous phase and the tie-chain segments (polymer chain segment which connects two crystalline phases) are fragmented. The chain flexibility has a direct bearing on melting point. The degree of entanglement of the long-chain molecules decreases as the tie-chains are degraded and therefore the chains gain higher mobility. Figure 6.15 shows a schematic of the hydrolytic degradation of PLA which shows that as the degradation progresses, the amorphous phase is consumed first and more and more chains are generated affecting the overall crystallinity of polymer.[31]

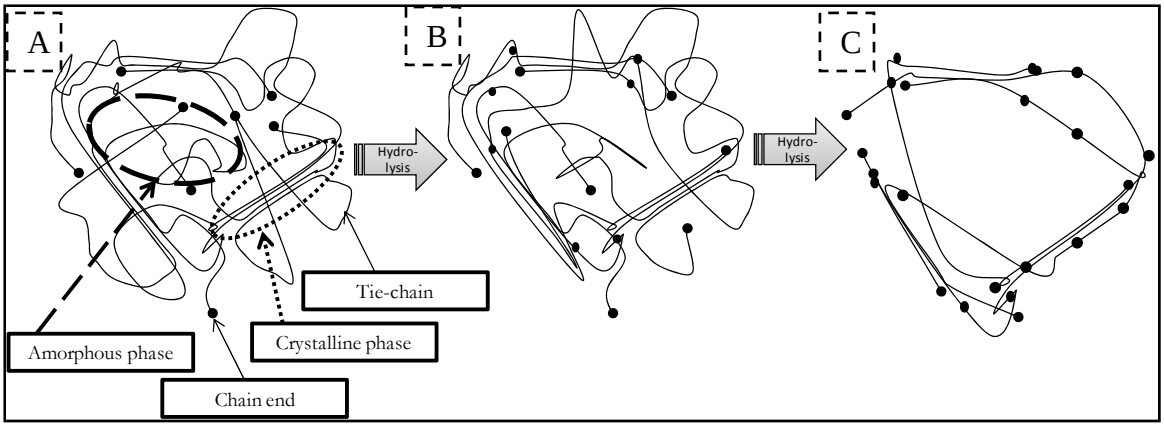

Figure 6.15. Schematic of hydrolytic degradation of PLA segments as a function of hydrolysis time.

The presence of impurities in a crystal lowers the melting point of crystalline substances.[32] Flory and co-workers developed the thermodynamics of melting in polymers and proposed that the melting point depression depends on the mole fraction of impurities in the crystallizable phase.[33-35] The polymer chain ends are chemically different from the polymer backbone and hence the chain ends contribute as impurities. The depression in melting point of a pure state can be given as:[36]

$$\frac{1}{T_m} - \frac{1}{T_m^0} = \frac{R}{\Delta H_m} \cdot \frac{2M_e}{M_n} \qquad 6.2$$

where T_m^0 and the T_m are melting points in the pure state and the impure state, respectively. R is the gas constant and ΔH_m is enthalpy of fusion. M_e and M_n are the molecular weights of end mer (and assuming that both ends are identical) and polymer chain respectively. Hence, as the hydrolysis progresses and chain scission results in an increase in chain ends with time, the melting point of hydrolyzed film is expected to decrease.

Figure 6.16 displays the DSC thermograms of PLA films hydrolyzed in water for 15 weeks. The endothermic melting peaks shifted towards lower temperature region and the peak areas increased initially followed by a maxima and finally decreased. The amorphous region can be easily penetrated by hydrolyzing media and degradation prevails in these non-crystalline phase. The disappearance of the glass transition step change begins immediately after the very first week and the transition is not observed at all after 3rd week for both PLA and FluoroPLAs. The melting point of PLA decreases from ca. 175 °C to ca. 158 °C after 15 week of hydrolysis in water. Similar decreases in the melting temperature of PLA in NaOH, HCl, and acetic acid solutions were observed. FluoroPLAs showed similar trends in all the hydrolytic solutions and the thermograms are shown in Appendix K. The decrease in the

melting transition can be attributed to the increase in the number of chain ends which acted as impurities for the crystalline regions and therefore made the crystallites imperfect.

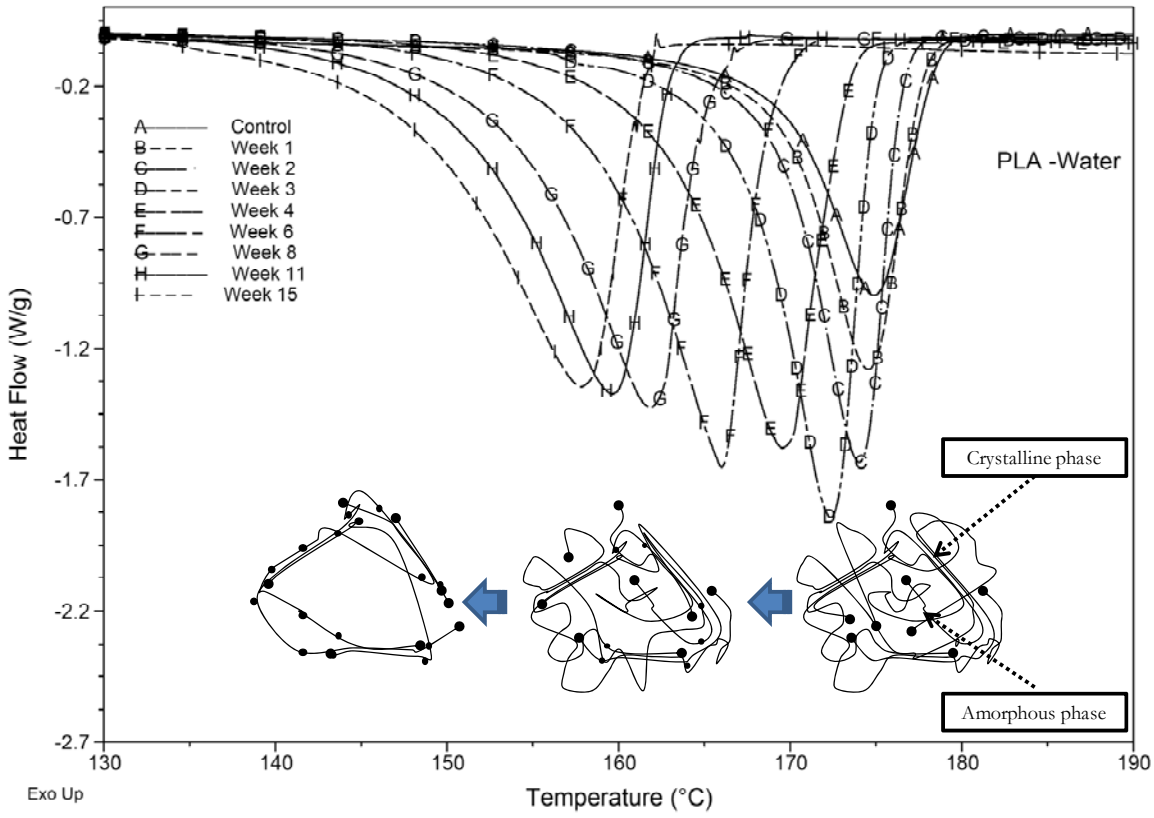

Figure 6.16. DSC thermograms of PLA films in water for different hydrolysis time.

Figure 6.17, Figure 6.18, Figure 6.19, and Figure 6.20 shows the melting temperature of PLA, FluoroPLA5(4.2k), FluoroPLA5(2.0k), and FluoroPLA5(1.5k) films in different hydrolytic solutions as a function of hydrolysis time. In sodium hydroxide solution, the depression in melting point is comparatively small for PLA and the FluoroPLAs as the films degraded before the 4th week. However, the maximum depression in melting temperature is observed for the hydrochloric acid treatment of PLA and the FluoroPLAs. PLA shows ca.

30 °C decrease in the melting temperature of films after 15 weeks of treatment in hydrochloric acid. FluoroPLA5(4.2k) shows the highest drop in melting point of ca. 43 °C where as FluoroPLA2(2.0k) and the FluoroPLA5(1.5k) show drops in melting temperature of ca. 37 and 35 °C respectively. However, the depression in melting points of PLA and FluoroPLAs films in water and acetic acid are in the range of 17-22 °C. The rate of depression of the melting point of PLA and FluoroPLAs for films in water, acetic acid and hydrochloric acid was similar up to 8 weeks, after that, however, the depression is sharper for the films hydrolyzed in hydrochloric acid. This is probably due to faster disintegration of films in hydrochloric acid due to strong acid-catalyzed hydrolysis.

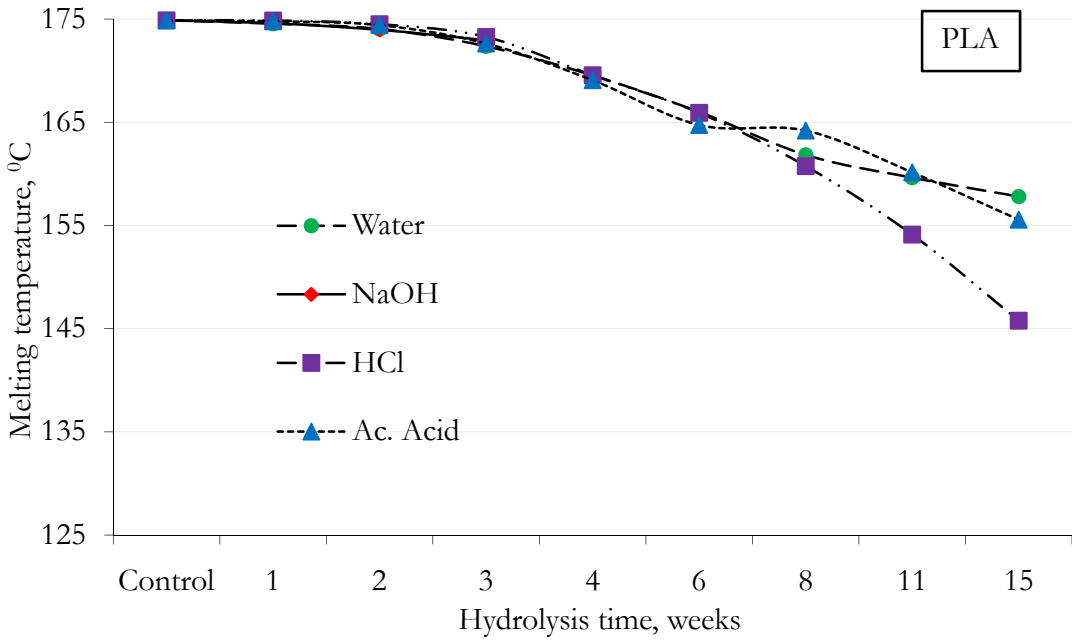

Figure 6.17. Melting temperature of PLA films in different hydrolytic solutions as a function of hydrolysis time.

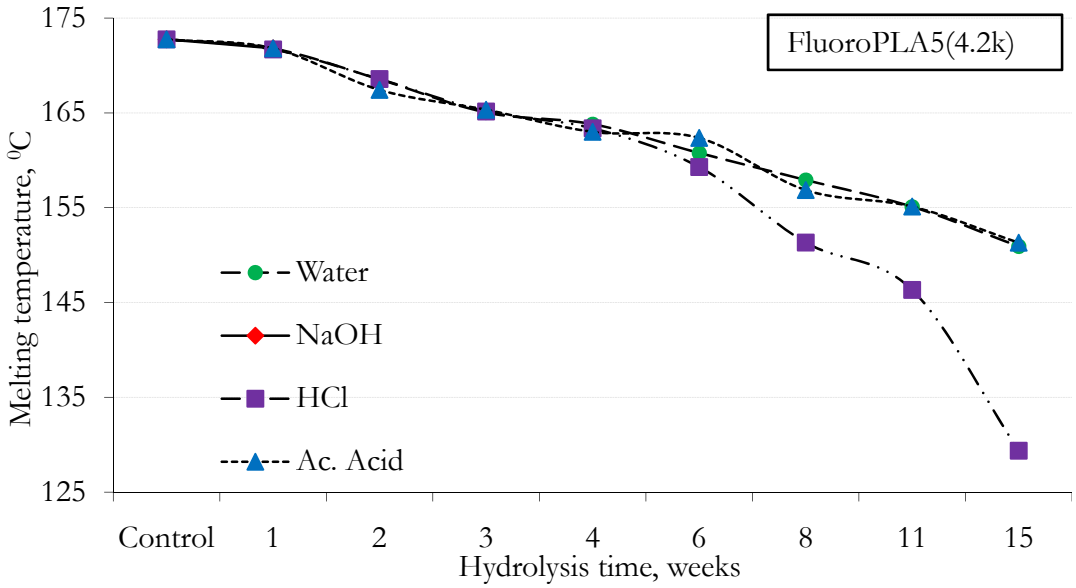

Figure 6.18. Melting temperature of FluoroPLA5(4.2k) films in different hydrolytic solutions as a function of hydrolysis time.

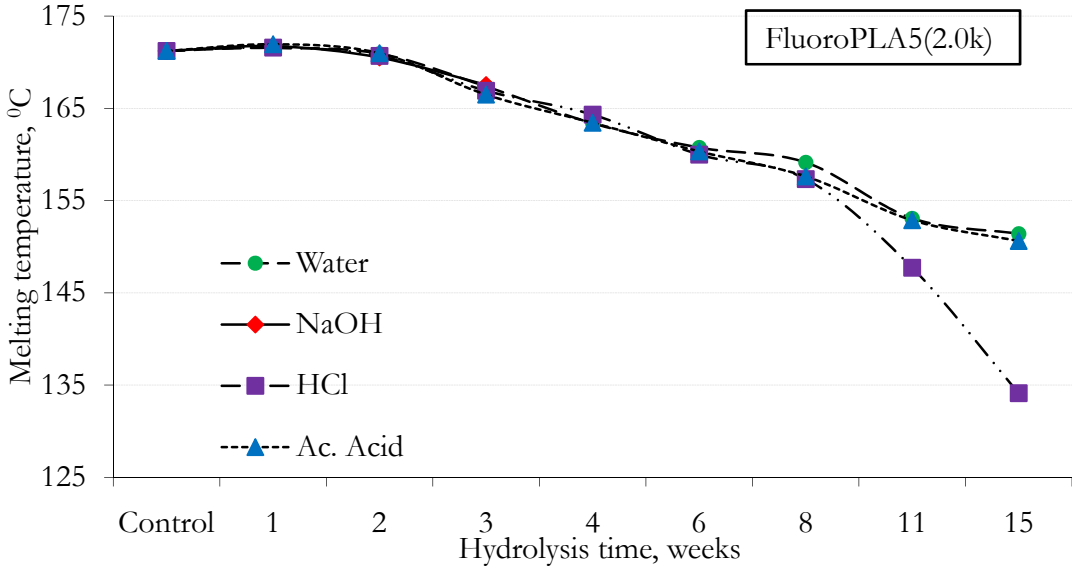

Figure 6.19. Melting temperature of FluoroPLA5(2.0k) films in different hydrolytic solutions as a function of hydrolysis time.

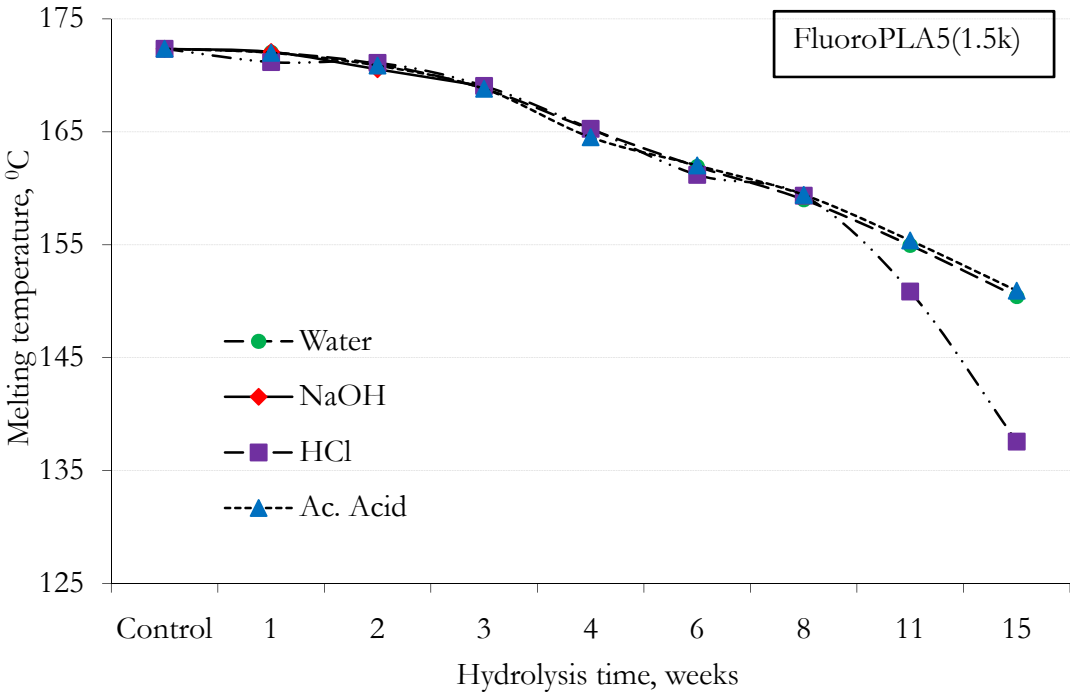

Figure 6.20. Melting temperature of FluoroPLA5(1.5k) films in different hydrolytic solutions as a function of hydrolysis time.

Figure 6.21, Figure 6.22, Figure 6.23, and Figure 6.24 show the variation in the heat of fusion of PLA and FluoroPLAs films hydrolyzed in different environments as a function of hydrolysis time. PLA and FluoroPLAs showed an increase in the heat of fusion as the hydrolysis proceeded for all the hydrolytic solutions. The hydrolytic solution easily penetrates in the amorphous phase in the semi-crystalline polymer and is consumed faster than the crystalline phase. The heat of fusion is associated with crystalline phase and as the amorphous phase is consumed (hydrolyzed), the relative concentration of crystalline phase increase in the film and overall, the material behaves as a higher crystalline material. Hence, the heat of fusion increases with hydrolysis time. Once, all the amorphous phase is

hydrolyzed, the increase in heat of fusion saturates or decreases as the crystalline lattice is destroyed. At the end (11^{th} and 15^{th} week), a slight decrease in heat of fusion was observed randomly in the case of FluoroPLAs. This is possibly due to the faster disintegration of the films.

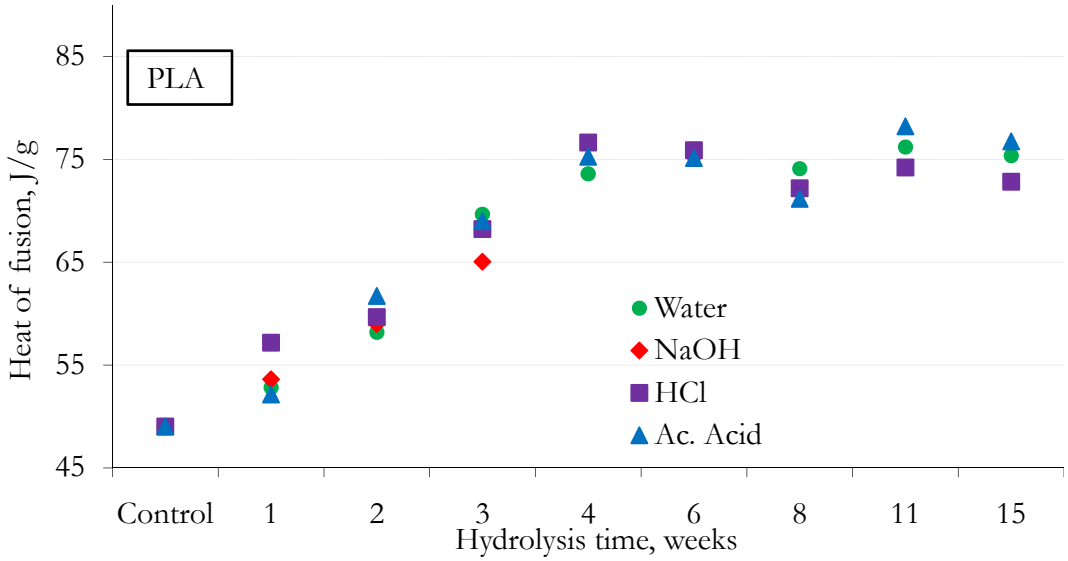

Figure 6.21. Heat of fusion for PLA films hydrolyzed in different solutions as a function of hydrolysis time.

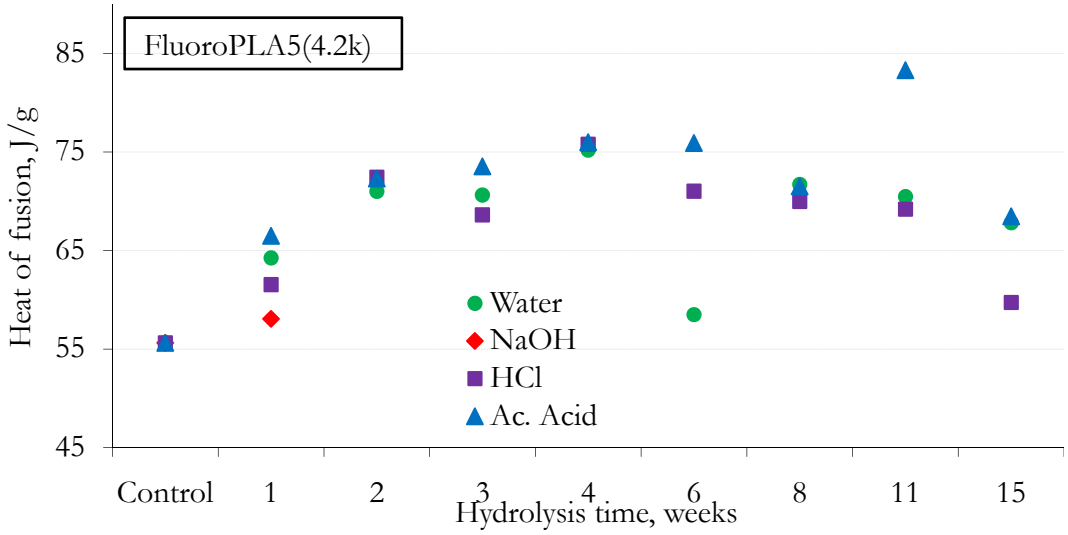

Figure 6.22. Heat of fusion for FluoroPLA5(4.2k) films hydrolyzed in different solutions as a function of hydrolysis time.

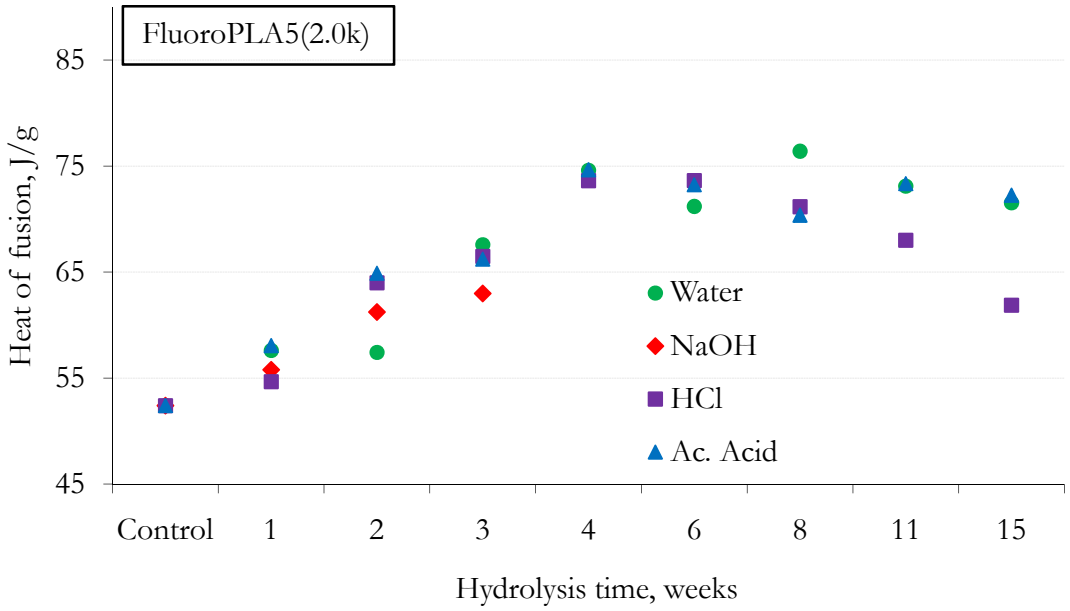

Figure 6.23. Heat of fusion for FluoroPLA5(2.0k) films hydrolyzed in different solutions as a function of hydrolysis time.

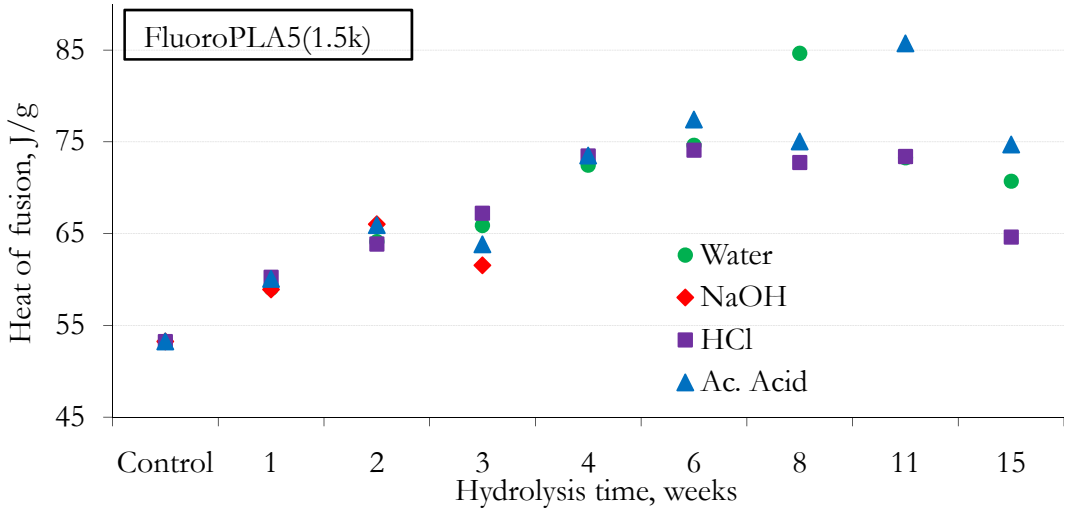

Figure 6.24. Heat of fusion for FluoroPLA5(1.5k) films hydrolyzed in different solutions as a function of hydrolysis time.

X-Ray Diffractometry

Figure 6.25 shows X-ray diffraction profiles of PLA films before (control) and after hydrolysis in water for 1, 2 and 11 weeks. The profiles exhibit diffraction peaks at 2θ values of 14.7, 16.5-16.7, 19.0 and 22.2° which are assigned to 010, 200/110, 203 and 205 reflections respectively[37,38] and are in agreement with the peaks reported by Ikada et al. (at 2θ values of 15, 16, 18.5 and 22.5°) for the optically pure PLA crystallizing in the α form with two 10_3 helices in a pseudo-orthorhombic unit cell (a= 1.07 nm, b = 0.595 nm, and c = 2.78 nm).[39,40] There is no significant change in the main peaks of PLA and FluoroPLAs, however, there are new peaks generated at 2θ value of ca. 44°

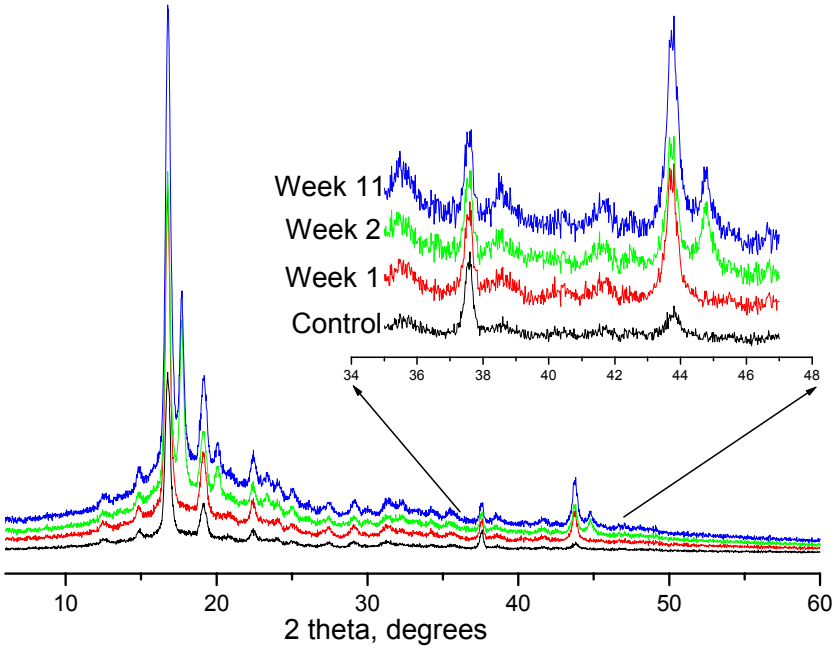

Figure 6.25. X-ray diffraction profiles of PLA films: before hydrolysis (Control) and after hydrolysis in water for 1, 2, 11 weeks.

Figure 6.26 shows X-ray diffraction profiles of FluoroPLA5(1.5k) films before (control) and after hydrolysis in water for 1, 2 and 11 weeks. After hydrolysis, in addition to the main peaks (similar to PLA), new peaks are observed at ca. 38 and 44° which are generated as the hydrolysis proceeds. The appearance of new peaks could be due to the annealing effect at 60 °C during the hydrolytic study which results in formation of small crystallites. Also, as hydrolysis progress, the bond cleavage reduces the degree of entanglement which could also lead to crystal formation and the appearance of new peaks in the diffraction pattern. Another possible reason for these low d-spacing peaks is an increase in the internal hydrogen bonding during the hydrolysis. Similar peaks are observed in case of FluoroPLA5(2.0k) and the FluoroPLA5(4.2k) as shown in Appendix L.

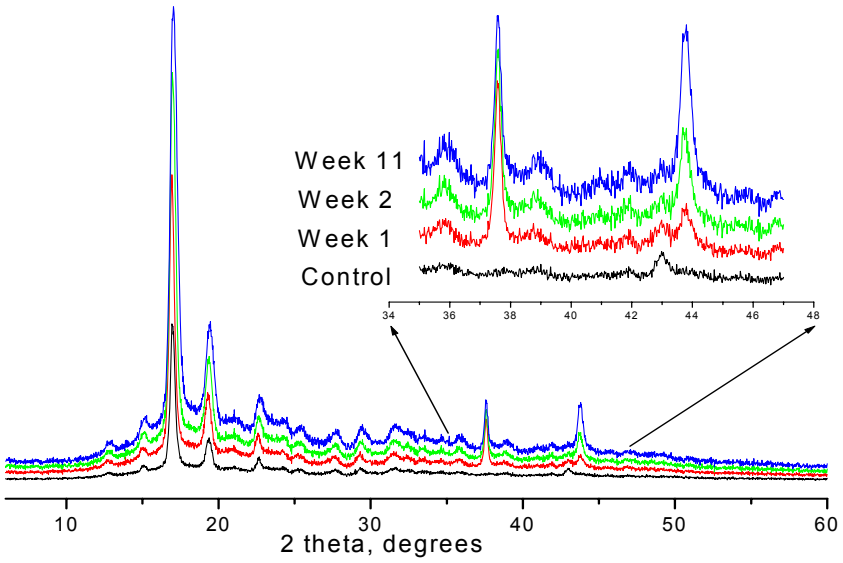

Figure 6.26. X-ray diffraction profiles of FluoroPLA5(1.5k) films: before hydrolysis (Control) and after hydrolysis in water for 1, 2, 11 weeks.

Morphology

SEM micrographs of the surfaces of the homopolymer PLA and the copolymers FluoroPLA5(2.0k) and the FluoroPLA5(1.5k) films hydrolyzed in alkaline solution for 3 weeks are shown in Figure 6.27. The FluoroPLA5(4.2k) film disintegrated/dissolved before the 3rd week. Lower molecular weight than the PLA, relatively lower crystallinity (heat of fusion) than FluoroPLA5(2.0k) and the FluoroPLA5(1.5k) makes FloroPLA5(4.2k) highly prone to hydrolysis. The surface erosion of PLA and FluoroPLAs films can be explained by the alkaline hydrolysis of ester groups on the surface due to the lower diffusion rate of bulkier hydroxide ions which are not regenerated unlike the protons, reducing the concentration of hydroxide ions in the core of film.[22] Also, the resultant oligomeric acids formed on the surface of the films are dissociated as $RCOO^-$ and have high hydrophilicity which enables these oligomers to diffuse into the hydrolytic solution, however, fresh hydroxide ions need to be supplied on the surface of the film. Hence, the hydrolysis of PLA and FluoroPLAs proceeds by the surface erosion mechanism in alkaline medium.[41]

The surface erosion of PLA and FluoroPLAs can be seen from the roughness on the surface of the films and disintegration of FluoroPLA5(2.0k) and the FluoroPLA5(1.5k) can be seen in SEM micrographs. The theoretical number of ester groups in PLA is ca. double the same in FluoroPLAs (based on number-average molecular weights) and hence it should take longer for PLA films to completely disintegrate than FluoroPLAs which is clearly observed from the SEM micrographs.

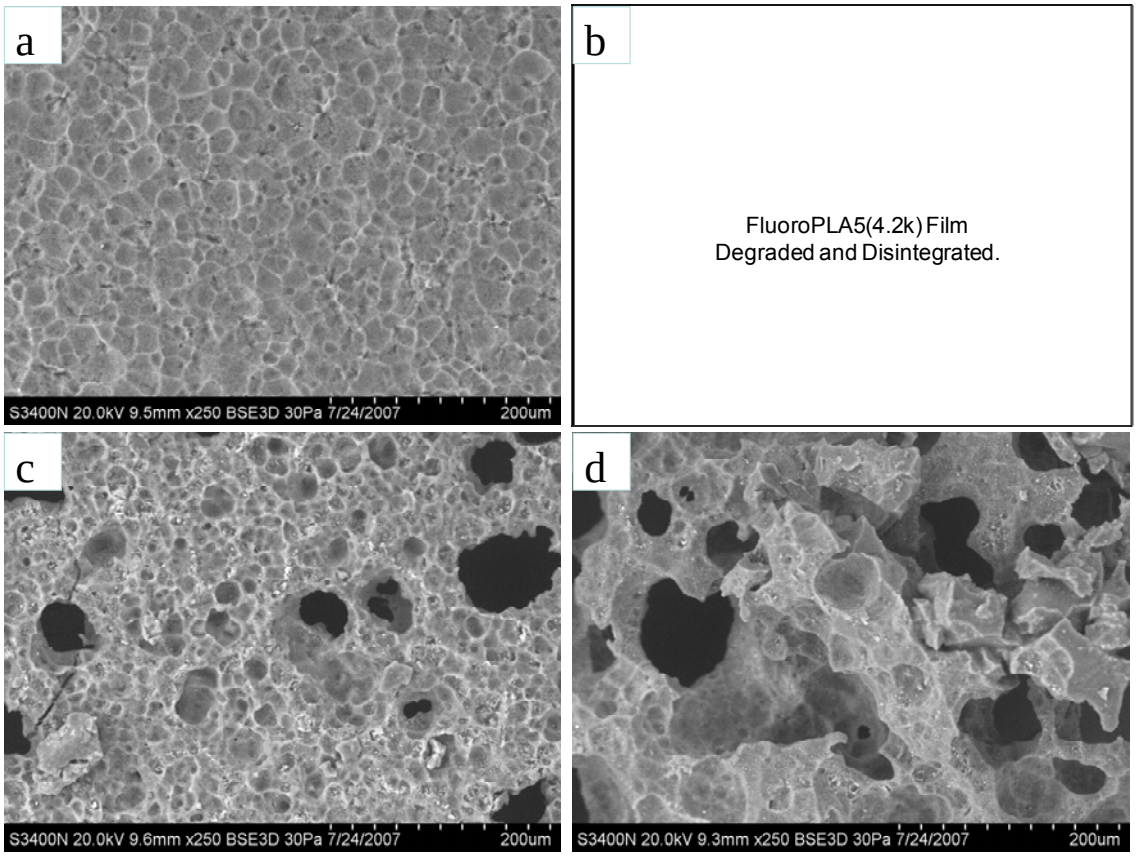

Figure 6.27. Scanning electron micrographs of (a) PLA, (c) FluoroPLA5(2.0k), and (d) FluoroPLA5(1.5k) films after alkaline degradation for 4 weeks. FluoroPLA5(4.2k) films dissolved after two weeks. Scale bar 200 μm.

SEM micrographs of the surfaces of PLA and the FluoroPLA5(4.2k), FluoroPLA5(2.0k) and the FluoroPLA5(1.5k) films hydrolyzed in water and acidic solutions did not show any significant change in morphology with hydrolysis time or among the different treatments.

Figure 6.28 shows the SEM micrographs of fractured cross-section of FluoroPLA5(1.5k) films unhydrolyzed (a) and hydrolyzed in water for 8 weeks (b). The

fractured surface of the unhydrolyzed film shows a ductile type failure. The fractured surface of hydrolyzed film shows the void, crack and brittle (smooth) profile. The circular features in hydrolyzed and unhydrolyzed films are spherulites. Surface erosion is not observed in water hydrolyzed films and the degradation products are part of the film. However, the film looses its mechanical properties due to the decrease in the molecular weight with hydrolysis time.

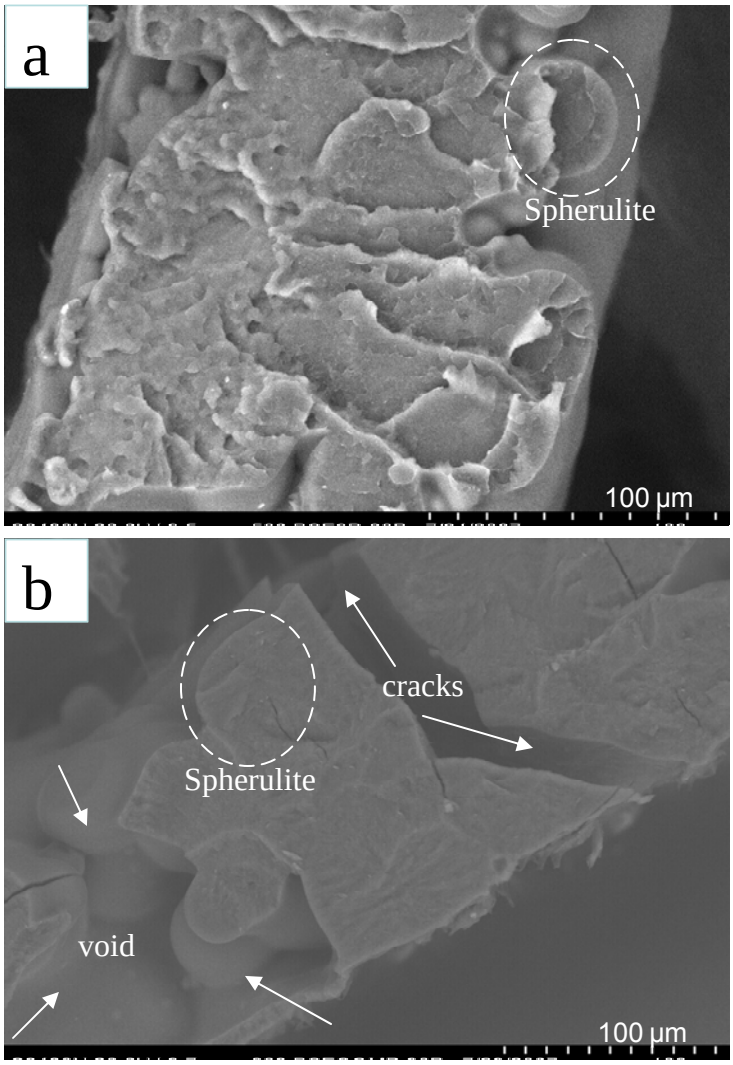

Figure 6.28. Scanning electron micrographs of fractured FluoroPLA5(1.5k) films in cross-section. Image (a) is before (control) and image (b) after 8 week hydrolysis in water.

Surface Erosion of PLA and FluoroPLA in Alkaline Solution

Figure 6.29 shows the schematic of alkaline hydrolysis of PLA and FluoroPLAs. FluoroPLAs show initial resistance to weight loss but after that the hydrolysis proceeds in similar fashion to PLA. The hydrolysis of PLA and FluoroPLAs can be explained by three main factors, namely, molecular weight, hydrophobicity and the crystallinity of the polymer films. The FluoroPLA5(1.5k) has the highest molar PFPE content and also has higher crystallinity (based on the heat of fusion) than the other FluoroPLAs and the PLA. Even though FluoroPLA5(1.5k) has lowest molecular weight (Mn~67 kD), it degrades similarly as PLA (Mn~144 kD). FluoroPLA5(4.2k) has the lowest molar PFPE content and lower crystallinity (based on the heat of fusion) compared to FluoroPLA5(2.0k) and FluoroPLA5(1.5k) and it has lower molecular weight (Mn~94 kD) than PLA and hence it degrades faster than PLA, FluoroPLA5(2.0k) and the FluoroPLA5(1.5k). The loss in molecular weight is observed for PLA and FluoroPLAs in all the media where as weight loss progresses by surface erosion in alkaline conditions and by the bulk erosion in acidic and neutral conditions. The surface erosion of FluoroPLAs has an induction period because of its hydrophobic surface whereas PLA shows almost linear weight loss with hydrolysis time.

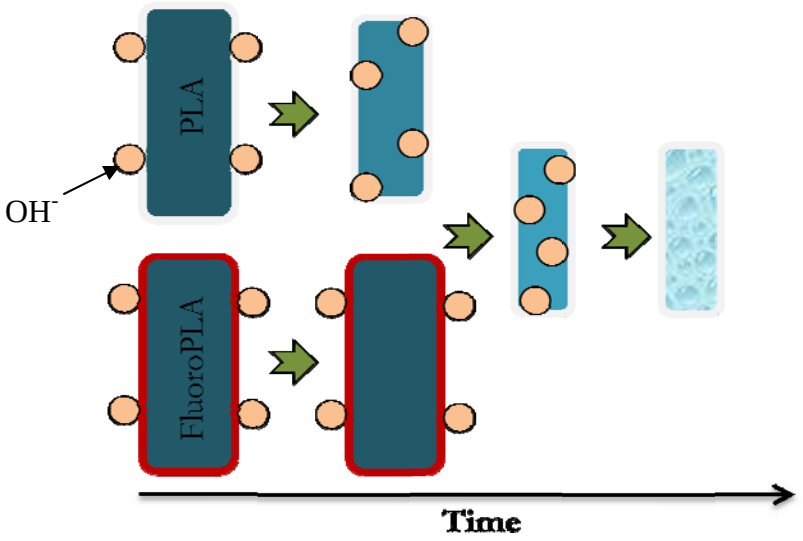

Figure 6.29. Schematic of surface erossion of PLA and FluoroPLA in alkaline environment.

6.4 Conclusions

The hydrolytic stability of PLA and FluoroPLAs in alkaline, acidic and neutral aqueous solutions were investigated by measuring the change in weight, molecular weight, melting temperature, heat of fusion and the morphology of annealed polymer films and the change in the pH of hydrolytic solutions as a function of hydrolysis time. The hydrolytic degradation of PLA and the FluoroPLAs were predominantly affected by molecular weight, hydrophobicity and crystallinity. The nucleating action of low surface energy, chemically different PFPE segments in FluoroPLAs increase their crystallinity in comparison to the PLA. FluoroPLA5(4.2k) has lowest crystallinity amongst FluoroPLAs and has a lower molecular weight than PLA. The combined effect of lower crystallinity and molecular weight makes it more sensitive to hydrolytic degradation. Based on the weight loss and the decrease in molecular weight of the films observed in different hydrolytic solution, the erosion of PLA and the FluoroPLAs films in alkaline solution proceeds mainly by the surface erosion; however, bulk erosion with an initial induction period dominates in the acidic and the neutral hydrolytic environments.

The molecular weight degradation does not show any induction period and was observed for all hydrolytic environments. This is probably due to the aqueous nature of the hydrolytic solutions and that the cleavage of ester linkage is a combined effect of auto and external catalysis. It was proposed that the hydrophobic effect of FluoroPLAs is for short time (less than a week) and the penetration of small size hydronium ions are not affected and hence, the molecular weight decreases with time for the PLA and FluoroPLAs in all the hydrolytic solutions.

As the hydrolysis proceeds, the polymer chains in the amorphous phase degraded (cleaved) faster than the chains in the crystalline phase. New peaks were observed in the diffraction spectra of PLA and FluoroPLAs at higher Brag's angle (ca. 44°). These new reflections could possibly be due to crystallite formation brought about by any or the combined effect of the annealing phenomena during hydrolysis, the rearrangements of chains upon cleavage and reduced entanglement or the increased hydrogen bonding between the cleaved chains. The degree of depression in the melting point of PLA and FluoroPLAs increases with the hydrolysis time. The generation of impurities such as chain ends during hydrolysis possibly decreases the melting point of hydrolyzed films. As hydrolysis progresses, the heat of fusion increases as the amorphous phase of the film is consumed faster than the crystalline phase. Hence, the relative crystallinity of PLA and FluoroPLAs films increases with hydrolysis time.

In conclusion, FluoroPLA5(1.5k) shows better stability to different hydrolytic solutions though it has the lowest molecular weight amongst PLA and FluoroPLAs and the enhanced stability is due to the higher crystallinity and hydrophobic properties. FluoroPLA5(4.2k) degrades faster and is prone to hydrolysis because of its comparatively lower molecular weight than the PLA and lower crystallinity than FluoroPLA5(1.5k) and FluoroPLA5(2.0k).

6.5 References

1. Albertsson, A.-C. & Karlsson, S. Degradable Polymers for the Future. *Acta Polymerica* **46**, 114-123 (1995).
2. Carothers, W. H., Dorough, G. L. & Natta, F. J. v. Studies of Polymerization and Ring Formation. X. The Reversible Polymerization of Six-Membered Cyclic Esters. *Journal of the American Chemical Society* **54**, 761-772 (1932).
3. Albertsson, A.-C. & Varma, I. K. Recent Developments in Ring Opening Polymerization of Lactones for Biomedical Applications. *Biomacromolecules* **4**, 1466-1486 (2003).
4. Tsuji, H. in *Biopolymers for Medical and Pharmaceutical Applications* (eds. Steinbüchel, A. & Marchessault, R. H.) 183-231 (Wiley-VCH, Weinheim, 2005).
5. Lunt, J. Large-Scale Production, Properties and Commercial Applications of Polylactic Acid Polymers. *Polymer Degradation and Stability* **59**, 145-152 (1998).
6. O'Keefe, B. J., Monnier, S. M., Hillmyer, M. A. & Tolman, W. B. Rapid and Controlled Polymerization of Lactide by Structurally Characterized Ferric Alkoxides. *J. Am. Chem. Soc.* **123**, 339-340 (2001).
7. Tsuji, H. & Fukui, I. Enhanced Thermal Stability of Poly(lactide)s in the Melt by Enantiomeric Polymer Blending. *Polymer* **44**, 2891-2896 (2003).
8. Piorkowska, E., Kulinski, Z., Galeski, A. & Masirek, R. Plasticization of Semicrystalline Poly(l-lactide) with Poly(propylene glycol). *Polymer* **47**, 7178-7188 (2006).

9. Park, P. I. P. & Jonnalagadda, S. Predictors of Glass Transition in the Biodegradable Poly-lactide and Poly-lactide-co-glycolide Polymers. *Journal of Applied Polymer Science* **100**, 1983-1987 (2006).

10. Fukuzaki, H., Yoshida, M., Asano, M. & Kumakura, M. Synthesis of Copoly(L-lactic acid) with Relatively Low Molecular Weight and *In Vitro* Degradation. *European Polymer Journal* **25**, 1019-1026 (1989).

11. Huffman, K. R. & Casey, D. J. Effect of Carboxyl End Groups on Hydrolysis of Polyglycolic Acid. *Journal of Polymer Science: Polymer Chemistry Edition* **23**, 1939-1954 (1985).

12. Leenslag, J. W., Pennings, A. J., Bos, R. R. M., Rozema, F. R. & Boering, G. Resorbable Materials of Poly(L-lactide) : VII. *In Vivo* and *In Vitro* Degradation. *Biomaterials* **8**, 311-314 (1987).

13. Pitt, C. G., Chasalow, F. I., Hibionada, Y. M., Klimas, D. M. & Schindler, A. Aliphatic Polyesters. I. The Degradation of Poly(ε-caprolactone) *In Vivo*. *Journal of Applied Polymer Science* **26**, 3779-3787 (1981).

14. Zhu, K. J., Hendren, R. W., Jensen, K. & Pitt, C. G. Synthesis, Properties, and Diodegradation of Poly(1,3-trimethylene carbonate). *Macromolecules* **24**, 1736-1740 (1991).

15. Tsuji, H., Ogiwara, M., Saha, S. K. & Sakaki, T. Enzymatic, Alkaline, and Autocatalytic Degradation of Poly(L-lactic acid): Effects of Biaxial Orientation. *Biomacromolecules* **7**, 380-387 (2006).

16. Göpferich, A. & Langer, R. Modeling of Polymer Erosion. *Macromolecules* **26**, 4105-4112 (1993).

17. Lee, W.-K. & Gardella, J. A. J. Hydrolytic Kinetics of Biodegradable Polyester Monolayers. *Langmuir* **16**, 3401-3406 (2000).

18. Proikakis, C. S., Mamouzelos, N. J., Tarantili, P. A. & Andreopoulos, A. G. Stability of Poly(D,L-lactic acid) in Aqueous Solutions. *Journal of Applied Polymer Science* **87**, 795-804 (2003).

19. Göpferich, A. Polymer Bulk Erosion. *Macromolecules* **30**, 2598-2604 (1997).

20. Pitt, C. G. & Gu, Z.-w. Modification of the Rates of Chain Cleavage of Poly(ε-caprolactone) and Related Polyesters in the Solid State. *Journal of Controlled Release* **4**, 283-292 (1987).

21. Nishida, H. et al. Theoretical Prediction of Molecular Weight on Autocatalytic Random Hydrolysis of Aliphatic Polyesters. *Macromolecules* **33**, 6595-6601 (2000).

22. Croll, T. I., O'Connor, A. J., Stevens, G. W. & Cooper-White, J. J. Controllable Surface Modification of Poly(lactic-*co*-glycolic acid) (PLGA) by Hydrolysis or Aminolysis I: Physical, Chemical, and Theoretical Aspects. *Biomacromolecules* **5**, 463-473 (2004).

23. Day, J. N. E. & Ingold, C. K. Mechanism and Kinetics of Carboxylic Ester Hydrolysis and Carboxyl Esterification. *Transactions of the Faraday Society* **37**, 686-705 (1941).

24. Ingold, E. H. & Ingold, C. K. Mechanism of the Hydrolysis of Carboxylic Esters with Special Reference to Acid Hydrolysis. *Journal of the Chemical Society*, 756 - 760 (1932).

25. Cohen, S. G. & Schneider, A. Cleavage of the Alkyl-Oxygen Bond in the Hydrolysis of Esters. *tert* -Butyl-2,4,6-trimethylbenzoate. *Journal of the American Chemical Society* **63**, 3382-3388 (1941).

26. Datta, S. C., Day, J. N. E. & Ingold, C. K. Mechanism of Hydrolysis of Carboxylic Esters and of Esterification of Carboxylic Acids. Acid Hydrolysis of an Ester with Heavy Oxygen as Isotopic Indicator. *Journal of the Chemical Society*, 838-840 (1939).

27. Roberts, I. & Urey, H. C. The Mechanisms of Acid Catalyzed Ester Hydrolysis, Esterification and Oxygen Exchange of Carboxylic Acids. *Journal of the American Chemical Society* **61**, 2584-2587 (1939).

28. Tsuji, H. & Nakahara, K. Poly(L-lactide). IX. Hydrolysis in Acid Media. *Journal of Applied Polymer Science* **86**, 186-194 (2002).

29. Shih, C. Chain-End Scission in Acid Catalyzed Hydrolysis of Poly (D,L-lactide) in Solution. *Journal of Controlled Release* **34**, 9-15 (1995).

30. Ellison, M. S., Fisher, L. D., Alger, K. W. & Zeronian, S. H. Physical Properties of Polyester Fibers Degraded by Aminolysis and by Alkaline Hydrolysis. *Journal of Applied Polymer Science* **27**, 247-257 (1982).

31. Chu, C. C. Hydrolytic Degradation of Polyglycolic Acid: Tensile Strength and Crystallinity Study. *Journal of Applied Polymer Science* **26**, 1727-1734 (1981).

32. Keller, A. et al. An Approach to the Formation and Growth of New Phases with Application to Polymer Crystallization: Effect of Finite Size, Metastability, and Ostwald's Rule of Stages. *Journal of Materials Science* **29**, 2579-2604 (1994).

33. Flory, P. J. Thermodynamics of Crystallization in High Polymers. IV. A Theory of Crystalline States and Fusion in Polymers, Copolymers, and Their Mixtures with Diluents. *The Journal of Chemical Physics* **17**, 223-240 (1949).

34. Mandelkern, L. & Flory, P. J. Melting and Glassy State Transitions in Cellulose Esters and their Mixtures with Diluents. *Journal of the American Chemical Society* **73**, 3206-3212 (1951).

35. Mandelkern, L., Garrett, R. R. & Flory, P. J. Heats of Fusion of Aliphatic Polyesters. *Journal of the American Chemical Society* **74**, 3949-3951 (1952).

36. Sperling, L. H. *Introduction to Physical Polymer Science* (Wiley-Interscience, New York, 2001).

37. Abayasinghe, N. K., Glaser, S., Perera, P. K. U. & Smith, D. W., Jr. Oligoethylene-End-Capped Polylactides. *Journal of Polymer Science Part A: Polymer Chemistry* **43**, 5257-5266 (2005).

38. Kobori, Y., Iwata, T., Doi, Y. & Abe, H. Synthesis, Solid-State Structure, and Surface Properties of End-Capped Poly(L-lactide). *Biomacromolecules* **5**, 530-536 (2004).

39. Ikada, Y., Jamshidi, K., Tsuji, H. & Hyon, S.-H. Stereocomplex Formation Between Enantiomeric Poly(lactides). *Macromolecules* **20**, 904-906 (1987).

40. Sarasua, J.-R., Prud'homme, R. E., Wisniewski, M., Le Borgne, A. & Spassky, N. Crystallization and Melting Behavior of Polylactides. *Macromolecules* **31**, 3895-3905 (1998).

41. Tsuji, H. & Ikada, Y. Properties and Morphology of Poly(L-lactide). II. Hydrolysis in Alkaline Solution. *Journal of Polymer Science Part A: Polymer Chemistry* **36**, 59-66 (1998).

CHAPTER 7

MELT FIBER SPINNING OF POLYLACTIDE AND POLYLACTIDE-PERFLUOROPOLYETHER BLOCK COPOLYMERS

7.1 Introduction

From its discovery in 1932 by Carothers (DuPont) to the mid 1990s, poly(lactic acid) (PLA) has mainly been used for medical and surgical applications due to its very high cost.[1,2] Recent technological developments in the production of raw materials has reduced the overall cost of PLA production and has made PLA available for commodity applications such as fibers, paper coating, films and nonwovens, etc. The production of PLA for commodity applications is currently ongoing by companies such as Shimadzu Corp., Japan (Lacty®); Mitsui Toatsu Chemicals, Inc., Japan (Lacea®); Cargill Dow Polymers LLC, United States (NatureWorks®) and many others.[1,3] The degradable and hydrolysable aliphatic polyester, PLA, has many advantages such as its renewable resource availability (corn), biodegradability and excellent processability.[4]

Spinning of PLA into fibers has been performed by various techniques such as melt spinning[5], wet spinning[6], dry-jet-wet spinning[7], electrospinning[8], etc. Melt and solution spinning of PLA is well reviewed by Agrawal and Bhalla.[9] Solution spinning of PLA results in high-strength fibers but requires solvents such as chloroform and toluene and has low production speed.[10] As-spun hollow fibers by dry-jet-wet spinning methods have been used extensively for drug delivery devices. Electrospinning methods provide fibers with high surface morphology and porosity which are required for biomedical applications. However, for commodity applications, high speed fiber production is required as well as very low cost. Melt spinning of PLA can be performed at higher production speeds with no solvent

requirements.[2] Engelberg and Kohn (1991) reported melt spun fibers with tensile modulus and strength of 3 GPa and 50 MPa respectively.[11]

The commodity and apparel uses of PLA fibers require higher thermal and hydrolytic properties compatible with the requirements of the application. Low surface energy polylactide-*b*-perfluoropolyether-*b*-polylactide block copolymer (FluoroPLA) were synthesized in our lab. In this chapter, the melt spinning of PLA and FluoroPLA5(2.0k) monofilament is discussed.

7.2 Materials and Methods

Materials

Structures of PLA and FluoroPLA are schematically illustrated in Figure 7.1 and the molecular and thermal properties of fibrous (precursor) PLA and FluoroPLA5(2.0k) materials are summarized in Table 7.1.

The detailed synthesis and properties of the PLA and FluoroPLA5(2.0k) are discussed in Chapter 4. The PLA and the FluoroPLA5(2.0k) polymers that were used for melt spinning were vacuum dried at 100 °C for 1 hr.

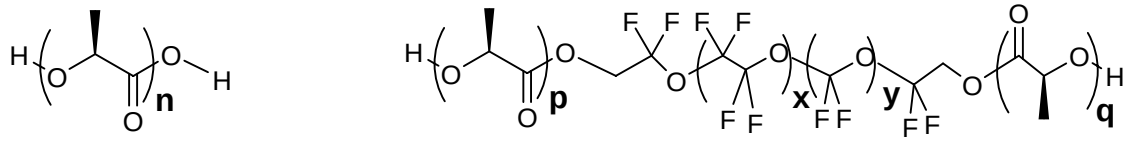

PLA
(Homopolymer)

FluoroPLA
(PLA-PFPE-PLA Block Copolymer)

Figure 7.1. Structure of PLA and FluoroPLA.

The shear viscosities of polymers were measured using a cone-and-plate fixture (Advanced Rheometric Expansion System, TA Instruments, New Castle, Delaware) with diameter of 25 mm and angular gap of 0.1 radian and data was analyzed using TA Instruments Orchestrator™ software. The shear viscosities of PLA and FluoroPLA5(2.0k) at 180 °C and a shear rate of 0.1/s were found to be ca. 472 Pa.s, and 74.2 Pa.s, respectively. The difference in the rheological behavior of PLA and FluoroPLAs is probably due to the

difference in their molecular weight since the FluoroPLA5(2.0k) only has a ca. 5 °C lower melting point than the PLA.

Table 7.1. The molecular characteristics and thermal properties of PLA and FluoroPLA5(2.0k) fiber precursor materials.

Polymer	Mn[a] kg mol^{-1}	PDI[a]	Tg[b] °C	Tc[b] °C	Tm[b] °C	Shear Viscosity[c] (Pa.s)
PLA	144	1.7	61.4	108.5	175.7	471.7
FluoroPLA5(2.0k)	83	1.7	55.7	103.3	170.3	74.2

[a] Results from gel permeation chromatography; [b] differential scanning calorimetry (DSC) data from 2nd heating cycle of annealed polymers samples heated at the rate of 10 °C/min; [c] shear viscosity at the shear rate of 0.1/s at 180 °C by cone and plate rheometer.

Fiber Production

A schematic of the melt spinning process is illustrated in Figure 7.2 (Instron Capillary Rheometer fitted with tailor-made spinneret with a single hole of diameter 250 μm). The barrel was filled with polymer materials under a dry nitrogen purge and heated to 190 °C for the case of PLA and to 185 °C for the case of FluoroPLA5(2.0k). The plungers were fitted with Teflon™ o-rings to fit perfectly with the barrel diameter (9.525 mm). As the desired temperature was achieved, the plunger was lowered at 0.06 cm/min and the molten polymer extruded into monofilament which was wound on to a spool, at a distance of ca. 1 meter from spinneret, rotating at 20 rpm.

The as-spun monofilaments were used for differential scanning calorimetric analysis and tensile testing. No post drawing on the fibers was performed. The melt spinning parameters used are as summarized below:

Spinneret hole diameter	-	250 μm
Winding speed	-	9.75 m/min
Throughput rate	-	0.05715 cm^3/min – 0.5715 cm^3/min
Spinning temperature	-	185-190 °C
Post drawing	-	None

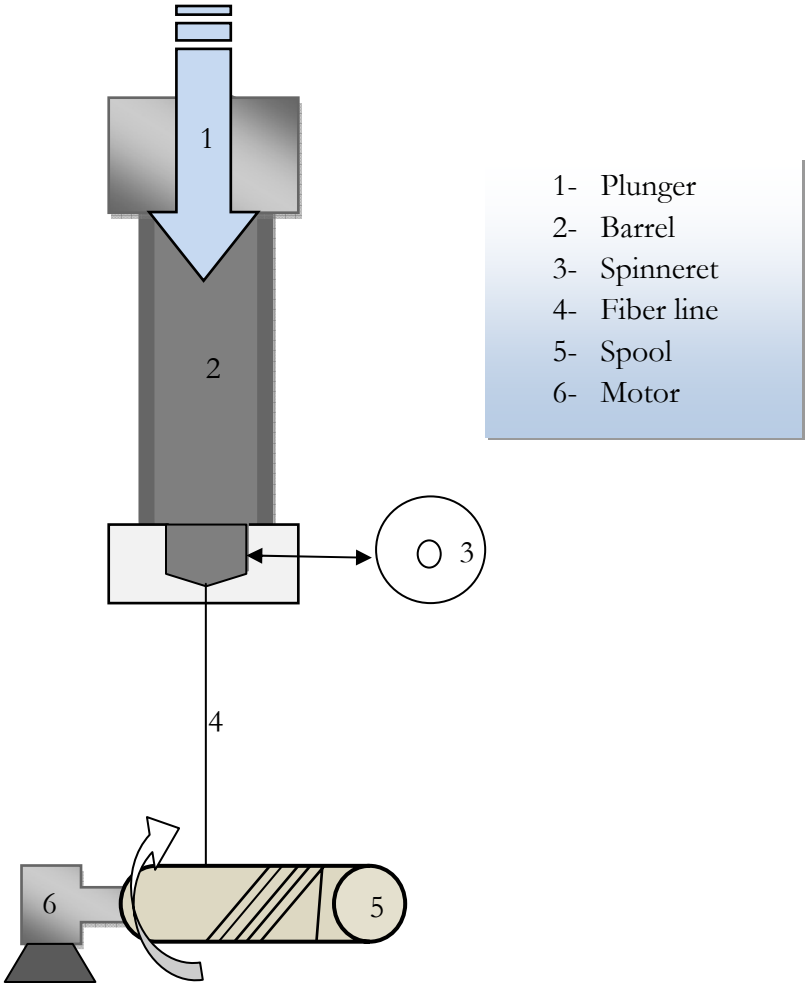

Figure 7.2. Schematic of melt extrusion process for PLA and FluoroPLA5(2.0k) fiber spinning.

Differential Scanning Calorimentry (DSC)

DSC analysis was conducted using a TA Instruments (New Castle, Delaware) Q1000 DSC. Data was analyzed using TA Instruments Universal Analysis 2000 version 4.1D software. The samples (6-8 mg in standard aluminum pans) were heated from 0 °C to 200 °C at a heating rate of 10 °C/min under a helium purge of 20 cm^3/min.

Wide-Angle X-Ray Diffraction (WAXD)

Diffraction patterns of as-spun fibers were collected at room temperature using a SCINTAG XDS 2000 (Scintag, Inc., Cupertino, CA) diffractometer equipped with Cu Kα source at a wavelength of 1.54 Å. The instrument was operated at 40 kV and 40 mA with a collimator diameter of 0.5 mm. Solution-cast polymer films (from Ch. 4) were scanned at 2°/min (2θ value) from 6° to 60°. Data were analyzed using DMSNT™ version 1.37 software.

Tensile Testing

The tensile testing of as-spun monofilament was performed using a Universal Materials Testing (Model 5582) Machine (Instron, Norwood, MA). American Society Testing & Materials (ASTM) D 3822 method for single filament testing was used with rate of 10 mm/min. Data was analyzed using Bluehill®2 version 2.4 software.

7.3 Results and Discussion

Melt spinning of PLA was performed at 190 °C whereas the spinning of FluoroPLA5(2.0k) could only be performed the lower temperature of 185 °C and this difference in the extrusion temperature of PLA and FluoroPLA5(2.0) was due to the disparity in the molecular weights and melting points of the polymers. Figure 7.3 shows photographs of spools with PLA and FluoroPLA5(2.0k) as-spun monofilaments spun at throughput rate of ca. 0.057 cm^3/min. The diameter of PLA and the FluoroPLA5(2.0k) as-spun monofilaments were measured to be 0.031 ± 0.004 mm and 0.037 ± 0.004 mm, respectively.

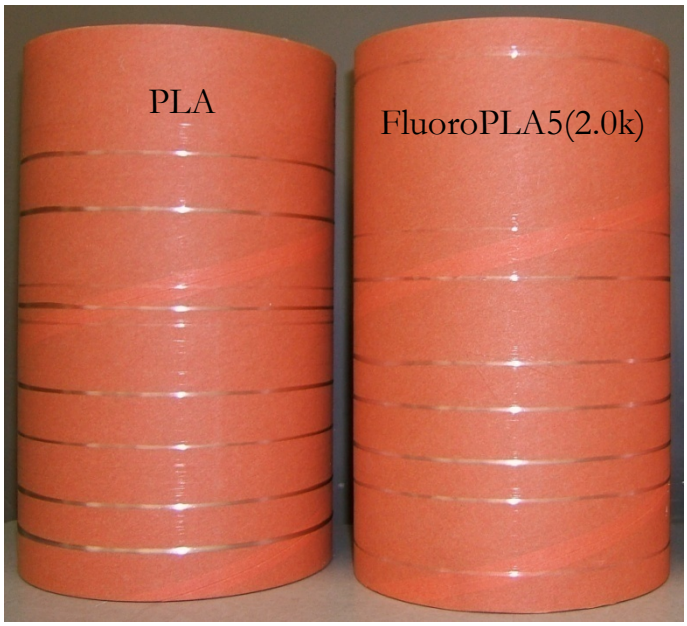

Figure 7.3. Photograph of PLA and FluoroPLA5(2.0k) as-spun monofilaments.

Wide-Angle X-ray Diffraction of PLA and FluoroPLA5(2.0k) As-spun Monofilaments

WAXD patterns of as-spun monofilaments of PLA and FluoroPLA5(2.0k) are shown in Figure 7.4. The inset in the Figure 7.4 shows the WAXD patterns of annealed solution cast films of precursor materials. Compared to the solution cast films, the as-spun monofilaments of PLA and FluoroPLA5(2.0k) are relatively amorphous and unoriented. While the PLA shows the presence of some crystallinity, the FluoroPLA5(2.0k) diffraction patterns exhibit no distinct crystalline bands. The amorphous nature of these monofilaments is probably the result of low take-up speed.

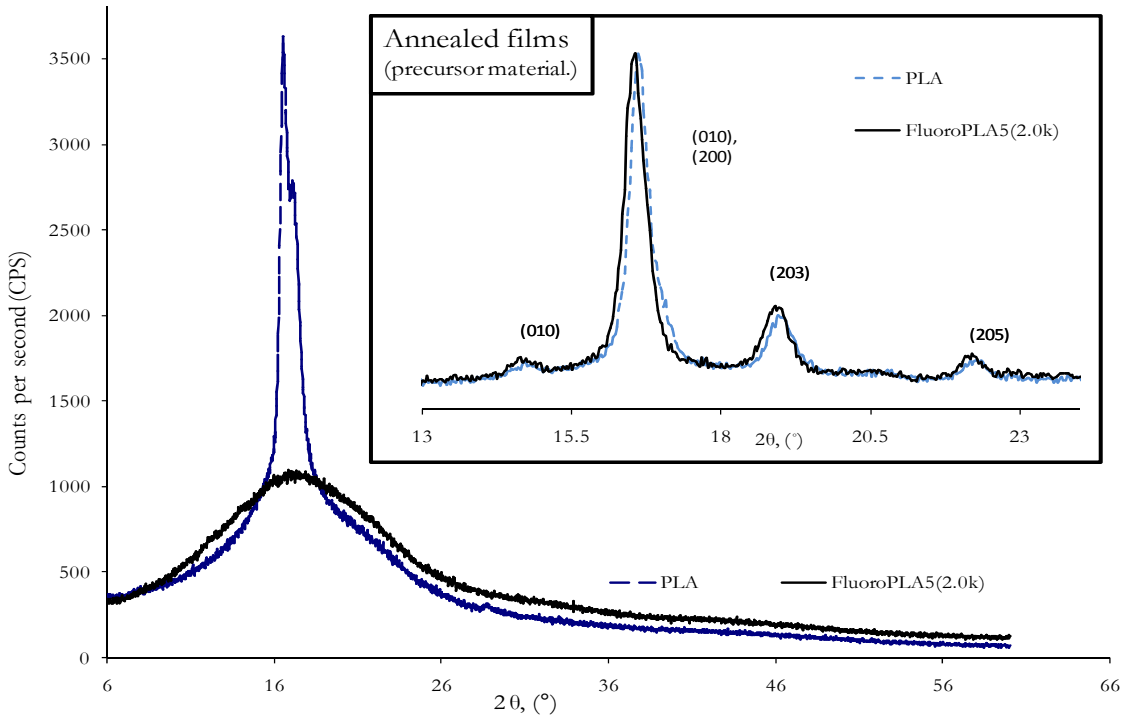

Figure 7.4. WAXD patterns of the PLA and FluoroPLA5(2.0k) as-spun monofilaments. Inset shows the WAXD patterns of annealed solution cast films of precursor materials.

Figure 7.5 shows the effect of the change in throughput rate on the WAXD pattern of FluoroPLA5(2.0k) as-spun monofilaments at a constant take-up speed of extrusion. FluoroPLA5(2.0k) monofilaments were spun at three different throughput rates of ca. 0.06, 0.2, and 0.6 cm^3/min at a constant take-up speed of ca. 9.75 m/min. As shown in Figure 7.5, no significant difference in the WAXD patterns was observed as the effect of throughput rate on the crystallinity of monofilaments was negligible and under the given spinning conditions it was not possible to attain higher crystallinity and tensile properties of PLA and FluoroPLA5(2.0k) monofilaments without post drawing.

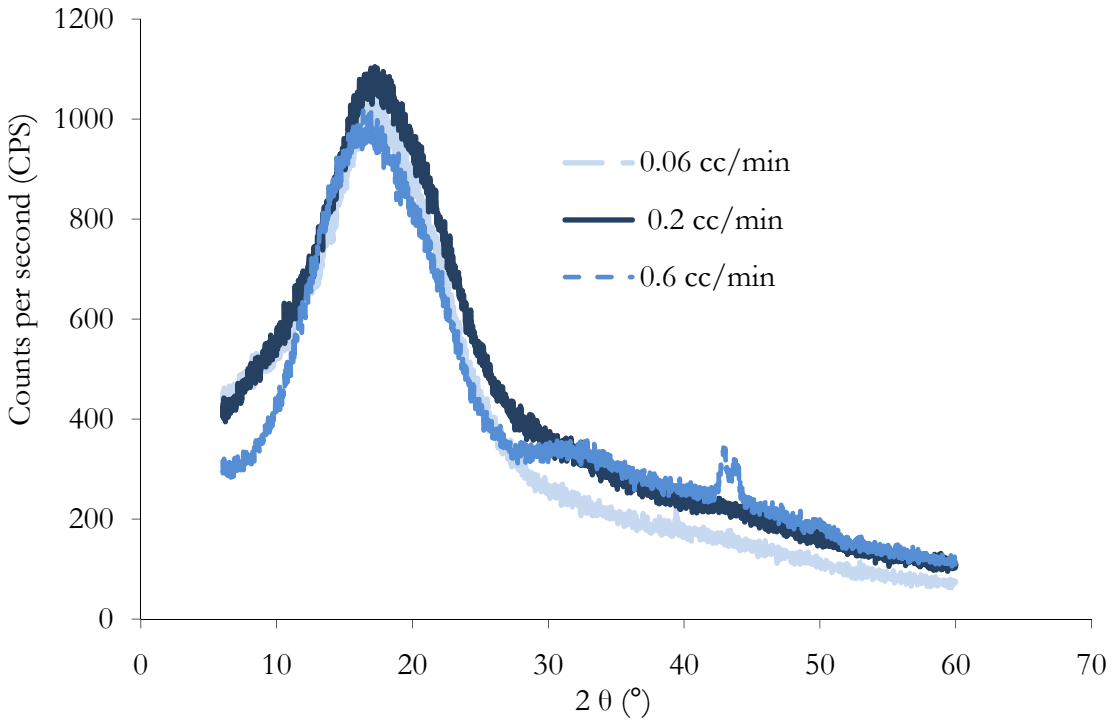

Figure 7.5. WAXD patterns of FluoroPLA5(2.0k) as-spun monofilaments at different throughput rates (0.057 cm^3/min, 0.19 cm^3/min, and 0.57 cm^3/min) with constant take-up speed.

Thermal Characterization of PLA and FluoroPLA5(2.0k) As-spun Monofilaments

The thermal properties of PLA and the FluoroPLA5(2.0k) as-spun monofilaments are summarized in Table 7.2 and representative DSC thermograms are illustrated in Figure 7.6. The major thermal transitions (glass transition, crystallization, and the melting) were clearly observed in the thermograms of both the monofilaments. As expected based on the x-ray diffraction data the DSC results show that the FluoroPLA5(2.0k) monofilaments were essentially amorphous, $\Delta Hc = 33.8$ J/g and the PLA slightly crystalline, $\Delta Hc = 12.1$ J/g. The Tc of PLA decreased from 108.5 °C (precursor material) to 77.3 °C (as-spun monofilaments) whereas the Tc of the FluoroPLA5(2.0k) was reduced from 103.3 °C (precursor) to 91.9 °C (as-spun monofilaments). The Tg's and Tm's of PLA and the FluoroPLA5(2.0k) did not differ significantly for the precursor materials (2^{nd} heating cycle) and the as-spun monofilaments.

Table 7.2. Thermal transitions and heat capacities of PLA and FluoroPLA5(2.0k) as-spun monofilaments and precursor materials.

Polymer	Tg °C	Tc °C	Tm °C	ΔHc J/g	ΔHm J/g
As-spun monofilaments[a]					
PLA	62.0	77.3	172.0	12.1	52.2
FluoroPLA5(2.0k)	56.6	91.9	170.1	33.8	58.1
Precursor materials (annealed films)					
PLA[a]	67.3	--	174.2	--	47.1
PLA[b]	61.4	108.5	175.7	28.8	43.0
FluoroPLA5(2.0k)[a]	67.2	--	170.2	--	48.9
FluoroPLA5(2.0k)[b]	55.7	103.3	170.3	31.5	48.4

[a] 1st heating cycle; [b] 2nd heating cycle.

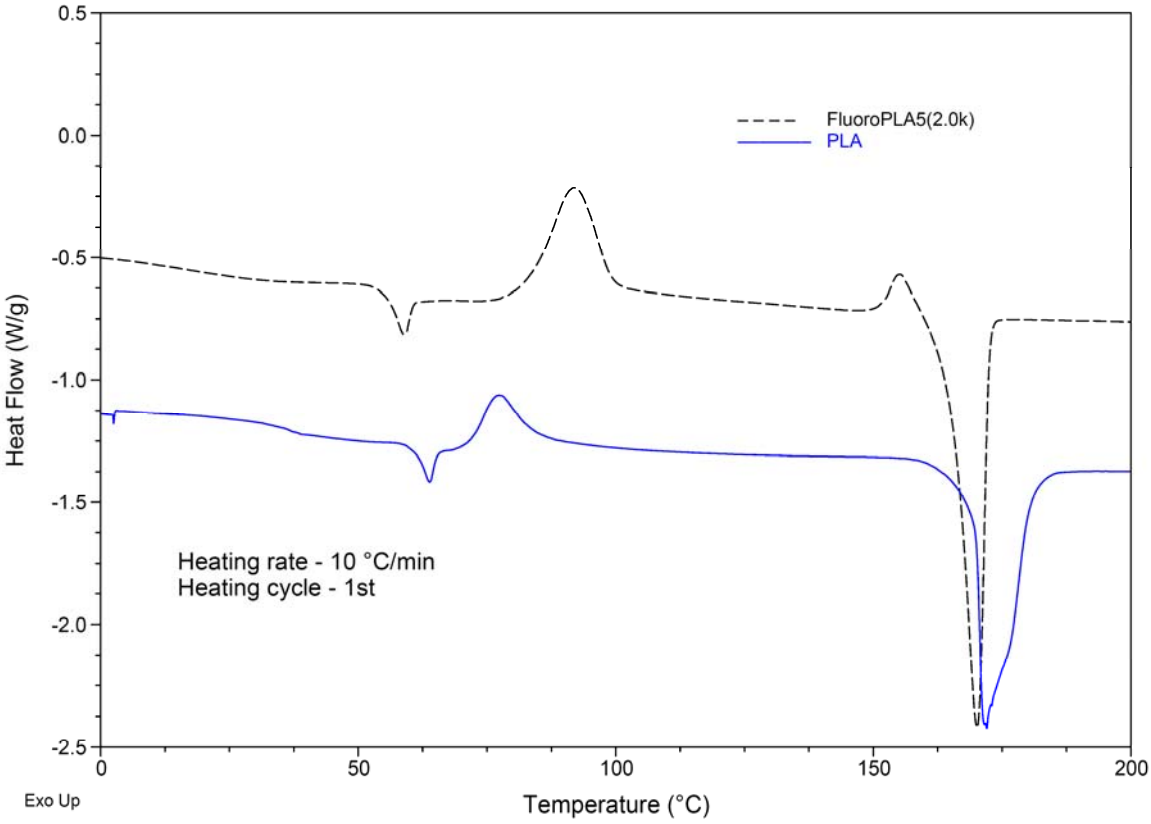

Figure 7.6. Thermal transitions of PLA and FluoroPLA5(2.0k) melt spun monofilaments by differential scanning calorimetry.

The shift in the Tc of PLA was 31.2 °C whereas shift for the FluoroPLA5(2.0k) was only 11.4 °C. As discussed in Chapter 5, it was explained that the higher crystallinity of FluoroPLA compared to the PLA was due to the nucleating action of PFPE. However, the (ΔHm- ΔHc) of as-spun PLA monofilaments is much higher than that of FluoroPLA5(2.0k). This is possibly due to two main difference between PLA and the FluoroPLA5(2.0k) i.e. the molecular weight and the melting temperature. The extrusion processes mainly rely on the knowledge of the rheological properties. The combined effect of the differences in

molecular weights and the melting temperatures of PLA and FluoroPLA5(2.0k) on their rheological properties is complex.

Tensile Properties of PLA and FluoroPLA5(2.0k) As-spun Monofilaments

Tensile properties of monofilaments are substantially affected by degree of crystallinity and orientation. Higher take-up speed during spinning or the post drawing of as-spun monofilaments improves the tensile strength because of the net increase in the orientation of polymer chains along the fiber axis. Figure 7.7 shows the percentage elongation of the as-spun monofilaments. The inset shown in Figure 7.7 illustrates the breaking strength (tensile) of the as-spun monofilaments. The strength of the PLA and the FluoroPLA5(2.0k) as-spun fiber was very similar and were measured as 96.5 ± 25.8 MPa and 90.6 ± 17.9 MPa, respectively. However, the percentage elongation (elongation at break) of FluoroPLA5(2.0k) monofilaments was found to be 297.7 ± 32.5 %, which was significantly higher than that of the PLA, measured as 73.9 ± 35.8 %.

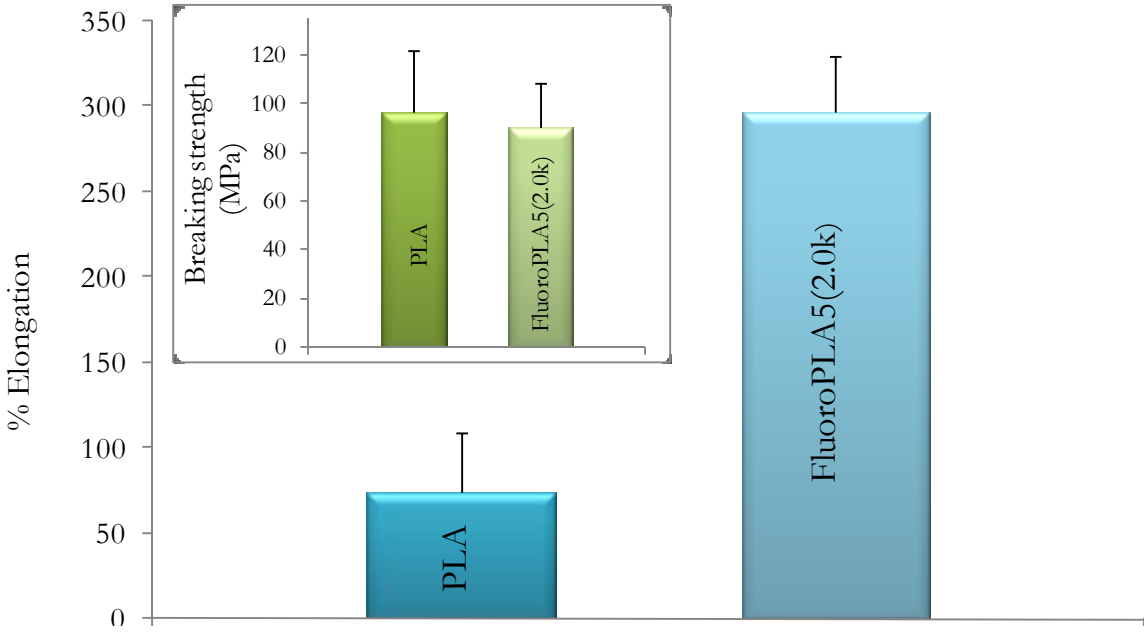

Figure 7.7. Percentage elongation and breaking strength (inset) of melt spun PLA and FluoroPLA5(2.0k) as-spun monofilaments.

The significant difference in the elongation-at-break of FluoroPLA5(2.0k) as-spun monofilaments compared to the PLA probably only reflects the difference in the crystallinity of PLA and FluoroPLA5(2.0k). The initial tensile moduli of the PLA and FluoroPLA5(2.0k) as-spun monofilaments were similar and ranged between 1.3 to 1.6 GPa. Figure 7.8 illustrates the stress-strain curve of the selective specimens which closely represents the elongation-at-break of PLA and the FluoroPLA5(2.0k) as-spun monofilaments. The FluoroPLA5(2.0k) fiber shows a yield stress followed by ductile behavior whereas no ductile (necking) type phenomenon was observed for the PLA as-spun monofilaments. Higher enlongation-at-break of FluoroPLA5(2.0k) compared to PLA is possibly due to the cold drawing of amorphous FluoroPLA5(2.0k) monofilaments.

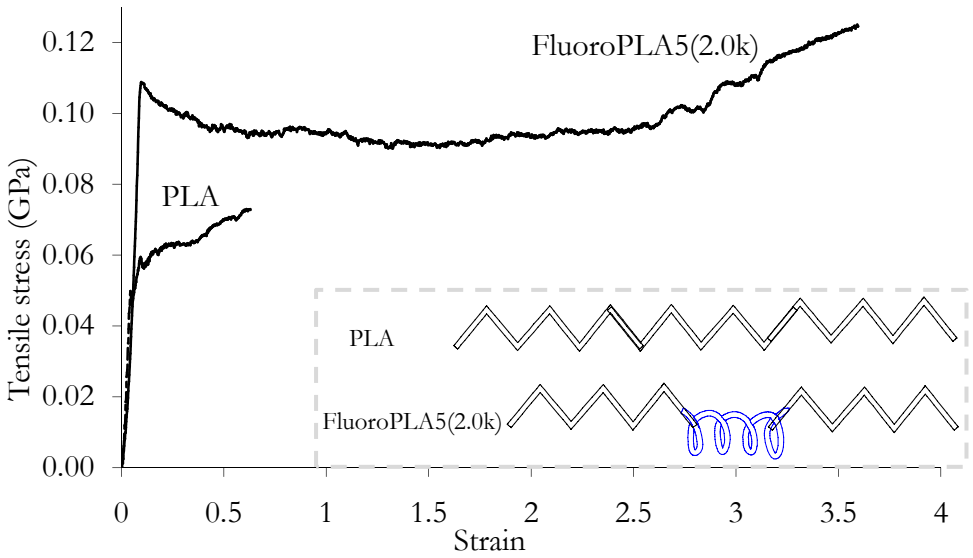

Figure 7.8. Stress-strain plot of the selectived PLA and FluoroPLA5(2.0k) as-spun monofilaments samples illustrating the comparative elongations of two different monofilaments.

7.4 Conclusions

As-spun monofilaments were produced from PLA and FluoroPLA5(2.0k) polymers by the melt spinning process. The equipment had limited take-up speed, therefore, resulting in the as-spun monofilaments of little to no crystallinity. As expected, at the given take-up speed (10 m/min), changing the throughput rate within the equipment limitations had almost no effect on the crystallinity of the FluoroPLA5(2.0k) as-spun monofilaments. The exact effect of incorporation of PFPE segments, in altering the elongation-at-break and toughness of FluoroPLAs monofilaments without any detrimental effect on tensile strength, would need to be investigated by comparing the PLA and FluoroPLAs monofilaments having similar crystallinity and orientation.

7.5 References

1. Lunt, J. & Shafer, A. L. Polylactic Acid Polymers from Corn. Applications in the Textiles Industry. *Journal of Industrial Textiles* **29**, 191-205 (2000).
2. Solarski, S., Ferreira, M. & Devaux, E. Characterization of the Thermal Properties of PLA Fibers by Modulated Differential Scanning Calorimetry. *Polymer* **46**, 11187-11192 (2005).
3. Perepelkin, K. E. Polylactide Fibres: Fabrication, Properties, Use, Prospects. A Review. *Fibre Chemistry* **34**, 85-100 (2002).
4. Cicero, J. A. et al. Supramolecular Morphology of Two-Step, Melt-Spun Poly(lactic acid) Fibers. *Journal of Applied Polymer Science* **86**, 2828-2838 (2002).
5. Fambri, L., Pegoretti, A., Fenner, R., Incardona, S. D. & Migliaresi, C. Biodegradable Fibres of Poly(L-lactic acid) Produced by Melt Spinning. *Polymer* **38**, 79-85 (1997).
6. Tsuji, H., Ikada, Y., Hyon, S.-H., Kimura, Y. & Kitao, T. Stereocomplex Formation Between Enantiomeric Poly(lactic acid). VIII. Complex Fibers Spun from Mixed Solution of Poly(D-lactic acid) and Poly(L-lactic acid). *Journal of Applied Polymer Science* **51**, 337-344 (1994).
7. van de Witte, P. et al. Formation of Porous Membranes for Drug Delivery Systems. *Journal of Controlled Release* **24**, 61-78 (1993).
8. Kim, K. et al. Control of Degradation Rate and Hydrophilicity in Electrospun Non-Woven Poly(D,L-lactide) Nanofiber Scaffolds for Biomedical Applications. *Biomaterials* **24**, 4977-4985 (2003).
9. Agrawal, A. K. & Bhalla, R. Advances in the Production of Poly(lactic acid) Fibers. A Review. *Polymer Reviews* **43**, 479 - 503 (2003).

10. Leenslag, J. W. & Pennings, A. J. High-Strength Poly(L-lactide) Fibers by a Dry-Spinning/Hot-Drawing Process. *Polymer* **28**, 1695-1702 (1987).

11. Engelberg, I. & Kohn, J. Physico-Mechanical Properties of Degradable Polymers Used in Medical Applications: A Comparative Study. *Biomaterials* **12**, 292-304 (1991).

CHAPTER 8

HIGH GLASS TRANSITION L-LACTIDE AND BISPHENOL A DERIVATIVES TERPOLYMER: SCALED-UP SYNTHESIS, CHARACTERIZATION AND APPLICATION

8.1 Introduction

The chemical industry uses ca. 12 % of fossil feedstocks for energy generation and as raw materials. The fossil feedstocks account for more than 90 % of the raw materials in the chemical industry and a large portion of the raw material is used for making polymers. But the oil crisis in 1973 has driven the chemical industry to try to find alternate sources for energy and raw materials.[1] In addition to the diminishing, non renewable oil resources, the environmental effects of non-biodegradable petroleum based polymers cannot be ignored in this global warming era. Biodegradable polymers from renewable resources are seen as one solution for some environmental problems and our dependency on the fossil resources.

One such biodegradable polymer is Polylactide / Poly(lactic acid) (PLA) and the first synthesis of aliphatic polyester, Poly(lactic acid), was reported by Carothers et al in 1932.[2] The medical applications of PLA and its copolymers for surgical implants and tissue repair began in the 1960s.[3] In addition to the biomedical and pharmaceutical applications, PLA and its copolymers are showing a significant rise in their use in commodity applications because they are made from a renewable monomer resource, they have comparable mechanical properties to petroleum-based polymers, they degrade in the natural environments with very low toxicity, and above all, recent developments in technology have lead to comparable prices to petroleum-based commercial polymers.[4] The widespread use of PLA as a commodity polymer is currently limited due to its lower glass transition

temperature (50-60 °C) compared to petroleum based polymers such as polystyrene and poly(methyl methacrylate) (ca. 100 °C).[5,6]

Various modification routes for PLA have been utilized to alter the intrinsic properties in recent approaches. The enhancement of properties by the use of novel catalysts and modifications by blending, plasticization and copolymerization with other polymers and/or compounds have recently been reported.[5,7-9] In this chapter, scaled-up synthesis, thermal and surface characterization and application of a high glass transition temperature polylactide and bisphenol A derivatives terpolymer are discussed. The bisphenol A based commodity monomers such as 4,4'-hexafluroisopropylidenediphenol (6F-Bis-A) and the diglycidyl ether of bisphenol A (DGEBA) were used to enhance the glass transition temperature of PLA.

8.2 Materials and Methods

L-Lactide (LA) was generously donated by Poly-Med Inc. (Pendleton, SC) and was recrystallized from ethyl acetate and vacuum dried to remove solvent and moisture. Polylactide (PLA Polymer 4042D) was generously donated by Cargill Dow Polymers, LLC (United States). Diglycidyl ether of bisphenol A (DGEBA), 4,4'-(hexafluoroisopropylidene)diphenol (6F-Bis-A) and 1-phenoxy-2-propanol (Dowanol™) were used as received from Dow Chemical Company (United States). The potassium chloride (KCl) and the 18-Crown-6 (18C6) were purchased from Sigma Aldrich (United States) and were used as received. All other chemicals and reagents were purchased from Fisher or Sigma Aldrich and used as received unless otherwise stated.

Scaled-up synthesis of terpolymer

The terpolymerization of LA, DGEBA and 6F-Bis-A was carried out in molar ratio of 1:1:1. KCl and 18C6E were stirred overnight in 10 ml Dowanol™ and then added to the reaction system. Reaction mixtures were prepared using the following recipe:

Reactants	Mole	
LA	1.0	
DGEBA	1.0	
6F-Bis-A	1.0	
KCl	2.7	$x10^{-3}$
18C6E	2.9	$x10^{-3}$
Dowanol	0.7	

The prepared reaction mixture (~300 g) was then added to the 600 ml capacity moveable reaction vessel (high pressure/moderate temperature stirred, series 4540, reactor,

Parr Instrument Company, Moline, IL), purged and sealed under 15 psi of inert (argon) atmosphere. The temperature was gradually (~2 °C/min) increased to 115 °C and held for 24 hrs with stirring (20 rpm) throughout. The terpolymerization product was removed from the bottom drain valve of the reactor and cooled. Extraction of the reaction product was carried out by dissolving in tetrahydrofuran followed by precipitation in methanol, then n-hexane sequentially. The precipitated terpolymer was then vacuum dried at 90 °C for 1 hour.

Characterization

FTIR spectroscopy was performed using a Thermo-Nicolet Magna - IR™ 550 spectrometer (Thermo Nicolet, Waltham, MA) equipped with a Thermo Spectra-Tech Foundation Series Endurance diamond attenuated total reflectance (ATR) accessory. Sample spectra were collected by performing 32 scans at a resolution of 4 cm^{-1} from 4000 cm^{-1} to 525 cm^{-1} and were ratioed against background spectra collected in the same fashion. Data was analyzed using OMNIC E.S.P. v 7.2 software.

Differential Scanning Calorimetry (DSC) analysis was conducted using a TA Instruments (New Castle, Delaware) Q1000 DSC. Data was analyzed using TA Instruments Universal Analysis 2000 version 4.1D software. The samples (6-8 mg in standard aluminum pans) were initially heated to 225 °C to erase the prior thermal history, then cooled to -50 °C, and finally heated from -50 °C to 225 °C. A heating rate of 10 °C was used for all of the segments described above. The glass transition temperatures were measured based on the inflection point of the step transition. Temperature values of the endothermic and exothermic peak maxima's were considered as the melting and crystallization temperatures,

and the integral of the peak areas was used to calculate heats of fusion and crystallization, respectively.

Thermal Gravimetric Analysis (TGA) was conducted using a TA Instruments (New Castle, Delaware) 2950 TGA. Data was analyzed using TA Instruments Universal Analysis 2000 version 4.1D software. Samples were heated at a rate of 10 °C/min from room temperature to 400 °C under a nitrogen purge.

Dynamic Mechanical Analysis (DMA) was performed using a DMS 210 Tension Module (Seiko Instruments Inc., Japan) with specimen dimensions of 40 mm x 10 mm and an effective gauge length of 20 mm. Samples were evaluated over a temperature range of -130 °C to 125 °C, at a heating rate of 2 °C/min at a frequency of 1 Hz and a deformation amplitude of 10 μm. Data were analyzed using EXSTAR6000 software.

Silicon wafers were oxidized by immersion in pirana solution (3 part 95-98% H_2SO_4 + 1 part 30% H_2O_2) at 80 °C for 45 minutes. The thickness of the resultant SiO_2 layer was measured by ellipsometry and found to be ca. 1.4 nm. Solutions of 2 % (w/v) homopolymer and terpolymer in chloroform were prepared and filtered through a Whatman 0.2 μm polytetrafluoroethylene membrane syringe filter. Dip coating of oxidized silicon wafers was carried out using a dip coater (Mayer Feintechnik D-3400, Göttingen, Germany). Dip coated samples were air dried and then the film thicknesses were measured using ellipsometry.

A Dimension 3100 (Veeco Inc., Woodbury, NY) atomic force microscope (AFM) equipped with Nanoscope IIIa controller was used to image the surface of the dip-coated polymer film on silicon wafers. All AFM characterization experiments were performed using a silicon AFM tip (MicroMash Inc., nominal force constant 40 N/m, tip radius <10 nm) in the non-contact (tapping) mode.

Static contact angle measurements were performed using the sessile drop method on a Drop Shape Analysis (KRÜSS Instruments, Hamburg, Germany) system. Liquid drops with an average volume between 5 to 10 μL were placed on the dip coated polymer films and the equilibrium contact angles were measured after an equilibration time of 30 seconds.

Electrospinning

Polymer solutions of concentrations between 25-35 (w/v) % in chloroform and tetrahydrofuran were electrospun using the electrospinning equipment illustrated in Figure 8.1. Solutions were placed in a 10 ml syringe and then pumped through a 16 ½ gauge needle at a rate of 6 ml/hr. A 15 kV voltage was applied to the needle and the polymer jet was collected on a grounded surface at distance of 10 cm. The electrospun sample was then vacuum dried at 60 °C for 1 hour.

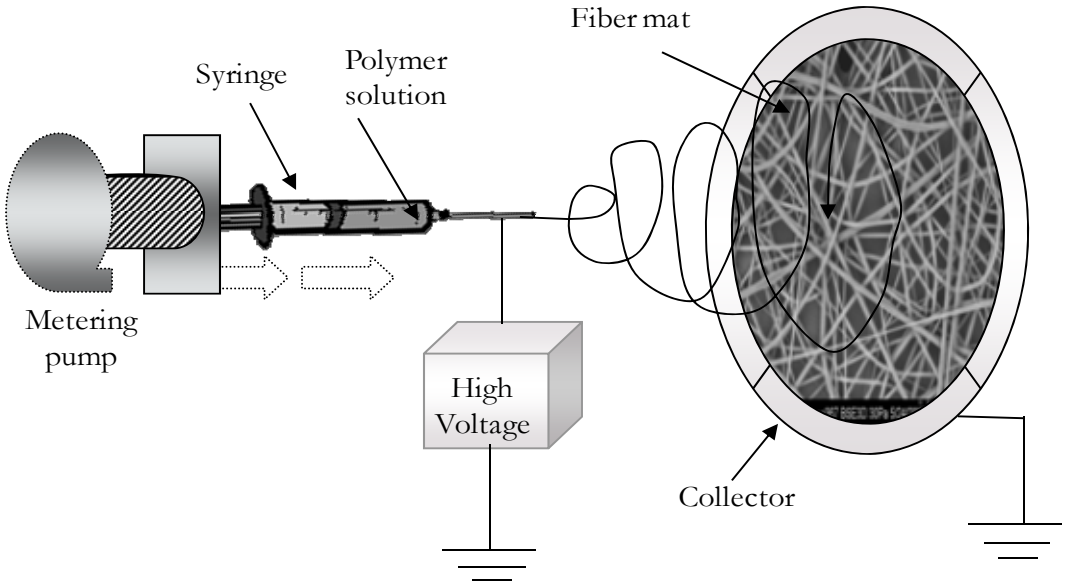

Figure 8.1. Schematic of electrospinning process for fiber spinning.

Scanning Electron Microscopy (SEM) images of electrospun fibers samples were obtained using a Hitachi S3400N (Hitachi High-Technologies, Japan) microscope at an accelerating voltage of 20 kV. A Hummer®6.2 (Anatech Ltd., Hayward, CA) sputter coater was used to pre-coat the samples with a 4-5 nm layer of platinum.

8.3 Results and Discussion

The synthesis L-lactide, 6F-Bis-A, DGEBA terpolymer (TP) was carried out as shown in the Scheme 8.1. The 18-Crown-6/KCl (18C6/KCl) complexes have been widely used for ring opening polymerization/polyaddition of epoxide with lactones and esters.[10,11] The effect of the feed ratio and solvent on the terpolymerization is discussed in detail by Abayasinghe et al.[6] The equimolar terpolymerization of L-Lactide, 6F-Bis-A and DGEBA at 115 °C for 24 hr resulted in terpolymers with molecular weight (Mn) of ca. 12 kg mol^{-1} and molecular weight distribution (Mw/Mn) of ca. 1.5 as determined by the gel permeation chromatography. The complexation of K^+ with 18C6 increases the concentration of the nucleophile Cl^- in system.[12] The carbanions generated by the attack of nucleophiles are stabilized by a tautomeric equilibrium with the enolate form. The propagation of the reaction proceeds by the alkyl-oxygen bond scission of the lactide.[13] The detailed mechanistic aspects of the reaction are described by Fish et al. and Jedlinski et al.[13,14]

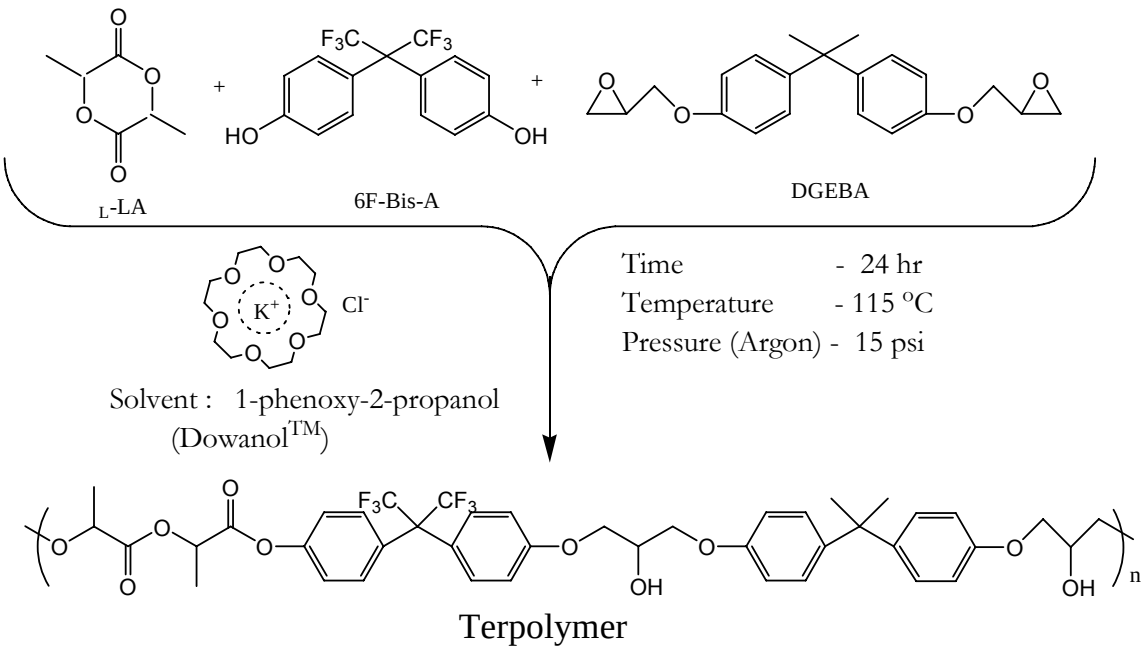

Scheme 8.1. Terpolymerization of L-Lactide and bisphenol A derivatives (DGEBA, 6F-Bis-A).

The confirmation of the incorporation of different moieties in the polymer chain of TP was measured using FTIR spectroscopy as shown in Figure 8.2. The FTIR spectrum of the TP shows the presence of a peak at 1743 cm^{-1} which corresponds to the carbonyl (C=O) peak in the lactide which occurs at 1753 cm^{-1} in the unreacted monomer. The peaks (strong) at ca. 1610 and 1510 cm^{-1} in 6F-Bis-A, DGEBA and TP correspond to the aromatic C=C stretch. The C-F stretch from CF_3 group in 6F-Bis-A and TP shows a strong peak at 1170 cm^{-1}. The epoxy stretching peak at 911 cm^{-1} in DGEBA completely disappears in the TP as expected, due to polymerization process which proceeds by opening of epoxy ring. Also, the Ph-O-C stretch is observed in the DGEBA and TP at 1297 cm^{-1}. All of the above

comparisons between the TP and monomers suggest the incorporation of monomer units in the TP backbone.

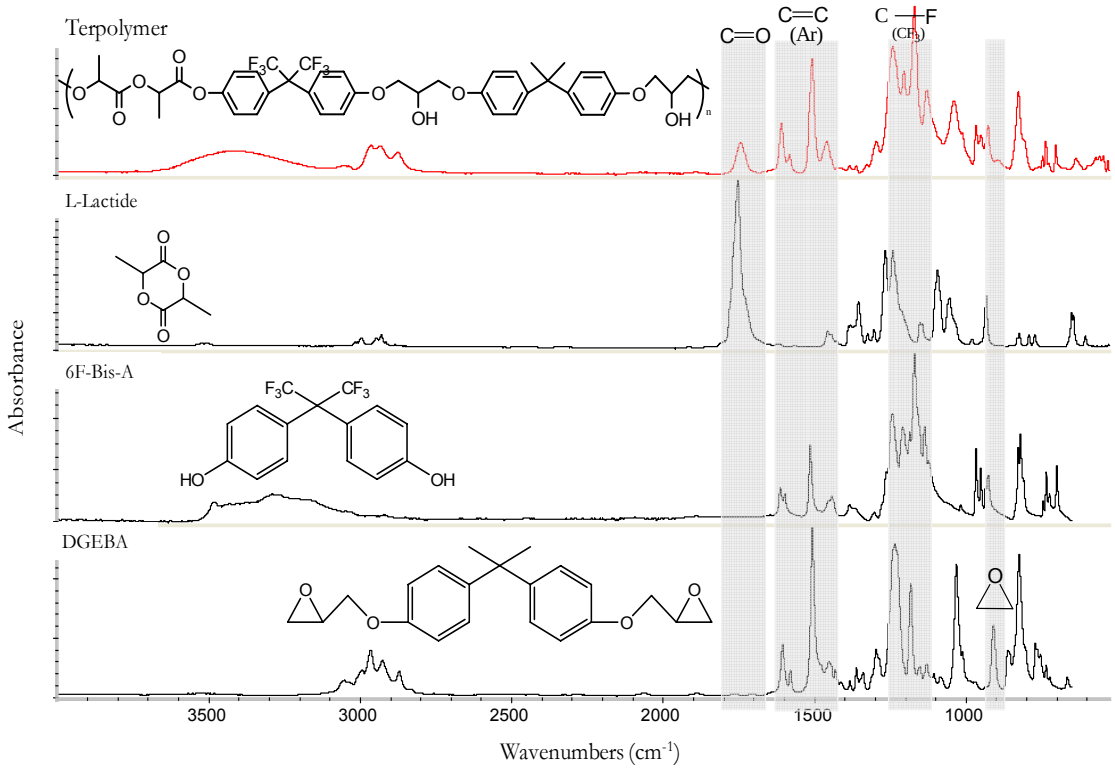

Figure 8.2. FTIR spectra for TP, L-Lactide, 6F-Bis-A and DGEBA.

As a result the progress of the reaction can also be monitored by the conversion of lactide and epoxide monomer to terpolymer by the decrease in intensity of carbonyl and epoxide peaks as the reaction proceeds. The FTIR peaks assignment for Lactide, 6F-Bis-A, DGEB and TP are summarized in Table 8.1.

Table 8.1. The FTIR peaks assignment for Lactide, 6F-Bis-A, DGEBA and TP.

Functinal group	FTIR peaks assignment, wavenumber (cm^{-1})			
	Lactide	6F-Bis-A	DGEBA	TP
C=O	1753	-	-	1743
Epoxy stretch	-	-	911	-
C=C (Aromatic)	-	1615/1515	1607/1508	1608/1510
C-F from $-CF_3$	-	1170	-	1170
Ph-O-C	-	-	1298	1297

The chemical structure of the polymer chain affects the thermal properties of the polymer. The structural characteristics, such as structural regularity, bond flexibility, close packing ability, and interactions, affects the thermal performance of a polymer.[15,16] The inclusion of aromatic units in the backbone increases the thermal resistance typical of the polymer as the aromatic ring systems possess high bond strength.[17] Representative weight loss curves (thermogravimetic analysis) for PLA and TP are shown in Figure 8.3 and the dependent axis on left side shows the percentage weight loss and on the right side shows the rate of weight loss as a function of temperature. The difference in the maxima of the rate of weight loss peaks of PLA and the TP is ca. 86 °C. Also, the complete degradation of TP is not seen untill 600 °C. This is possibly due to very high thermal stability of the aromatic units. Hence, the TP has much higher thermal stability than PLA.

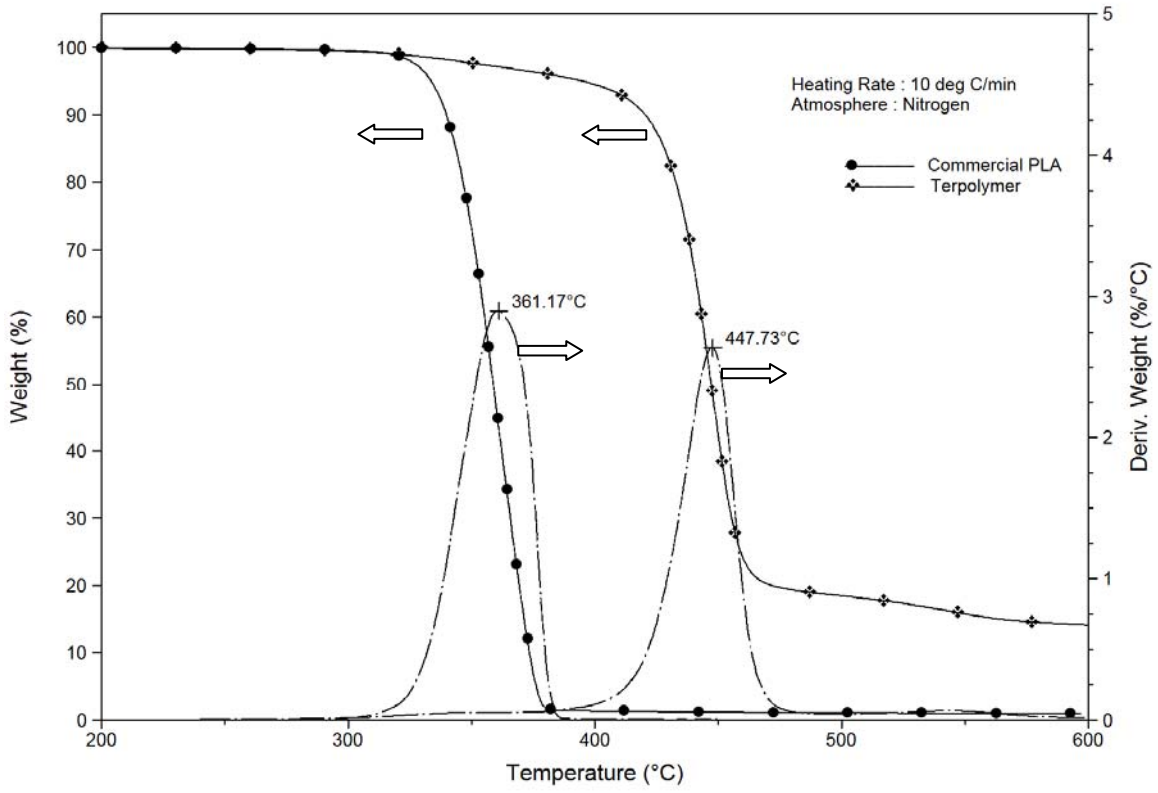

Figure 8.3. Thermogravimetric analysis of PLA and TP demonstrating the percentage weight loss and rate of weight loss as a function of temperature.

The inclusion of aromatic units in the polymer chain should certainly increase the melting temperature of polymers as the rigidity of backbone is improved.[15] But both the bisphenol A derived monomers contain bulky groups and these bulky groups could possibly hinder the packing of chains and formation of crystalline polymer domains is restricted. The calculated glass transition temperature for TP by Bicerano module was about 105 °C using Polymer-Design Tools™ version 1.1 (DTW Associates, Inc, PA, USA) software. As shown by the comparison of the DSC thermograms in Figure 8.4, the glass transition temperature of TP is above one hundred (102 °C) which is ca. 40 °C higher than commercial PLA. The

glass transition temperature of the TP is in the range of the Tg of polystyrene (ca. 100 °C). No melting peak was observed in case of TP whereas the PLA showed melting peak at ca. 145 °C. In TP, polymer chains lack the ability to pack closely and hence the formation of crystalline domains is inhibited. This and the rigidity of the backbone makes TP an amorphous polymer with a high glass transition temperature. The TP resembles petroleum-based amorphous polymers such as polystyrene and poly(methyl methacrylate).

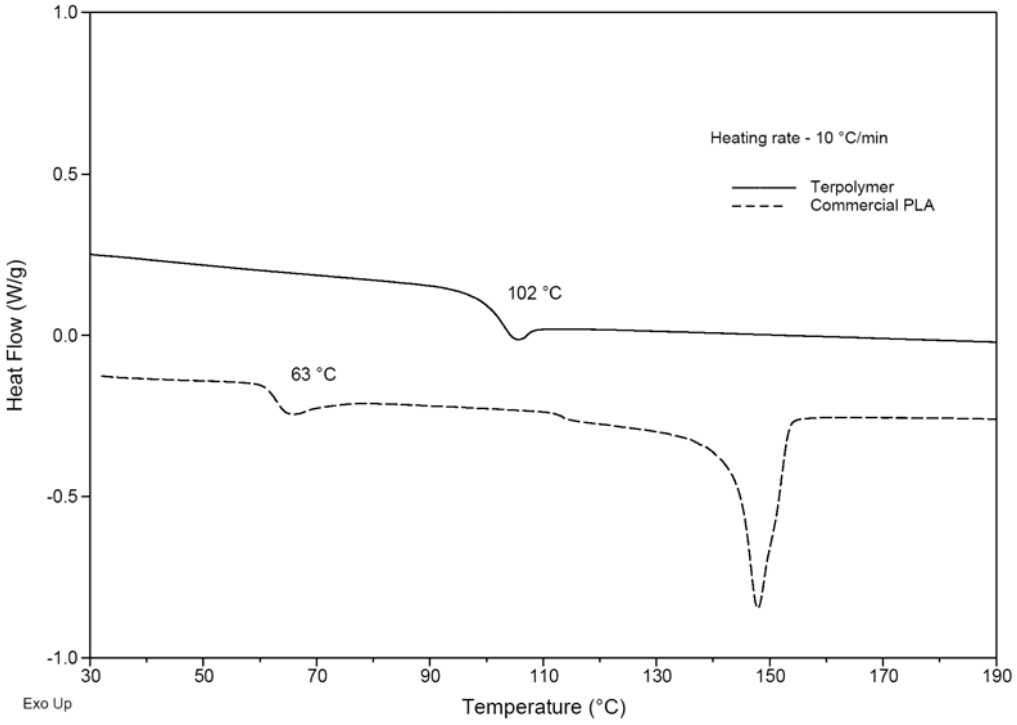

Figure 8.4. DSC thermograms comparing the observed thermal transitions for PLA (dashed line) and the TP (solid line).

The relationship between the glass transition temperature and the molecular weight of polymers is well explained by Fox and Flory and can be approximated by equation 8.1:[18,19]

$$T_g = T_{g\infty} - \frac{C}{Mn} \quad 8.1$$

where $T_{g\infty}$ is glass transition temperature at an infinite molecular weight and C is a positive constant depending on the polymer. The dependence of T_g on the molecular weight is very strong below the critical molecular weight (M_C) of a polymer (due to the large free volume associated with the chain ends). The M_C for PLA[20] is ca. 9.6 x 10^3 g mol^{-1} which is very close to the molecular weight of the TP. Hence, there is possibility that the glass transition temperature of the TP can be increased further by increasing the molecular weight of the TP.

Figure 8.5 shows the plot of the storage modulus, loss modulus and loss factor (tan δ) as a function of temperature for the TP. Analysis was performed on a compression molded article (40 mm x 10 mm x 1.6mm) of TP. The mechanical properties of polymers are strongly associated with its molecular weight and for any useful tensile property the molecular weight should be well above the critical molecular weight of the polymer. The TP shows a storage modulus of < 2 MPa at lower temperature range and this is due to the moderate molecular weight. The tan δ shows a peak at ca. 98 °C which is consistent with the DSC data and further confirms that the TP has a much higher Tg (ca. 100 °C) than PLA.

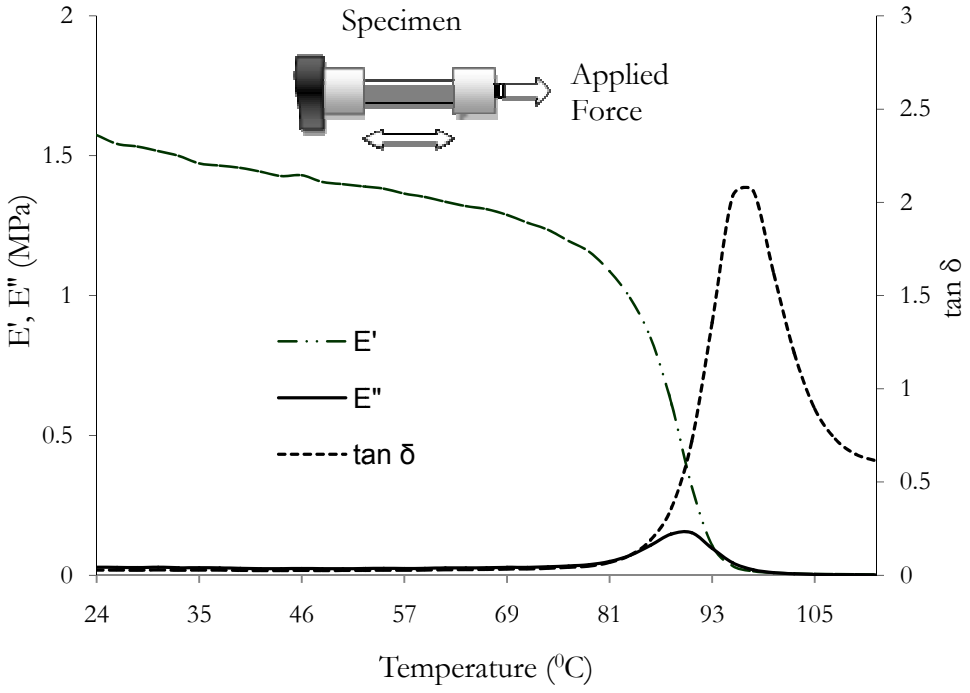

Figure 8.5. Dynamic mechanical anaysis curve with storage modulus (E'), loss modulus (E") and loss factor (tan δ) for TP.

Surface Morphology and Energy

Atomic force microscopy (AFM) analysis in the non-contact (tapping) mode was performed on the dip coated films obtained by immersion of oxidized silicon wafer in 2%(w/v) polymer solution in chloroform. The AFM surface topography images of PLA and the TP are shown in Figure 8.6. PLA shows a very flat morphology whereas the TP shows a distinct morphology in comparison to PLA. The contrast observed in the morphology of TP and PLA is possibly due to the difference in the solubility and viscosity of polymers in chloroform. The solubility parameter (δ) of PLA and TP are very similar ($\delta_{PLA} \sim 18.7\ J^{1/2}cm^{-3/2}$, $\delta_{TP} \sim 19.9\ J^{1/2}cm^{-3/2}$ as calculated by Bicerano module). However, the higher crystallinity and molecular weight of the polymer adversely affects its solubility in any solvent.[21] As observed in DSC analysis (Figure 8.4), PLA is semicrystalline polymer and TP is completely amorphous as no melting transition was observed. The molecular weight difference between PLA (Mn ca. 144 kD) and TP (Mn ca. 12 kD) is very large. Based on above observations and calculations, the solubility of aforementioned TP in chloroform is possibly higher than that of the PLA and the viscosity of PLA solution is very high. Also, the thickness of dip coated PLA film was ca. 86 nm wheareas TP film thickness was only ca. 40 nm and this difference in the thickeness could have been related to the viscosity difference in 2%(w/v) polymer solutions of PLA and TP in chloroform.

During the dip coating, drying of films occur as a result of exposure to air and the lower viscosity solution can possibly result in the contrast surface morphology due to rapid drying whereas very high viscosity PLA solution does not allow the rapid drying and resulted in flattened morphology.

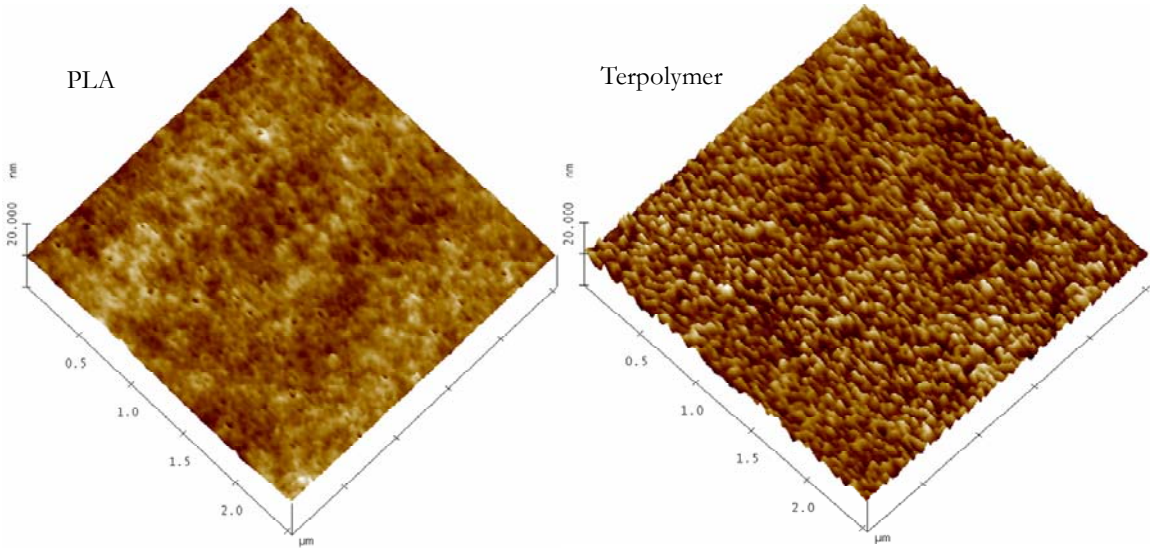

Figure 8.6. AFM topography images of PLA (left) and TP (right) with a scan size of 2.5 µm x 2.5 µm.

Static contact angle measurements were performed using the sessile drop method with an equilibration time of 30 seconds. Plots of the contact angles of five probe liquids on PLA (synthesized by ring-opening polymerization, for details see Chapter 4) and TP are shown in Figure 8.7. Water has a relatively high surface tension (72 mN/m) and interfacial forces have a significant contribution from intermolecular forces such as hydrogen bonding. In the case of n-hexadecane, which has a surface tension of 27 mN/m, only dispersion forces contribute to the interfacial tension. No significant difference in the contact angles of PLA and TP was noted for all liquids except for slightly lower contact angle of TP with n-hexadecane. This is possibly due to the fact that the TP films started dissolving in n-hexadecane thereby making the measurements difficult and less reliable.

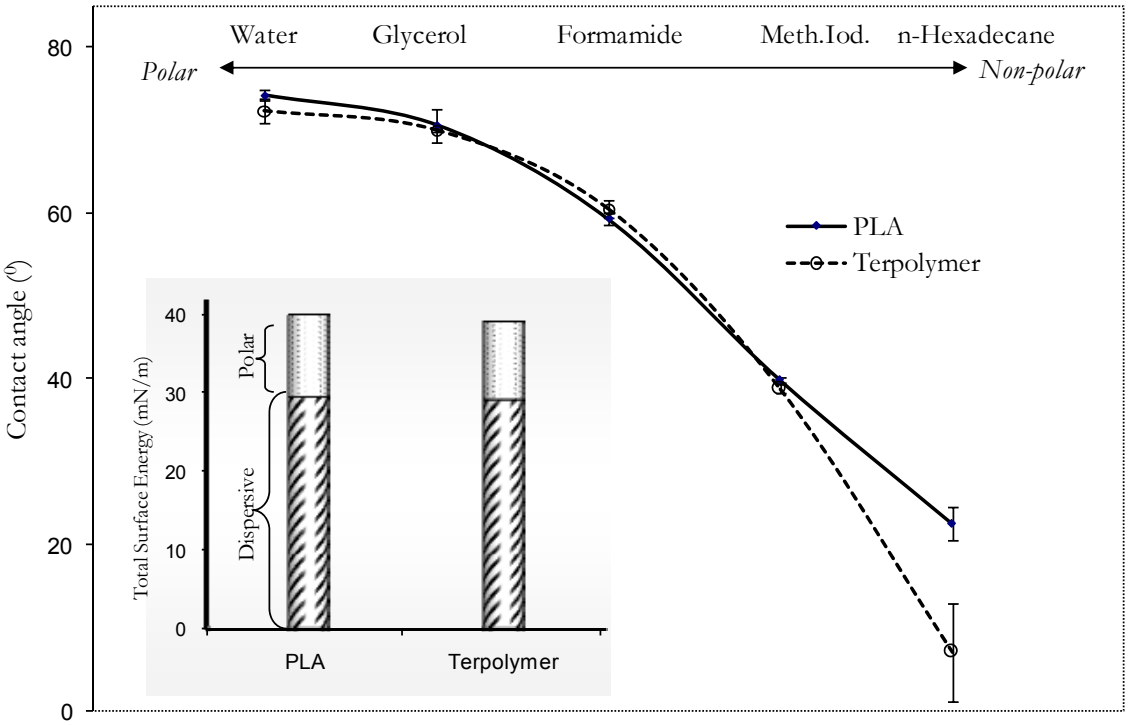

Figure 8.7. Static contact angle of water, glycerol, formamide, methylene iodide and n-hexadecane on PLA and TP dip coated on silicon wafers. Surface free energy and its components for PLA and TP by the Kaelble method.

The Owens-Wendt-Rabel-Kaelble (WORK) method was used to investigate the surface energies of PLA and TP. The dispersive and polar components of the total surface energies of PLA and TP was obtained by WORK equation 2.

$$\frac{(1+\cos\theta)}{2}\cdot\left(\frac{\gamma_l}{\sqrt{\gamma_l^d}}\right)=\sqrt{\gamma_s^d}+\sqrt{\gamma_s^p}\cdot\left(\frac{\sqrt{\gamma_l^p}}{\sqrt{\gamma_l^d}}\right) \qquad 8.2$$

The plots of $\frac{\gamma_l \cdot (1+\cos\theta)}{2\sqrt{\gamma_l^d}}$ vs $\frac{\sqrt{\gamma_l^p}}{\sqrt{\gamma_l^d}}$ for both Rabel and Kaelble methods are shown in Appendix E and Appendix F, respectively. The results from using these two methods were in good agreement and no significant difference in dispersive, polar and total surface energies of PLA and TP was observed using either. The inset in Figure 8.7 shows the polar and dispersive component of surface energies of PLA and TP by the Kaelble method. The dispersive component of surface energy for PLA and TP was 29.7 mN/m and 29.4 mN/m respectively and the polar component of surface energy for PLA and TP was 10.5 mN/m and 10.0 mN/m. Hence, the surface energies of PLA are not altered significantly by the inclusion of aromatic moieties in the backbone.

Electrospinning of TP

Electrospinning, introduced by Formhals in 1934,[22] allows for production of continuous fibers from micron to nanometer scale diameter. In the mid-1990s, the interest in the field was rejuvenated due to progress in the nanoscience and nanotechnology research.[23,24] Electrospinning is a versatile, flexible and easy technique compared to other nanostructure fabricating methods such as phase separation and template synthesis. The applications for nanofibers include tissue scaffolds, nanocatalysis, protective clothing, filtration and electronics.[25,26]

Electrospinning of polymer solutions was performed by the application of high voltage (15 kV) to the needle attached to capillary tube. The schematic showing the electrospinning process set-up is shown in Figure 8.1 in the experimental section. Figure 8.8 shows the SEM images of fibers electrospun from a 25% (w/v) of TP in chloroform. Image (a) and (b) shows ribbon-like fibers with a few cylindrically shaped fibers. The shape of fiber is strongly dependent on the concentration and thus viscosity of the polymer solution.[27] Concentrations lower than 20% (w/v) resulted in bead formation and breakage in the fibers. The low molecular weight of the TP required higher feed concentration to achieve a suitable viscosity for electrospinning. Images (c) and (d) shows cross-section views of electrospun fibers that were freeze fracture in liquid nitrogen. Image (c) shows the ribbon-like structure and image (d) shows the nearly cylindrical shape. The brittle fracture can be seen from the cross-section of image (c) and (d) as the cross-section is very smooth. The brittle fracture is possibly also due to very low molecular weight of TP.

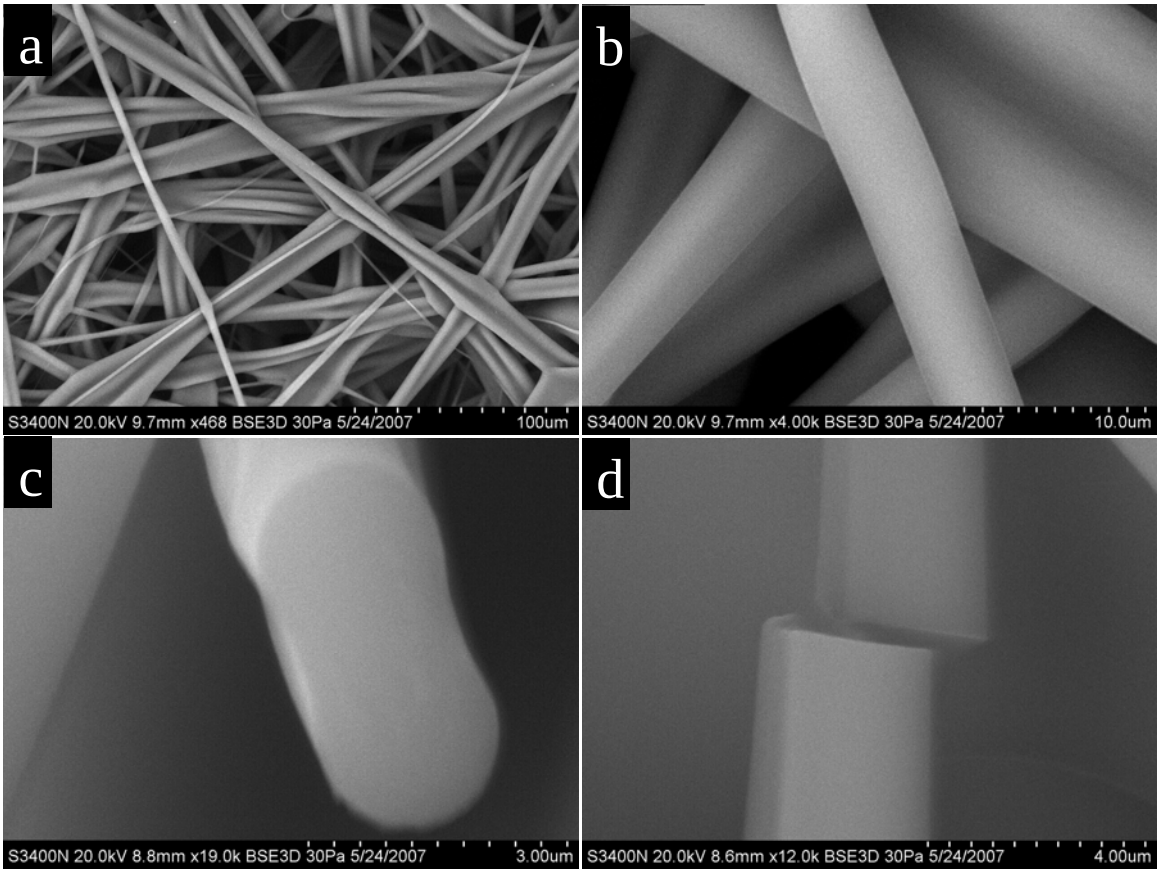

Figure 8.8. SEM images of TP fibers electrospun from $CHCl_3$. Images (a) and (b) are at different magnification and images (c) and (d) shows the cross-section of fiber after freeze fracture.

Figure 8.9 shows the SEM images of electrospun fibers from 35% (w/v) solution of TP in tetrahydrofuran (THF). Images (a), (b) and (c) shows the SEM of the fiber mat at different magnification levels and image (d) shows the cross-section of an electrospun fiber that was freeze fractured in liquid nitrogen. The fibers spun at 35% (w/v) were all cylindrical in shape with diameters ranging from 1 to 10 μm with an average diameter ca. 3 μm.

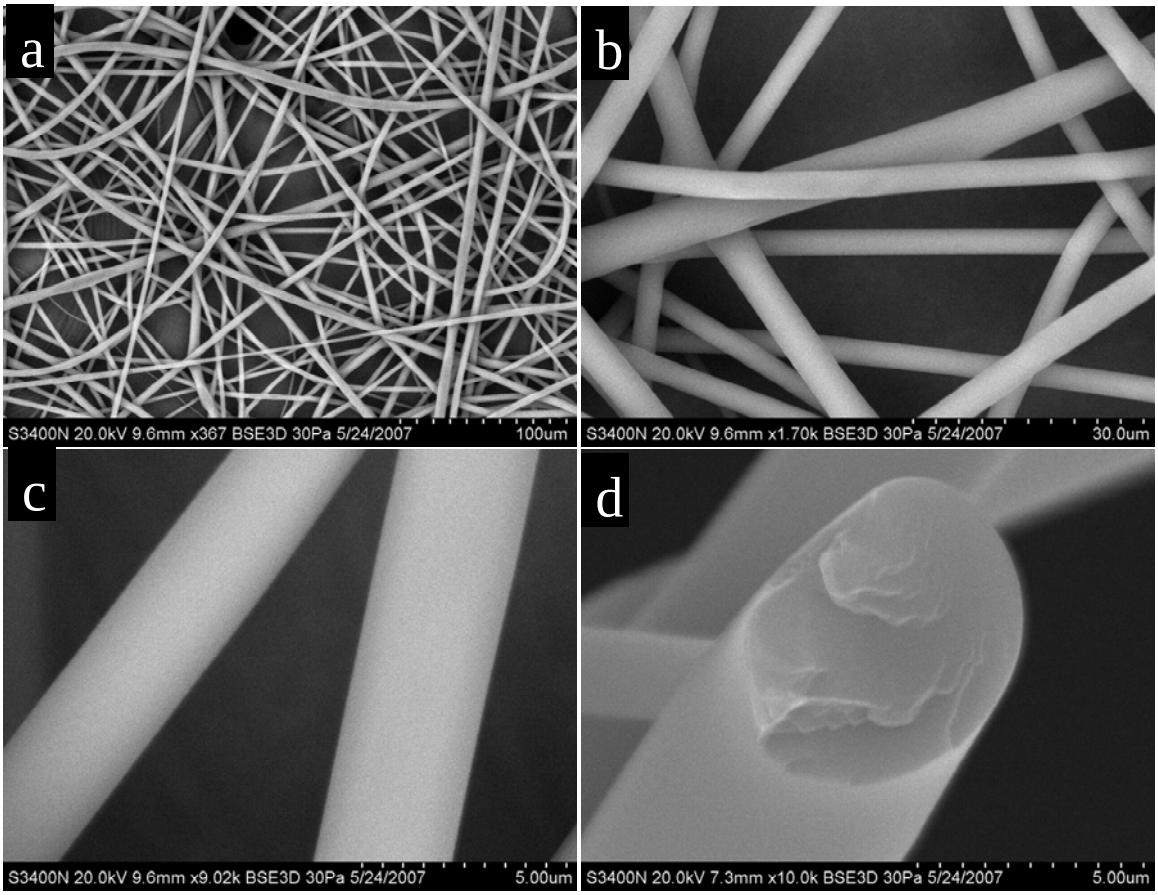

Figure 8.9. SEM images of TP fibers electrospun from THF. Images (a), (b) and (c) are at different magnification and image (d) shows the cross-section of fiber after freeze fracture.

8.4 Conclusion

The terpolymerization of lactide and bisphenol A derivatives resulted in moderate molecular weight, ca. 12 kg/mol, TP. The inclusion of aromatic moieties resulted in a significantly higher glass transition temperatures as compared to PLA homopolymer. The resultant TP also exhibited significantly higher thermal stability than PLA homopolymer. The mechanical properties of the TP were not acceptable for most commodity applications because of the moderate molecular weight. The incorporation of the co-monomers in the TP did not alter the surface energy when compared to PLA. The components and total surface energy of TP and PLA were very similar and this is indicative that no significant change occurred in the hydrophilicity and other bulk intrinsic properties of PLA. Despite the moderate molecular weight, it was possible to successfully electrospin TP from chloroform and tetrahydrofuran solutions.

8.5 References

1. Mecking, S. Nature or Petrochemistry? - Biologically Degradable Materials. *Angewandte Chemie International Edition* **43**, 1078-1085 (2004).
2. Carothers, W. H., Dorough, G. L. & van Natta, F. J. Studies of Polymerization and Ring Formation. X. The Reversible Polymerization of Six-Membered Cyclic Esters. *Journal of the American Chemical Society* **54**, 761-772 (1932).
3. Albertsson, A.-C. & Varma, I. K. Recent Developments in Ring Opening Polymerization of Lactones for Biomedical Applications. *Biomacromolecules* **4**, 1466-1486 (2003).
4. Tsuji, H. in *Biopolymers for Medical and Pharmaceutical Applications* (eds. Steinbüchel, A. & Marchessault, R. H.) 183-231 (Wiley-VCH, Weinheim, 2005).
5. Piorkowska, E., Kulinski, Z., Galeski, A. & Masirek, R. Plasticization of Semicrystalline Poly(L-lactide) with Poly(propylene glycol). *Polymer* **47**, 7178-7188 (2006).
6. Abayasinghe, N. K. & Smith, D. W., Jr. Terpolymers from Lactide and Bisphenol A Derivatives: Introducing Renewable Resource Monomers into Commodity Thermoplastics. *Macromolecules* **36**, 9681-9683 (2003).
7. O'Keefe, B. J., Monnier, S. M., Hillmyer, M. A. & Tolman, W. B. Rapid and Controlled Polymerization of Lactide by Structurally Characterized Ferric Alkoxides. *Journal of the American Chemical Society* **123**, 339-340 (2001).
8. Tsuji, H. & Fukui, I. Enhanced Thermal Stability of Poly(lactide)s in the Melt by Enantiomeric Polymer Blending. *Polymer* **44**, 2891-2896 (2003).

9. Park, P. I. P. & Jonnalagadda, S. Predictors of Glass Transition in the Biodegradable Polylactide and Poly(lactide-*co*-glycolide) Polymers. *Journal of Applied Polymer Science* **100**, 1983-1987 (2006).

10. Chen, B.-Q., Kameyama, A. & Nishikubo, T. New Polymers with Mesogens in the Side Chain and Kinked Aromatic Structures in the Main Chain from the Polyaddition of Bis(epoxide)s and Di(ester)s. *Journal of Polymer Science Part A: Polymer Chemistry* **38**, 988-998 (2000).

11. Nishikubo, T., Kameyama, A. & Kawakami, S. A Novel Synthesis of Poly(ester-*alt*-sulfide)s by the Ring-Opening Alternating Copolymerization of Oxiranes with γ-thiobutyrolactone Using Quaternary Onium Salts or Crown Ether Complexes as Catalysts. *Macromolecules* **31**, 4746-4752 (1998).

12. Abayasinghe, N. K. Renewable Resource Lactide Derived Novel Materials: Synthesis and Characterization of Fluorinated Polylactides, Epoxy Terpolymers, Oligoethylene-End-Capped-Polylactides and Poly(ester amide)s. *PhD Dissertation. Clemson University.* 1-178 (2004).

13. Fish, R. H. & Dupon, J. W. Regioselective Carbon-Oxygen Bond Cleavage Reactions of Aromatic Ethers and Esters with Potassium Metal/18-Crown-6/THF as the Electron-Transfer Reagent. *Journal of Organic Chemistry* **53**, 5230-5234 (1988).

14. Jedlinski, Z., Kurcok, P. & Kowalczuk, M. Polymerization of β-lactones Initiated by Potassium Solutions. *Macromolecules* **18**, 2679-2683 (1985).

15. Wilfong, R. E. Linear Polyesters. *Journal of Polymer Science* **54**, 385-410 (1961).

16. Sperling, L. H. *Introduction to Physical Polymer Science* (Wiley-Interscience, New York, 2001).

17. Odian, G. *Principles of Polymerization* (Wiley-Interscience, New York, 1991).

18. Fox, J., Thomas G. & Flory, P. J. Second-Order Transition Temperatures and Related Properties of Polystyrene. I. Influence of Molecular Weight. *Journal of Applied Physics* **21**, 581-591 (1950).

19. Ajroldi, G., Marchionni, G. & Pezzin, G. The Viscosity-Molecular Weight Relationships for Diolic Perfluoropolyethers. *Polymer* **40**, 4163-4164 (1999).

20. Zhang, J.-F. & Sun, X. in *Biodegradable polymers for industrial applications* (ed. Smith, R.) 251-288 (CRC Press, Washington, DC, 2005).

21. Bicerano, J. *Prediction of Polymer Properties* (Marcel Dekker, New York, 2002).

22. Formhals, A. Process and Apparatus for Preparing Artificial Threads. 1975504.United States.(1934).

23. Teo, W. E. & Ramakrishna, S. A Review on Electrospinning Design and Nanofibre Assemblies. *Nanotechnology* **17**, R89-R106 (2006).

24. Dosunmu, O. O., Chase, G. G., Kataphinan, W. & Reneker, D. H. Electrospinning of Polymer Nanofibres from Multiple Jets on a Porous Tubular Surface. *Nanotechnology* **17**, 1123-1127 (2006).

25. Wang, Y. K., Yong, T. & Ramakrishna, S. Nanofibres and their Influence on Cells for Tissue Regeneration. *Australian Journal of Chemistry* **58**, 704-712 (2005).

26. Li, W.-J., Laurencin, C. T., Caterson, E. J., Tuan, R. S. & Ko, F. K. Electrospun Nanofibrous Structure: A Novel Scaffold for Tissue Engineering. *Journal of Biomedical Materials Research* **60**, 613-621 (2002).

27. Jaeger, R., Schonherr, H. & Vancso, G. J. Chain Packing in Electro-Spun Poly(ethylene oxide) Visualized by Atomic Force Microscopy. *Macromolecules* **29**, 7634-7636 (1996).

CHAPTER 9

SUMMARY AND CONCLUSIONS

9.1 Summary

In this research, the goal of improving the properties of polylactide (PLA) was successfully achieved by modifying the surface, thermal, and crystallization properties. The novel polymers were processed into commodity item such as melt and electrospun fibers.

High molecular weight poly(L-lactide) (PLA) homopolymer was synthesized by ring-opening polymerization (ROP) of L-lactide using $Sn(Oct)_2$ as the catalyst. The low surface energy polylactide-perfluoropolyether-polylactide (FluoroPLAs) block copolymers were synthesized by ROP of L-lactide using $Sn(Oct)_2$ as the catalyst and perfluoropolyether (PFPE) as the macro-initiator.

Incorporation of flexible PFPE linkages with low glass transition temperatures (Tg) into PLA backbone, lowered the Tg of PLA. As a result, FluoroPLAs showed lower Tg in comparison to homopolymer PLA. Similar to the decrease in Tg, the crystallization temperature (Tc), the melting temperature (Tm), and the degradation temperature (Td) of PLA dropped upon copolymerization with PFPE and the extent of decrease was proportional to the molar content of PFPE. The low surface energy PFPE altered the surface properties of PLA and the surface energy of PLA dropped from 35-40 mN/m to 16-20 mN/m.

The crystallization rate and overall crystallinity increased upon copolymerization and FluoroPLA5(1.5k) exhibited the highest heat of fusion. Annealing processes enhanced the crystallinity of FluoroPLAs and saturation in heats of fusion were attained faster than for PLA.

The hydrolytic stability of PLA and FluoroPLAs were studied in acidic, alkaline, and, neutral media. The weight loss in acid and neutral media, showed an induction period for both PLA and FluoroPLAs whereas in alkaline medium, PLA showed almost linear weight loss with hydrolysis time whereas FLuoroPLAs showed resistance to weight loss initially possibly because of their hydrophobic nature. However, PLA and FluoroPLAs films were completely disintegrated in alkaline solution by the 4th week. No significant weight loss for PLA and FluoroPLAs films were noted in acidic and neutral medium until 4th week. The trend of loss in the molecular weight is similar for PLA and FluoroPLAs. The melting temperature and the heat of fusion of both polymers were affected upon degradation. The polymer chains in the amorphous region are cleaved faster and thus the amorphous phase is consumed faster than the crystalline phase. Hence the heat of fusion and sample crystallinity increases and attains saturation. The chain cleavage generates more chain ends and increasing chain ends in crystalline phase act as impurity and hence the melting temperature decreases with degradation time.

Melt fiber spinning was successfully performed with PLA and FluoroPLAs polymers. As-spun fibers with diameter of ca. 30 μm were produced. The FluoroPLAs as-spun fibers have very high elongation-at-break compared to those of PLA as-spun fibers without any detrimental effect on the tensile strength.

Successful terpolymerization of bisphenol A derivatives with lactides resulted in a terpolymer with number average molecular weight of ca. 12 kg/mol. Terpolymer was completely amorphous as no melting peak was observed in differential scanning calorimetry thermograms. Increased glass transition findings were supported by the dynamic mechanical analysis of terpolymer. The surface energy of terpolymer was found to be very similar to that

of PLA. However, the atomic force microscopy data clearly indicated a difference in surface morphology. Successful electrospinning of terpolymer resulted in micro-level fibers with potential for high temperature applications.

9.2 Conclusions

Molar concentrations of the initiator affected the resultant molecular weight of polymers and hence, the homopolymer PLA mol. wt. was 144 kg/mol and the copolymers, FluoroPLAs, were between 93 kD to 68 kD depending on the molar concentration of PFPE. The extent of decrease in glass transition temperature of FluoroPLAs was found to be proportional to the molar content of PFPE. The Tg of PLA decreased from ca. 61 °C to ca. 50 °C with the incorporation of 4.6 x 10^{-3} mole of PFPE (2000 g/mol). The molar content of PFPE did not affect the surface energy of copolymer as there was no significant difference among the surface energies of three FluoroPLAs. FluoroPLAs showed better hydrophobic and lipophobic properties than PLA. High density and low surface energy PFPE acts as nucleating agents for the PLA chains, hence, FluoroPLAs possess enhanced overall crystallinity. The crystallization half times ($t_{1/2}$) for FluoroPLAs were shorter than that for PLA below 110 °C which would make FluoroPLAs a more processable commodity polymer. Higher crystallinity and hydrophobic FluoroPLAs show better resistance to degradation in all the environments even though PLA has the highest molecular weight. However, FluoroPLA(4.2k) shows lower stability amongst the PLA and FluoroPLAs and this is because it has lower molecular weight compared to PLA and it also has lower crystallinity compared to the other two FluoroPLAs. FluoroPLA polymer could be seen as a potential resin for fiber in filtration and waterproof clothing applications. Incorporation of rigid monomers (diglycidyl ether of bisphenol A and 4,4'-(hexafluoroisopropylidene)diphenol) in PLA backbone increased the glass transition temperature of terpolymer (T_g ca. 100 °C) significantly.

CHAPTER 10

RECOMMENDATIONS FOR FUTURE WORK

In addition to the findings reported in this dissertation, the following investigations are recommended to further enhance the potential of PLA as commodity polymer:

- Incorporation of low surface energy PFPE in the PLA backbone decreases the surface energy of the copolymer, FluoroPLA. Further investigation should be carried out to characterize the influence of molar content of PFPE in lowering the surface energy of FluoroPLA.
- The nucleating action of PFPE improved the crystallization rate and overall crystallinity (based on heat of fusion) of FluoroPLA. Thorough investigation should be carried out to explore the nucleation mechanism and also the effect of molar content and block length effects of PFPE on its nucleating action.
- As-spun FluoroPLA fibers have higher elongation-at-break in comparison to the as-spun PLA fibers. The tensile properties of fully drawn PLA and FluoroPLA fibers should be compared.
- Terpolymers of lactide and bisphenol A derivatives have high glass transition temperature. The molecular weight of these high glass transition terpolymers must be improved to enhance their mechanical properties.
- The biodegradation and hydrolytic stability of high glass transition terpolymers should be investigated.

APPENDICES

Appendix A

^{19}F NMR Spectra

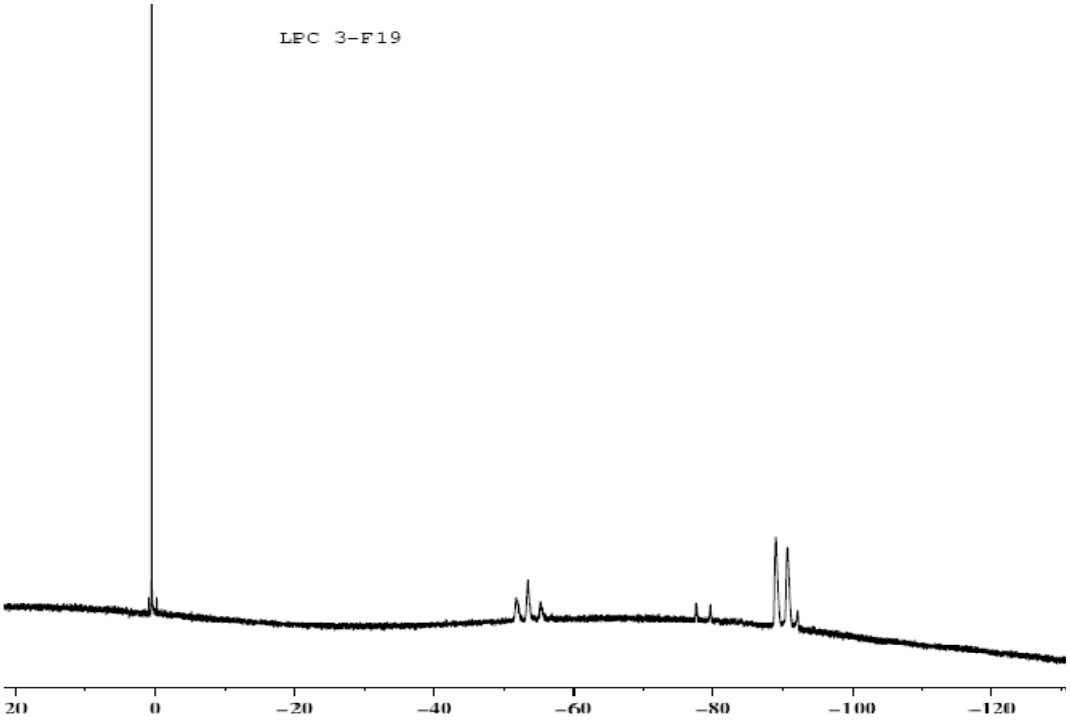

Figure A.1. ^{19}F NMR spectrum of FluoroPLA5(2.0k).

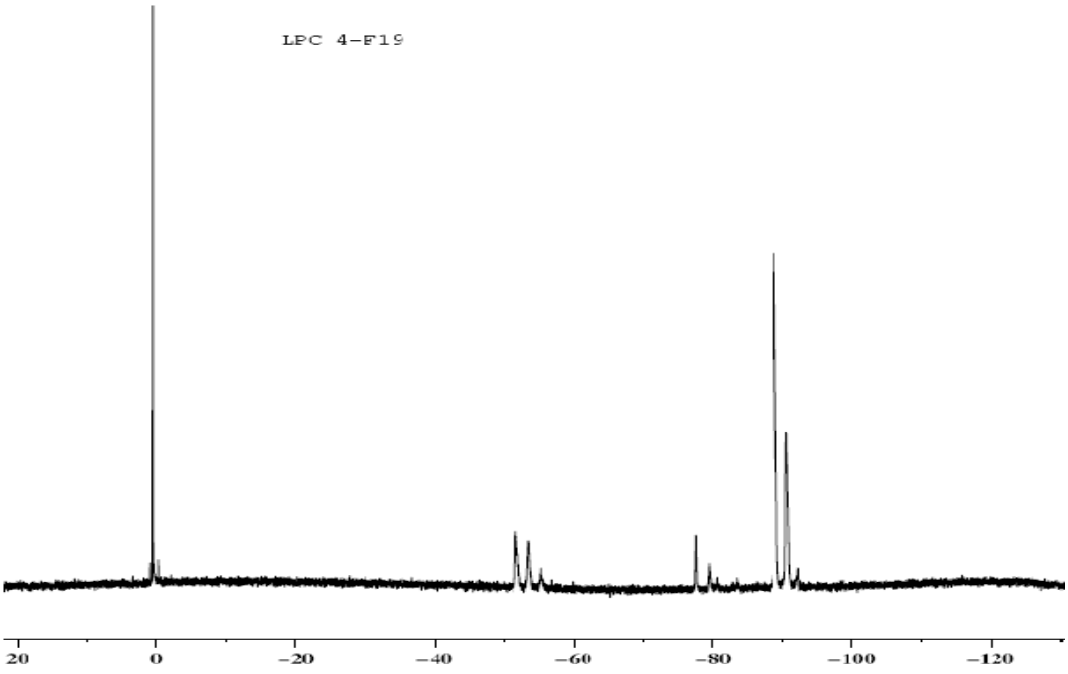

Figure A.2. ^{19}F NMR spectrum of FluoroPLA5(1.5k).

Appendix B

Gel Permeation Chromatography Standards and Their Chromatograph.

Table B.1. Polystyrene standards used for gel permeation chromatography data. Elution time and mol. wt.

	Elution Volume (ml)	Mol Wt (Daltons)	Log Mol Wt	Calculated Weight (Daltons)	% Residual	Ignore Point	Manual Point	Standard Type
1	12.796	990500	5.995854	883065	12.166	☐	☐	Narrow
2	13.082	600000	5.778151	611431	-1.870	☐	☐	Narrow
3	13.326	400000	5.602060	451151	-11.338	☐	☐	Narrow
4	14.010	200000	5.301030	201895	-0.939	☐	☐	Narrow
5	14.499	111500	5.047275	117838	-5.379	☐	☐	Narrow
6	15.384	50000	4.698970	47297	5.714	☐	☐	Narrow
7	16.405	20000	4.301030	17550	13.960	☐	☐	Narrow
8	17.835	4000	3.602060	4504	-11.200	☐	☐	Narrow
9	20.091	436	2.639486	427	2.188	☐	☐	Narrow

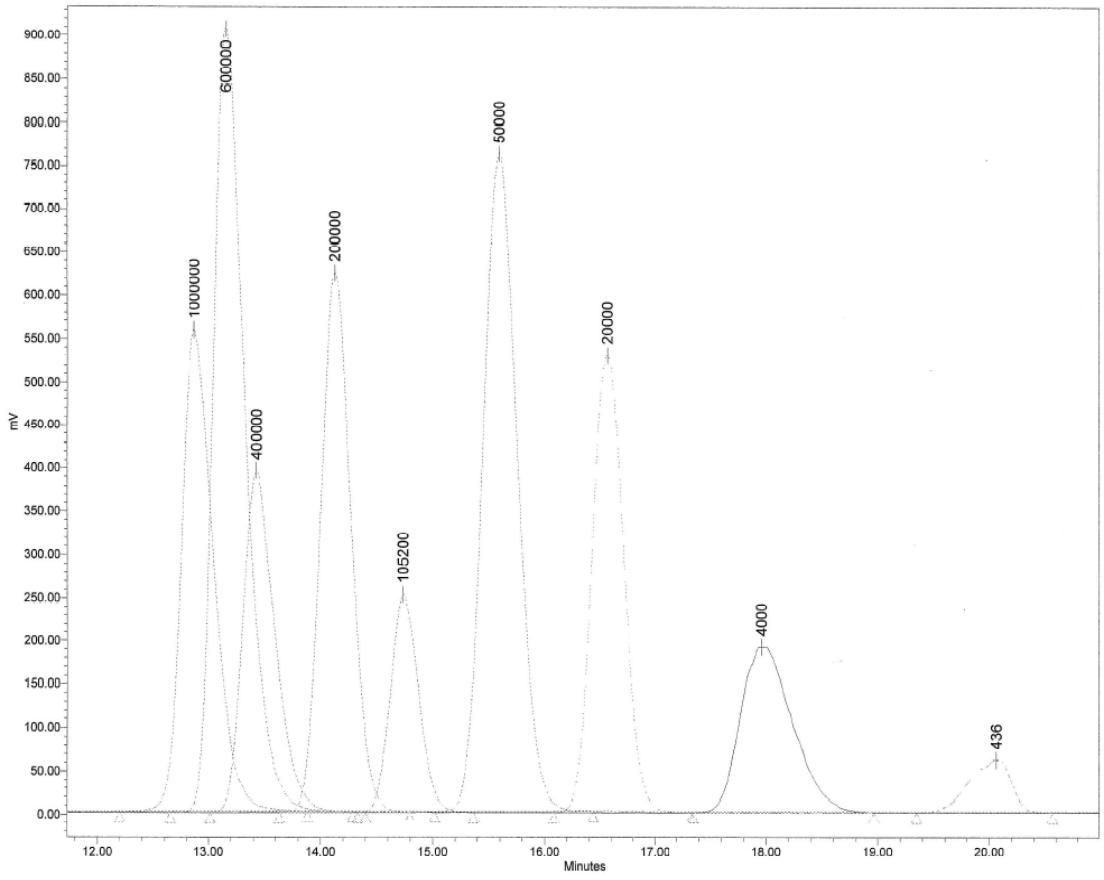

Figure B.1. Overlay of chromatograms of polystyrene standards.

Appendix C

Cole-Cole Plot of PLA and FluoroPLAs

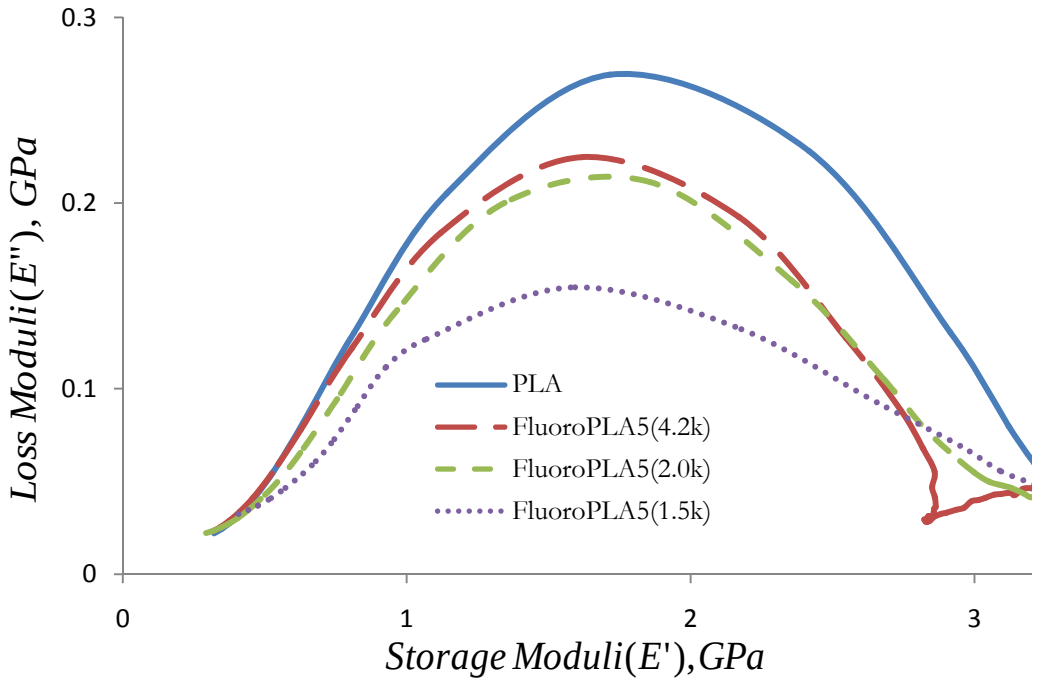

Figure C.1. Cole-Cole plot for PLA and FluoroPLAs through glass transition region.

Appendix D

Rheological Properties and Contact Angles of PLA and FluoroPLAs

The processability of thermoplastic polyesters are inconvenient due to the low crystallization rate and also due to the higher processing temperatures. The processing temperature is usually determined by the rheological properties of the materials and thus it is critical to study these properties. The PLA and FluoroPLA samples were subjected to steady shear rate sweep tests from 0.1 s^{-1} to 100 s^{-1} at 180 °C. The shear-thinning behavior of PLA and FluoroPLAs are shown in Figure D.1. The shear viscosity, at a shear rate of 0.1/s, for PLA (~460 Pa.s) is much higher than any of the FluoroPLAs (>100 Pa.s). This difference in the behavior of PLA and FluoroPLAs is due to the differences in their melting phenomenon. The low melting FluoroPLAs have lower shear viscosities. In addition, the molecular weight difference can not be neglected. Hence, FluoroPLAs are better processable materials compared to PLA and can be easily molded into articles.

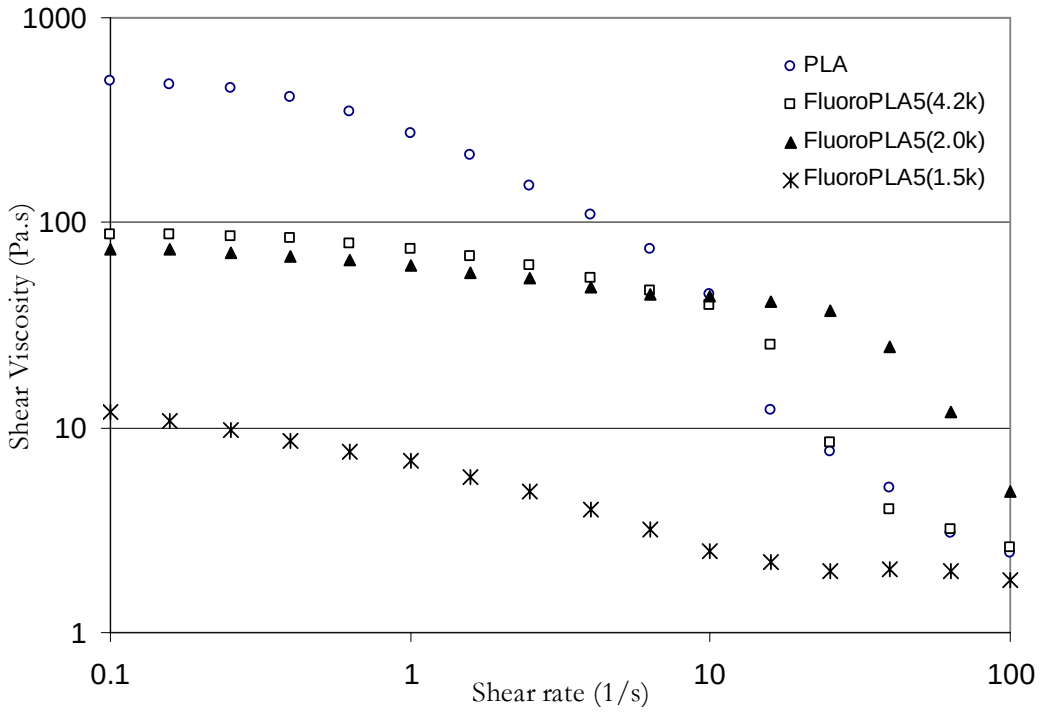

Figure D.1. Shear-thinning of PLA and FluoroPLAs at 180 °C by steady shear rate sweep test using the cone-and-plate rheometer.

Table D.1. Contact angles of water, glycerol, formamaide, methylene iodide, and n-hexadecane on PLA and FluoroPLAs.

Polymer	Liquid	Θ_1	Θ_2	Θ_3	AVERAGE	Std Dev.
PLA	Water	74.8	73.6	74.4	74.3	0.6
	Glycerol	69.3	72.8	69.7	70.6	1.9
	Formamide	59.5	58.6	60	59.4	0.7
	Methylene Iodide	39.9	40.2	39.6	39.9	0.3
	n-Hexadecane	24.3	23.2	20.4	22.6	2.0
FluoroPLA5(4.2k)	Water	104.7	103.9	103.9	104.2	0.5
	Glycerol	94.4	99.1	95.2	96.2	2.5
	Formamide	88.2	89.2	91.5	89.6	1.7
	Methylene Iodide	73.5	74	73.5	73.7	0.3
	n-Hexadecane	59.5	56.7	60.3	58.8	1.9
FluoroPLA5(2.0k)	Water	104.4	103.6	104.3	104.1	0.4
	Glycerol	98	99.6	99.9	99.2	1.0
	Formamide	94	93.7	94.6	94.1	0.5
	Methylene Iodide	76.4	78.3	77.9	77.5	1.0
	n-Hexadecane	60.2	60.4	55.7	58.8	2.7
FluoroPLA5(1.5k)	Water	105.2	104.6	104.3	104.7	0.5
	Glycerol	101.5	100.7	101.3	101.2	0.4
	Formamide	93.1	92.3	94.5	93.3	1.1
	Methylene Iodide	76.5	74.9	75.9	75.8	0.8
	n-Hexadecane	55.9	62.2	63.7	60.6	4.1

Appendix E

Surface Energy by Rabel Method

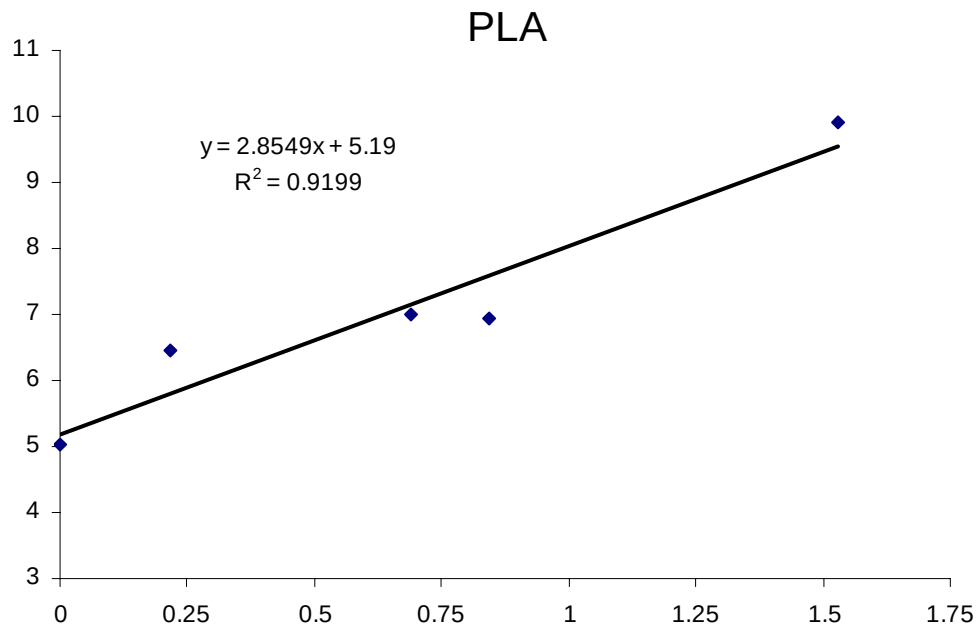

Figure E.1. Plot of $\frac{1+Cos\theta}{2}\frac{\gamma_l}{\sqrt{\gamma_l^d}}$ vs $\sqrt{\frac{\gamma_l^p}{\gamma_l^d}}$ for PLA.

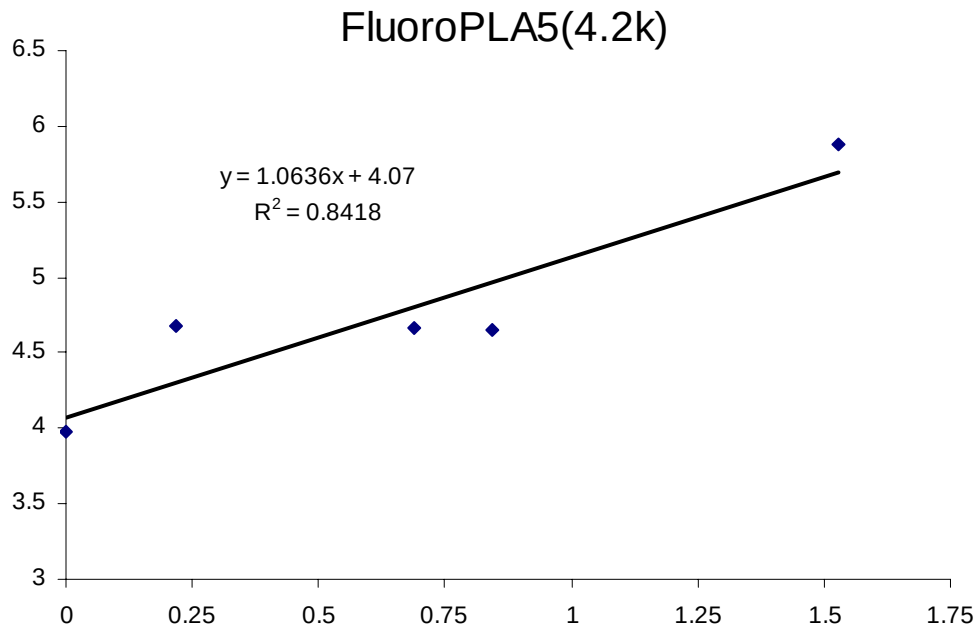

Figure E.2. Plot of $\frac{1+Cos\theta}{2}\frac{\gamma_l}{\sqrt{\gamma_l^d}}$ vs $\sqrt{\frac{\gamma_l^p}{\gamma_l^d}}$ for FluoroPLA5(4.2k).

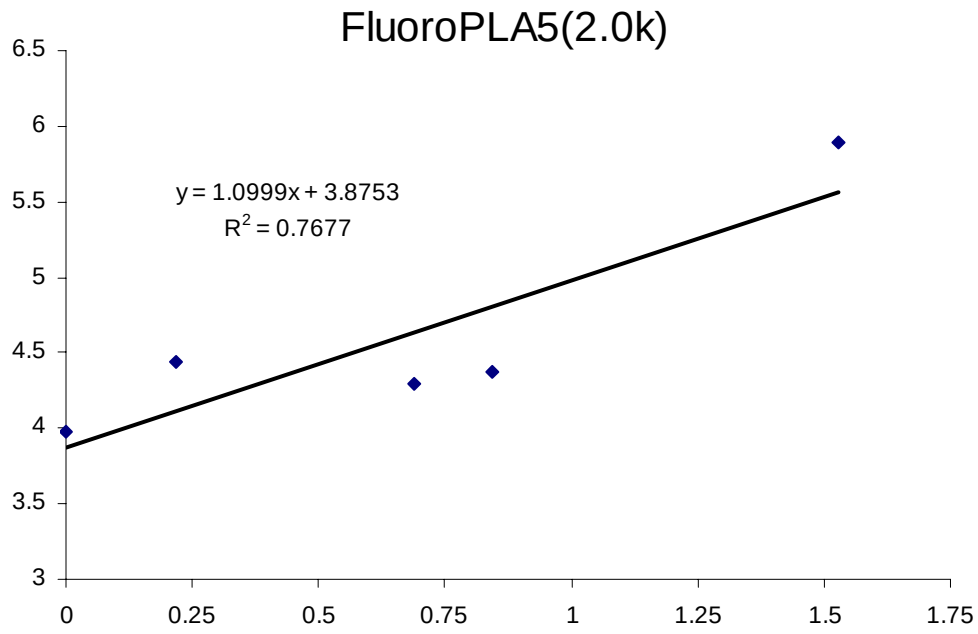

Figure E.3. Plot of $\frac{1+Cos\theta}{2}\frac{\gamma_l}{\sqrt{\gamma_l^d}}$ vs $\sqrt{\frac{\gamma_l^p}{\gamma_l^d}}$ for FluoroPLA5(2.0k).

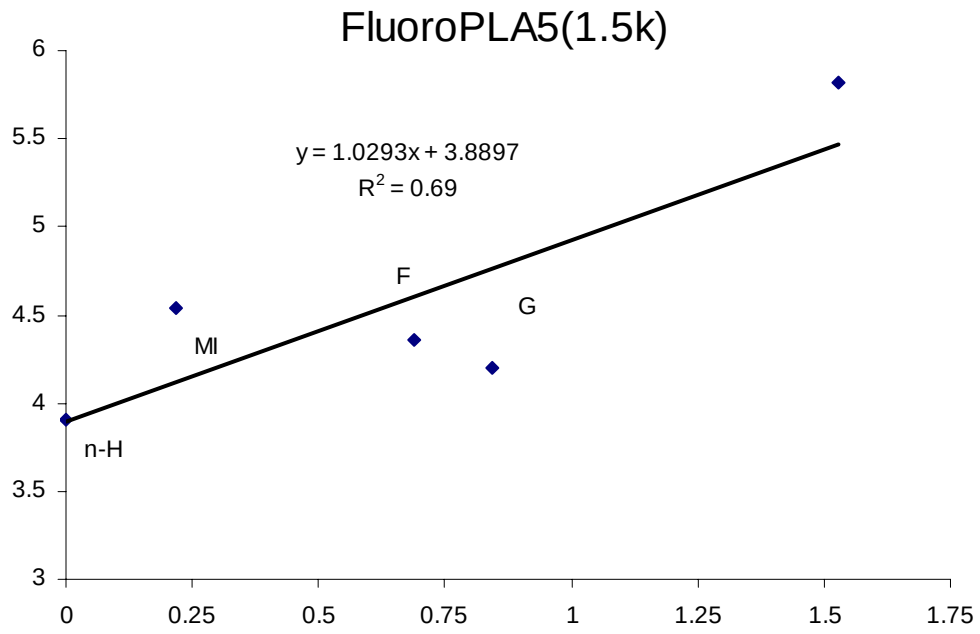

Figure E.4. Plot of $\frac{1+Cos\theta}{2}\frac{\gamma_l}{\sqrt{\gamma_l^d}}$ vs $\sqrt{\frac{\gamma_l^p}{\gamma_l^d}}$ for .FluoroPLA5(1.5k).

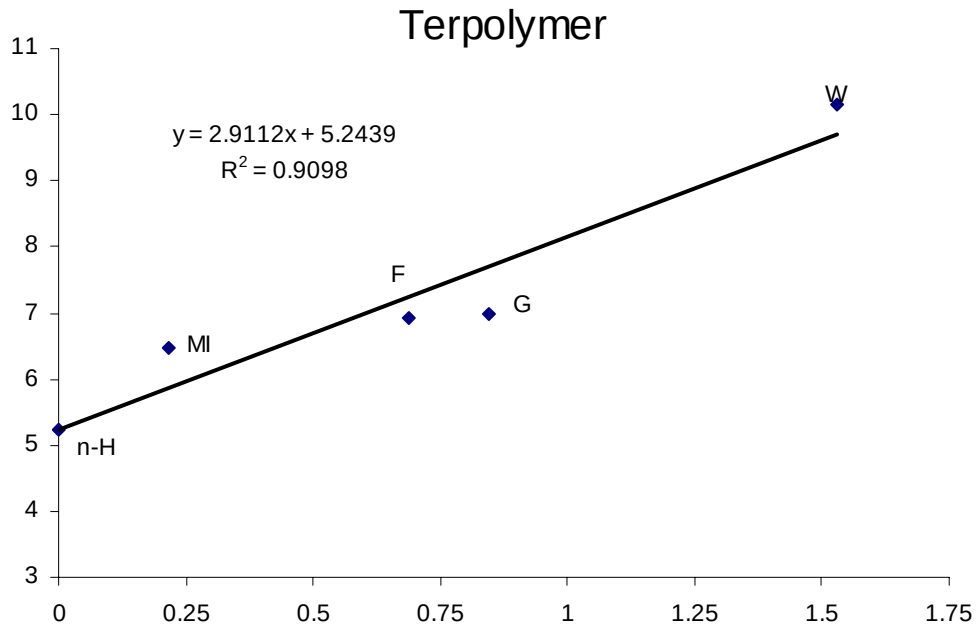

Figure E.5. Plot of $\frac{1+Cos\theta}{2}\frac{\gamma_l}{\sqrt{\gamma_l^d}}$ vs $\sqrt{\frac{\gamma_l^p}{\gamma_l^d}}$ for L-lactide and bispenol A derivatives terpolymer.

Appendix F

Surface Energy by Kaelble Method

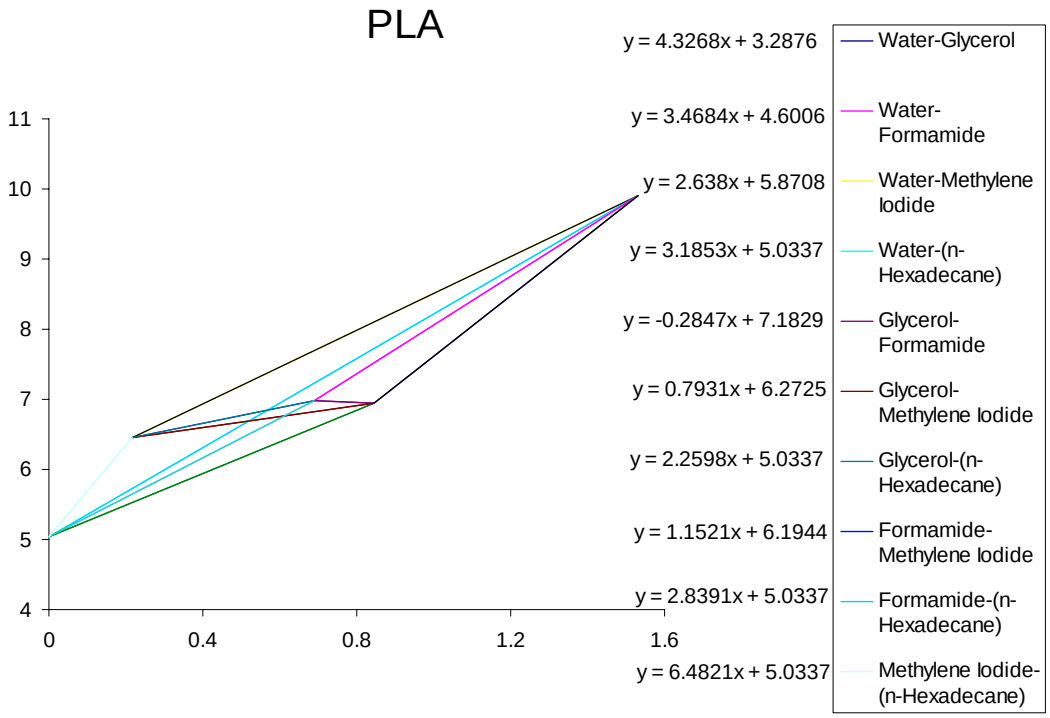

Figure F.1. Plot of $\frac{1+Cos\theta}{2}\frac{\gamma_l}{\sqrt{\gamma_l^d}}$ vs $\sqrt{\frac{\gamma_l^p}{\gamma_l^d}}$ for PLA.

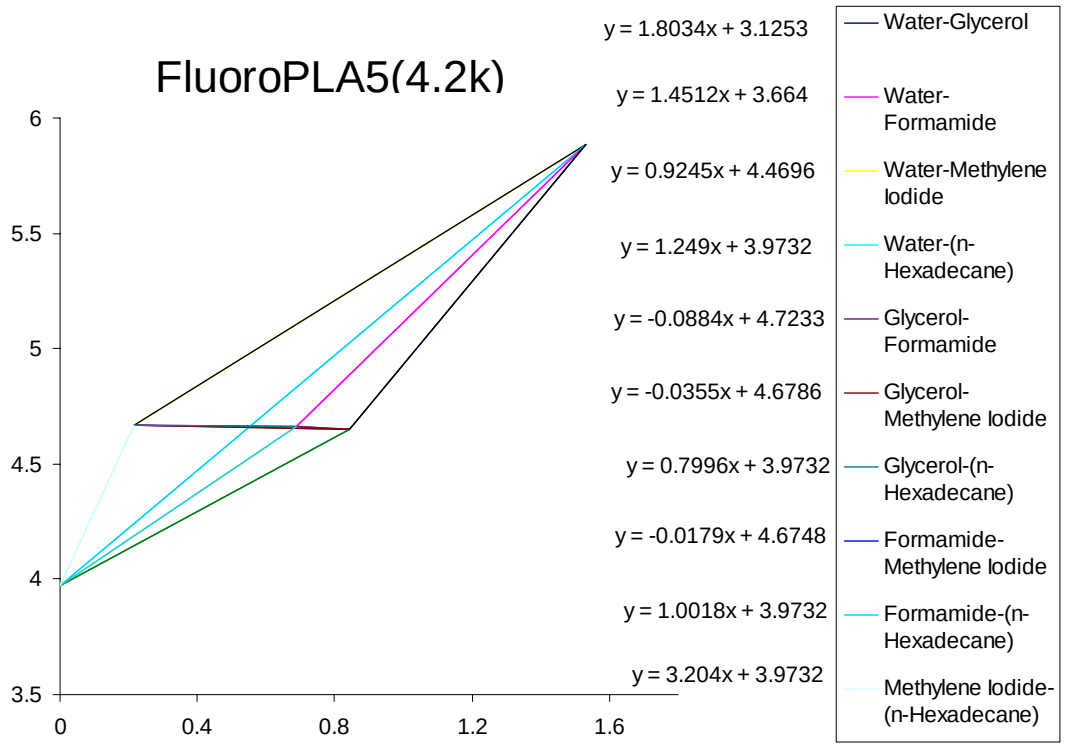

Figure F.2. Plot of $\frac{1+Cos\theta}{2}\frac{\gamma_l}{\sqrt{\gamma_l^d}}$ vs $\sqrt{\frac{\gamma_l^p}{\gamma_l^d}}$ for FluoroPLA5(4.2k).

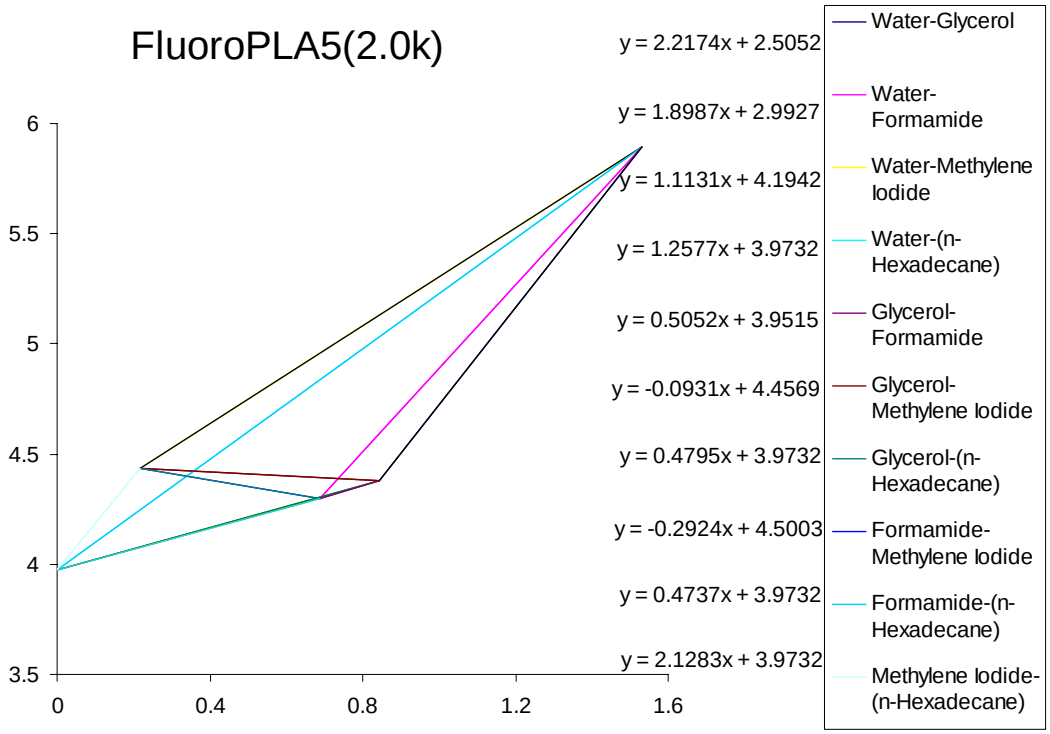

Figure F.3. Plot of $\frac{1+Cos\theta}{2}\frac{\gamma_l}{\sqrt{\gamma_l^d}}$ vs $\sqrt{\frac{\gamma_l^p}{\gamma_l^d}}$ for FluoroPLA5(2.0k).

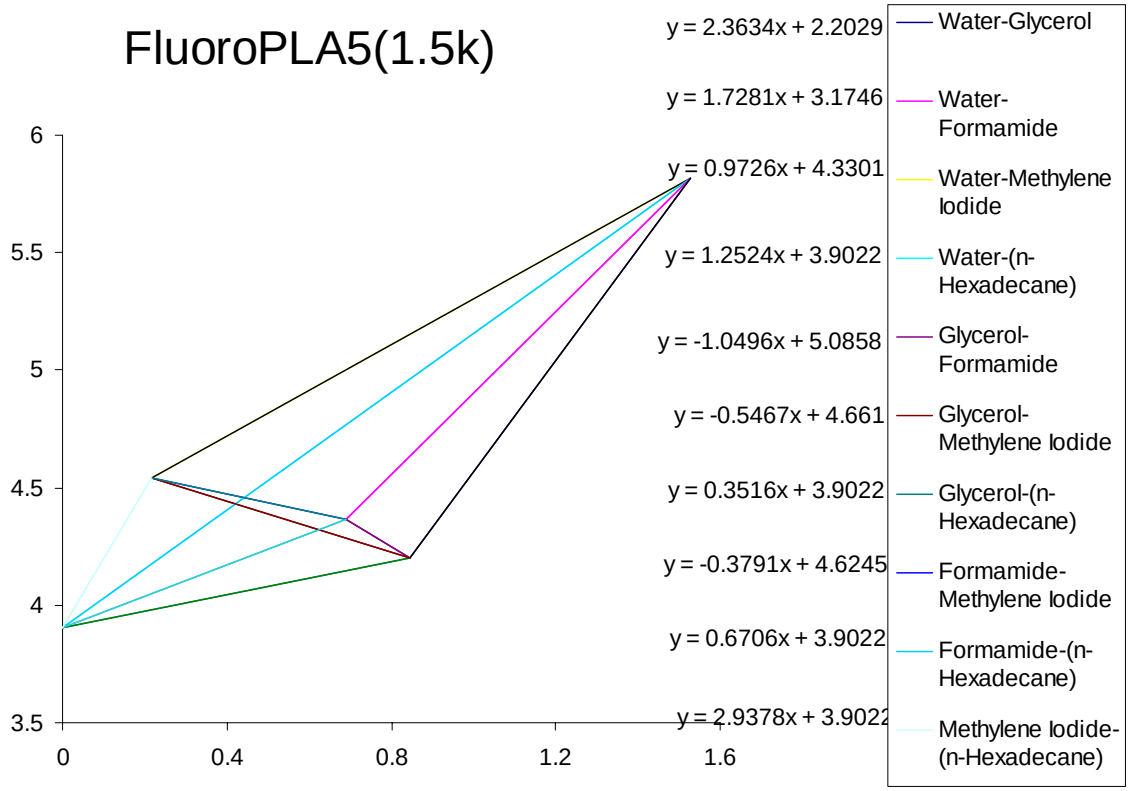

Figure F.4. Plot of $\frac{1+Cos\theta}{2}\frac{\gamma_l}{\sqrt{\gamma_l^d}}$ vs $\sqrt{\frac{\gamma_l^p}{\gamma_l^d}}$ for .FluoroPLA5(1.5k).

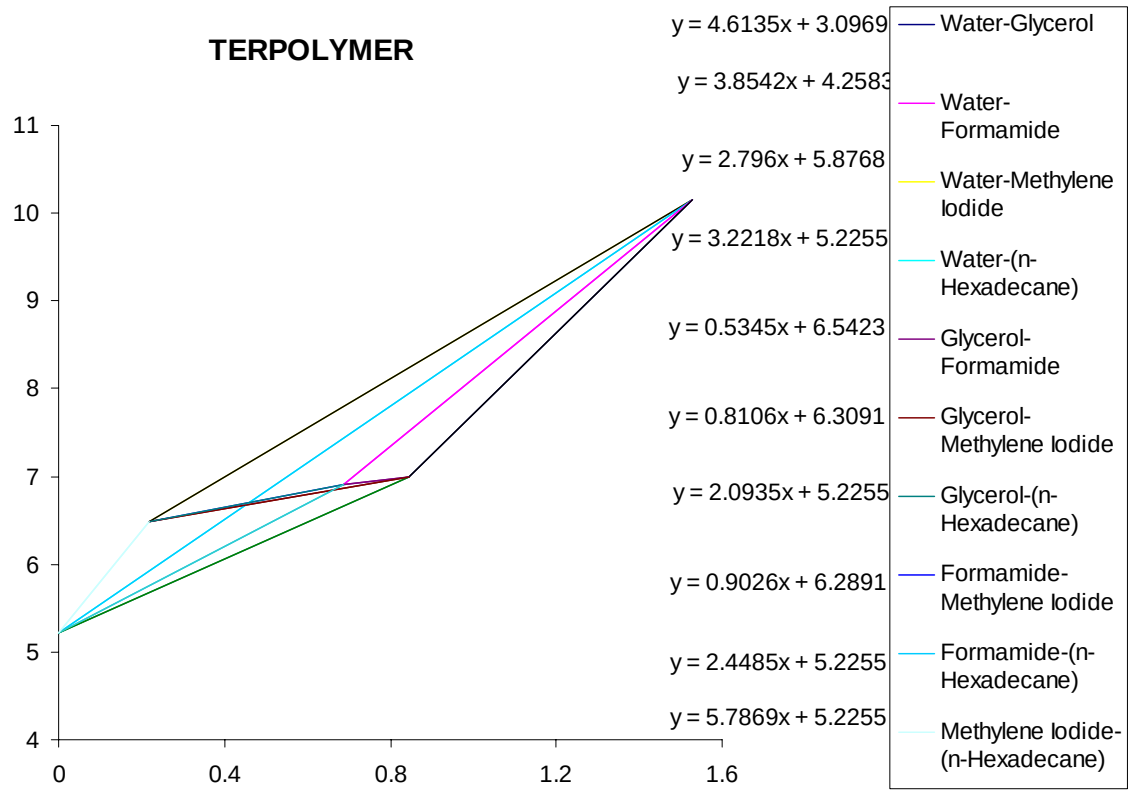

Figure F.5. Plot of $\frac{1+Cos\theta}{2}\frac{\gamma_l}{\sqrt{\gamma_l^d}}$ vs $\sqrt{\frac{\gamma_l^p}{\gamma_l^d}}$ for L-lactide and bispenol-A derivatives terpolymer.

Appendix G

X-ray Diffraction Data for PLA and FluoroPLAs

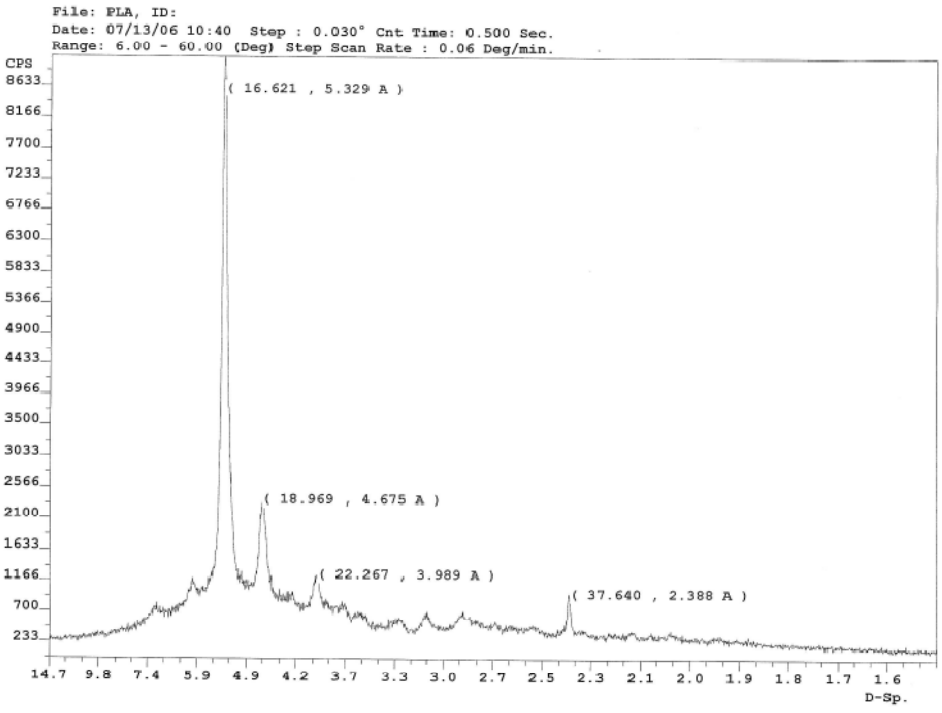

Figure G.1. Wide angle x-ray diffraction spectrum of annealed PLA films.

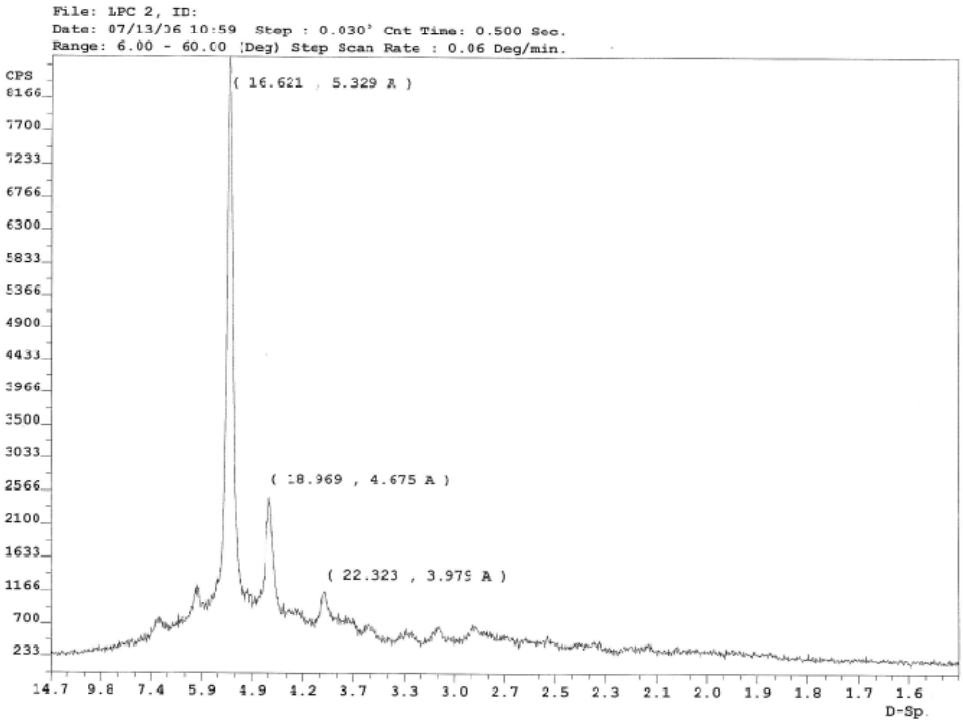

Figure G.2. Wide angle x-ray diffraction spectrum of annealed FluoroPLA5(4.2k) films.

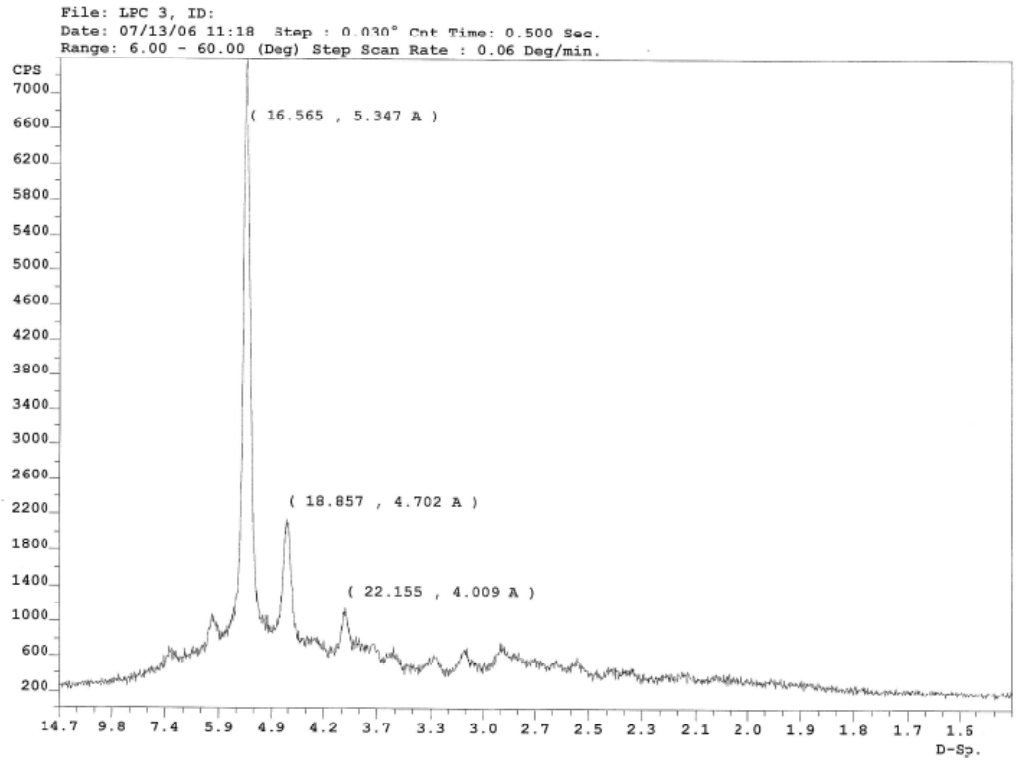

Figure G.3. Wide angle x-ray diffraction spectrum of annealed FluoroPLA5(2.0k) films.

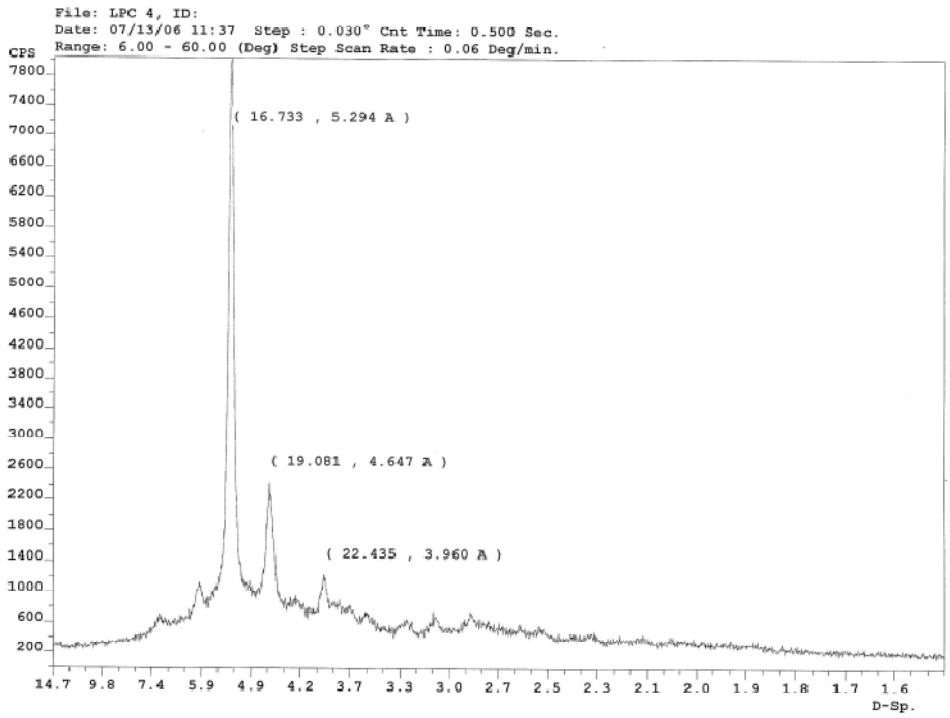

Figure G.4. Wide angle x-ray diffraction spectrum of annealed FluoroPLA5(1.5k) films.

Appendix H

Transmission Electron Microscopy (TEM) for PLA and FluoroPLA5(1.5k).

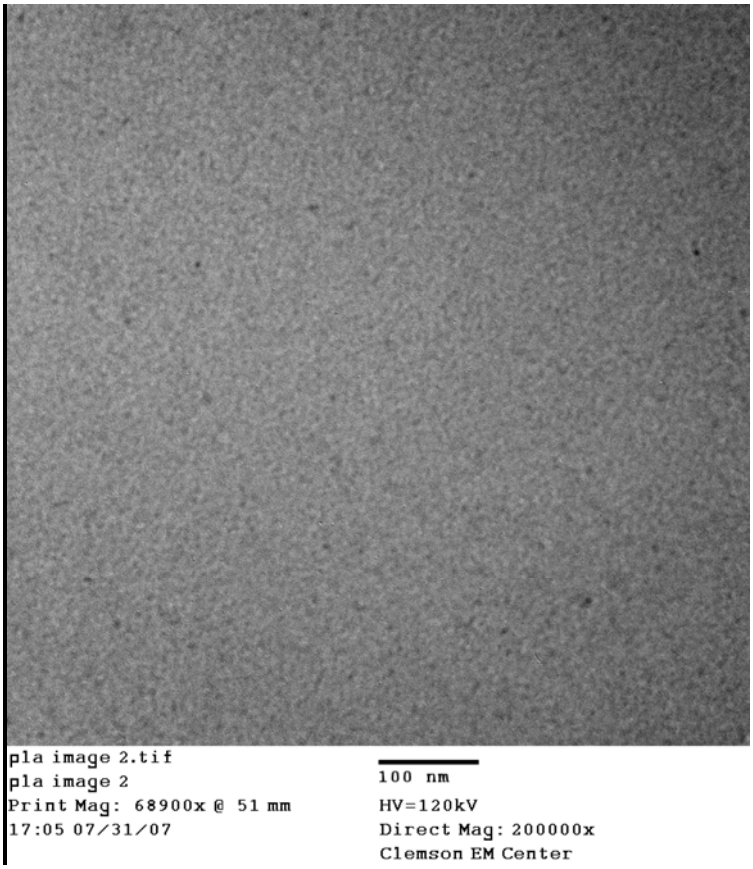

Figure H.1. TEM image of PLA.

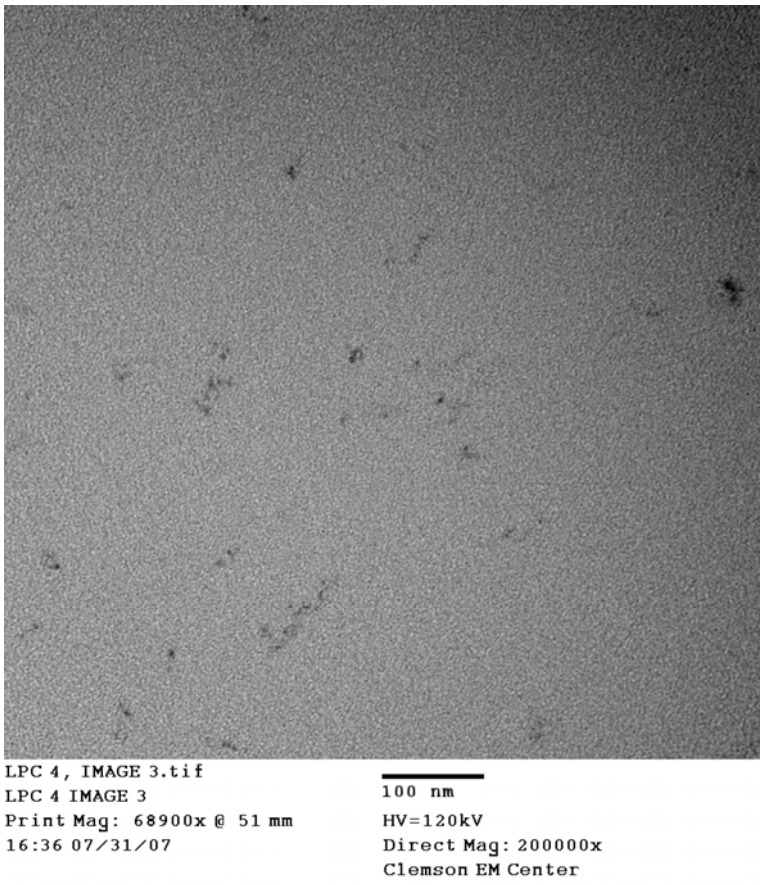

Figure H.2. TEM image of FluoroPLA5(1.5k).

Appendix I

Spherulitic Growth Rates of PLA and FluoroPLAs

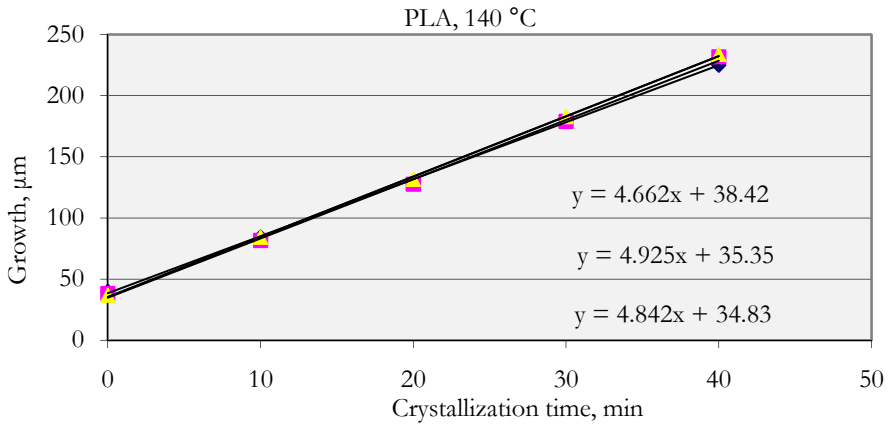

Figure I.1. Diameter of PLA spherulites as a function of crystallization time at 140 °C.

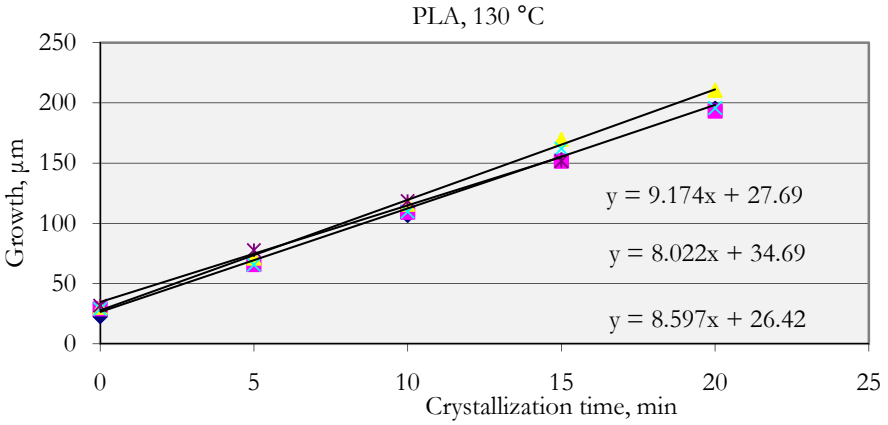

Figure I.2. Diameter of PLA spherulites as a function of crystallization time at 130 °C.

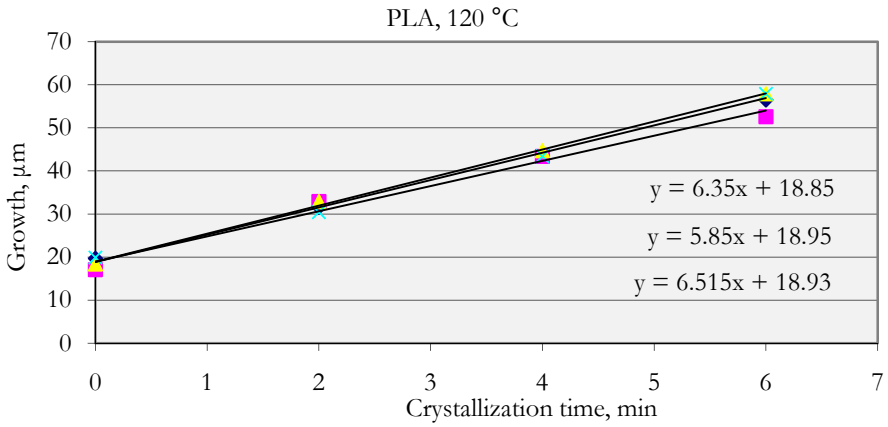

Figure I.3. Diameter of PLA spherulites as a function of crystallization time at 120 °C.

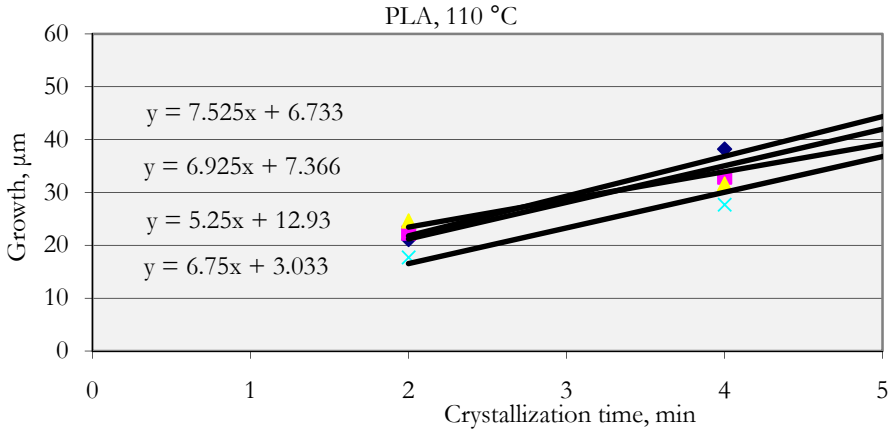

Figure I.4. Diameter of PLA spherulites as a function of crystallization time at 110 °C.

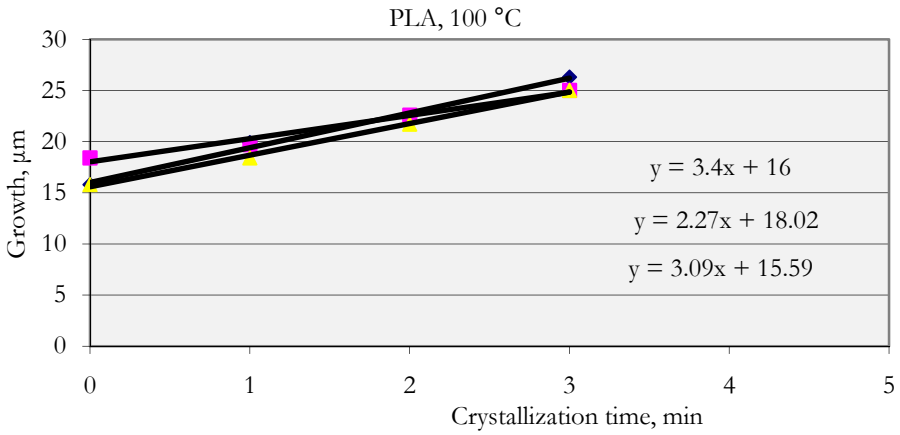

Figure I.5. Diameter of PLA spherulites as a function of crystallization time at 100 °C.

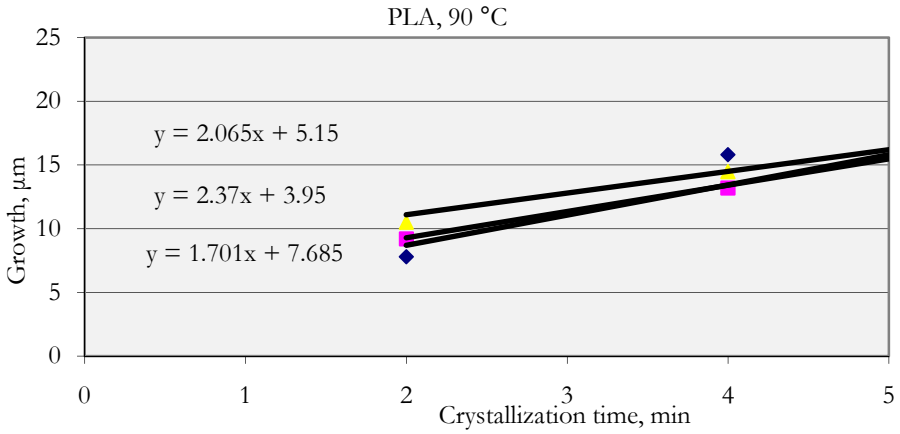

Figure I.6. Diameter of PLA spherulites as a function of crystallization time at 90 °C.

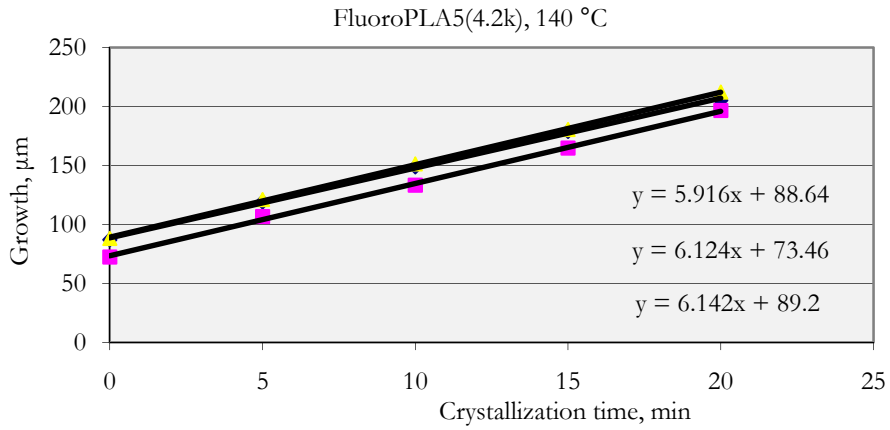

Figure I.7. Diameter of FluoroPLA5(4.2k) spherulites as a function of crystallization time at 140 °C.

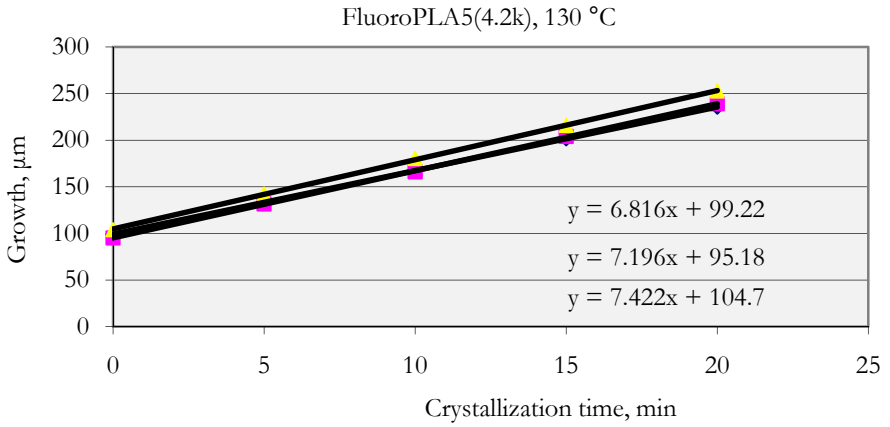

Figure I.8. Diameter of FluoroPLA5(4.2k) spherulites as a function of crystallization time at 130 °C.

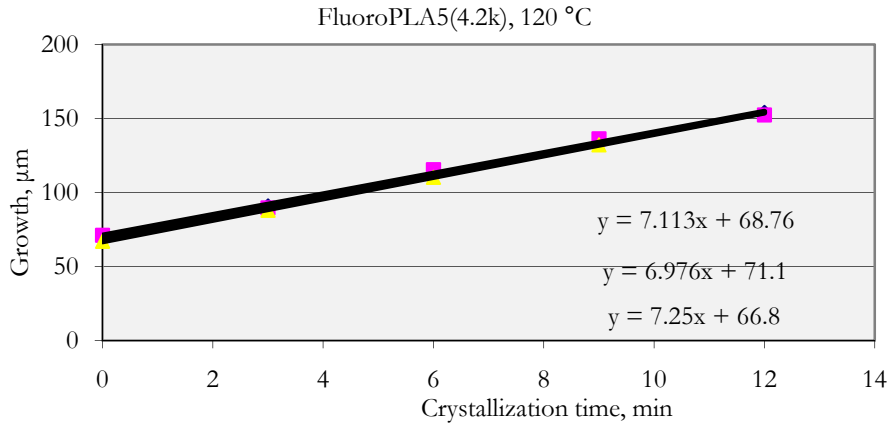

Figure I.9. Diameter of FluoroPLA5(4.2k) spherulites as a function of crystallization time at 120 °C.

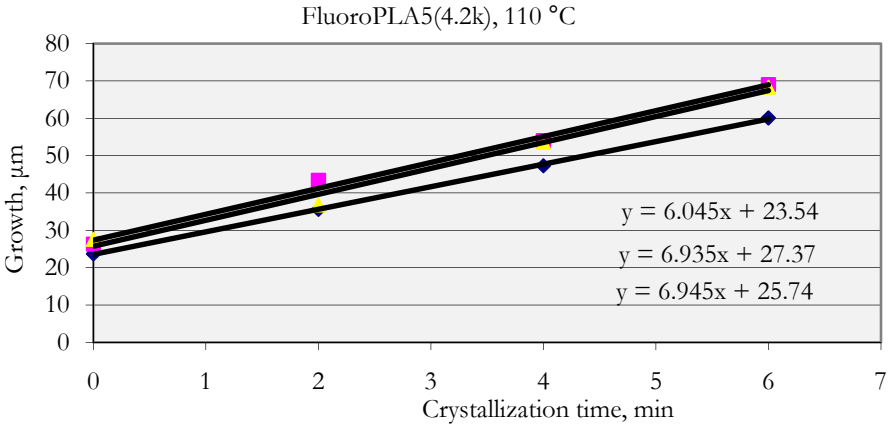

Figure I.10. Diameter of FluoroPLA5(4.2k) spherulites as a function of crystallization time at 110 °C.

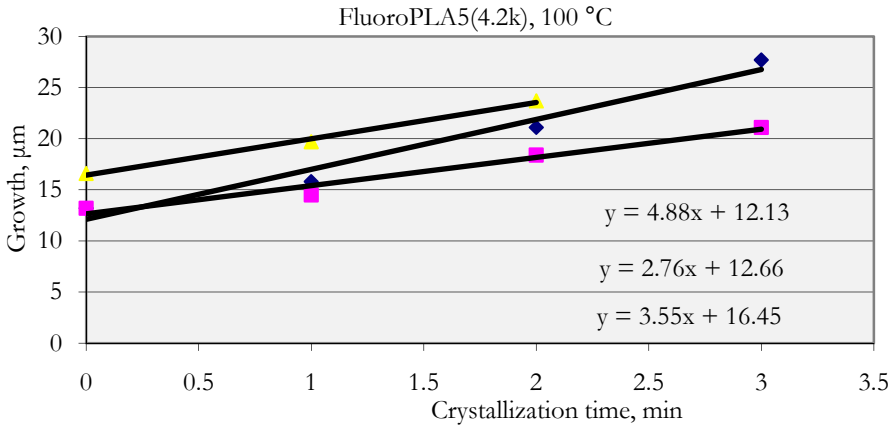

Figure I.11. Diameter of FluoroPLA5(4.2k) spherulites as a function of crystallization time at 100 °C.

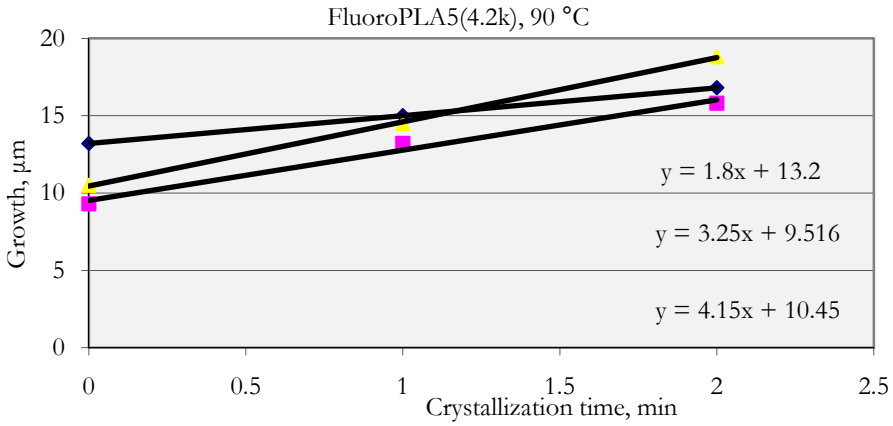

Figure I.12. Diameter of FluoroPLA5(4.2k) spherulites as a function of crystallization time at 90 °C.

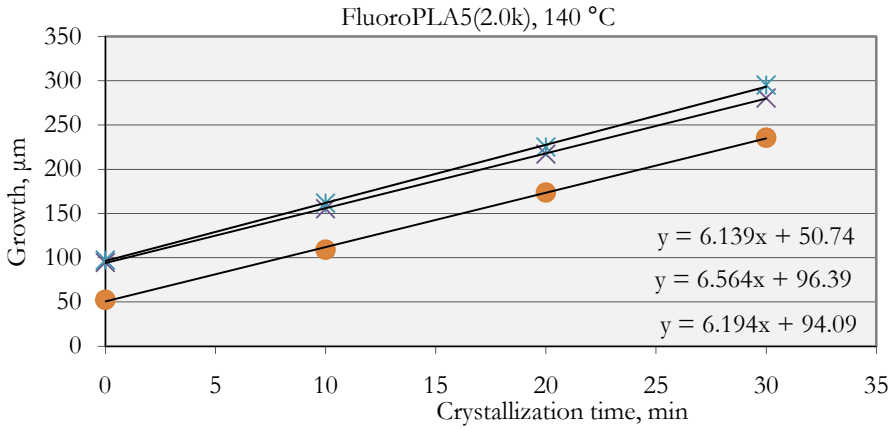

Figure I.13. Diameter of FluoroPLA5(2.0k) spherulites as a function of crystallization time at 140 °C.

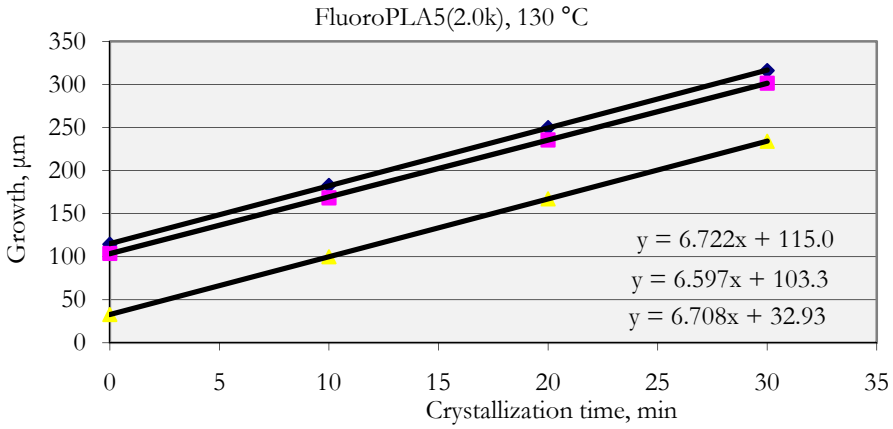

Figure I.14. Diameter of FluoroPLA5(2.0k) spherulites as a function of crystallization time at 130 °C.

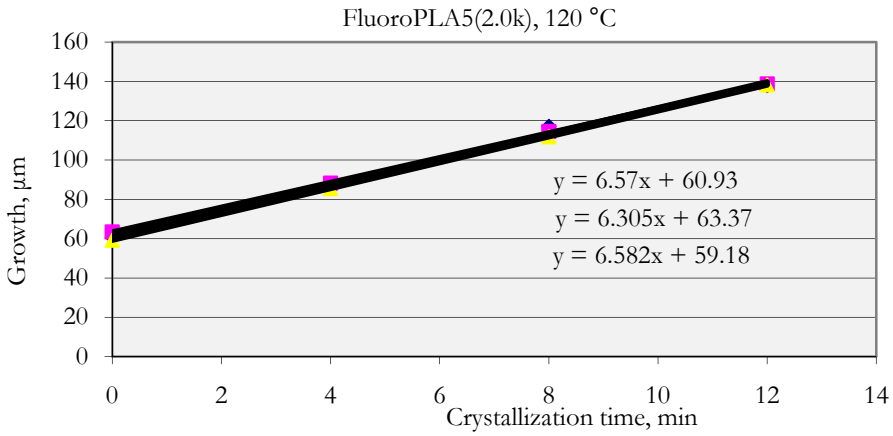

Figure I.15. Diameter of FluoroPLA5(2.0k) spherulites as a function of crystallization time at 120 °C.

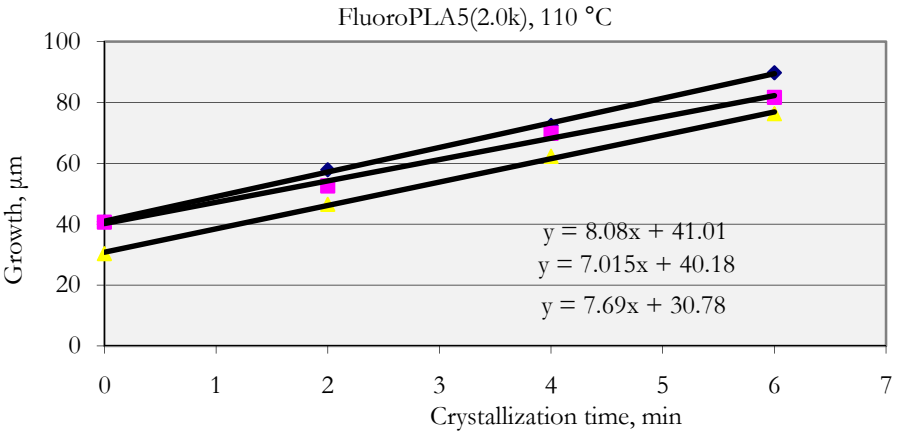

Figure I.16. Diameter of FluoroPLA5(2.0k) spherulites as a function of crystallization time at 110 °C.

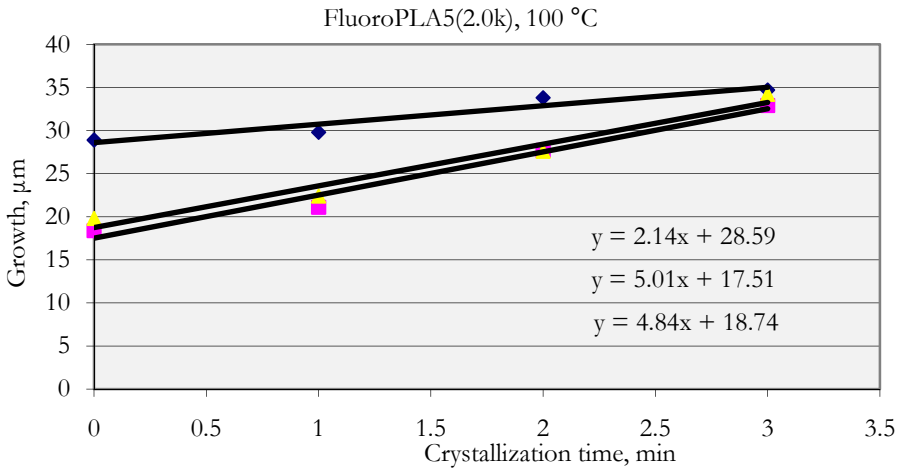

Figure I.17. Diameter of FluoroPLA5(2.0k) spherulites as a function of crystallization time at 100 °C.

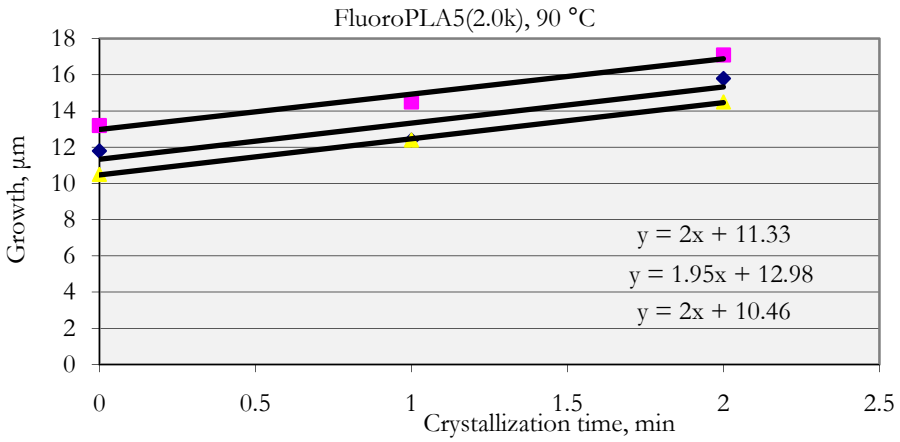

Figure I.18. Diameter of FluoroPLA5(2.0k) spherulites as a function of crystallization time at 90 °C.

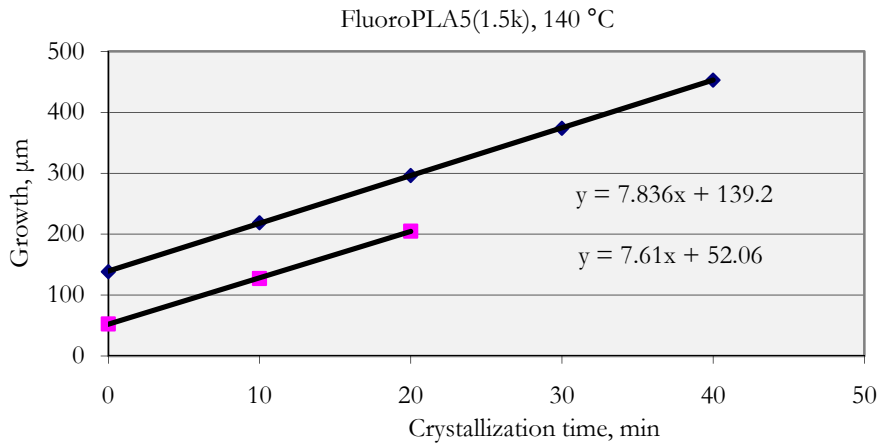

Figure I.19. Diameter of FluoroPLA5(1.5k) spherulites as a function of crystallization time at 140 °C.

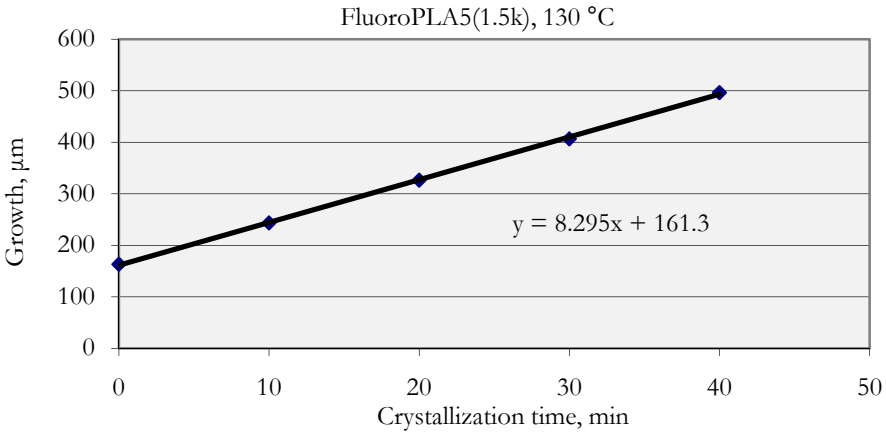

Figure I.20. Diameter of FluoroPLA5(1.5k) spherulites as a function of crystallization time at 130 °C.

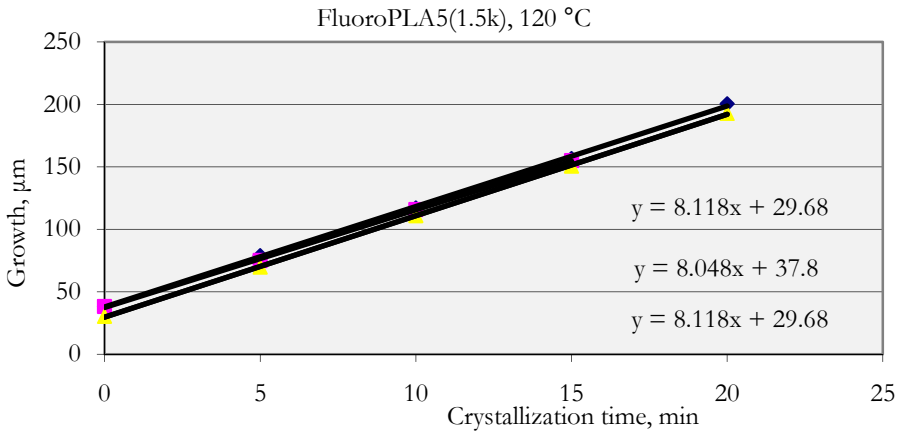

Figure I.21. Diameter of FluoroPLA5(1.5k) spherulites as a function of crystallization time at 120 °C.

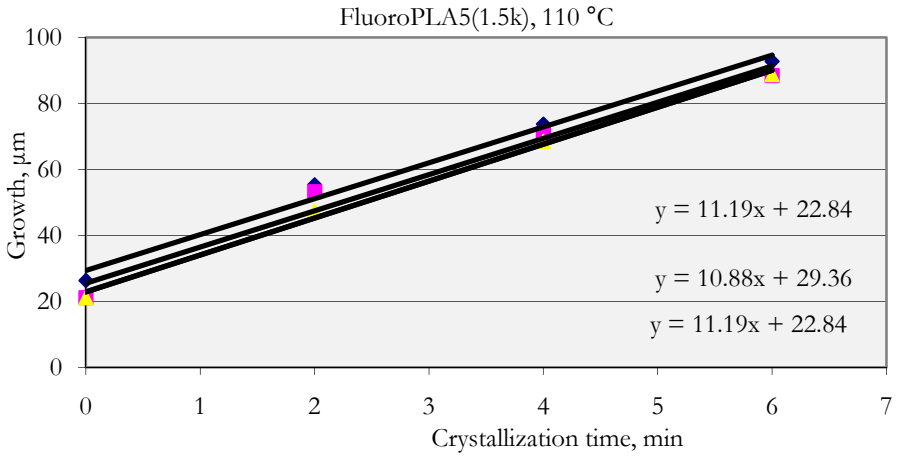

Figure I.22. Diameter of FluoroPLA5(1.5k) spherulites as a function of crystallization time at 110 °C.

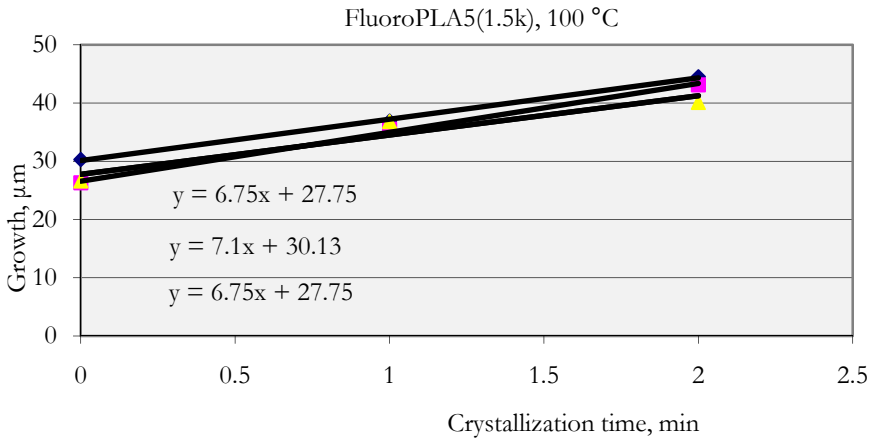

Figure I.23. Diameter of FluoroPLA5(1.5k) spherulites as a function of crystallization time at 100 °C.

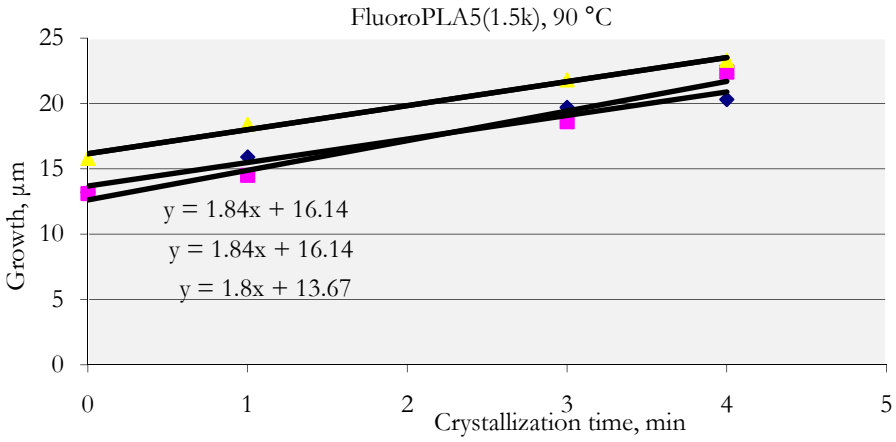

Figure I.24. Diameter of FluoroPLA5(1.5k) spherulites as a function of crystallization time at 90 °C.

Appendix J

Non-Isothermal Cold Crystallization of PLA and FluoroPLAs

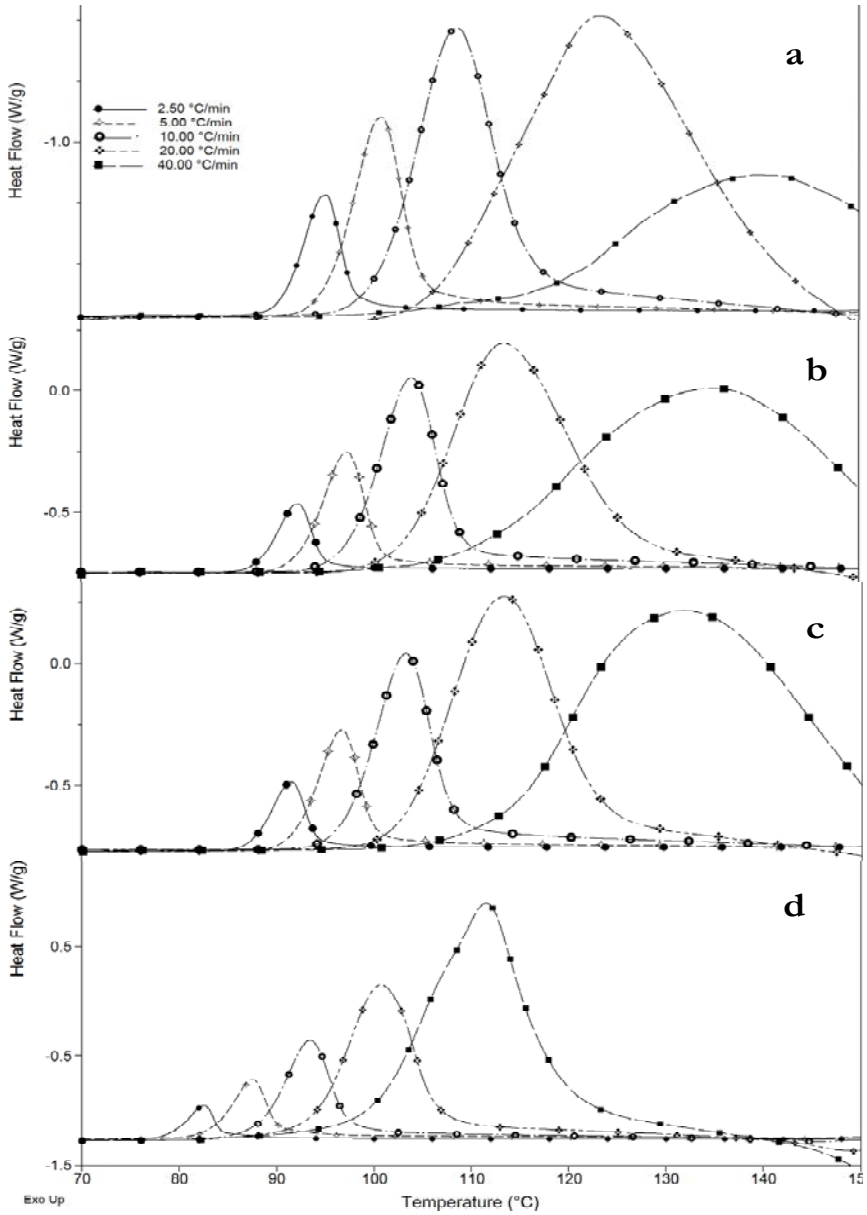

Figure J.1. Heat flow curves for non-isothermal cold crystallization of PLA (a), FluoroPLA5(4.2k) (b), FluoroPLA5(2.0k) (c) and FluoroPLA5(1.5k) (d) obtained during various heating rates.

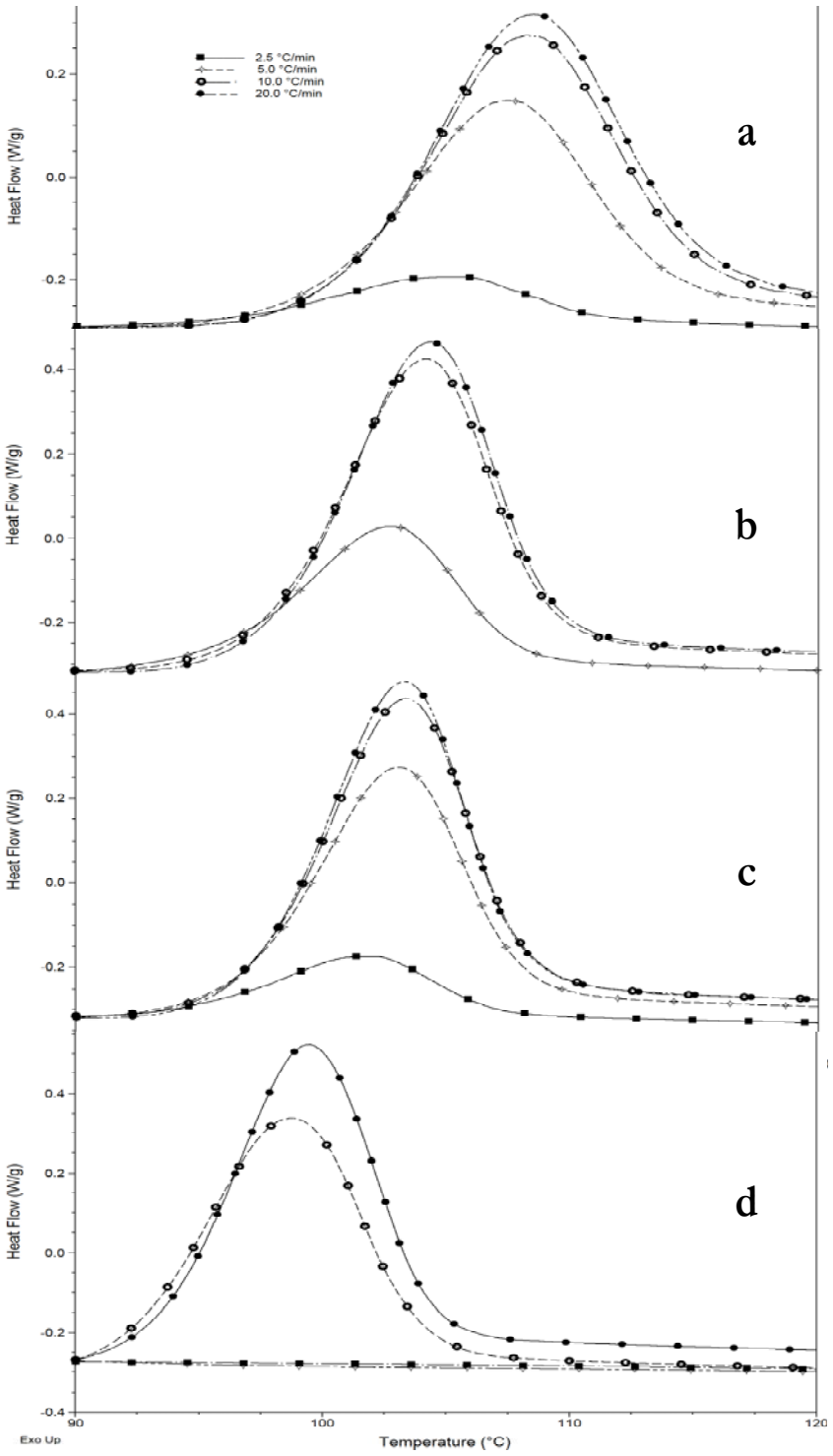

Figure J.2. Heat flow curves for non-isothermal cold crystallization of PLA (a), FluoroPLA5(4.2k) (b), FluoroPLA5(2.0k) (c) and FluoroPLA5(1.5k) (d) obtained by heating samples (obtained by four different cooling rates 20, 10, 5, 2.5 °C/min) at constant rate of 10 °C/min.

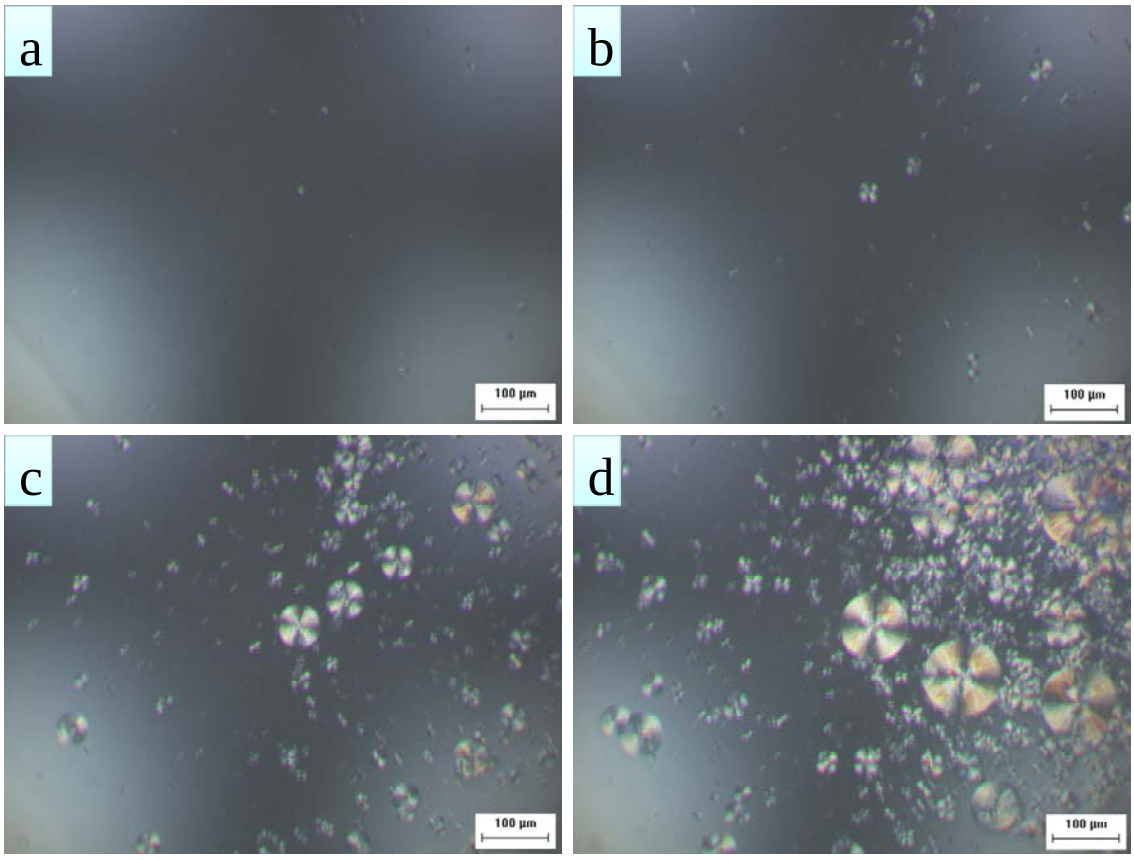

Figure J.3. Polarized optical micrographs of PLA at different cooling rate [20 °C/min (a), 10 °C/min (b), 5 °C/min (c), and 2.5 °C/min (d)].

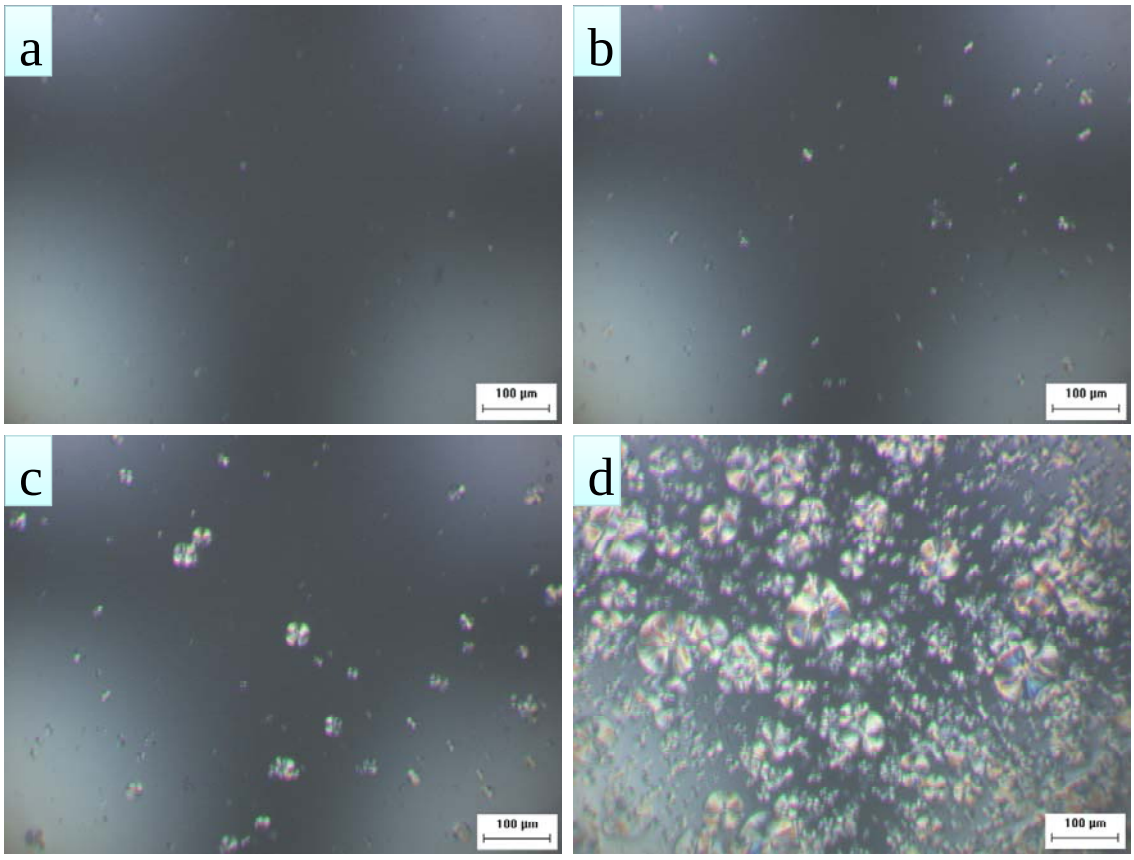

Figure J.4. Polarized optical micrographs of FluoroPLA5(1.5k) at different cooling rate [20 °C/min (a), 10 °C/min (b), 5 °C/min (c), and 2.5 °C/min (d)].

Appendix K

Effect of Hydrolysis Time on the Melting Transition of PLA and FluoroPLAs

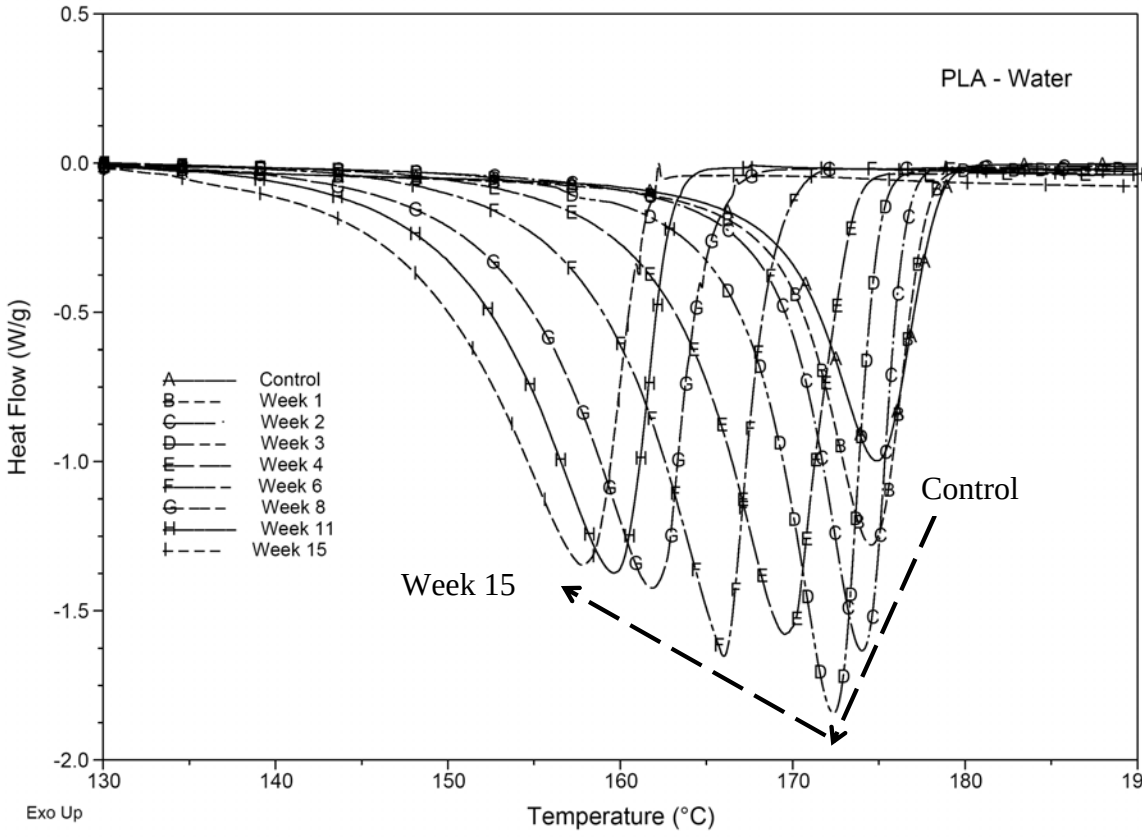

Figure K.1. DSC thermograms of PLA films in water for different hydrolysis time.

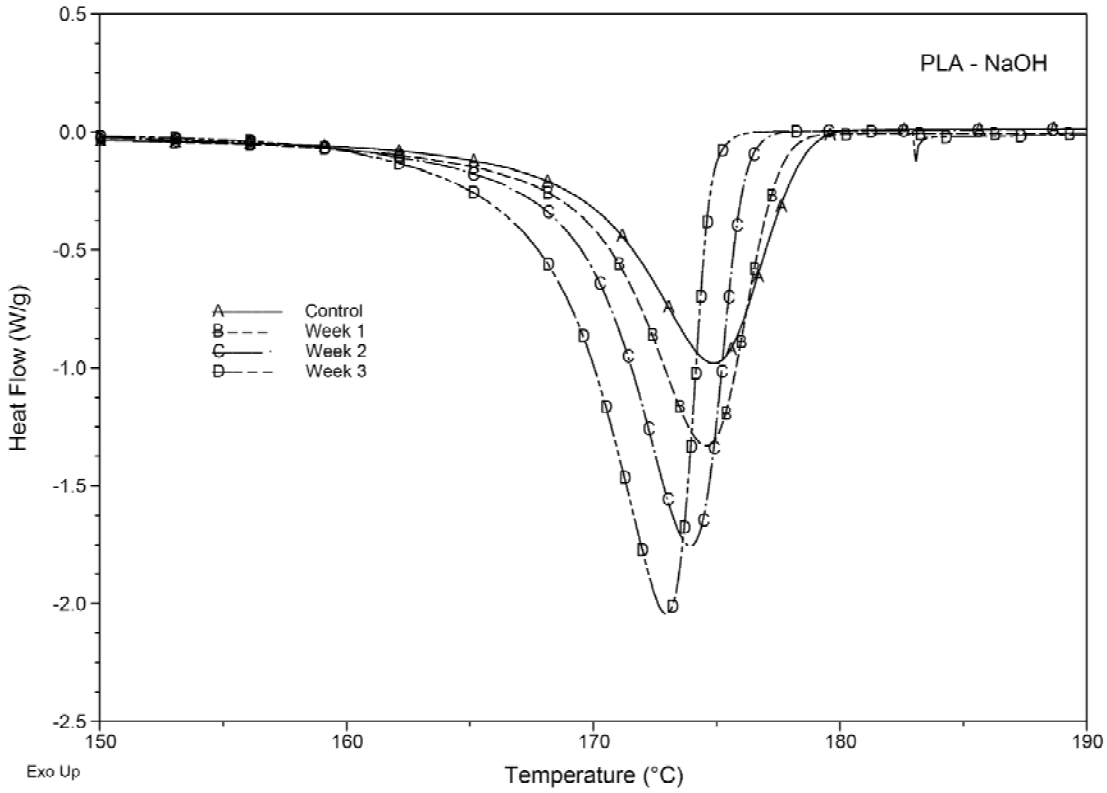

Figure K.2. DSC thermograms of PLA films in NaOH for different hydrolysis time.

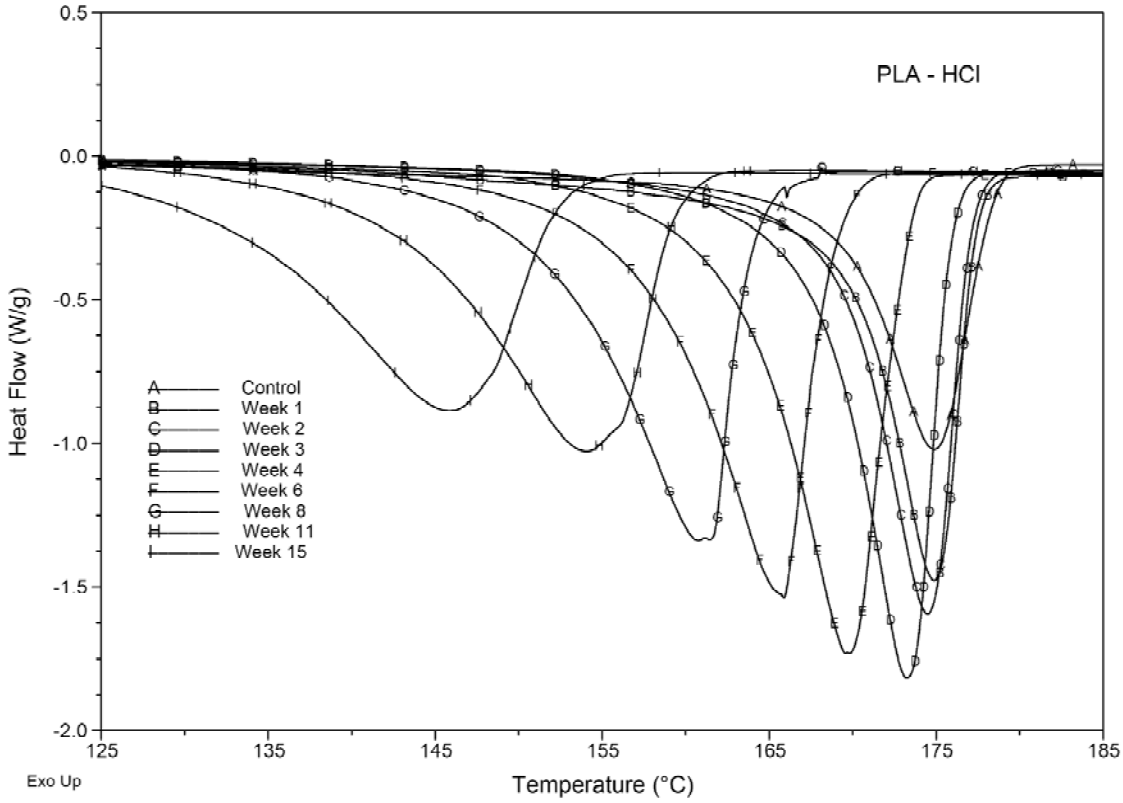

Figure K.3. DSC thermograms of PLA films in HCl for different hydrolysis time.

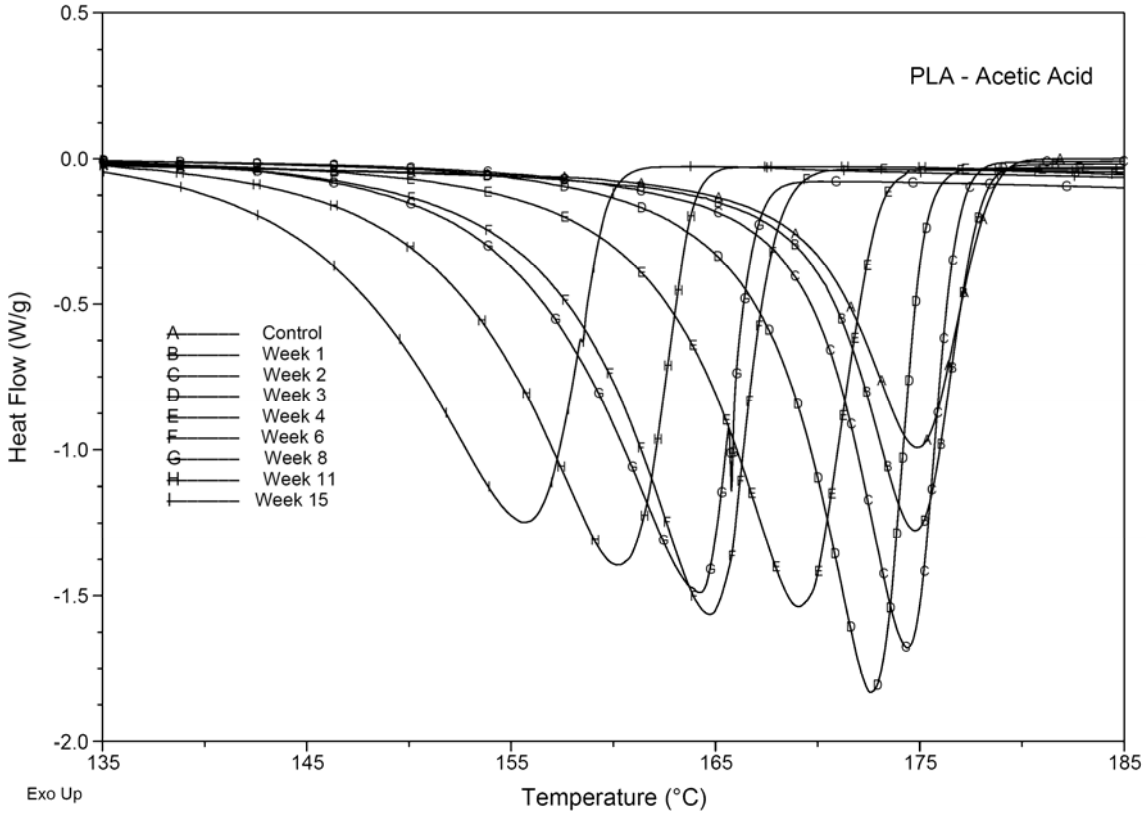

Figure K.4. DSC thermograms of PLA films in acetic acid for different hydrolysis time.

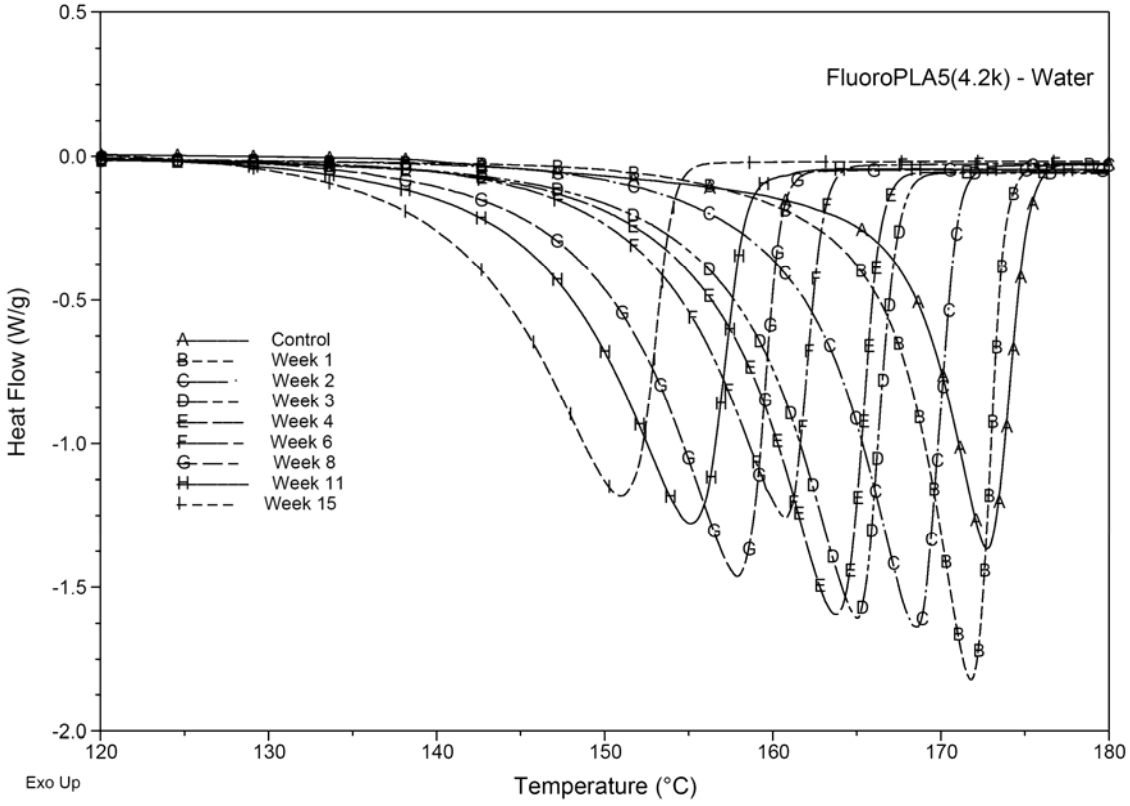

Figure K.5. DSC thermograms of FluoroPLA5(4.2k) films in water for different hydrolysis time.

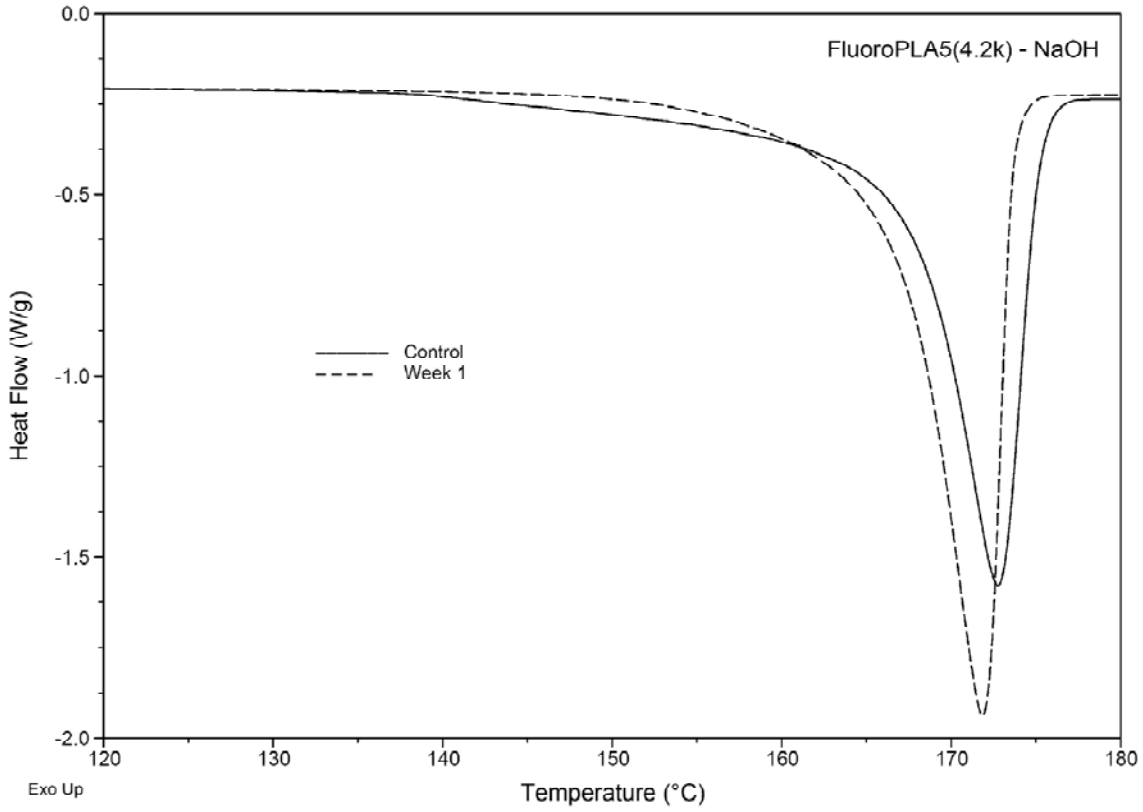

Figure K.6. DSC thermograms of FluoroPLA5(4.2k) films in NaOH for different hydrolysis time.

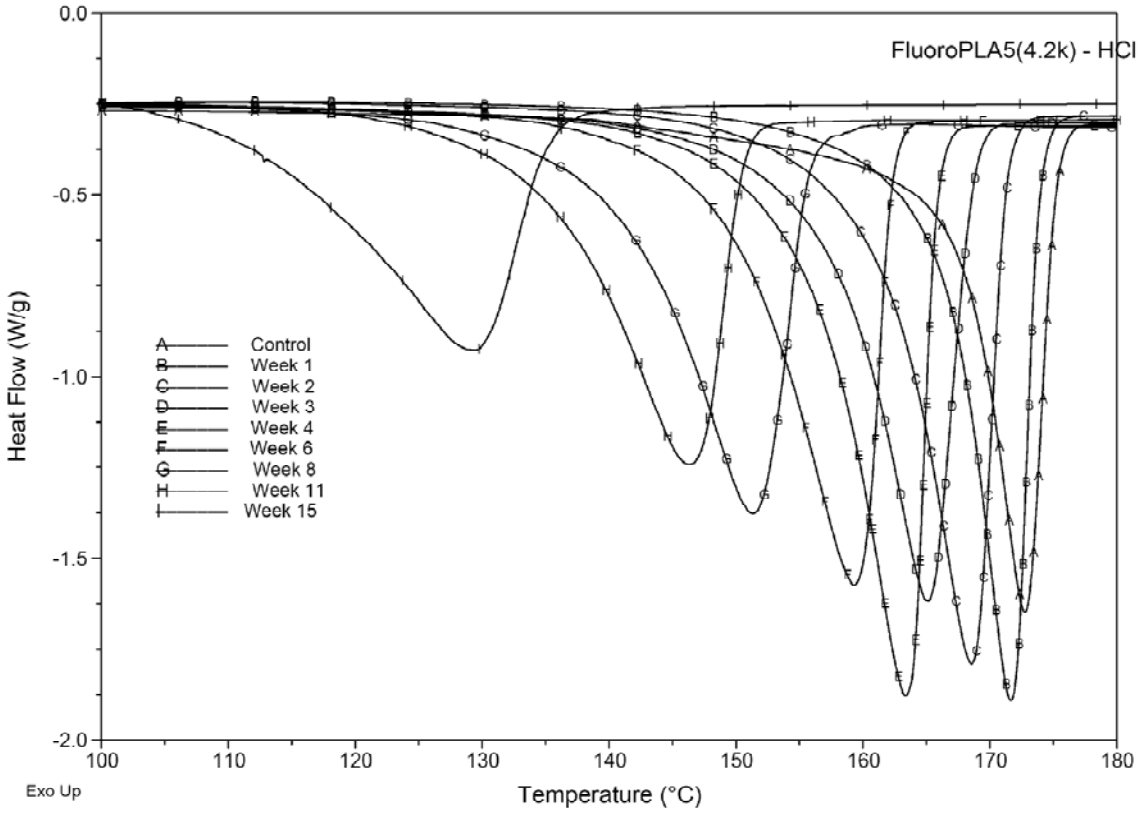

Figure K.7. DSC thermograms of FluoroPLA5(4.2k) films in HCl for different hydrolysis time.

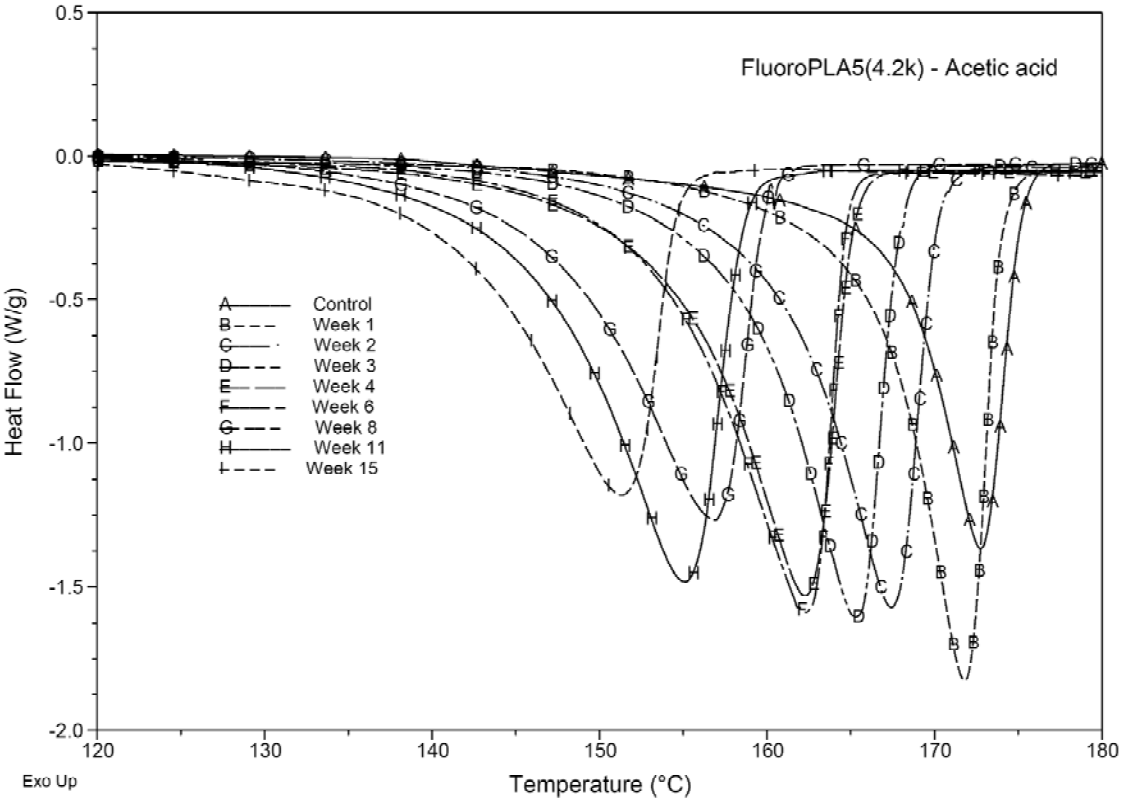

Figure K.8. DSC thermograms of FluoroPLA5(4.2k) films in acetic acid for different hydrolysis time.

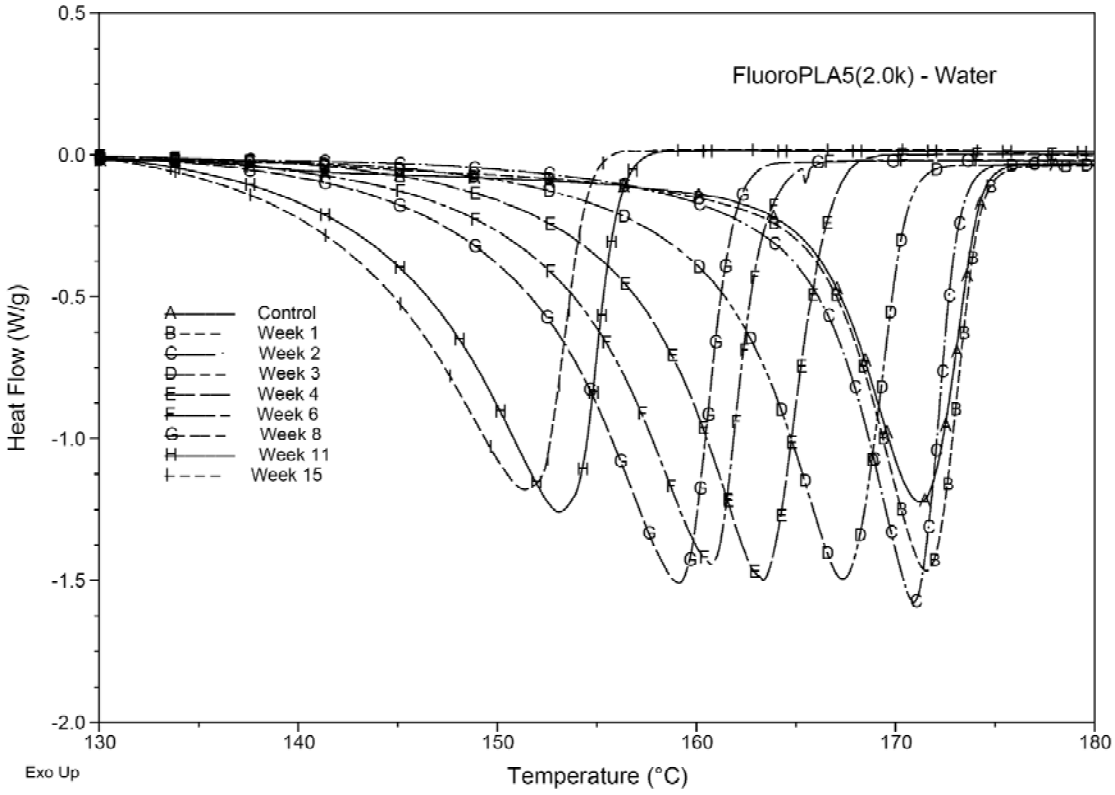

Figure K.9. DSC thermograms of FluoroPLA5(2.0k) films in water for different hydrolysis time.

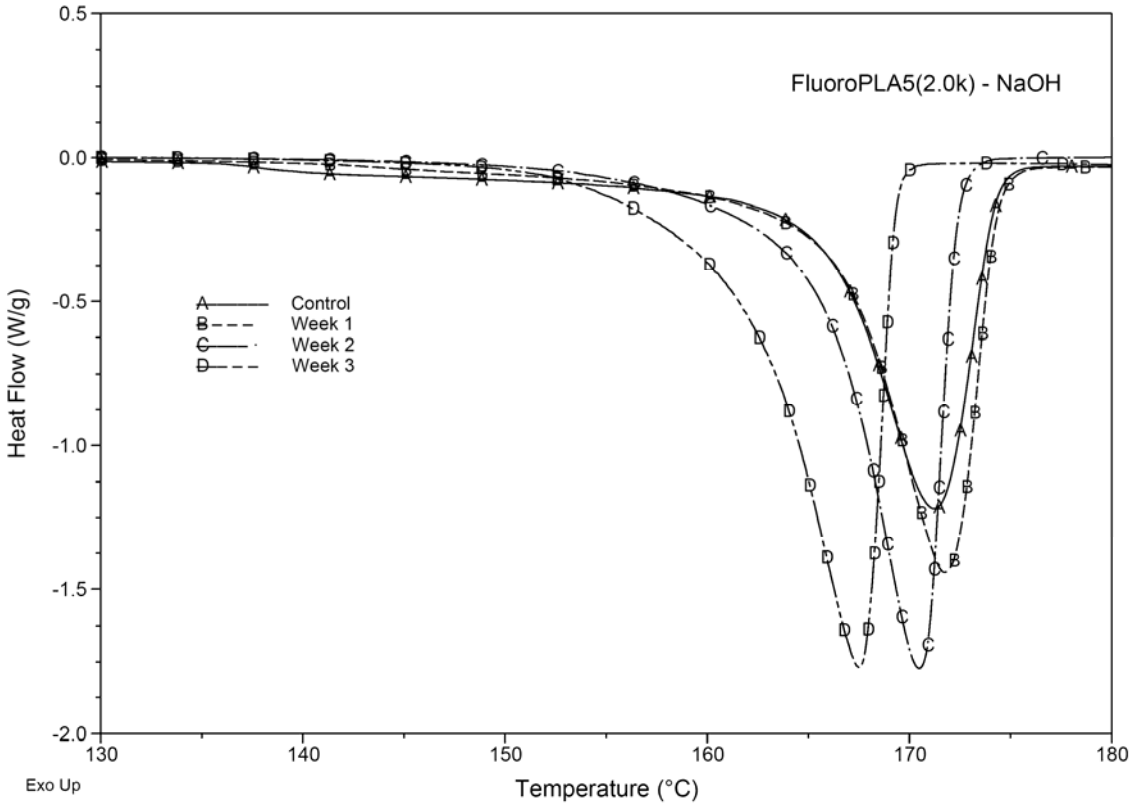

Figure K.10. DSC thermograms of FluoroPLA5(2.0k) films in NaOH for different hydrolysis time.

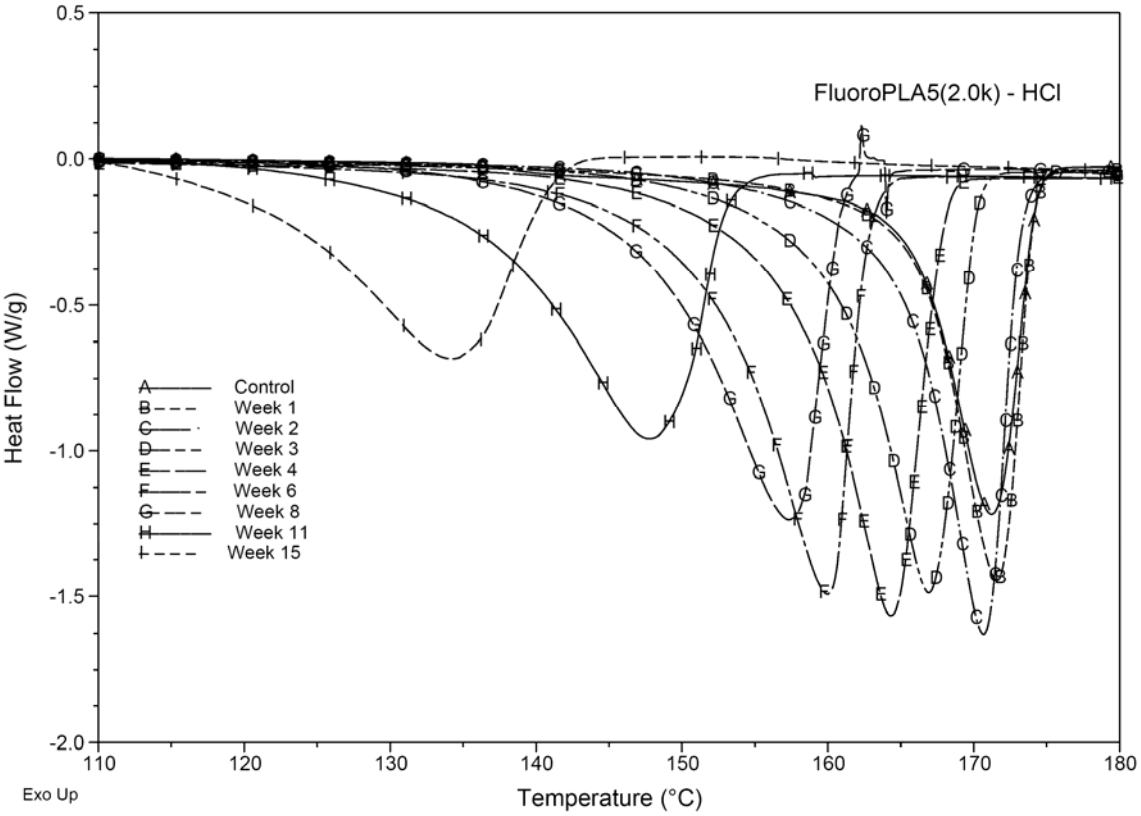

Figure K.11. DSC thermograms of FluoroPLA5(2.0k) films in HCl for different hydrolysis time.

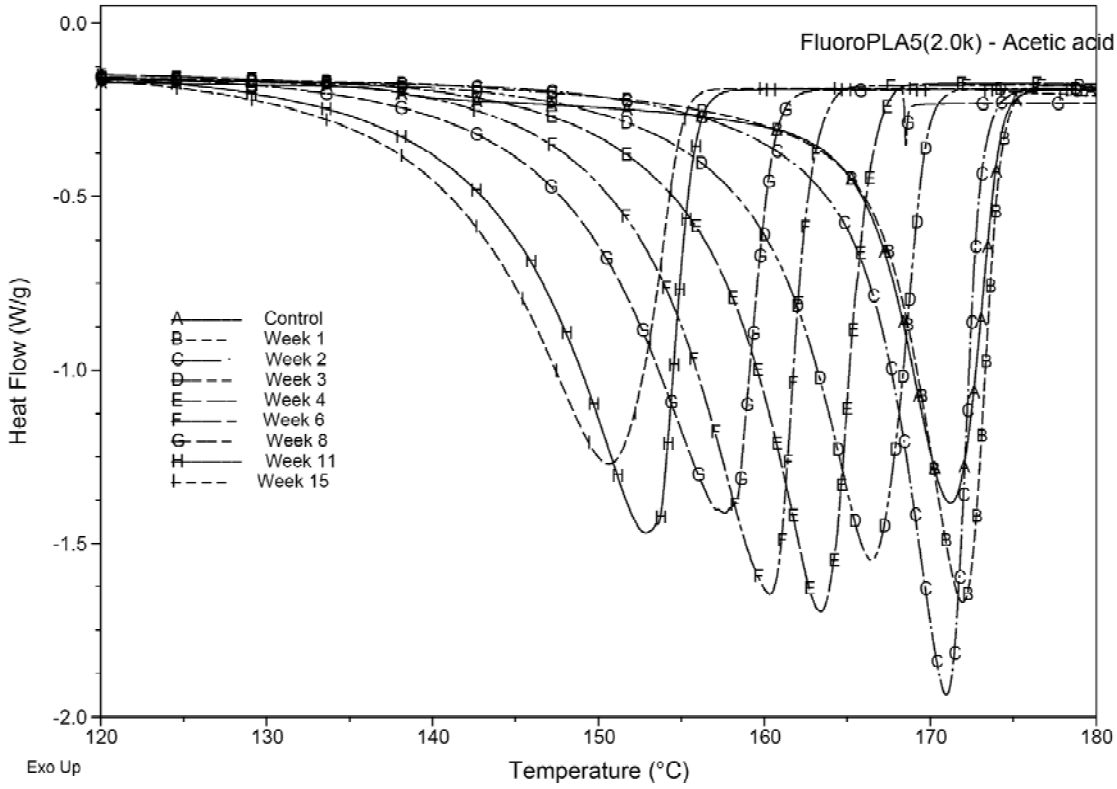

Figure K.12. DSC thermograms of FluoroPLA5(2.0k) films in acetic acid for different hydrolysis time.

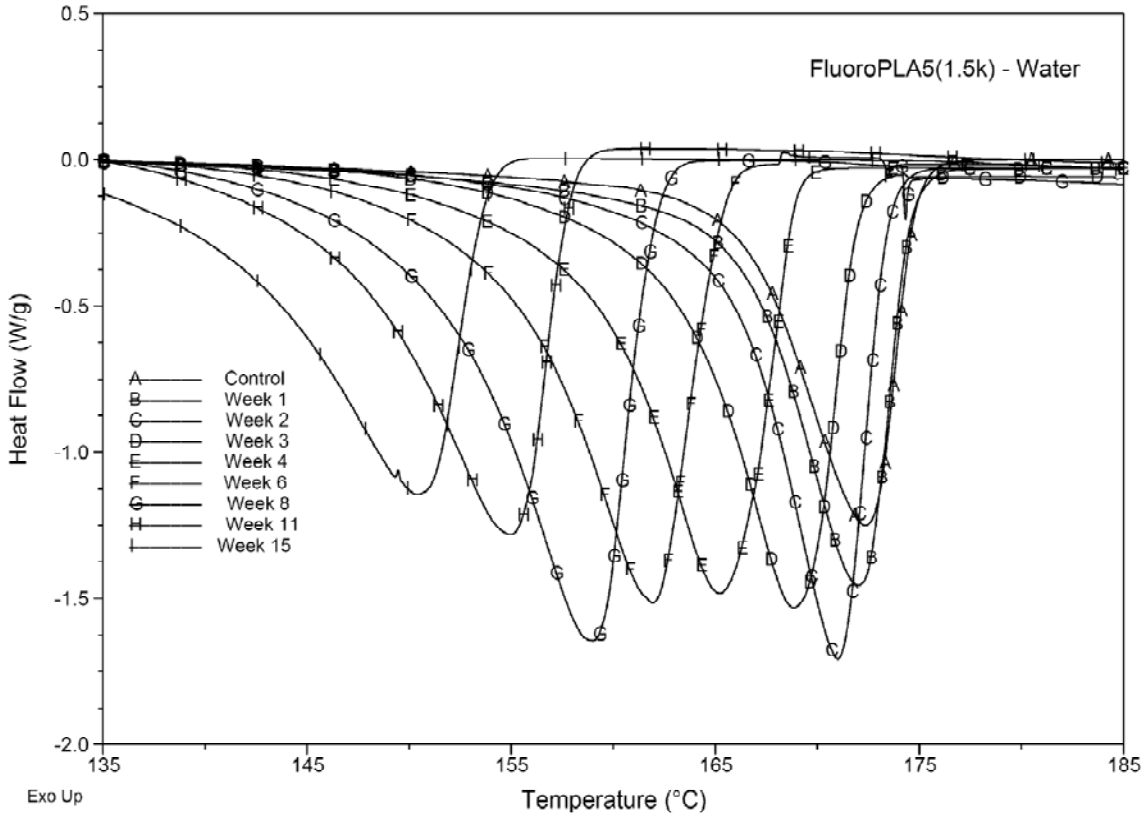

Figure K.13. DSC thermograms of FluoroPLA5(1.5k) films in water for different hydrolysis time.

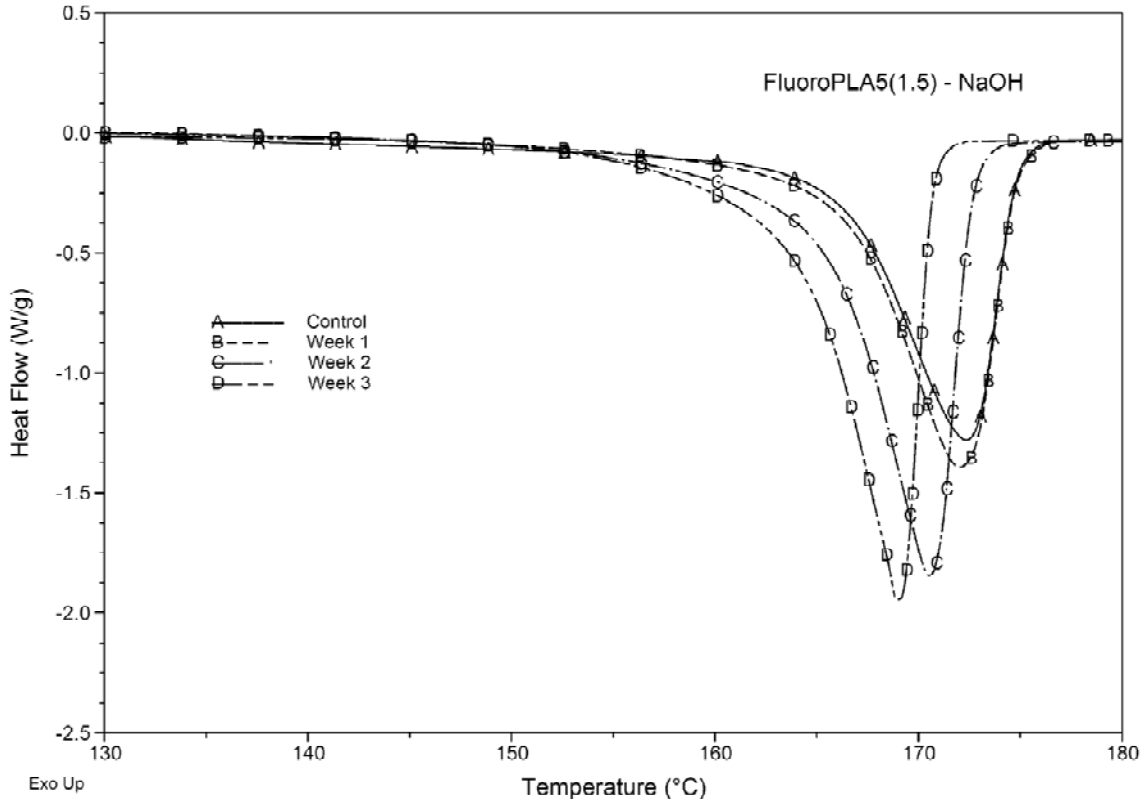

Figure K.14. DSC thermograms of FluoroPLA5(1.5k) films in NaOH for different hydrolysis time.

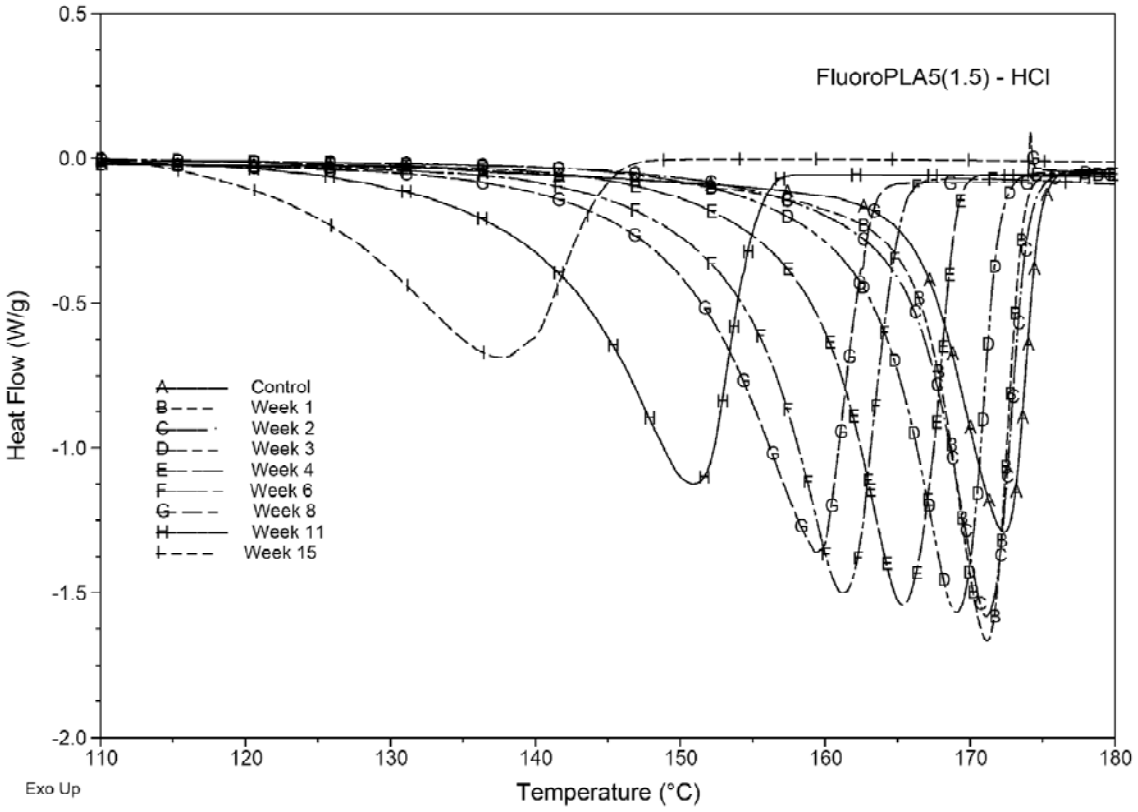

Figure K.15. DSC thermograms of FluoroPLA5(1.5k) films in HCl for different hydrolysis time.

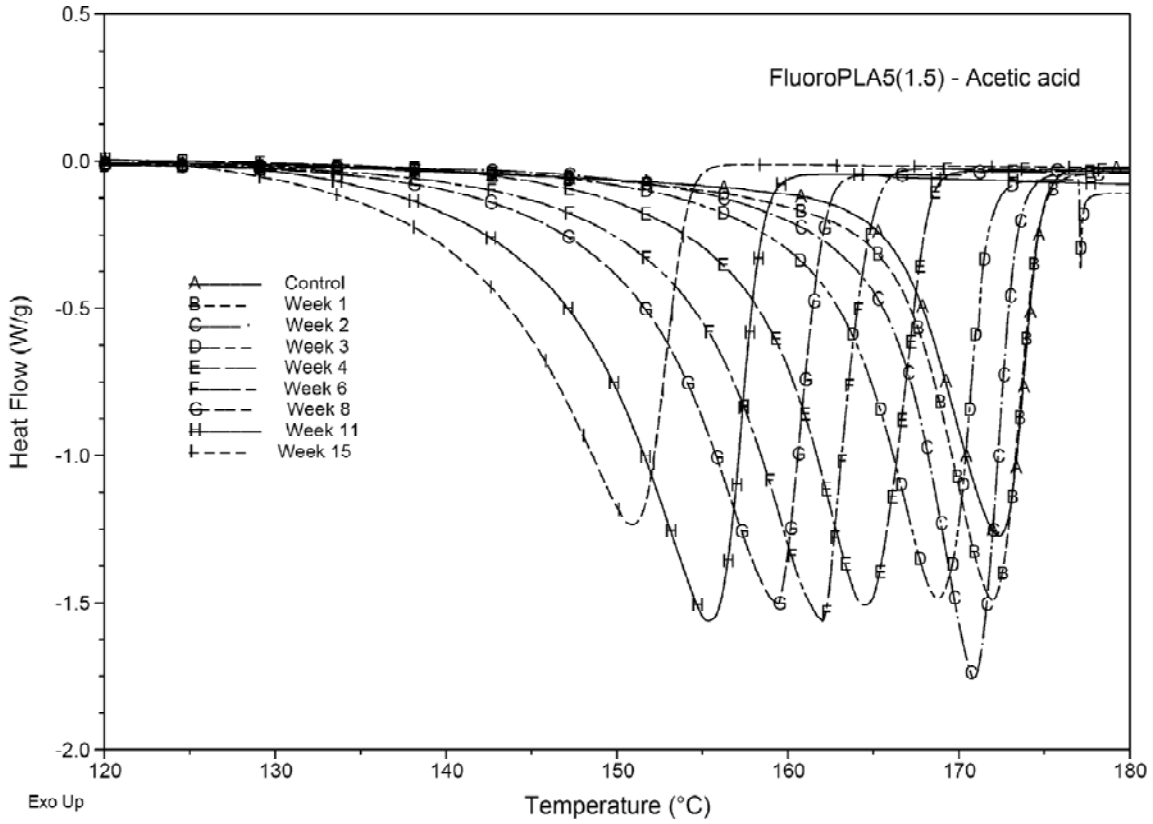

Figure K.16. DSC thermograms of FluoroPLA5(1.5k) films in acetic acid for different hydrolysis time.

Appendix L

X-ray Diffraction Data for Hydrolyzed PLA and FluoroPLAs films.

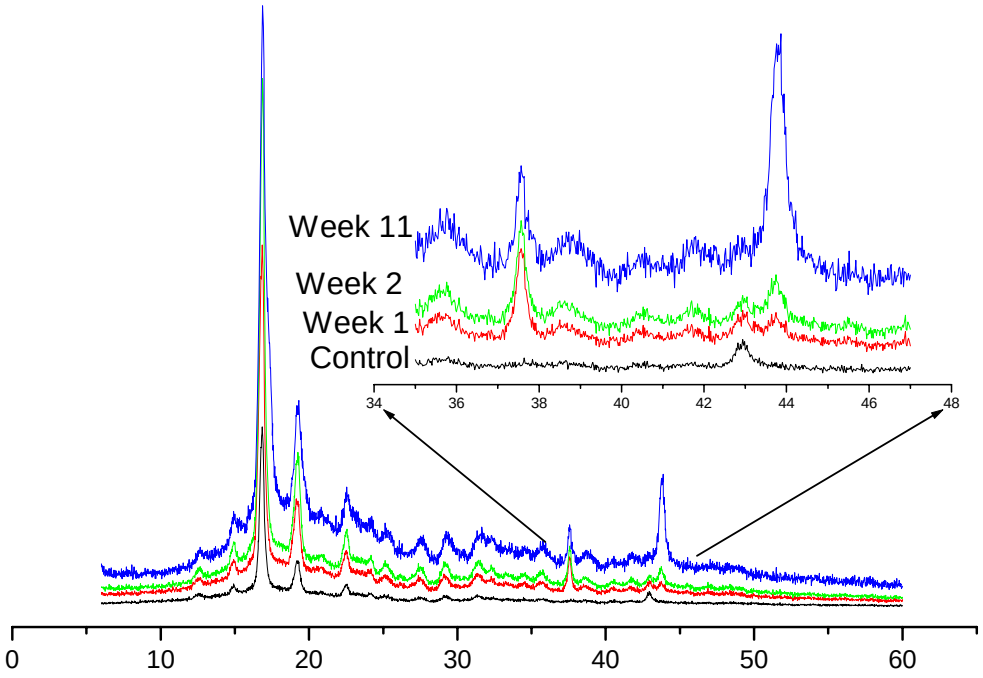

Figure L.1. X-ray diffraction profiles of FluoroPLA5(4.2k) films: before hydrolysis (Control) and after hydrolysis in water for 1, 2, 11 weeks.

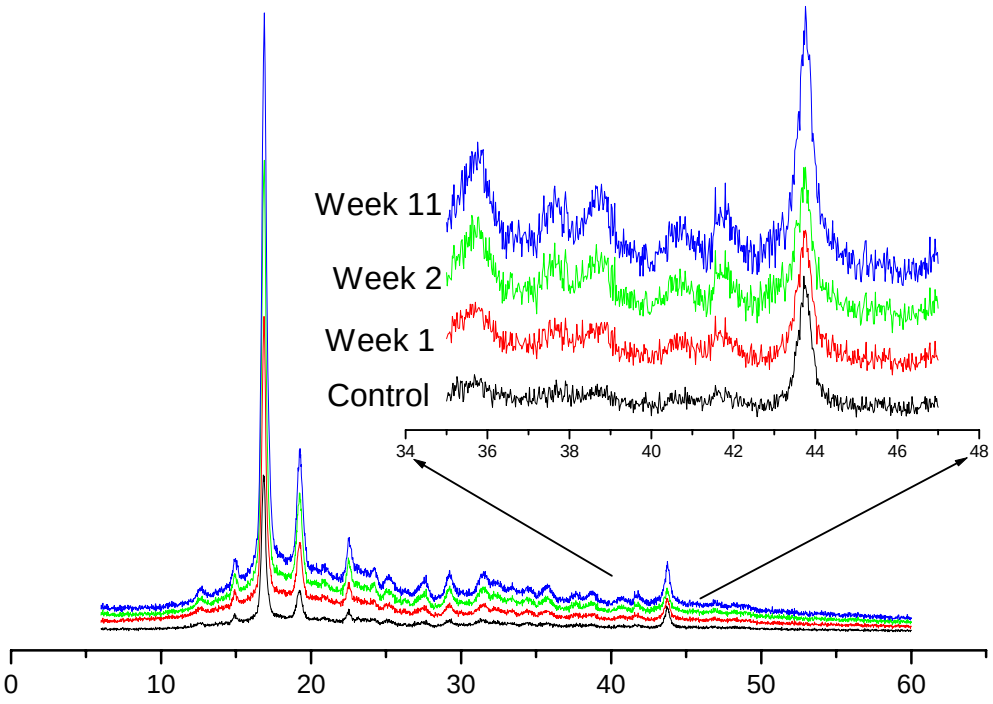

Figure L.2. X-ray diffraction profiles of FluoroPLA5(2.0k) films: before hydrolysis (Control) and after hydrolysis in water for 1, 2, 11 weeks.

Appendix M

Tensile Properties of PLA and FluoroPLA Melt Spun Fibers

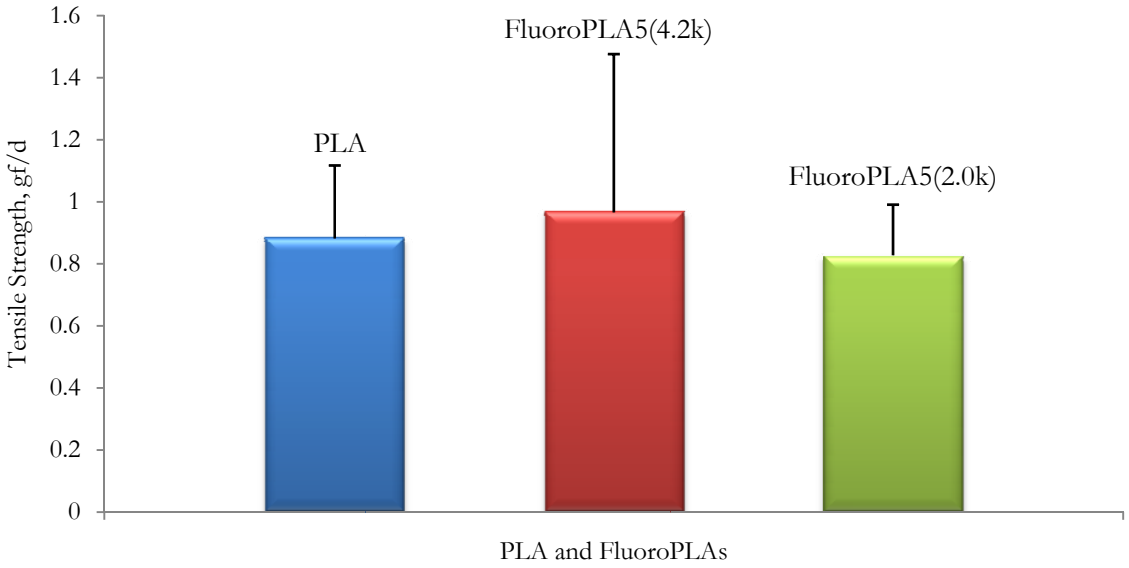

Figure M.1. Tensile strength (g/d) of PLA, FluoroPLA5(4.2k), and FluoroPLA5(2.0k) melt spun fibers.

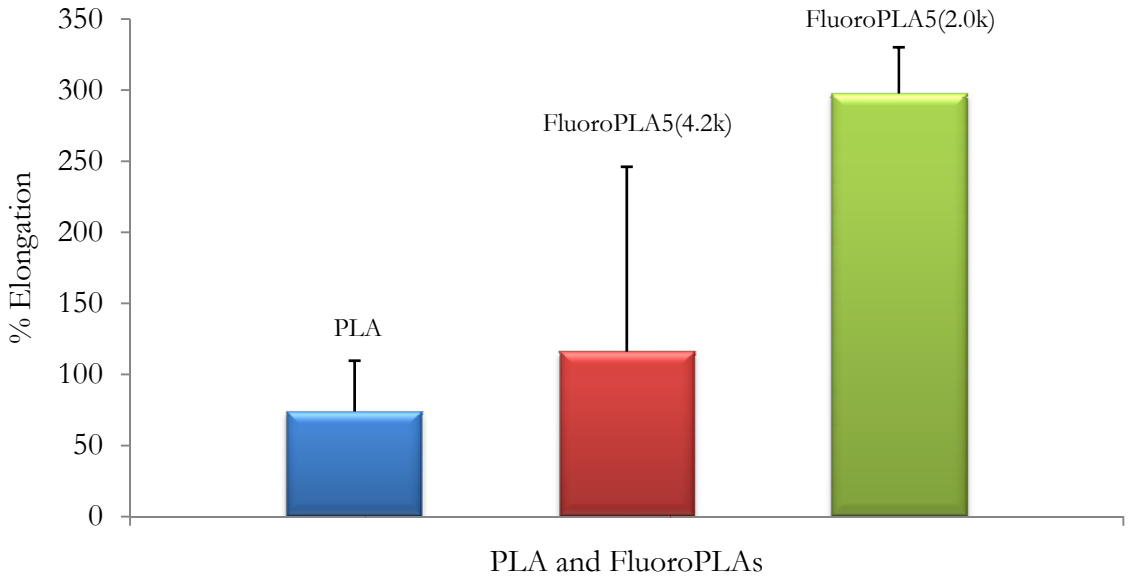

Figure M.2. Percentage elongation-at-break of PLA, FluoroPLA5(4.2k), and FluoroPLA5(2.0k) melt spun fibers.

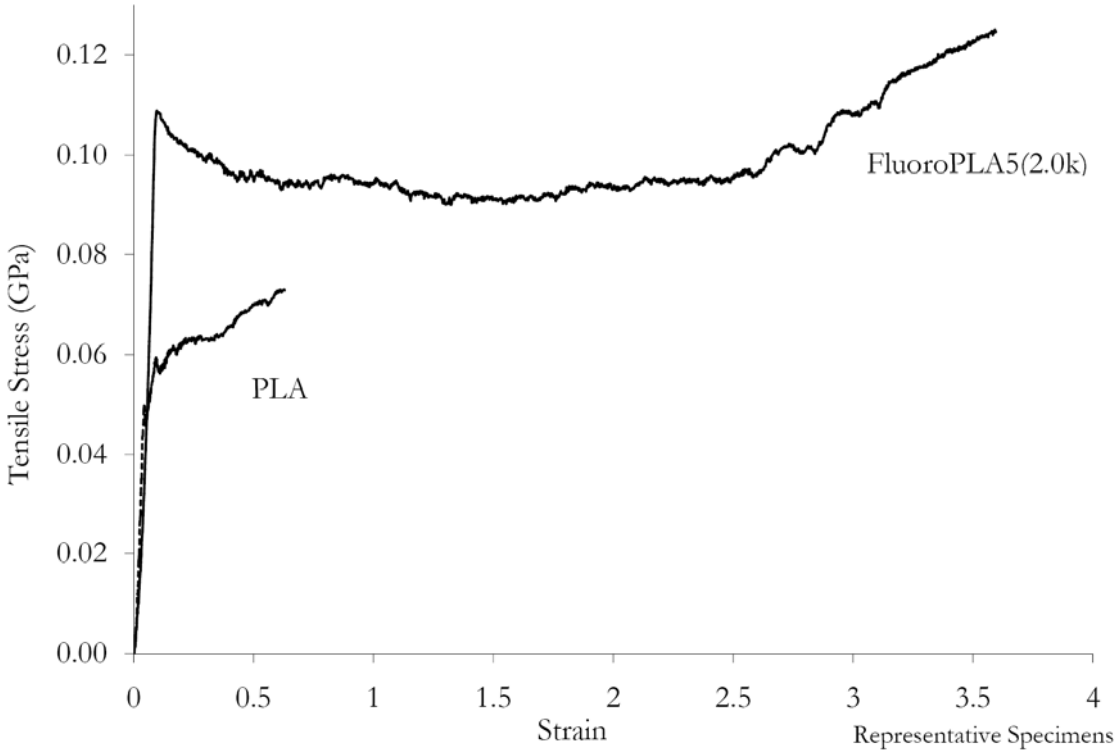

Figure M.3. Stress-strain curve of a single specimen of melt spun PLA and FluoroPLA5(2.0k) fibers.

Appendix N

Dynamic Mechanical Analysis of Melt Spun PLA and FluoroPLA Fibers

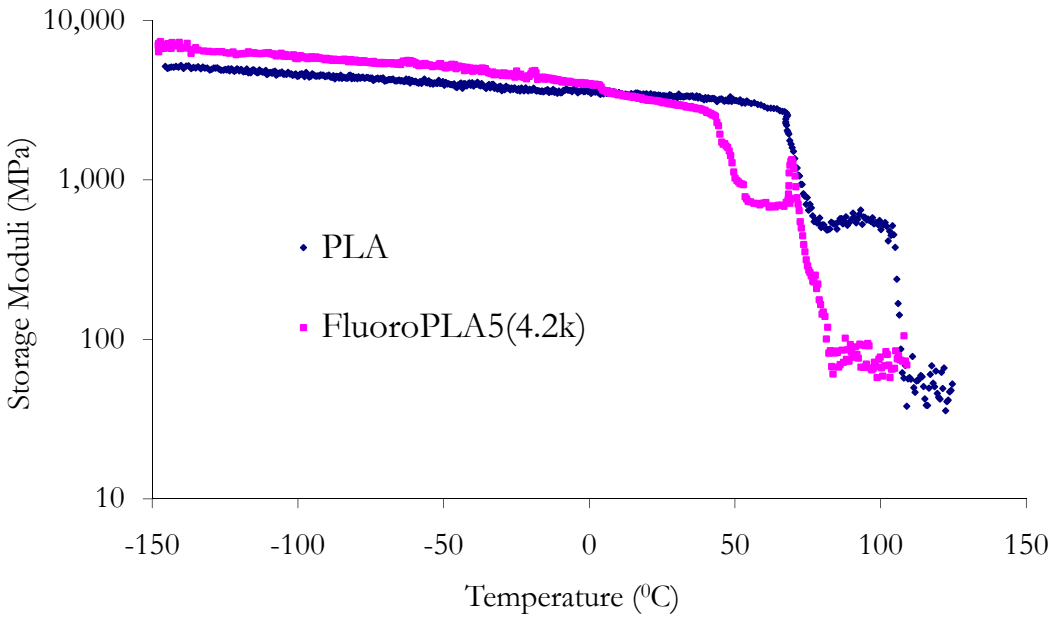

Figure N.1. Storage moduli of PLA and FluoroPLA5(4.2k) melt spun fibers as a function of temperature.

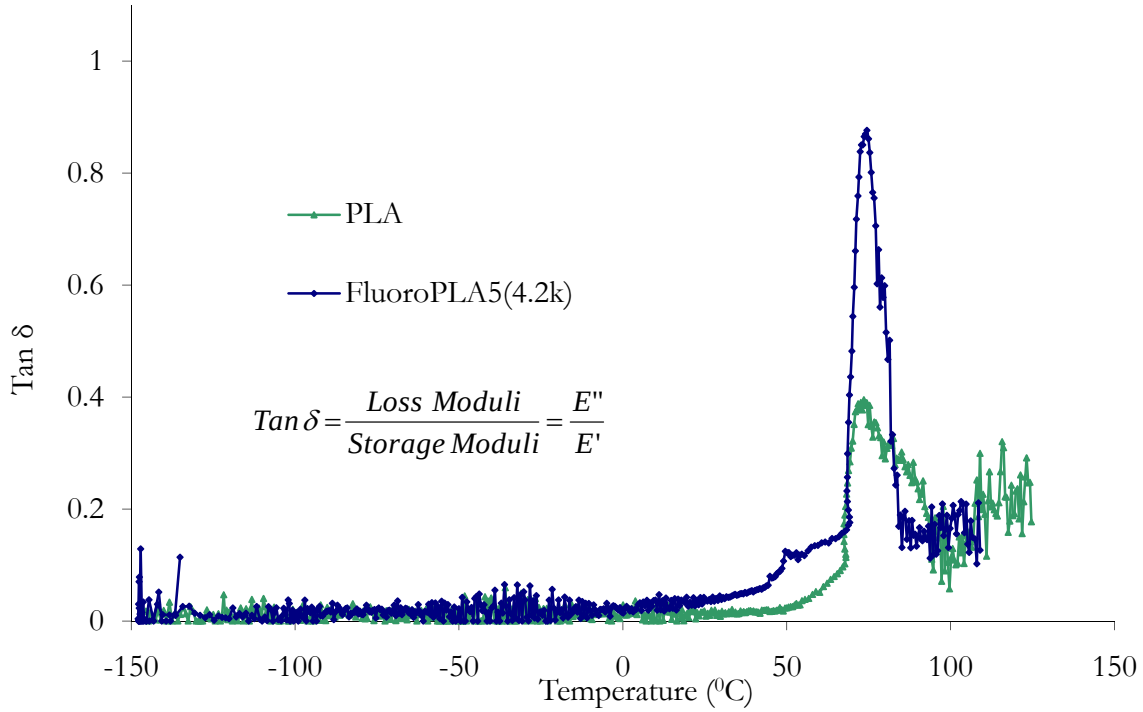

Figure N.2. Loss factor (tanδ) of PLA and FluoroPLA5(4.2k) melt spun fibers as a function of temperature.